Integrating paleoseismic studies with geochronology and thermochronology to understand the timing of rifting, volcanism, and uplift in the Rukwa Rift Basin, Tanzania

Thesis submitted by

Hannah Louise Hilbert-Wolf

June 2016

For the Degree of Doctor of Philosophy
James Cook University

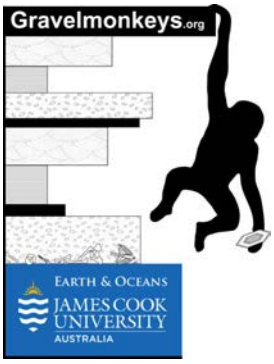

Statement of Access

I, the undersigned author of this thesis, understand that James Cook University will make this thesis available for use within the university library and allow access in other approved libraries after its submission. All users consulting this thesis will have to sign the following statement:

In consulting this thesis I agree not to copy or closely paraphrase it in whole or in part without the written consent of the author; and to make proper public written acknowledgement for any assisstance which I have obtained from it.

Beyond this, I do not wish to place any restrictions on access to this thesis.

Hannah L. Hilbert-Wolf
June 2016

Declaration

I declare that this thesis is my own work and has not been submitted in any form for another degree or diploma at any university or other institute or tertiary education. Information derived from the published or unpublished work of others has been acknowledged in the text and a list of references is given.

Hannah L. Hilbert-Wolf
June 2016

Every reasonable effort has been made to gain permission and acknowledge the owners of copyright material. I would be pleased to hear from any copyright owner who has been omitted or incorrectly acknowledged.

Statement on the contributions of others

Nature of Assistance	Contribution	Names & affiliations of co-contributors
Intellectual support	Supervision	Dr. Eric Roberts, JCU Dr. Paul Dirks, JCU
	Proposal writing	Dr. Eric Roberts, JCU
	Data analysis	Dr. Eric Roberts, JCU Dr. Carl Spandler, JCU Bob Downie, Heritage Oil Ltd. Dr. Edward Simpson, KU
	Editorial assistance	Dr. Eric Roberts, JCU Bob Downie, Heritage Oil Ltd. Dr. Paul Dirks, JCU Dr. Patrick O'Connor, OU Dr. Nancy Stevens, OU
Financial support	Research funding	NSF (US) American Assoc. of Petroleum Geologists Heritage Rukwa Tanzania Ltd. (provided well cutting samples)
	Stipend	JCU IPRS
External data collection	**(**U-Th)/He lab	Travelled to University of Glasgow to perform analyses under supervision of Dr. Rod Brown, UG
	U-Pb and FT lab	Apatite to Zircon, Inc.

Statement of Contribution

Chapter	Publication on which chapter is based	Nature and extent of intellectual input
1	Hilbert-Wolf, H. and Roberts, E. (2015). PLoS ONE. doi: 10.1371/journal.pone.0129051	Roberts contributed to primary idea discussion, fieldwork, and provided editorial assistance.
2	Hilbert-Wolf, H., Roberts, E., and Simpson, E. (in review; submitted 9/2015). Sedimentary Geology.	Roberts contributed to primary idea discussion, fieldwork, and provided editorial assistance.
3	Hilbert-Wolf, H., Roberts, E., Downie, B., Mtelela, C., Stevens, N., and O'Connor, P. (in review; submitted 1/2016). The AAPG Bulletin.	Roberts contributed to concept development and primary idea discussion, fieldwork, sample collection, data analysis, and provided editorial assistance.

I confirm the candidate's contribution to these papers and consent to the inclusion of these papers in this thesis.

Name: Dr. Eric Roberts

Signature:

Date: 18/01/2016

Statement of Contribution

Chapter	Publication on which chapter is based	Nature and extent of intellectual input
2	Hilbert-Wolf, H., Roberts, E., and Simpson, E. (in review; submitted 9/2015). Sedimentary Geology.	Simpson contributed to concept development, primary idea discussion, and provided editorial assistance.

I confirm the candidate's contribution to this paper and consent to the inclusion of this paper in this thesis.

Name: Dr. Edward Simpson

Signature:

Date: 1/19/2016

Statement of Contribution

Chapter	Publication on which chapter is based	Nature and extent of intellectual input
3	Hilbert-Wolf, H., Roberts, E., Downie, B., Mtelela, C., Stevens, N., and O'Connor, P. (in review; submitted 1/2016). The AAPG Bulletin.	Downie contributed to primary idea discussion, fieldwork, sample collection, and provided editorial assistance.

I confirm the candidate's contribution to this paper and consent to the inclusion of this paper in this thesis.

Name: Bob Downie

Signature:

Date: 19th January 2016

Statement of Contribution

Chapter	Publication on which chapter is based	Nature and extent of intellectual input
3	Hilbert-Wolf, H., Roberts, E., Downie, B., Mtelela, C., Stevens, N., and O'Connor, P. (in review; submitted 1/2016). The AAPG Bulletin.	O'Connor contributed to fieldwork and provided editorial assistance.

I confirm the candidate's contribution to this paper and consent to the inclusion of this paper in this thesis.

Name: Dr. Patrick O'Connor

Signature:

Date: 19 January 2016

Statement of Contribution

Chapter	Publication on which chapter is based	Nature and extent of intellectual input
3	Hilbert-Wolf, H., Roberts, E., Downie, B., Mtelela, C., Stevens, N., and O'Connor, P. (in review; submitted 1/2016). The AAPG Bulletin.	Stevens contributed to fieldwork and provided editorial assistance.

I confirm the candidate's contribution to this paper and consent to the inclusion of this paper in this thesis.

Name: Dr. Nancy Stevens

Signature:

Date: 19 January 2016

Statement of Contribution

Chapter	Publication on which chapter is based	Nature and extent of intellectual input
3	Hilbert-Wolf, H., Roberts, E., Downie, B., Mtelela, C., Stevens, N., and O'Connor, P. (in review; submitted 1/2016). The AAPG Bulletin.	Mtelela contributed to fieldwork and sample collection.

I confirm the candidate's contribution to this paper and consent to the inclusion of this paper in this thesis.

Name: Cassy Mtelela

Signature:

Date: 19th Jan, 2016

Acknowledgments

There are many people who have contributed to my education, experiences, and growth throughout my work on this thesis over the last few years. Although I cannot thank each person here individually, I sincerely appreciate everyone's contributions, as the value each person has added to my time working on my PhD has been immense.

I owe the greatest debt of thanks and sincere appreciation to my advisor and mentor, Dr. Eric Roberts. To say that Eric is the best advisor one could wish for is an understatement. As just one timely example, he reviewed parts of this thesis while braving 30 ft+ waves on a ship to Antarctica. Eric: I have grown as a person, a scientist, and as an academic because of your unending support, enthusiasm, guidance, wisdom, and because of the many opportunities you have presented me with. You have truly taught me how to be a smarter scientist, and I very much look forward to future projects and field adventures with you. No 'thanks' here is enough.

I owe a great deal also to Doc (Dr. Ed Simpson), who I sincerely thank for his unending support since the very beginning. Doc: Thank you for leading me on this path, and for first taking me out into the field in Utah and showing me how exciting, challenging, and rewarding it is to be a geologist. I would not be here without your influence and faith in my abilities, and I am looking forward to future collaborations and adventures!

I also want to thank my advisor Professor Paul Dirks, especially for our on-going adventures in South Africa. I would not have learned as much without Dr. Carl Spandler always keeping his door open to me and always willing to talk about geochronology and carbonatite tuffs. I am grateful also to Dr. Jan Martin for good advice and laughs often on my way to the tearoom.

Sincere gratitude is due to the staff of the SEES (CSTE and CSE), especially to Melissa, Beth, Bec, Jo and Judy. You all helped to make Townsville a home away from home for me, and I am grateful for all of the energy and time you have put towards all I have been able to do here. I sincerely appreciate the staff at the AAC, particularly Yi, Kevin, Shane, Gordon, and Brendan, for assistance with analytical work. I am also indebted to everyone who taught me about (U-Th)/He thermochronology at the University of Glasgow and SUERC. A special thanks is due to Bob Downie, as I have learned so much from you both in and out of the field, and thank you kindly for your hospitality in Glasgow.

It has been really great to share this time also with the rest of the PhD, honours, and masters students over the years – thank you for the comradery. Thank you to Rob! I also want to thank my fellow soccer players, especially the Smurfs. I have so much gratitude for all of the members of the Rukwa Rift Basin Project, who made my experiences in the field unforgettable, and rich with learning and discovery - thank you, and here's to many more!

There is certainly no way I could have accomplished this without Johannes. Thank you so much for reminding me often to be happy, as I have two arms and two legs. You have believed in me each step of the way, and there is nothing I could appreciate more.

Last, but absolutely not least, thank you to all of my family. Most importantly, thank you Mom and Dad (Deb and John) for absolutely everything. I have the best parents in the world, and without your positive perspectives, your incredible support, constant love, wit, wisdom, and more, no part of this would have been as good as it was. Thank you for always reminding me that what I am doing is important.

Thesis Abstract

Although continental rifting has contributed to shaping the Earth's landmasses and landscapes for arguably a large part of our planet's history, the archetypal East African Rift System is one of very few active continental rifts on the Earth today. Research to better understand rifting mechanisms and rift evolution is of great interest because rifts are natural laboratories for understanding how continents break up. Furthermore, rifts result in the accumulation of thick sediments with the potential to form both hydrocarbon resources and rich fossil archives of past ecosystems and climates. The break-up of lithosphere also leads to significant disturbances of the Earth's surface, and consequently rift regions are regarded as geologic hazards, involving large magnitude earthquakes, volcanic eruptions, debris flows, and more. In an effort to elucidate some of the complexities of the active East African Rift System, this research has focused on a lesser-studied segment of the western branch of the East African Rift System, the Rukwa Rift Basin, located in southwestern Tanzania. Developed within the Paleoproterozoic Ubendian orogenic belt between the margins of Archean cratons, the Rukwa Rift Basin is unique because it preserves one of the thickest (~9-11 km) and best-exposed sedimentary sequences in East Africa, containing sedimentary units deposited from the Permian – Recent times, including a rare window into the late Oligocene and late Miocene continental records that are not exposed anywhere else in subequatorial Africa.

The common objective of the studies presented here was to decipher how a sedimentary basin within a continental rift zone records the complex relationships between the generation of accommodation space, uplift, volcanism, faulting, and sediment drainage and depositional patterns in response to rifting. Previous work on the rift flanks, volcanic rocks, and stratigraphy provided only a limited view into this important basin, and so an integrated approach to basin analysis was devised in order to understand the above associations via a sedimentary perspective. U-Pb geochronology has been combined with (U-Th)/He and fission track low-temperature thermochronology and applied to detrital zircons and apatites from the sedimentary sequences of the Rukwa Rift. U-Pb dating of newly discovered tuffs and detrital zircons from well cuttings revealed that after initial rifting in the late Oligocene, renewed volcanism and sediment accumulation began again by at least 8.7 Ma in the Rukwa Rift Basin. Provenance studies of the Lake Beds succession that contains these late Miocene tuffs reveal that the Rukwa Rift Basin was internally draining through to at least the Pliocene, implying that rift flank and volcanic topography impeded drainage inlets and outlets.

A new approach for utilizing hydrocarbon exploration well cuttings for detrital zircon analysis, specifically to obtain maximum depositional age control, was developed as

a part of this study on the Lake Beds, and has the potential to become a powerful new tool for stratigraphic dating and correlation for hydrocarbon exploration. Detrital low-temperature thermochronology data suggests that there was minimal uplift associated with either pulse of rifting and sedimentation (at ~25 and ~9 Ma) recorded in the Rukwa Rift Basin, and therefore much of the high topography and incised landscape observed today in this part of eastern Africa likely developed during the late Pliocene to Quaternary. Multiple populations of cooling ages spanning the Paleoproterozic to Late Cretaceous obtained from detrital zircon and apatite low-temperature thermochronology suggests that the Rukwa Rift and vicinity was subject to repeated far-field tectonic stresses.

The sedimentary record in the Rukwa Rift also preserves a rare archive of seismicity, in the form of soft-sediment deformation features (seismites). This research has documented several new seismite morphologies, expanding the database of seismogenic sedimentary structures, which is important for future seismic hazard preparations and predictions. Extensive seismites from the Late Quaternary to Recent upper Lake Beds have been documented, including a decameter-scale clastic 'megablock complex' correlative to similarly sized recumbent folds over 35 km away; evidence for Late Pleistocene large magnitude earthquakes in the Rukwa Rift Basin. In addition, new seismogenic sedimentary structures from the Cretaceous Namba Member of the Galula Formation, termed 'balloon-shaped inflation structures', formed primarily by gas-escape as opposed to the more commonly called upon mechanism, water-escape. This discovery not only has shed light on the longevity of seismic activity within the Rukwa Rift Basin, but also serves as an important discovery for the re-examination of the classification scheme of soft-sediment deformation structures.

The results of combined zircon and apatite detrital- and tephro-geochronology and thermochronology have been integrated with sedimentology-based paleoseismic investigations to provide new insights into the history of the Rukwa Rift Basin, which has important implications for documenting the evolutionary record and for documenting previously unknown seismic activity. Constraining the magnitude and timing of rifting events, magmatism, faulting, and uplift is critical because these processes created and fundamentally changed the landscape, redirected drainages, affected local climate, and more, all of which have major implications for the flora and fauna, including hominins, that evolved along the East African Rift valleys.

Table of Contents

.

Contents of Digital Appendices

List of Tables

List of Figures

Chapter 4

Introduction to Thesis

The East African Rift System (EARS) is considered Earth's archetypal example of an active continental rift, and consequently, it has attracted considerable scientific interest from members across the geoscience community. The rift system is composed of many different active rift segments that align over several thousands of kilometers, forming the eastern and western rift branches. Over a century of research in the rift has focused on the various segments to better comprehend not only rifting processes and the origin of the East African Rift System, but also to understand fundamental aspects of plate tectonics and continental breakup throughout Earth's history. Indeed, the East African Rift is a natural laboratory for investigating how plate tectonics have shaped, and will continue to drive, Earth's geologic, topographic, and biologic evolution. Extensive work with geophysical data such as seismic profiles and well data from hydrocarbon exploration, structural and volcanic studies, and more, have focused on the rift's deep origins, fueling a long-standing debate on the influence of mantle plume and tectonic plate movements on the rift's behavior (Ebinger and Sleep, 1998; Pik, 2011; Koptev et al., 2015). At the other end of the spectrum, the East African Rift is also known as the 'cradle of humankind', and much focus has been directed towards understanding the relationship between rifting (and associated landscape change) and vertebrate evolution— particularly, human evolution (Trauth et al., 2007; Passey et al., 2010; Stevens et al., 2013).

The thick sedimentary record preserved in the Rukwa Rift Basin in Tanzania, a segment of the western branch of the East African Rift System, is the focus of this project, and represents one of the best places in eastern Africa to investigate Paleogene-Quaternary tectonic, sedimentologic and faunal evolution (Fig. 1). My thesis is divided into two distinct, but interrelated components, focused on: 1) investigating the evidence and implications of paleoseismicity in the rift; and 2) using sedimentary provenance analysis to assess the timing and magnitude of critical landscape changes in the rift, and in eastern Africa more generally. This PhD thesis aims to contribute to answering questions about both modern hazards for people living in and around the rift and the tectonic evolution of this portion of the western branch of the rift system, in an effort to understand the tectonic events that controlled sediment deposition and rift flank uplift. The data sets that have been generated and interpreted create a foundation for describing the interplay between landscape change, environmental change, and vertebrate evolution in this part of eastern Africa. The studies presented here have approached these questions from the often-overlooked perspective of the sedimentary record, as preserved in the Rukwa Rift Basin, which contains the thickest continental sedimentary sequence along the East African Rift (~9-11 km).

The first distinct aspect of this thesis deals with the ever-present consequence of active

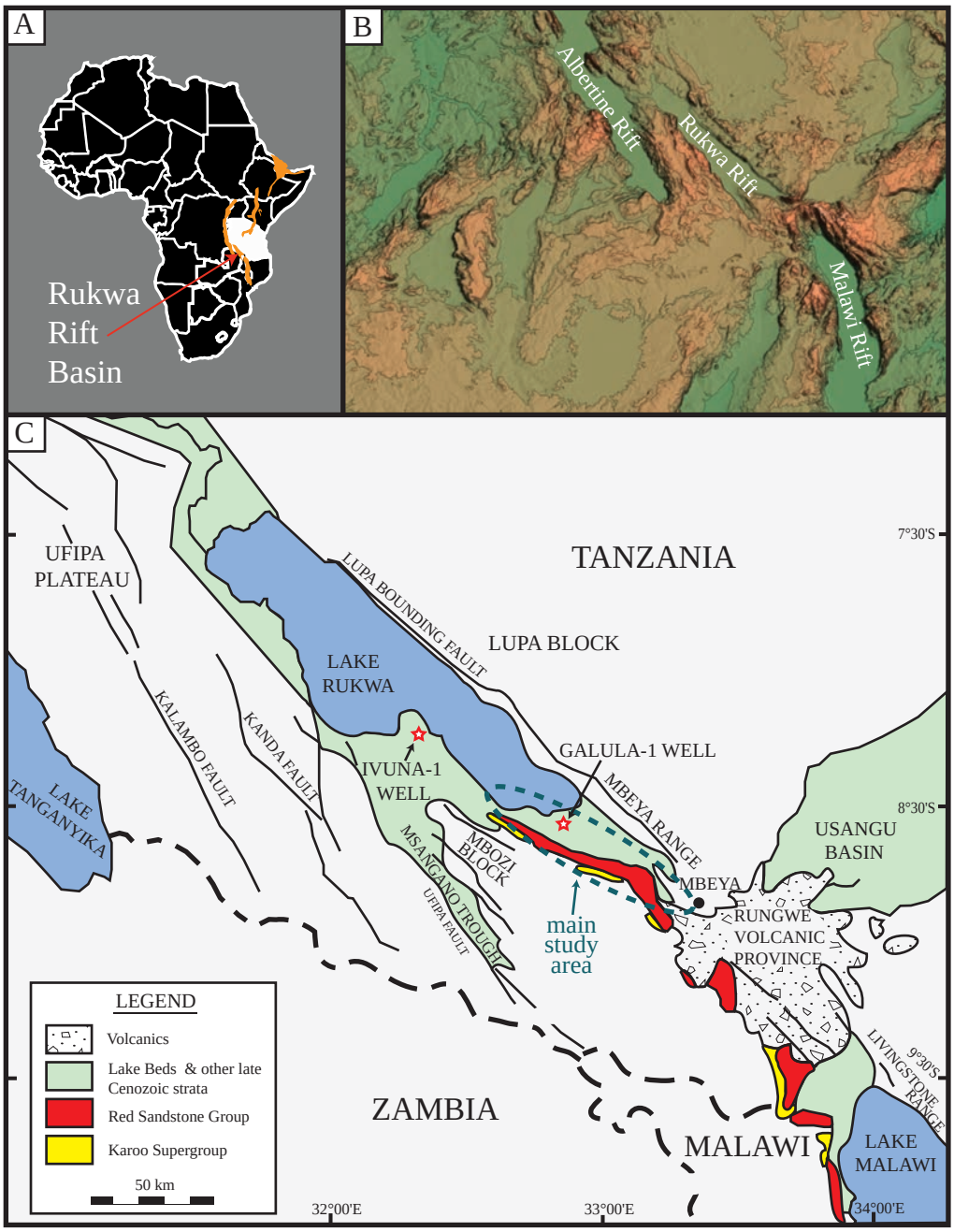

Fig. 1. Maps showing the location of the Rukwa Rift Basin and the study and sampling sites. A. Generalized map of Africa highlighting the East African Rift System in orange. Tanzania is colored in white. B. DEM map modified from the Arc-Minute Global Relief Model (Amante and Eakins, 2009) of the southern western branch of the East African Rift System. C. Geologic map of the Rukwa Rift Basin showing major tectonic elements and the distribution of Phanerozoic sedimentary deposits (modified from Roberts et al., 2010).

rifting: seismicity. Since seismicity can have significant impacts in sedimentary settings both during and after deposition, a crucial part of this thesis focuses on examining records and consequences of paleoseismicity in the Rukwa Rift Basin. New seismogenic sedimentary structures (seismites) are described from Cretaceous and Pleistocene strata. Through careful description and understanding of the mechanisms that generated these seismites, seismic activity can be reconstructed through time and tell us about the frequency and magnitude of movements along the rift faults. New sedimentary structures in seismites

described for the first time here from the Cretaceous Galula Formation and from the Pleistocene Lake Beds expand our capacity for recognizing seismogenic soft-sediment deformation features in the rock record. Giant seismites correlated over 35 km + and dated to the same time period are described herein from the upper Lake Beds succession (Chapter One; Hilbert-Wolf and Roberts, 2015), and suggest that the Rukwa Rift region experienced repeated, large-magnitude earthquakes that significantly disrupted the paleosurface in the very recent geologic past. Moreover, seismites in the Rukwa Rift are also documented in strata as old as Cretaceous (Chapter Two), including novel expressions of gas-generated soft-sediment deformation in near-surface deposits, which highlight both the complexity and recurrence of seismic deformation in the rift.

The Rukwa Rift Basin lies between the Tanganyika and Malawi rift segments in southwestern Tanzania (Fig. 1). Superimposed on a structurally weakened, Paleoproterozoic shear belt, the Rukwa Rift has been tectonically reactivated numerous times from the late Paleozoic onwards (Delvaux et al., 2012). Since tectonic events (dominantly extensional) in the East African Rift System are marked by sedimentation and magmatism, the age and provenance of both detrital and volcanic tuff-derived minerals from the Rukwa Rift Basin strata provide important and reliable insight into the timing of rift development, volcanism and erosion linked to uplift and landscape change in the western branch throughout the evolution of the rift. As such, the second major component of this thesis involves the study of the sedimentary record of the Rukwa Rift Basin. Radioisotopic dating of newly discovered volcanic tuffs intercalated in the rift sediments demonstrates that after initial rifting between 26 and 24 Ma, renewed volcanism and sediment accumulation began again by at least 8.7 Ma in the Rukwa Rift Basin, suggesting a long hiatus before the second phase of rifting began in the late Miocene. Chapters Three and Four of this thesis integrate radioisotopic dating of tuffs for age control with detrital geochronology and thermochronology to illuminate the relative timing and magnitude of movement and sediment contribution from the rift flanks and surrounding areas during the Miocene to Recent. One of the ultimate aims of this work is to constrain the time of formation (uplift) and development of the present anomalously high topography of eastern Africa, which remains a topic of intense debate (Nyblade and Robinson, 1994; Pik et al., 2008; Moucha and Forte, 2011). For example, was the topography established by 26-24 Ma as a product of the first phase of rifting, or sometime during the second phase of rifting from ~8.7-3 Ma, or was the topographic development entirely restricted to the latest phases of rifting during the Quaternary? Provenance investigation helps us to understand sediment routing systems, indicating from where and by what means sediments that filled the basin were sourced, and therefore revealing the behavior of the Rukwa Rift hinterlands during tectonic episodes. By constraining the relationship and timing between rifting events, sedimentation, and uplift in the western branch of the East African Rift System, we hope to better understand

the influence of dynamic landscapes, volcanism, and seismicity on the development of modern African flora and fauna, including humans, in East Africa (Sepulchre et al., 2006; Spiegel et al., 2007).

This research project has been conducted in concert with paleontologists in the Rukwa Rift region, as part of a joint research effort known as the "Rukwa Rift Basin Project", which is focused on developing late Mesozoic-Quaternary records of faunal evolution in this portion of the rift (e.g., Krause et al., 2003; Stevens et al., 2005; O'Connor et al., 2006; O'Connor et al., 2010; Roberts et al., 2010; Roberts et al., 2012; Stevens et al., 2013; Gorscak et al., 2014; McCartney et al., 2014; Roberts et al., 2016). In the past decade sedimentological, paleontological, and geochronological studies have documented a complex, long-lived history for the western branch of the EARS, extending the initiation of the Rukwa Rift Basin back to 25 Ma (Fig. 2; Roberts et al., 2012; Stevens et al., 2013). Nearly 14 years of exploration in the upper Oligocene Nsungwe Formation (~25 Ma) in the Rukwa Rift Basin has resulted in the recovery of the only known continental Oligocene ecosystem from subequatorial Africa, including fossil evidence for the earliest divergence of Old World monkeys and apes (Stevens et al., 2013), the oldest venomous elapid snake from mainland Africa (McCartney et al., 2014), the earliest evidence of the endemic frog family Ptychadenidae (Blackburn et al., 2015), and an array of other invertebrate and vertebrate groups. The Nsungwe Formation is significant in that it captures the Paleogene-Neogene transition, when major tectonic and environmental changes drastically affected the landscape, climate and biotas. Stratigraphically above the Nsungwe Formation lies the Lake Beds succession (Fig. 2), the least studied stratigraphic interval in the rift. Our work in this unit has resulted in the discovery of multiple, previously unrecognized stratigraphic subdivisions (i.e., new formations) within the Lake Beds and the discovery of an entirely new and previously unknown Mio-Pliocene fossil fauna from this portion of the East African Rift System. Among the fossil discoveries are the skulls of a potentially new species of Hippopotamidae and of a large crocodyliform, both recovered from these strata. This thesis provides geologic context for this important, new vertebrate fauna, presenting new data from sedimentologic, geochronologic, and thermochronologic studies to understand this ancient ecosystem and obtain a rare glimpse into an under-sampled region and time period in Africa's history. One of the key, unanswered questions of East African landscape evolution is whether significant uplift accompanied stages of basin development. We test this question using (U-Th)/He and fission track dating of fossiliferous sediments.

In addition, chronologies of rifting and uplift in combination with sedimentary provenance have significant implications for modeling thermal and burial history of strata, critical for establishing the probability of working hydrocarbon systems in this portion of the rift. The East African Rift System is considered to be one of the next hydrocarbon frontiers, and

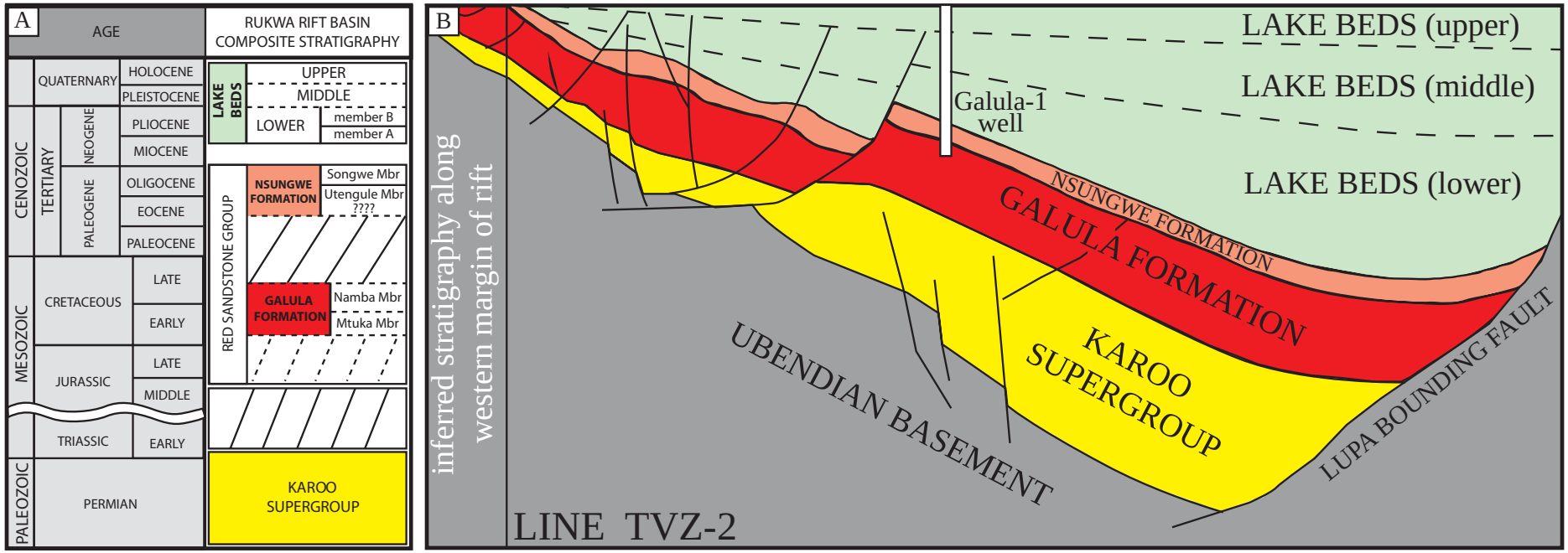

Fig. 2. A. Stratigraphy and nomenclature for stratigraphic sequences in the Rukwa Rift Basin. Note that the nomenclature for the Lake Beds succession is informal. B. Cross section through the Rukwa Rift Basin oriented perpendicular to the rift axis (SW to NE) near the Galula-1 well. Interpretation is based on seismic line TVZ-2 (Tanzanian Petroleum Development Corporation, Dar es Saalam).

assessing essential elements of the petroleum system, such as basin structure and thermal history, hinges on the accurate dating of sedimentary successions and understanding the relationship between key events such as rift lake development, volcanism, and uplift, which all have a major impact on hydrocarbon prospectivity. The application of U-Pb detrital zircon geochronology for constraining maximum depositional ages through hydrocarbon exploration wells using drill cuttings is demonstrated here and proposed as a complementary or alternative dating technique to more traditional biostratigraphy in basin analysis.

Together, the four individual studies presented in this thesis provide new insights into the history of the Rukwa Rift Basin and serve as a baseline for considering future earthquake-related hazards in the area. The aim of this thesis was to investigate the severely understudied sedimentary record of this portion and time period of eastern Africa and use these findings to refine our understanding of the tectonic, sedimentary, and evolutionary history of a critical segment of the western branch of the East African Rift System.

Thesis introduction references:

Amante, C. and Eakins, B.W., 2009, ETOPO1 1 Arc-Minute Global Relief Model: Procedures, Data Sources and Analysis: NOAA Technical Memorandum NESDIS NGDC-24, National Geophysical Data Center, NOAA.

Blackburn, D.C., Roberts, E.M., and Stevens, N.J., 2015, The earliest record of the endemic African frog family Ptychadenidae from the Oligocene Nsungwe Formation of Tanzania: Journal of Vertebrate Paleontology, v. 35, doi 10.1080/02724634.2014.907174.

Delvaux, D., Kervyn, F., Macheyeki, A.S., Temu, E.B., 2012, Geodynamic significance of the TRM segment in the East African Rift (W-Tanzania): Active tectonics and paleostress in the Ufipa plateau and Rukwa basin: Journal of Structural Geology, v. 37, p. 161-180.

Ebinger, C.J., and Sleep, N., 1998, Cenozoic magmatism throughout East Africa resulting from impact of a single plume: Nature, v. 395, p. 788-791.

Gorscak, E., O'Connor, P.M., Stevens, N.J., and Roberts, E.M., 2014, The basal titanosaurian Rukwatitan bisepultus (Dinosauria, Sauropoda) from the middle Cretaceous Galula Formation, Rukwa Rift Basin, southwestern Tanzania: Journal of Vertebrate Paleontology, v. 34, p. 1133-1154, doi 10.1080/02724634.2014.845568.

Hilbert-Wolf, H.L., and E.M. Roberts, 2015, Giant seismites and megablock uplift in the East African Rift: Evidence for Late Pleistocene large magnitude earthquakes: PLOS One, doi 10.1371/journal.pone.0129051.

Koptev, A., Calais, E., Burov, E., Leroy, S., and Gerya, T., 2015, Dual continental rift systems generated by plume-lithosphere interaction: Nature Geoscience, v. 8, p. 388-

392, doi 10.1038/ngeo2401.

Krause, D.W., Gottfried, M.D., O'Connor, P.M., and Roberts, E.M., 2003, A Cretaceous mammal from Tanzania: Acta Palaeontologica Polonica, v. 48, p. 321-330.

McCartney, J.A., Stevens, N.J., and O'Connor, P.M., 2014, The earliest Colubroid-dominated snake fauna from Africa: Perspectives from the Late Oligocene Nsungwe Formation of southwestern Tanzania: PLoS ONE, doi 10.1371/journal.pone.0090415.

Moucha, R., and Forte, A.M., 2011, Changes in African topography driven by mantle convection: Nature Geoscience, v. 4, p. 707-712.

Nyblade, A., and Robinson, S., 1994, The African Superswell: Geophysical Research Letters, v. 21, p. 765-768.

O'Connor, P.M., Gottfried, M.D., Stevens, N.J., Roberts, E.M., Ngasala, S., Kapilima, S., and Chami, R., 2006, A new vertebrate fauna from the Cretaceous Red Sandstone Group, Rukwa Rift Basin, southwestern Tanzania: Journal of African Earth Sciences, v. 44, p. 277-288.

O'Connor, P.M., Sertich, J.J.W., Stevens, N.J., Roberts, E.M., Gottfried, M.D., Hieronymus, T.L., Jinnah, Z.A., Ridgely, R., Ngasala, S.E., and Temba, J., 2010, The evolution of mammal-like crocodyliforms in the Cretaceous period of Gondwana: Nature, v. 466, p. 748-751, doi 10.1038/nature09061.

Passey, B.H., Levin, N.E., Cerling, T.E., Brown, F.H., and Eiler, J.M., 2010, High-temperature environments of human evolution in East Africa based on bond ordering in paleosol carbonates: Proceedings of the National Academy of Sciences USA, v. 107, p. 11245-11249, doi 10.1073/pnas.1001824107.

Pik, R., 2011, East Africa on the rise: Nature Geoscience, v. 4, p. 660-661.

Roberts, E.M., O'Connor, P.M., Stevens, N.J., Gottfried, M.D., Jinnah, Z.A., Ngasala, S., Choh, A.M., and Armstrong, A., 2010, Sedimentology and depositional environments of the Red Sandstone Group, Rukwa Rift Basin, southwestern Tanzania: New insight into Cretaceous and Paleogene terrestrial ecosystems and tectonics in sub-equatorial Africa: Journal of African Earth Science, v. 57, p. 179-212.

Roberts, E.M., Stevens, N.J., O'Connor, P.M., Dirks, P.H.G.M., Gottfried, M.D., Clyde, W.C., Armstrong, R.A., Kemp, A.I.S., and Hemming, S., 2012, Initiation of the western branch of the East African Rift coeval with the eastern branch: Nature Geoscience, v. 5, doi 10.1038/NGEO1432.

Roberts, E.M., Todd, C.N., Aanen, D.K., Nobre, T., Hilbert-Wolf, H.L., O'Connor, P.M., Tapanila, L., Mtelela, C., and Stevens, N.J., 2016, Oligocene termite nests with *in situ* fungus gardens from the Rukwa Rift Basin, Tanzania, support a Paleogene African origin for insect agriculture: PLoS ONE, doi 10.1371/journal.pone.0156847.

Sepulchre, P., Ramstein, G., Fluteau, F., Schuster, M., Tiercelin, J.-J., and Brunet, M., 2006, Tectonic uplift and eastern African aridification: Science, v. 313, p. 1419, doi 10.1126/science.1129158.

Spiegel, C., Kohn, B.P., Belton, D.X., and Gleadow, A.J.W., 2007, Morphotectonic evolution of the central Kenya rift flanks: Implications for late Cenozoic environmental change in East Africa: Geology, v. 35, p. 427-430.

Stevens, N.J., O'Connor, P.M., Gottfried, M.D., Roberts, E.M., and Ngasala, S., 2005, An anthropoid primate humerus from the Rukwa Rift Basin, Paleogene of southwestern Tanzania: Journal of Vertebrate Paleontology, v. 25, p. 986-989.

Stevens, N.J., Seiffert, E.R., O'Connor, P.M., Roberts, E.M., Schmitz, M.D., Krause, C., Gorscak, E., Ngasala, S., Hieronymus, T.L., and Temu, J., 2013, Palaeontological evidence for an Oligocene divergence between Old World monkeys and apes: Nature, v. 497, p. 611-614.

Trauth, M.H., Maslin, M.A., Deino, A.L., Strecker, M.R., Bergner, A.G.N., and Dühnforth, M., 2007, High- and low-latitude forcing of Plio-Pleistocene East African climate and human evolution: Journal of Human Evolution, v. 53, p. 475-486, doi 10.1016/j.jhevol.2006.12.009.

Thesis Structure

It is intended that the entire contents of this thesis will be published in internationally recognised, peer reviewed science journals. At the time of submission of this thesis, Chapter One is published in PLoS ONE (Hilbert-Wolf and Roberts, 2015; see Appendix 1); Chapter Two is published in Sedimentary Geology (Hilbert-Wolf et al., 2016; see Appendix 3); and Chapter Three has been accepted for publication in The AAPG Bulletin. Chapter Four is being prepared for submission in late 2016. Some of the outcomes of this project have also been published as part of co-authored papers in both Chemical Geology (Spandler et al., 2016; see Appendix 2) and PLoS ONE (Roberts et al., 2016; see Appendix 4). In addition to what is presented in this thesis, the author (Hilbert-Wolf) has contributed to other Rukwa Rift Basin Project studies ranging in focus from sedimentology and stratigraphy, to petroleum prospectivity, and paleontology, some of which at this time have resulted in co-authored published reports (e.g., Roberts et al., 2014 and Roberts et al., 2015) and others that will be forthcoming papers (e.g., Mtelela et al., in preparation).

This thesis consists of four chapters, each of which represents an independent body of work and is presented in a format resembling a published manuscript. Hence, the structure of this thesis has unavoidably led to some repetition of sections, such as the geological setting and methodologies. However, it should be noted that the analytical methods applied vary from chapter to chapter, and the resulting conclusions drawn from each piece of work are unique. A single reference list follows "Chapter Five: Thesis Summary and Future Work" at the end of this work.

Although each chapter constitutes a stand-alone piece of work; together, all of the chapters are complementary and are related to the central theme of this thesis: understanding the timing of rifting and seismicity, volcanism, and uplift in the Rukwa Rift Basin of the East African Rift System. The focus of this research particularly on detrital minerals and on seismicity recorded in the sedimentary record affords us a unique record of rift behavior, as recorded by the sedimentary fill in a rift basin, instead of that recorded by the more-studied rift flanks. Chapters One and Two focus on paleoseismicity, describing new sedimentary structures in seismites and revealing for the first time the Rukwa Rift's capacity for large-scale, frequent earthquakes in the geologic past, expanding the earthquake record much beyond the instrumental records for this area from the early 1900s. Chapter One presents two newly discovered decameter-scale seismites, dated to ~28,000 years BP, from alluvial and lacustrine strata of the Lake Beds succession, including a clastic 'megablock complex' in shallow subsurface sediments near the regional capital of Mbeya. This work serves to better understand how seismicity deforms near-surface sediments, critical for predicting and preparing for modern seismic hazards in populated rift regions. Chapter Two is focused on newly recognized sedimentary structures in seismites from the Cretaceous Galula Formation, termed "balloon-shaped inflation structures" and "surface fractures with linked sandstone splays". These structures are exceptional because they show evidence for formation via gas-escape, in addition to the typically called upon mechanism of water-escape during seismic shaking. This documentation is important because it emphasizes the need for re-examination of the classification scheme that is used for soft-sediment deformation structures. This scheme is currently focused on the concept that fluid-escape is responsible for generating such structures, yet this study demonstrates that secondary sedimentary structures may also be associated with gas-escape. The documentation of these remarkable examples of seismite expands the database of seismogenic sedimentary structures.

The Cretaceous Galula Formation and the Oligocene Nsungwe Formation have been studied in some detail in the past, so a major focal point of this thesis was to investigate the late Miocene-Recent Lake Beds succession, not only to illuminate the most recent stage of rifting in the western branch, but also to investigate this succession for hydrocarbon prospectivity. In Chapter Three the first radioisotopic ages from both detrital zircon U-Pb maximum depositional ages and U-Pb dated tuffs are presented, constraining the initiation of the latest phase of basin formation, volcanism and sedimentation to ~8.7 Ma. This chapter also outlines an innovative outcome of this thesis: successful application of U-Pb detrital zircon geochronology to small-volume drill cuttings from hydrocarbon exploration wells as an alternative and complement to traditional biostratigraphic dating. We demonstrate the effectiveness of this technique in the Rukwa Rift Basin and make suggestions for appropriate methodology and applications to other hydrocarbon prospective continental

strata that lack age-diagnostic fossil material.

In order to detect rifting events and uplift, a suite of geochronologic and thermochronologic methodologies were applied to Cretaceous, Oligocene, and Miocene-Recent successions in the Rukwa Rift Basin. This "Sedimentary Triple Dating" approach to basin analysis constitutes Chapter Four of this thesis. Chapter Four presents a detailed provenance study focused on the origins of the Lake Beds sediments, the uppermost sedimentary package in the Rukwa Rift Basin, which has been radioisotopically dated for the first time here. Chapter Four also contains the results of detrital zircon and apatite fission track and (U-Th)/He thermochronology, spanning Cretaceous – Pliocene sediments from the rift. It is here that we detect that the Rukwa Rift has been an internally draining basin for most of it's history, and has not undergone major, rapid uplift events associated with the initiation of rifting or volcanism in the area. This chapter integrates geochronology, thermochronology, and provenance analysis to relate the initiation of rifting events to regional dynamic uplift, and interpret the far-reaching climatic and evolutionary consequences of fluctuating rift flank topography.

Thesis structure references:

Hilbert-Wolf, H.L., and Roberts, E.M., 2015, Giant seismites and megablock uplift in the East African Rift: Evidence for Late Pleistocene large magnitude earthquakes: PLoS ONE, doi 10.1371/journal.pone.0129051.

Hilbert-Wolf, H.L., Roberts, E.M., and Simpson, E.L., 2016, New sedimentary structures in seismites from SW Tanzania: Evaluating gas- vs. water-escape mechanisms of soft-sediment deformation: Sedimentary Geology, doi 10.1016/j.sedgeo.2016.03.011.

Mtelela, C., Roberts, E.M., **Hilbert-Wolf, H.L.**, Downie, B., Hendrix, M.S., O'Connor, P.M., and Stevens, N.J., in preparation, Sedimentology and paleoenvironments of a richly fossiliferous late Neogene-Quaternary sedimentary succession in the Rukwa Rift Basin, Tanzania: Journal of African Earth Sciences.

Roberts, E., **Hilbert-Wolf, H.**, and Mtelela, C., 2014, LA-ICPMS U-Pb zircon geochronology of ten detrital zircon samples from the Galula-1 well cuttings: technical report for Heritage Oil Ltd.

Roberts, E., Agyemang, P.O., and **Hilbert-Wolf, H.L.**, 2015, Combined U-Pb detrital zircon/titanite geochronology on volcaniclastic sandstone and 40Ar/39Ar sanidine geochronology on volcanic tuff from the GEKL-001 borehole, Kyela, Tanzania for age and sedimentary provenance analysis: technical report for Heritage Oil Ltd.

Roberts, E., Todd, C.N., Aanen, D.K., Nobre, T., **Hilbert-Wolf, H.L.**, O'Connor, P.M., Tapanila, L., Mtelela, C., and Stevens, N.J., 2016, Oligocene termite nests with *in*

situ fungus gardens from the Rukwa Rift Basin, Tanzania, support a Paleogene African origin for insect agriculture: PLoS ONE, doi 10.1371/journal.pone.0156847.

Spandler, C., Hammerli, J., Sha, P., **Hilbert-Wolf, H.**, Hu, Y., Roberts, E., and Schmitz, M., 2016, MKED1: A new titanite standard for in situ microanalysis of Sm-Nd isotopes and U-Pb geochronology: Chemical Geology, doi 10.1016/j.chemgeo.2016.01.002.

Chapter One

Giant Seismites and Megablock Uplift in the East African Rift: Evidence for Late Pleistocene Large Magnitude Earthquakes

Published in *PLoS ONE*

Abstract

In lieu of comprehensive instrumental seismic monitoring, short historical records, and limited fault trench investigations for many seismically active areas, the sedimentary record provides important archives of seismicity in the form of preserved horizons of soft-sediment deformation features, termed seismites. Here we report on extensive seismites in the Late Quaternary-Recent (~ 28,000 years BP) alluvial and lacustrine strata of the Rukwa Rift Basin, a segment of the Western Branch of the East African Rift System. We document examples of the most highly deformed sediments in shallow, subsurface strata close to the regional capital of Mbeya, Tanzania. This includes a remarkable, clastic 'megablock complex' that preserves remobilized sediment below vertically displaced blocks of intact strata (megablocks), some in excess of 20 m-wide. Documentation of these seismites expands the database of seismogenic sedimentary structures, and attests to large magnitude, Late Pleistocene-Recent earthquakes along the Western Branch of the East African Rift System. Understanding how seismicity deforms near-surface sediments is critical for predicting and preparing for modern seismic hazards, especially along the East African Rift and other tectonically active, developing regions.

1. Introduction

Earthquakes not only trigger geohazards such as surface ruptures, tsunamis, and landslides, but are also linked to significant, catastrophic soft-sediment deformation. Despite recent events associated with devastating liquefaction and fluidization of near-surface sediments, such as the 2011 New Zealand and Japan earthquakes and the ongoing Lusi mud eruptions in Indonesia, the dangers to life and infrastructure from soft-sediment deformation are often overlooked. In 1910 7.5 million people lived in Tanzania when the most powerful earthquake in Africa of the twentieth century (Ms 7.4) struck the Lake Rukwa region, collapsing houses, initiating standing waves in nearby water bodies, causing ground deformation, and triggering liquefaction and fluidization of saturated subaerial and submarine deposits (Ambraseys, 1991; Ambraseys and Adams, 1991). By 2050 roughly 138 million people will live in Tanzania (Haub et al., 2012), largely in constructed urban environments. This growth particularly affects the seismically active rift valleys of East Africa, where people concentrate near productive rift lakes and volcanic soils, on substrate that is susceptible to liquefaction and seismite generation and preservation (Rodríguez-Pascua et al., 2000).

A combination of approaches to investigate prehistoric seismicity, such as archaeoseismic research, seismic-stratigraphic correlation of event horizons, and characterization of soft-sediment deformation features, are vital for constraining earthquake recurrence intervals and magnitude (Obermeier, 1996; Rodríguez-Pascua et al., 2000). In Africa, historical records alone can limit the recognition of long-term earthquake trends due to deficiencies in station numbers, global station distribution, epicentral accuracy, and short instrumental coverage period of only the last ~100 years. Given the potential societal impacts, understanding sediment responses to earthquake activity is an underappreciated aspect of seismic hazard evaluation. Additionally, the ability to recognize and document large-scale soft-sediment deformation and injectite features in outcrop is increasingly advantageous in light of heightened interest in the association of large-scale sandstone intrusions and hydrocarbons.

2. Seismicity in the Rukwa Rift

The Rukwa Rift Basin is a nexus of tectonic activity (Fig. 1), and with one of the thickest continental sedimentary successions in Africa, it records repeated rifting, volcanism, and sedimentation from the Permian to Recent (Delvaux et al., 2012; Roberts et al., 2012). At its southern extremity the Rukwa Rift Basin splits into the Msangano and Songwe (study area) valleys (Fig. 1). Over the last century, the Songwe Valley has been characterized by particularly high micro-seismicity, moderate and strong earthquakes ($5 \leq M \leq 7.4$),

and significant Holocene fault movements (Camelbeeck and Iranga, 1996; Vittori et al., 1997; Kervyn et al., 2006; Delvaux et al., 2012). Related to Miocene-Recent rifting, the Lake Beds Succession (LBS) is the youngest deposit in the Rukwa Rift Basin, comprised of semi-consolidated volcaniclastic siltstones, mudstones, sandstones and conglomerates deposited by fluvial deltaic, alluvial, and lacustrine processes.

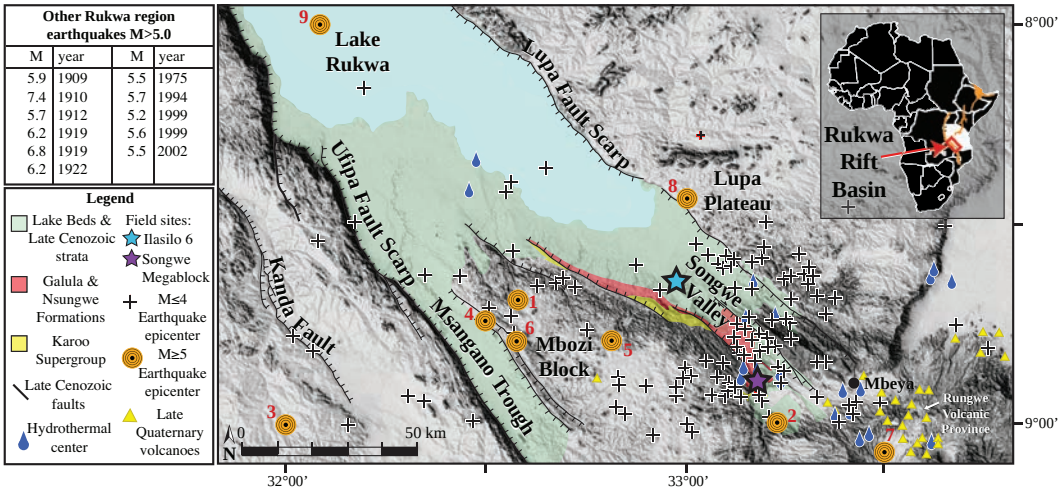

Fig 1. DEM map displaying neotectonic elements of the Songwe Valley, Rukwa Rift Basin (Delvaux et al., 1993). Camelbeeck and Iranga's seismic network recorded 199 microearthquake ($M \leq 4$) events in the Rukwa Rift Basin from 1992-1994 (Camelbeeck and Iranga, 1996). A sample of these epicenters is plotted on the map (+ symbols) to show the general distribution of activity, highlighting the Songwe Valley as the most seismically active area [8]. Historical earthquake epicenters in the mapped region with $M \geq 5$ include: 1 —1968, M 5.0; 2 —1972, M 5.0; 3 —1979, M 5.3; 4 —1984, M 5.4; 5 —1985, M 5.1; 6 —1988, M 5.0; 7 —1994, M 5.0; 8 —2012, M 5.0; 9 —2013, M 5.0. Other comparable earthquakes that plot just off the map are listed in the table (Ambraseys and Adams, 1991; ISC, 2012; USGS Global Earthquake Catalogue).

Numerous soft-sediment deformation features of possible seismic origin have been identified at a variety of different localities spanning the Paleozoic-Recent sedimentary succession in the Rukwa Rift Basin. Indeed, a number of other workers have noted the presence of such secondary sedimentary features, particularly in the Cretaceous-Paleogene Red Sandstone Group strata, and they have also interpreted a seismic origin for many of these features (Milga, 1994; Roberts et al., 2010; Delvaux et al., 2011). This paper is the first to report soft-sediment deformation features from the Pleistocene-Recent Lake Beds Succession in the rift. We have documented numerous such features, of centimeter- to dekameter-scale and varying character, in the Lake Beds Succession at many stratigraphic levels and at numerous localities in the southern portion of the Rukwa Rift where we have concentrated our research. Here we focus on two particularly spectacular occurrences of soft-sediment deformation exposed at two, stratigraphically correlative outcrop localities ~35 km apart (Ilasilo 6: 502917 E 9044472 N; and the Songwe Megablock Site: 522904 E 9015130 N; zone 36, ARC 1960 datum; Fig. 1).

3. Methods

3.1. Permits

The Tanzanian Commission for Science and Technology and the Tanzanian Antiquities Unit granted us permission to carry out our field studies and to take samples. Our field studies did not involve endangered or protected species.

3.2. Fieldwork and Analyses

Fieldwork was conducted in the southern Rukwa Rift Basin, Tanzania (Fig.1), during the Austral winter, from 2012-2014. Outcrops were evaluated using standard sedimentologic techniques. For example, stratigraphic sections were measured with the aid of a Jacob's staff and Brunton compass.

Data analysis was carried out at James Cook University, Australia. Sediment size and dispersion was measured on a Mastersizer 2000 via laser diffraction, capable of measuring particles of 0.02 – 2000 μm diameter. Five sediment samples were analyzed and corresponding liquefaction potential was modeled from the recorded data and used to create gradation curves. Sediment samples containing fossilized organic material from 1.5 m below the deformed horizon at Ilasilo 6 and in situ fossilized reed fragments from the megablock siltstone unit of the megablock complex at the Songwe Megablock Site were dated using the Accelerator Mass Spectrometry (AMS) method by Beta Analytic Inc. The samples were pretreated with an acid wash, and conventional radiocarbon ages were corrected for total fractionation effects and rounded to the nearest 10 years per conventions of the 1977 International Radiocarbon Conference. Calibrated ages were calculated using the IntCal13 database (Reimer et al., 2013).

4. Large-Scale Soft-Sediment Deformation Features

4.1. Description

4.1.1. Megablock Complex

Here we describe for the first time a 50 m-tall cliff face exposure of a spectacular, large-scale (10 m-tall x 20 m-wide in cross-sectional surface area), soft-sediment deformation feature that we term the 'Songwe Megablock Complex' (Figs. 2 and 3). The Songwe Megablock Site is characterized by an angular unconformity that separates the Upper Pleistocene, upper Lake Beds Succession from underlying, undeformed Cretaceous

sandstones that gently dip consistently across the outcrop (~311°, 14° NE). The base of the Lake Beds Succession consists of an upward fining, polymictic, pebble-cobble orthoconglomerate. This unit preserves weak horizontal bedding, remnant trough cross-bedding, weak pebble imbrication, and no obvious deformation. Above the conglomerate a buttress unconformity separates red, dominantly coarse-grained Lake Beds strata to the south (left of the megablock complex in Fig. 2D) from dominantly fine-grained Lake Beds strata to the north (right of the megablock complex in Figs. 2D and 3), which hosts the megablock complex. The coarse-grained strata is comprised of a basal conglomeratic unit, and overlain by repeated, interbedded sequences of fine-medium sandstone at the base with 1-3 mm pumice clasts, fining upwards into ash-rich siltstone with floating clasts, including ≤ 5 cm metamorphic and caliche pebbles. To the north, the fine-grained units are characterized by finely laminated, tuffaceous siltstone (the strata from which the megablock was derived), and were deposited within an erosionally incised depression that formed along the buttress unconformity surface, against which the fine-grained facies thin. Continuous horizons of thin (~10-20 cm) white cross-bedded ashes are present near the top of the outcrop, along with several massive, color banded, ash-rich siltstone horizons above this (Figs. 2 and 3).

A large-scale, soft-sediment deformation feature dominates the finer-grained Lake Beds Succession facies. Deformation is contained between the buttress unconformity and the top of the modern-day cliff face. A 10 m-tall x 20 m-wide block of intact siltstone from the unit immediately above the basal conglomerate appears to have been uplifted ~10 m. The block is supported by a massive, fine-grained foreign body of tuffaceous material, not correlative with the laminated strata on either side of the soft-sediment deformation. This same ‘parent material’ that supports the megablock extends upwards via irregular dykes that surround the displaced blocks of bedded, cohesive sediment. A 5 cm-wide clastic injection dyke emerges from the top of the basal Lake Beds Succession conglomerate, crosscutting the intrusive sediment and uplifted megablock, where it expands gradually into a “V”-shape, up to 2.5 m in diameter at the top of the outcrop. The lower dyke contains metamorphic cobbles (4–20 cm diameter) from the basal Lake Beds Succession conglomerate and abundant pumice clasts (Fig. 2C). Metamorphic cobbles and 5-25 cm clasts of the megablock unit infill the uppermost “V”-shaped dyke.

4.1.2. Asymmetric Recumbent Folds

Thirty-five km to the northwest of the Songwe Megablock Site, at a locality called Ilasilo 6, dekameter-scale asymmetrical, recumbent folds occur in a 3 m-thick, horizontally bedded, tuffaceous siltstone unit (Figs. 4C and 4D), stratigraphically correlative to the deformed horizon (the megablock complex) at Songwe. The folds are overlain and underlain by undeformed, horizontally bedded, volcaniclastic siltstone units of the same lithology.

The asymmetric, recumbent fold crests are systematically directed to the southwest. The deformed horizon is truncated by the overlying siltstone, cutting off the tops of the folds.

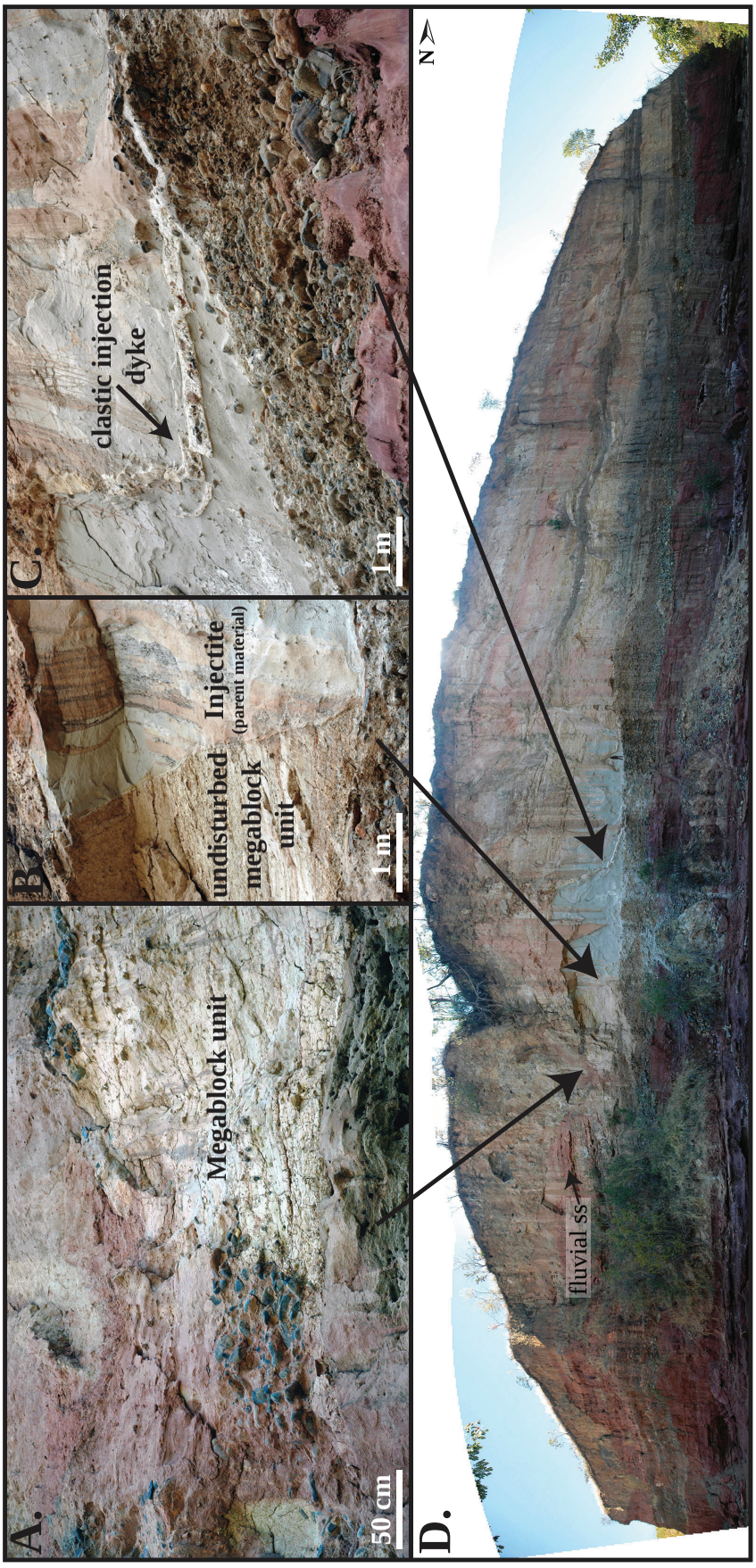

Fig 2. Field photographs of the megablock complex at the Songwe Megablock Site. (A) Megablock unit and offset conglomerate unit. (B) "Blowout" fault bounding the left side of the injectite. (C) Clastic injection dyke emerging from basal LBS conglomerate. Note the pebbles and cobbles entrained in the dyke, as well as the offset dyke segments. (D) Panoramic photograph of injectite complex outcrop, highlighting its position within undeformed, horizontal Lake Beds strata. Person is for scale on the lower right of the injectite.

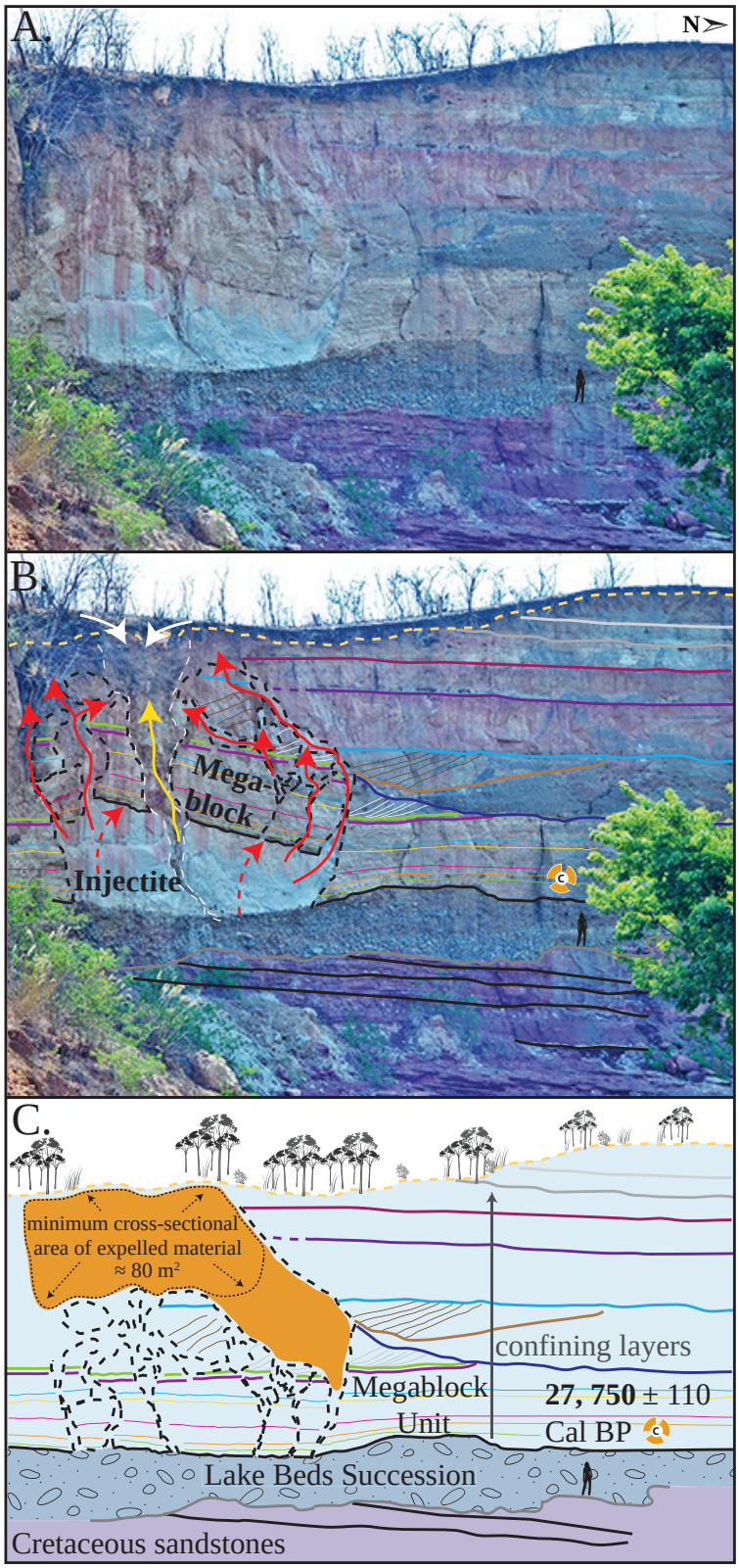

Fig 3. Outcrop exposure of injectite and megablock complex at the Songwe Megablock Site. (A) Photograph of megablock complex outcrop. (B) Trace of intact stratigraphy and displaced megablock. Red arrows indicate flow of injectite material. Yellow arrow indicates path of clastic injection dyke. White arrows represent surface alluvium and clasts of the sidewall infilling the top of the clastic injection dyke. (C) Reconstructed megablock in original stratigraphic position. An estimate is made of the cross-sectional surface area of material ejected onto the surface after formation of injectite and vertical displacement of megablock.

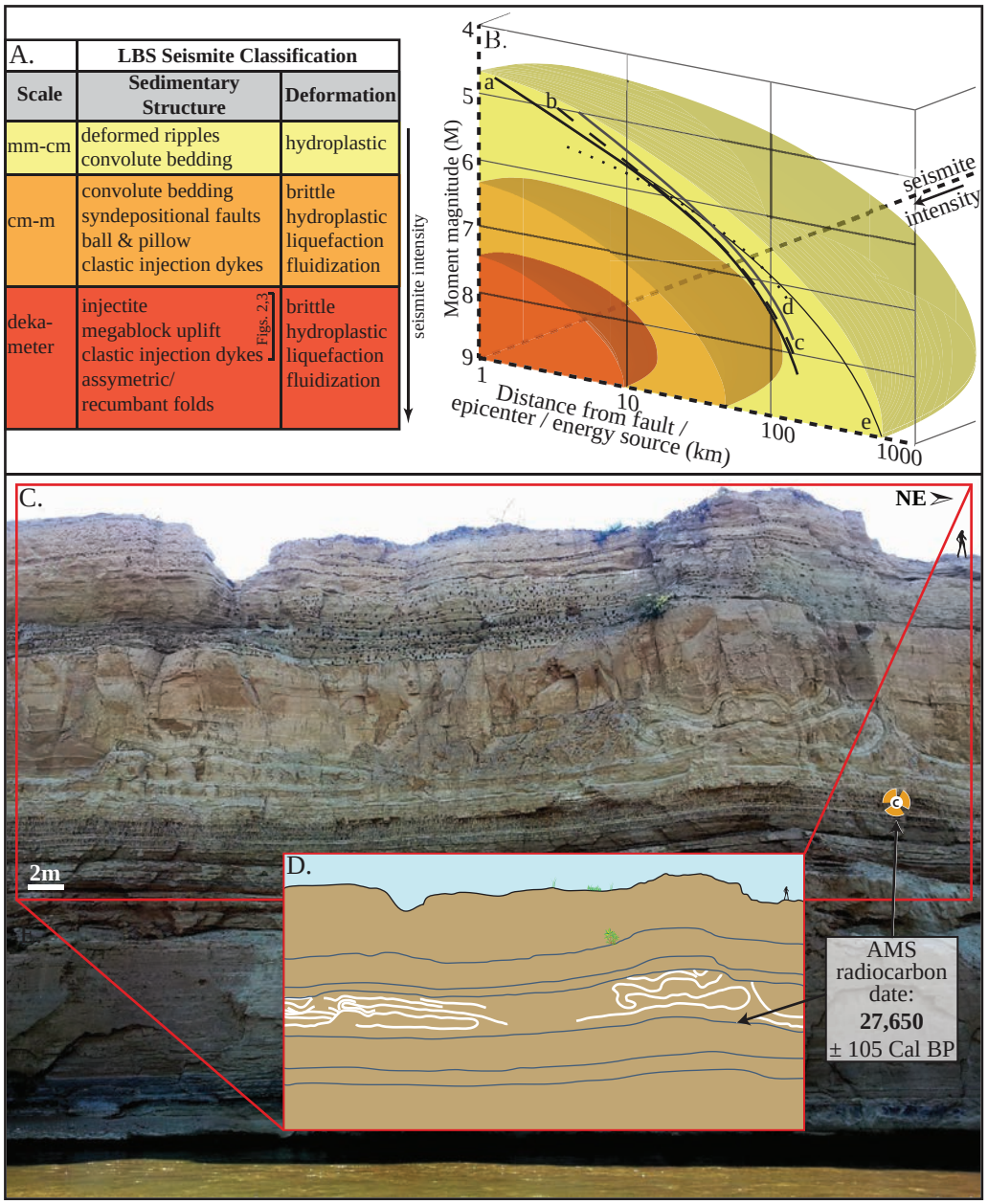

Fig 4. Classification and genetic relationship of liquefaction features in the Songwe Valley. (A) Classification scheme for seismites in the study area (after Lowe, 1975 and Hilbert-Wolf et al., 2009). (B) Model relating qualitative seismite intensity (refer to Fig. 4A) to distribution (distance from fault/epicenter/energy source) and earthquake magnitude. Curve a: upper bound from energy source for worldwide, shallow focus earthquakes (Ambraseys, 1988); curves b-c: bound from fault (Papathanassiou et al., 2005); curve d: bound from fault for earthquakes $5.5 \leq Ms \geq 7.1$ (Papathanassiou et al., 2005); and curve e: bound from epicenter for worldwide, shallow focus earthquakes (Ambraseys, 1988). The seismite intensity scale (Fig. 4A) reported here describes the soft-sediment deformation features recorded from the Lake Beds Succession only; however, the curves reported in part B are global averages. (C) Asymmetric/recumbent folds at Ilasilo 6, illustrated in (D).

4.2. Interpretation of Large-Scale Soft-Sediment Deformation Features

4.2.1. Megablock Complex

The Lake Beds Succession at the Songwe Megablock Site is characterized by older fluvial-dominated facies and younger lacustrine facies, separated by an erosional unconformity. Prior to the deposition of the lacustrine facies preserved on the north end of the outcrop, a portion of the fluvial units was deeply incised by erosional downcutting. Fluvial incision created a topographical depression, into which lacustrine sedimentation (fine-grained, siltstone dominated facies) records the presence of a network of small, isolated, shallow wetland ponds and lakes. This major decrease in grain size, coupled with a dramatic increase in volcaniclastic sediments (Fig. 5) in the lacustrine facies suggests that these units (in which the megablock complex is hosted) were deposited relatively rapidly, preserving reedy plant macrofossils and are associated with a period of intense volcanism and base level rise.

The megablock complex lies on top of the undisturbed, basal Lake Beds Succession conglomerate. This soft-sediment deformation complex displays a unique combination of seismogenically-remobilized sediment coupled with brittle deformation features. It is comprised of (1) an injected body of fluidized volcanic ash that hydraulically displaced (2) an equally sized, semi-consolidated block of intact strata (megablock); both of which were subsequently intruded by (3) a clastic injection dyke (Figs. 2 and 3). The buttress unconformity between the basal conglomerate and sealing siltstone above (unit from which megablock was derived) likely served as an initial conduit for lateral flow of fluidized sediment. The parent unit is not found intact or in its original stratigraphic position anywhere along the exposed cliff face. The injected material is lithologically similar to the megablock unit, so we invoke horizontal flow from a laterally correlative unit as a source for the injected parent ash/water slurry (sensu Rodríguez-Pascua et al., 2000 and Hurst et al., 2011). The ash-dominated parent material was remobilized when pore fluid pressure

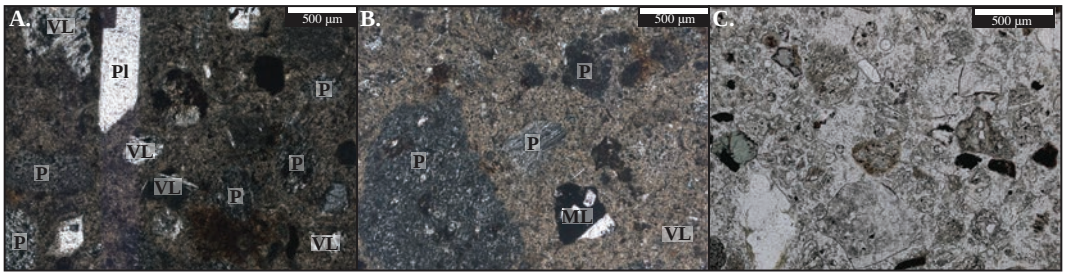

Fig 5. Thin section images from megablock complex samples. (A and B) Thin section of the clastic injection dyke in plane polarized light (PPL), containing abundant pumice and ~90% glassy fragments. (C) Thin section of grain mount of injectite material in PPL. The injectite material is composed primarily of volcanic glass, but also contains few dense mineral grains, including zircon and chlorite. "VL" = volcanic lithic; "ML" = metamorphic lithic; "P" = pumice; "Pl" = plagioclase.

rose above the hydrostatic pressure gradient (Delvaux and Hanon, 1993). When pore fluid pressure also rose above the fracture pressure gradient of the sealing siltstone unit, the confining layer was hydrofractured into an enormous megablock, along with smaller blocks, of intact strata, bound by reverse "blowout" faults (Montenant et al., 2007; Fig. 2B). Once fluidized, the parent material appears to have been remobilized and driven laterally to the site of the megablock complex by overpressure, where it then hydrofractured, intruded, and hydraulically lifted the overlying volcaniclastic siltstone, similar to the popping of a champagne cork. The megablock and smaller blocks of consolidated, undeformed siltstone were transported upward as the fluidized parent material from below was forced upwards into zones of weakness, flowing around the cohesive megablock(s) towards the paleosurface (Fig. 3B).

We interpret strong ground shaking due to seismicity as the source of pore fluid overpressuring, leading to liquefaction and fluidization of the tuffaceous sediment, as discussed in detail below. Cyclic stresses (i.e. seismicity) and/or aftershocks (Quigley et al., 2013) allowed for the overprinting of a brittle structure (clastic injection dyke) on ductile structures (fluidized parent unit and associated megablock), as the sediment was re-deformed after regaining strength following initial fluidization. The clastic injection dyke was formed after the uplift of the megablock complex, as evidenced by its superposition on both the injectite and megablock. Brittle fracturing of the dyke demonstrate that its emplacement was soon after the megablock uplift event, before the fluidized parent material fully dewatered, when post-seismic settling ultimately compacted the injection dyke and led to its deformation. We interpret the upper "V-shaped" portion of the clastic injection dyke as a blowout cone (sensu Nichols et al., 1994; Loope et al., 2013), representing the top of the dyke where it intersected with the paleosurface. Metamorphic cobbles and 5-25 cm clasts of the megablock unit infill the blowout cone, presumably after injected material was extruded onto the paleosurface (Vigorito et al., 2008), and material fell into the cone opening from above.

This megablock complex is significant because it is one of the few continental, outcrop examples of very large-scale soft-sediment deformation associated with injectite features (Hurst et al., 2011; Vigorito et al., 2008; Thompson et al., 2007), in comparison to the significant subsurface submarine record of sandstone injectite complexes. The megablock complex also stands out because it occurs in rather homogenous, tuffaceous sandstone, compared to the more common scenario of sandstone injectites in mudstone hosts (Huuse et al., 2007; Scott et al., 2009; Vigorito and Hurst, 2010). Similarly, the hydraulic lifting of the megablock by fluidized injected volcanic ash, defies traditional concepts of downward displaced blocks of coherent sediment, usually due to collapse from overloading, liquefaction, and density inversions. This unique seismite formation illustrates the

powerful effects of overpressured systems and active seismicity in this region on near-surface sediments. Consequently, this deformation indicates significant surface stability hazards associated with seismicity in the region, and other parts of the East African Rift System.

4.2.2. Asymmetric Recumbent Folds

The large-scale asymmetric, recumbent folds at Ilasilo 6 record hydroplastic soft-sediment deformation in a quiet, shallow lake or pond. The orientation of the folds suggests a very low slope (0.5°-2°) at the time of deformation. The folded horizon is truncated, indicating that the deformed unit was at the sediment/water interface at the time of deformation.

5. Discussion

5.1. Identification of a seismic triggering mechanism

Seismites are horizons of secondary sedimentary structures generated close to the surface by earthquakes of great enough magnitude ($M \geq 5 \pm 0.5$; Atkinson, 1984; Allen, 1986; Ambraseys, 1988; Audemard and de Santis, 1991; Obermeier et al., 1993; Galli, 2000) to sufficiently increase intergranular pore pressure and cause liquefaction and/or fluidization of the affected sediment (Lowe, 1975). There are no unequivocal criteria for identifying seismogenic soft-sediment deformation structures, as morphological expression varies widely and is dependent on lithology and depositional history, no two of which are ever the same. However, many authors refer to sets of criteria proposed by Sims (1975), Obermeier (1996; 2009), and summarized by many others, to link deformation structures with seismic events. These criteria generally include: 1) association with seismically active faults; 2) liquefiable sediments; 3) similarity to structures formed experimentally or by recent earthquakes; 4) horizons of deformation that are correlative over large areas; 5) deformed zones surrounded by undeformed strata; 6) deformation that increases in intensity towards the inferred epicenter; and 7) the exclusion of other triggering mechanisms (Sims, 1975; Hempton and Dewey, 1983; Obermeier, 2009).

However, the above conditions are not diagnostic, and often these criteria can also fulfill the requirements for triggers other than seismicity. In contrast, some workers advocate a context-based approach (Molina et al., 1998; Jones and Omoto, 2000; Owen and Moretti, 2011) to identify a trigger mechanism as either autogenic or allogenic, based on sedimentological and paleoenvironmental setting. In light of the problematic methodology for identifying a trigger mechanism for soft-sediment deformation, we use a combination of published criteria and depositional environment- and deformation style-based evidence to

infer a seismic trigger for the large-scale megablock complex and asymmetric, recumbent folds at Ilasilo 6.

The following field-based evidence is used to meet the above criteria and to diagnose a seismic trigger for the soft-sediment deformation in the Lake Beds Succession in the southern Rukwa Rift Basin:

1) Deposition of the volcaniclastic, Late Pleistocene-Recent Lake Beds Succession occurred simultaneously with active volcanism and active faulting in the southern Rukwa Rift (Fig.1). Refer to "Implications" section below for details.

2) Grain size analysis suggests the deformed sediment is highly susceptible to liquefaction (Fig. 6). The upper surface of the folded horizon at Ilasilo 6 resembles an erosional surface, an indication of liquefaction at the sediment/water interface (Figs. 4C and 4D; Owen and Moretti, 2011). Additionally, clastic dykes and the injectite of the megablock complex show evidence of water-escape.

3) Large-scale deformation features are correlated via radiocarbon dates over 35+ km (Figs. 7 and 8).

4) Folds at Ilasilo 6 are overlain and underlain by undeformed, horizontally bedded siltstones. The megablock complex is positioned within undisturbed, horizontal bedding and preserves intact, correlative stratigraphy on either side (Figs. 2-4).

5) Soft-sediment deformation horizons are not only a common and repeated occurrence in the Lake Beds strata, but have also been abundantly recognized in Permian – Paleogene strata of the Rukwa Rift Basin. For example, stratigraphic sections at Ilasilo 6 and elsewhere in the Rukwa Rift Basin record diverse forms of soft-sediment deformation, including: flame structures; cm- to m-scale folded beds; ball-and-pillow structures; syn-sedimentary faults; sand injection features; and m-dkm-scale clastic injection dykes (Fig. 9). Clastic injection dykes are most common (n >15), occurring at many localities, where they vary in length from <30 cm to >10 m, and from a few mm to >25 cm in width. Many initiate in sand beds, cut confining horizons of distinct sandstone, mudstone, or siltstone lithologies, and contain cm-scale angular fragments of the side wall rock.

The circumstantial evidence presented above strongly suggests a seismic triggering mechanism for the large-scale soft-sediment deformation in the southern Rukwa Rift Basin. However, because seismite criteria can be ambiguous, we also consider other likely triggering mechanisms. Sediment loading can be ruled out because of the homogeneity of tuffaceous, silt-sized lithology that dominates the outcrops at both localities, eliminating overloading and inverse density gradients as triggers. Additionally, truncation of the folds at the top of the deformed unit at Ilasilo 6 indicates formation near the sediment/water interface (Anketell et al., 1969). Likewise, the megablock complex is positioned to within

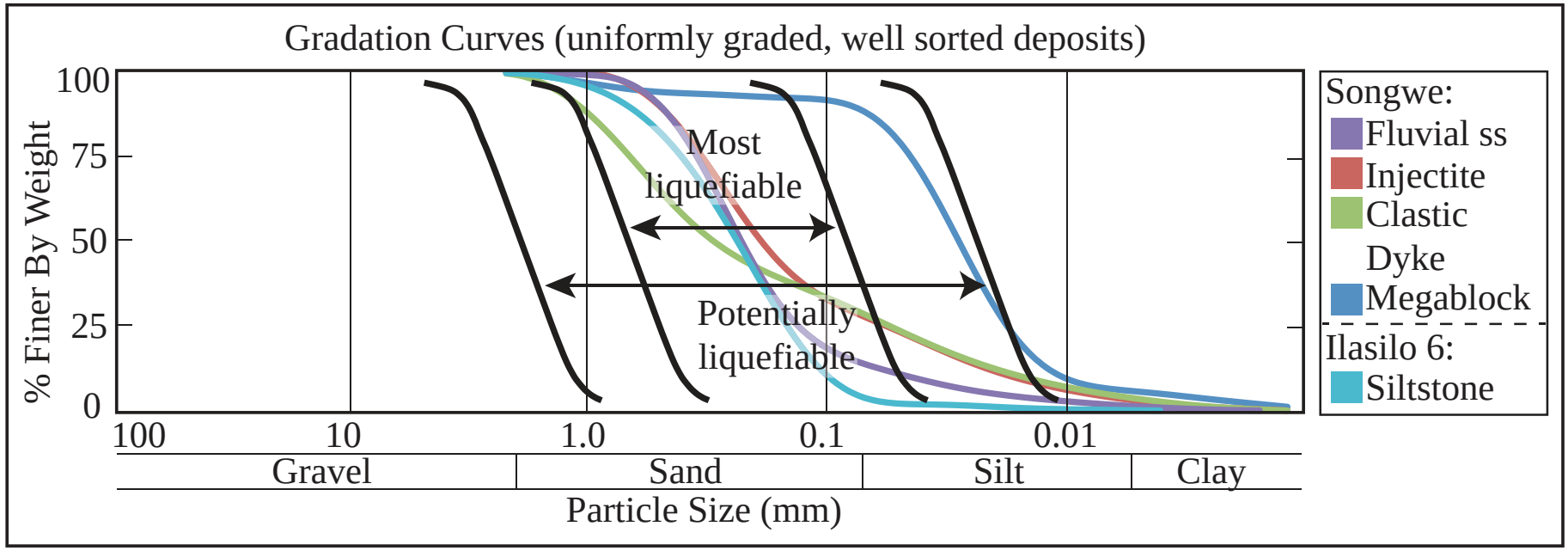

Fig 6. Gradation curves modeling the susceptibility of sediment from the Rukwa Rift Basin to liquefaction (Tsuchida and Hayashi, 1971). The sealing unit of the megablock complex is represented by the sample labeled "Megablock". Note that this lithology is the least liquefiable, in comparison to the fluidized parent unit ("injectite") and clastic dyke material, which plot within the "most liquefiable" zone. Sediment size and dispersion was measured on the Mastersizer 2000 via laser diffraction. The "fluvial ss" sample is located on Fig. 2D. This unit represents the fluvial facies incised into by the buttress unconformity and against which the lacustrine siltstones of the megablock complex were deposited.

A. Sample	Conventional Radiocarbon Age	13C/12C	Calibrated Age, years BP (2σ)	
Organic sediment 710142GAL6	23,530 +/- 90 BP	-17.1 o/oo	27,650 ± 105	This study
Organic sediment 6/23/12-6	23,650 +/- 100 BP	-15.1 o/oo	27,750 ± 110	This study
Coelatura cf. *ujujiensis* Songwe section	18,360 +/- 60 BP	Indet.	22,010 ± 320	Cohen et al. (2013)
Bivalve shell S. of Galula	9,740 +/- 140 BP	-2.45 o/oo	11,070 ± 200	Cohen et al. (2013)
Bivalve shell 8 km S. of Galula	8,060 +/- 120 BP	-1.36 o/oo	8,950 ± 190	Cohen et al. (2013)
Bivalve shell S. of Galula	8,030 +/- 30 BP	Indet.	8,910 ± 90	Cohen et al. (2013)
Lavigeria sp. shell Galula Station	6,340 +/- 50 BP	-1.8 o/oo	7,270 ± 60	Cohen et al. (2013)

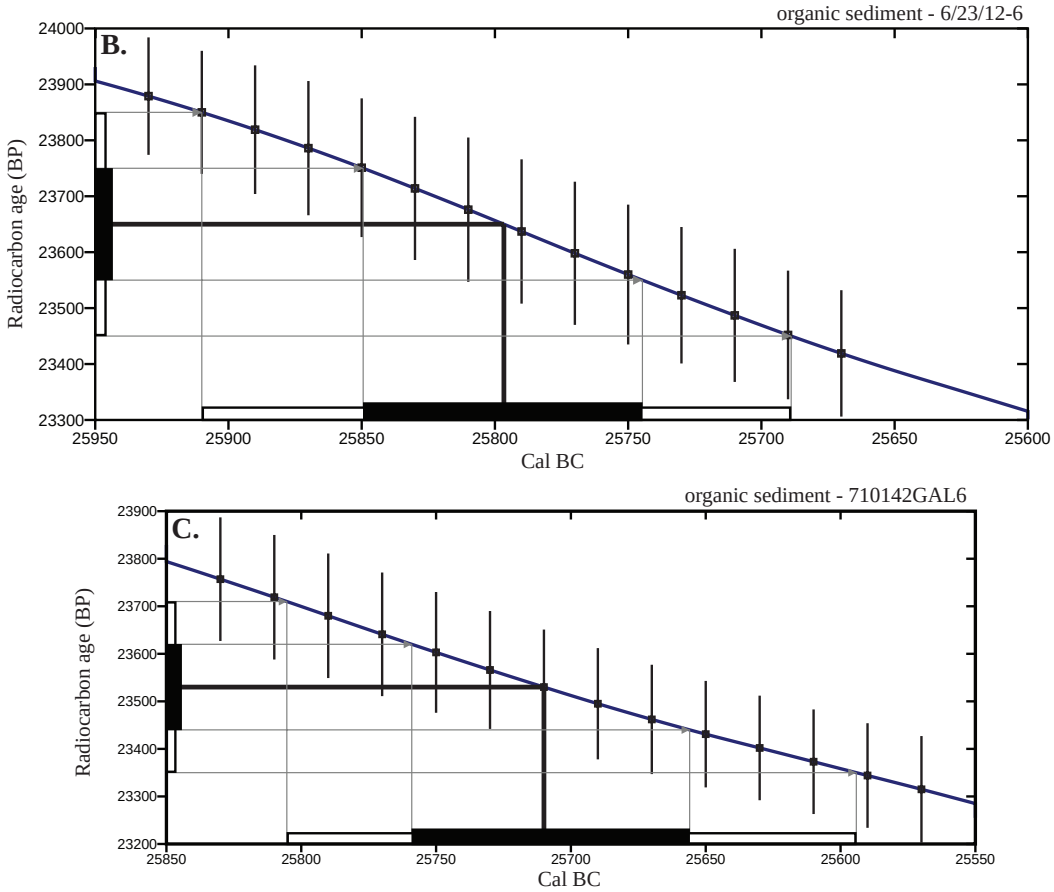

Fig 7. AMS radiocarbon dates from the Songwe Valley region. (A) Dates from the Ilasilo 6 seismite, Songwe Megablock site, and samples from Cohen et al. (2013) sourced near Ilasilo 6. (B and C) The intersection of the megablock unit sample (see Fig. 3) and Ilasilo 6 seismite sample radiocarbon dates (see Fig. 4), respectively, with the calibration curve (Reimer et al., 2013).

~10 m of the paleosurface. At the Songwe site, the intrusion of massive sediment from an underlying or stratigraphically equivalent parent body demonstrates horizontal and vertical injection as the driving mechanism. At both localities we interpret the facies to represent a flat lying lake floor unit. Vertical displacement of the megablock and block-bounding faults displaying reverse orientation also rule out a trigger originating from the sedimentary

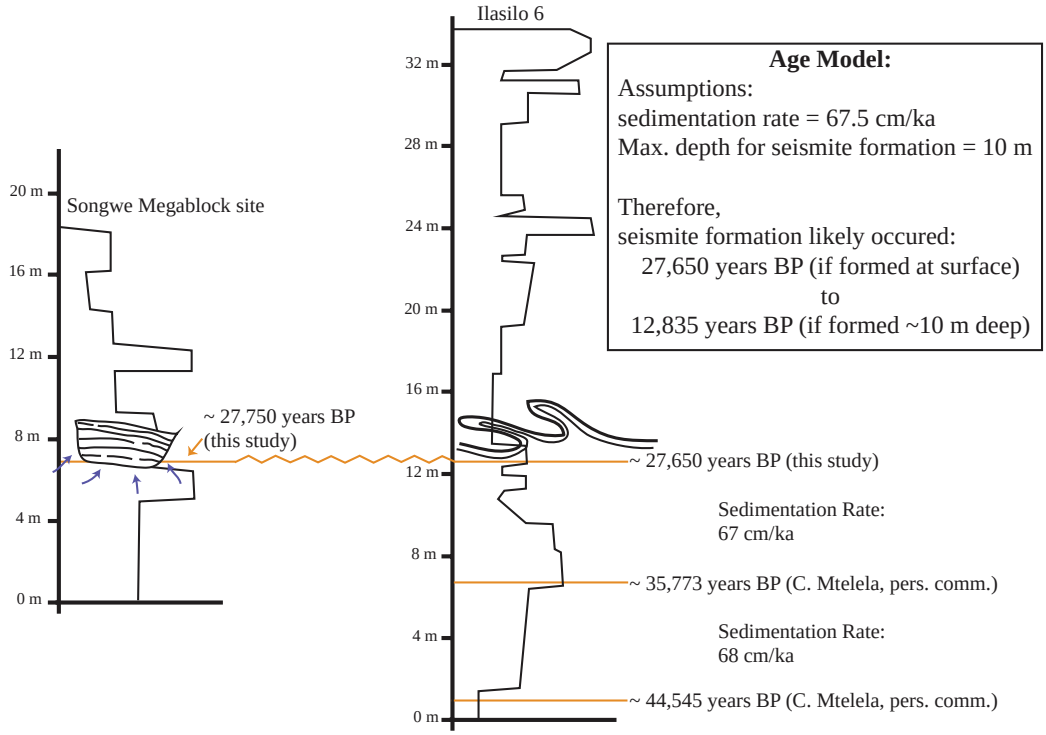

Fig 8. Correlation of Ilasilo 6 and the Songwe Megablock sites, with model approximating age of deformation. The Songwe Megablock Site radiocarbon sample is from an organic-rich layer containing macrofossil reeds of the unit that was fractured and uplifted, forming the megablock (UTM: 522904 E 9015130 N, zone 36, ARC 1960 datum). The Ilasilo 6 radiocarbon sample is from a black, fossiliferous, organic-rich unit ~1.5 meters below the large-scale seismite (UTM: 502917 E 9044472 N, zone 36, ARC 1960 datum). These two indistinguishable radiocarbon dates provide a tie point for the correlation of the two deformed outcrops over 35 km, and support the hypothesis for synchronous deformation of the megablock complex and asymmetric, recumbent folds.

depositional environment itself. At Ilasilo 6, the directional element within the folding suggests the aid of a downslope force. Assuming paleo-slope was similar to the present day maximum lake floor slopes (0.5°-2°), and considering fold asymmetry, these seismogenic slump folds were likely gravity-driven, related to slope failure, and seismicity is again the favored mechanism to have reduced sediment shear strength to allow for such hydroplastic deformation (Field et al., 1982; Moretti and Sabato, 2007; Alsop and Marco, 2013). Radiocarbon age correlation with the seismogenic Songwe megablock complex supports this interpretation. Storm waves are also discarded as a trigger mechanism because the finely laminated, horizontally bedded siltstone strata reflects relatively still-water conditions, and there is no evidence of tempestites, storm currents, or gravity-driven density currents. It is possible that other processes that produce high fluid pressures were present, and enhanced

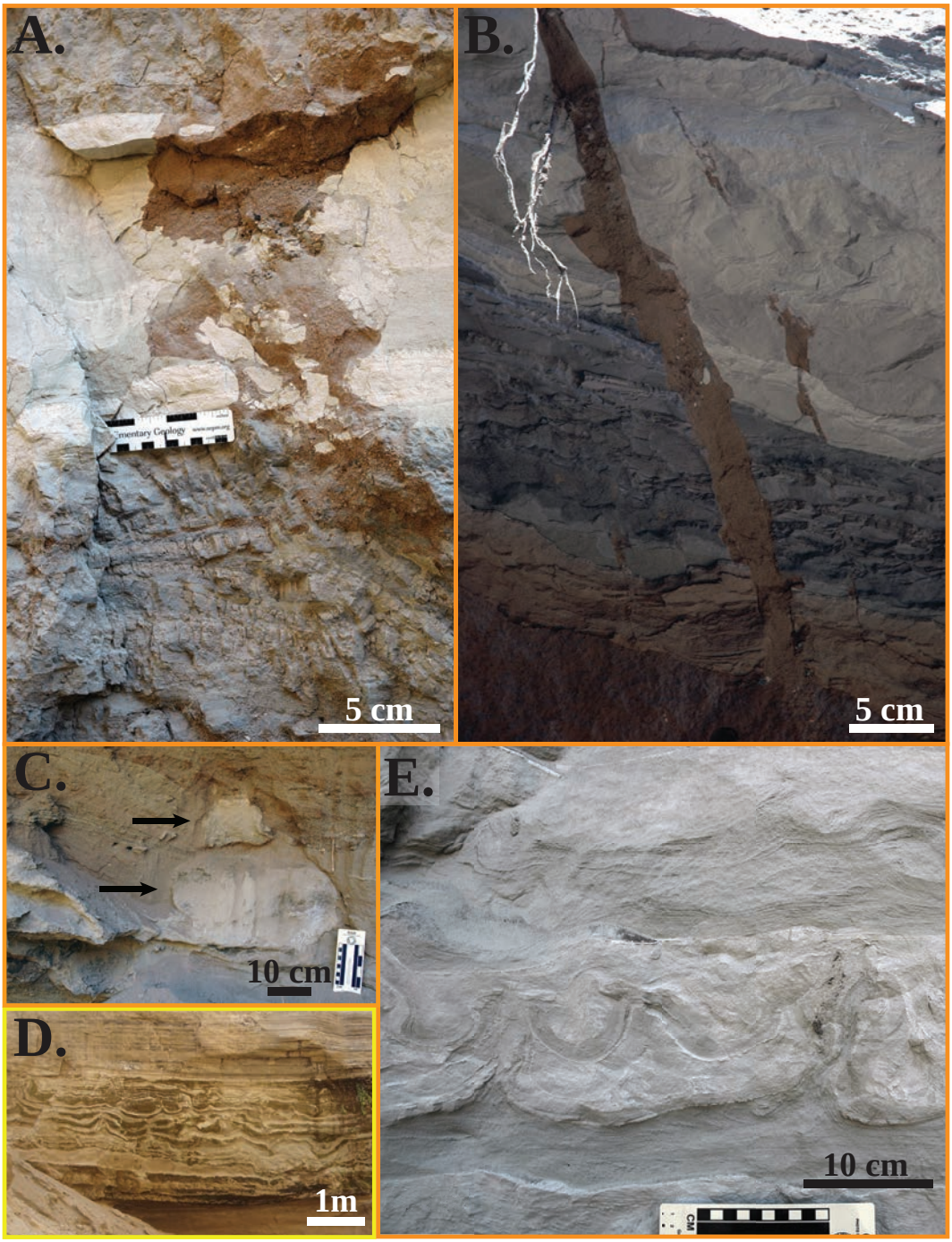

Fig 9. Seismites from the Lake Beds Succession at Ilasilo 6. (A and B) Clastic injection dykes. Vertical movement of clasts of the sidewall rock and sandstone parent bodies present below the field of view of the photographs indicate upward-directed injection. Bottom scale in (A) is in cm. (C) Ball-and-pillow structure. (D) Cm-scale convolute bedding. (E) Convolute bedding, folds, flame structures, and evidence of vertical fluid escape. Refer to Fig. 4 for color-coding. Soft sediment deformation features were photographed on vertical, southwest- (A and B), northeast- (C and D), and southeast-facing (E) canyon walls of LBS strata, exposed by down cutting of modern-day rivers.

by seismicity. For example, abundant hydrothermal vents exist throughout the Songwe Valley and may have intensified overpressure, increasing the risk for seismically triggered liquefaction in the Rukwa Rift Basin. In summary, the large-scale dimensions; highly liquefiable, low energy, tuffaceous, lacustrine lithologies (Figs. 2, 3, and 6); stratigraphic recurrence; regional extent; deformation morphology; in combination with proximity to active faults; and fulfillment of established seismite criteria, suggests deformation triggered by strong seismic shocks for the features described in this paper.

Large-scale (hundreds of meters to hundreds of kilometers) clastic injectite networks, extrudite deposits, load casts, and slumps have been previously identified, and their generation has been attributed to thermal destabilization (Backeberg and Rowe, 2009), fluid overpressure due to rapid sedimentation (Løseth et al., 2012), catastrophic triggering mechanism such as seismicity, subaqueous landslides, and bolide impacts (Cartwright, 2010; Sherry et al., 2012), lateral pressure transfer (Cartwright, 2010), etc., although the triggering mechanisms are not well understood (Cartwright, 2010). The megablock complex we describe here is similar to these previously reported deformation structures only in scale, but differs in that it is the first seismically generated injectite complex that features uplifted megablocks of intact sediment, in non-marine strata, which represents a process and variety of seismite not previously recognized. This spectacular, large-scale deformation feature suggests intense, Late Pleistocene to Recent seismic shaking in the Rukwa region.

6. Implications: Large magnitude earthquake risk

6.1. Age Estimate for Deformation

The Songwe megablock complex and recumbent folds at Ilasilo 6 likely occur along the same stratigraphic surface, as indicated by two radiocarbon dates (Figs. 7 and 8), signifying synchronous deformation. An age model (Fig. 8) suggests that deformation and related seismicity occurred in the Late Pleistocene, between ~ 27,650 ± 105 and 12,835 ± ~100 years ago (based on sedimentation rates calculated from radiocarbon ages from a stratigraphic section at Ilasilo 6; Fig. 8). The upper truncation of folds at Ilasilo 6 and the surface breach of the clastic dyke at Songwe imply that the deformed horizon was at or near the paleosurface at the time of liquefaction and fluidization, suggesting a significant seismic event closer to ~27,650 years ago. There is documented crustal seismicity at this time, demonstrated by fault scarps, faceted spurs, tilted Quaternary deposits, volcanism, and recorded seismicity (Vitorri et al., 1997), as well as by activity of Late Quaternary normal faults in the center of the basin and at the southwestern rift flank (Delvaux et al., 2012; Skobelev et al., 2004).

6.2. Earthquake Magnitude Estimate

We suggest that earthquakes of M ≥ 6 were responsible for the soft-sediment deformation features we report here, based on minimum magnitude capable of liquefaction, and circumstantial evidence, as discussed below. However, relating seismites to earthquake magnitude is equivocal, due to complexities including distance from the causal fault, attenuation of ground motion, and sediment susceptibility to liquefaction, which could not be quantitatively measured here. Many studies (Atkinson, 1984; Allen, 1986; Ambraseys, 1988; Audemard and de Santis, 1991; Obermeier et al., 1993; Galli, 2000) have reported M5 ± 0.5 as the lower limit of earthquake energy capable of triggering liquefaction. Empirical relationships have been established between earthquake magnitude and the farthest distance of observed liquefaction (Ambraseys, 1988; Papathanassiou et al., 2005; Galli, 2000), and these curves also support this estimate of minimum magnitude. Seismicity responsible for the Lake Beds Succession seismites could have originated at the Kanda Fault (also the proposed source of the 1910 Rukwa earthquake), as nearby LBS deposits record related, Pleistocene–Holocene faulting (Delvaux et al., 1998). One technique for interpreting the strength of paleo-earthquakes, the magnitude-bound method (Ambraseys, 1988), estimates a minimum M ~7.5 earthquake for seismites in the Songwe Valley, if sourced from the Kanda Fault (Fig. 10). A second possible seismic source, the active Mbeya Range-Galula Fault, lies just 10-15 km E/NE of the Songwe Megablock Site. This fault system continues beneath Lake Rukwa, where a series of steeply dipping faults are typically syndepositional with the youngest lake sediments. The longest segment of the Mbeya Range-Galula Fault, measuring ~23 km, could be capable of producing an earthquake of M = 6.7-7, as estimated by regression relations of moment magnitude on surface rupture length (Wells and Coppersmith, 1994; Stirling et al., 2002). A third likely candidate, the Lupa boundary fault, is continuous over 200 km, and has been significantly active, causing major basin forming events (and earthquakes) on intervals of thousands of years (Morley et al., 2000). If we assume deformation does not extend pass the Songwe Megablock Site, the magnitude-bound method estimates a minimum earthquake M6 produced by the Lupa Fault for soft-sediment deformation ~20 km away from the source (Ambraseys, 1988; Fig. 10).

Rodríguez-Pascua et al. (2000) qualitatively related particular seismite morphologies to earthquake magnitudes. Clastic injection dykes in lacustrine and fluvial deposits were interpreted to form from earthquakes ranging from 5≤ M ≥8 (Rodríguez-Pascua et al., 2000). Cobbles (4–20 cm diameter) from the basal Lake Beds Succession conglomerate contained within the lower meter of the injectite and within the clastic dyke required high injection velocities (Rodríguez-Pascua et al., 2000; Hurst et al., 2011), and this displacement is additional evidence for larger magnitude earthquakes (possibly up to M8 by estimates of Rodríguez-Pascua et al., 2000). However, we interpret these relationships with caution,

as soft-sediment response to seismicity is not only dependent on magnitude, but is also related to ground acceleration, proximity to the source, and other local factors. Minimally, we estimate that the paleo-earthquake magnitude was M > 5 ± 0.5, the minimum energy for triggering liquefaction. However, taking the size of the uplifted megablock and of the Ilasilo 6 folds, their morphologies, and the transport of large cobbles as proxy evidence, we suggest triggering by a higher-magnitude event at that time, especially when compared to the smaller-scale convoluted laminations, clastic dykes, and other seismites we report from underlying and overlying horizons (Fig. 9). We estimate a minimum earthquake of M ~6+, taking the most conservative magnitude estimate calculated using the magnitude bound method (from the Lupa Fault). Since 1900, at least 20 earthquakes of M ≥ 5 have been documented in the Songwe Valley region (Ambraseys and Adams, 1991; ISC, 2012; USGS; Fig. 1). The sedimentary evidence for recurring, similarly intense palaeoseismic events presented herein emphasizes the potential for damaging surface deformation in the region, and identifies a significant seismic hazard in southwest Tanzania, and indeed throughout the East African Rift System.

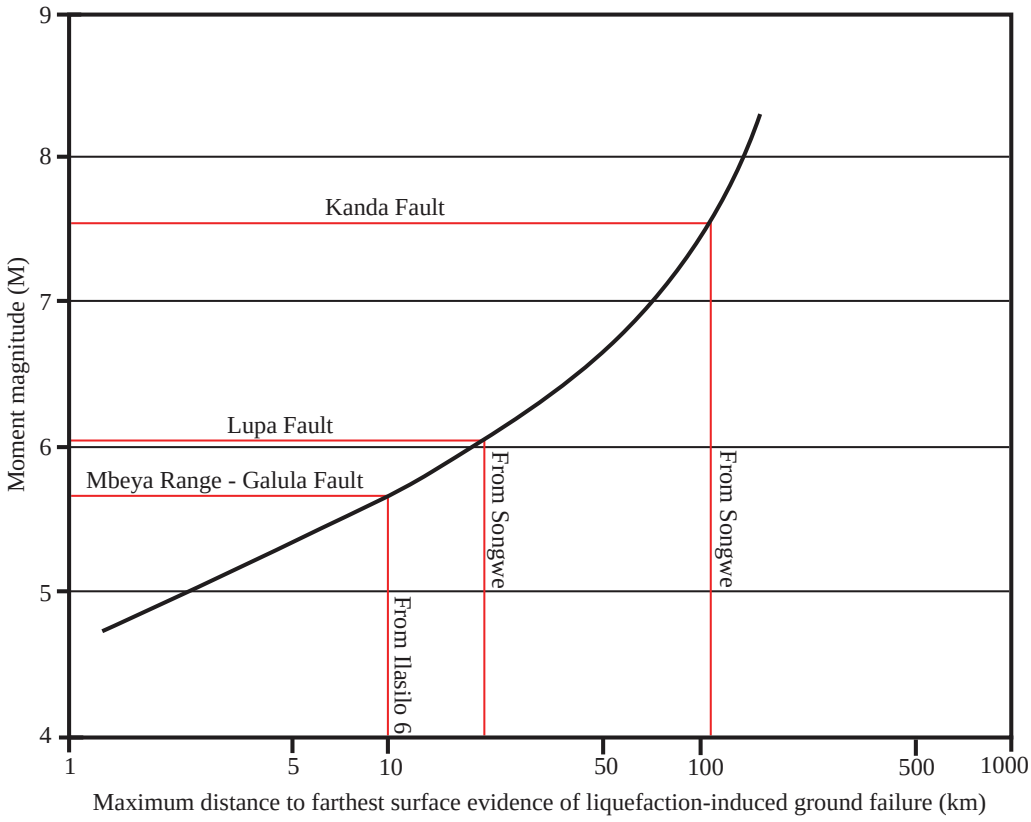

Fig 10. Paleo-earthquake magnitude estimates using the magnitude-bound method. Estimates of minimum paleo-earthquake magnitudes necessary for the formation of liquefaction features at either Ilasilo 6 or the Songwe Megablock Site using the magnitude-bound method of Ambraseys (1988). Distance to farthest evidence of liquefaction was estimated using the distance from either Ilasilo 6 or the Songwe Megablock site to each suspect fault (site furthest away was chosen). Note that this is a minimum estimate of furthest surficial liquefaction features.

7. Conclusions

Outcrop exposure of exceptional, large-scale soft-sediment deformation, including the uplift of a bus-sized megablock by fluidized, injected material; fluidization of large cobbles at Songwe; formation of giant, recumbent folds at Ilasilo 6; and numerous smaller scale clastic dykes and seismites, occur over at least 35 km in the RRB. These unique features suggest potential for dangerous surface deformation related to the seismically active East African Rift System. Our documentation provides evidence for M ~6+ Late Pleistocene earthquakes, similar to the M7.4 earthquake at the same location in 1910, extending the record of large-magnitude earthquakes beyond the last century, and contributing valuable data to better constrain recurrence intervals of high magnitude earthquakes in the Western Branch of the East African Rift. Our discovery is consistent with high-resolution seismic reflection data from Lake Rukwa, which provided evidence for high-frequency changes in boundary fault activity that occurs with a periodicity of thousands to tens-of-thousands of years (Morley et al., 2000). Documenting new seismite morphologies, such as the one presented here, is essential for understanding surface dynamics and assessing seismic hazards and risks, particularly in rift settings where seismite records remain poorly studied. The nature of the Late Pleistocene to Recent deposits of the Lake Beds strata in the Rukwa Rift Basin, typified by repeated transitions between coarse-grained alluvial/fluvial strata and fine-grained volcanic ash-rich lacustrine strata, provide perfect conditions for land surface deformation and serious hazards associated with seismic shaking, as exemplified by the unique, highly disruptive nature of the megablock complex. With population centers such as Mbeya, Tukuyu, Sumbawanga, and Mpanda all within tens of kilometers from the Songwe Megablock Site or the 1910 M7.4 earthquake epicenter, documenting and predicting the near-surface sediment behavior under seismic stress is critical information for the understanding and modeling of earthquake hazards in rift settings in East Africa.

Chapter Two

New sedimentary structures in seismites from SW Tanzania: Evaluating gas- vs. water-escape mechanisms of soft-sediment deformation

Published in *Sedimentary Geology*

Abstract

Seismite horizons are abundant in Cretaceous sandstones of the Rukwa Rift Basin, southwestern Tanzania. Diverse morphologies of soft-sediment deformation are preserved, including two new, unusual sedimentary structures, herein referred to as: 1) balloon-shaped inflation structures and 2) surface fractures with linked sandstone splays. This original description of new sedimentary structures contributes to the growing catalogue of seismically induced deformation features. Their unusual morphologies bring to the forefront an important, though seldom touched upon, question of how to differentiate between gas- and water-escape in soft-sediment deformation features. The recognition of the spectrum of soft-sediment deformation structures contained in strata and their deformational mechanisms is important because it permits the differentiation between triggering mechanisms, particularly seismic activity, and can constrain such events spatially and temporally. We interpret the surface fractures and linked sandstone splays to reflect a high gas effusion rate, formed by the release of high-pressure gas followed by a limited expulsion of water. The balloon-shaped inflation structures reflect lower gas effusion rates due to expulsion of lower pressure gas that did not breach the Cretaceous surface seal. When these gas pulses did breach the paleosurface, they formed gas-discharge pits. These seismogenic structures are consistent with deposition of Cretaceous strata in the Rukwa Rift during periods of active carbonatite volcanism, seismicity, and possibly hot spring activity. This documentation serves as an important data point for the re-examination of the classification scheme of soft-sediment deformation structures as primarily water-escape structures to accommodate for the genesis of some secondary sedimentary features by gas-escape.

1. Introduction

Soft-sediment deformation is attributed to the overpressuring of pore fluids in unconsolidated sediment, resulting in the modification and often destruction of primary sedimentary structures and the formation of new, secondary sedimentary structures (Lowe, 1975). A variety of mechanisms can initiate such conditions, including: bedform shear, loading, slumping, seismicity, and many other actualistic processes (Allen, 1982; Obermeier, 1996; Owen, 1996; 1997; Jones and Omoto, 2000; Owen and Moretti, 2011). Water is universally called upon as the medium facilitating liquefaction and fluidization. Gases (e.g., biogenic, hydrothermal, etc.) however are also a common component of sedimentary environments and may similarly instigate soft-sediment deformation. Although an extensive body of literature on soft-sediment deformation features exists, few studies have actually sought to distinguish between water- and gas-escape mechanisms of deformation and the resultant end products.

The majority of sedimentary structures formed by soft-sediment deformation are attributed to overpressure of the pore fluid, including: convoluted bedding, folding, ball and pillow structures, flame structures, injectites, sand volcanoes, and many more types. Sedimentary structures solely attributable to gas expulsion are rarely documented (Cloud, 1960; Pralle et al., 2003; Jianhua et al., 2004; Frey et al., 2009). Some occurrences of gas-escape through sediments have been reported, although they are dominantly recognized and preserved in argillaceous and marine settings (Fleischer et al., 2001). Examples include: chimneys and pockmarks related to gas hydrates (Cathles et al., 2010), air discharge pits on point bars (Jianhua et al., 2004), molar tooth structures in carbonates (Frey et al., 2009), circular gas-escape pits at a track site (Rindsberg, 2005), and gas bubble release due to biogenic gas build-up (Maxson, 1940; Cloud, 1960).

For soft-sediment deformation structures, the recognition of specific depositional settings, morphologies, and distributions are used to infer genesis via seismicity (McCalpin, 1996; Ettensohn et al., 2002; Reicherter et al., 2009), but identifying the triggering mechanism is often problematic (Owen and Moretti, 2011). Herein, we report on two, new, small-scale soft-sediment deformation features identified in Cretaceous sandstones from the Rukwa Rift Basin, Tanzania. Based on several lines of evidence these features are most likely attributable to seismic activity that caused the overpressuring and subsequent vertical migration of water and gas phases responsible for the preserved deformation. The newly identified balloon-shaped inflation structures and associated surface fractures with sandstone splays expand the understanding of gas migration effects on the generation of sedimentary structures, particularly in sand-sized sediments, and highlight the importance of considering gas-escape as a formation mechanism for soft-sediment deformation.

2. Geologic Setting

The Rukwa Rift Basin (RRB) in southwestern Tanzania is a half-graben basin segment of the western branch of the East African Rift System (EARS; Fig. 1; Chorowicz, 2005). The thick deposits record changes in the kinematic stress regime throughout the polyphase history of the RRB from the Permian to Recent, including multiple phases of rifting (Kilembe and Rosendahl, 1992; Wheeler and Karson, 1994; Delvaux et al., 1998; 2012). The sedimentary packages preserved in the Rukwa Rift are valuable archives of long-lived fluvial and lacustrine deposition and provide key insights into the effects of volcanism and seismicity on deposition in a rift basin through time (Roberts et al., 2010; Hilbert-Wolf and Roberts, 2015).

The RRB records four episodes of rifting and associated sedimentary deposition. The Red Sandstone Group of the RRB was deposited above a thick, Carboniferous-Permian succession (the Karoo Supergroup) after a ~150 Ma hiatus, and is subdivided into the older Galula Formation and the younger Nsungwe Formation (Roberts et al., 2010). The Galula Formation is assigned a Cretaceous age based on paleontological, geological, and radioisotopic age constraints (Gottfried et al., 2004; Roberts et al., 2004; O'Connor et al., 2006), whereas the Nsungwe Formation has been firmly established as Oligocene, based on radioisotopic dating, magnetostratigraphy, and mammalian biostratigraphy (Roberts et al., 2010, 2012; Stevens et al., 2013). The Red Sandstone Group is overlain by the thick, upper Neogene to Recent, Lake Beds succession (Grantham et al., 1958) that caps the rift fill sediment and is also an important archive of recent high magnitude seismic activity in the rift (Hilbert-Wolf and Roberts, 2015).

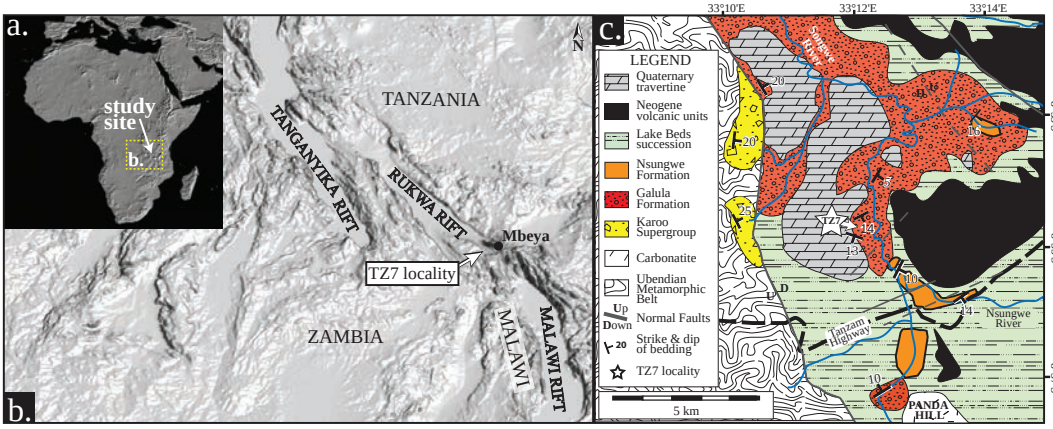

Fig. 1. Locality maps of the study site in the Rukwa Rift Basin. (a) Inset map showing the general location of the study area (yellow box) within eastern Africa. (b) Map of eastern Africa, highlighting the Tanganyika-Rukwa-Malawi rift segments. The arrow marks the study site in the Rukwa Rift Basin, southwestern Tanzania. Maps are modified from the NASA Shuttle Radar Topography Mission collection (http://www2.jpl.nasa.gov/srtm/cbanddataproducts.html). (c) Detailed geologic map of the TZ7 site in the Songwe sub-basin of the Rukwa Rift displaying volcanic and structural features (modified from Roberts et al., 2010).

The Cretaceous Galula Formation is dominated by cross-bedded sandstones with minor conglomerates and thin mudstones that accumulated in a large amalgamated braided stream setting, which flowed northwest across the continent into the Congo Basin (Roberts et al., 2012). Sedimentation in the overlying Nsungwe Formation is characterized by a vertical progression from alluvial to fluvial to lacustrine settings, which indicates that at least a portion of the western branch of the East African Rift System developed into an internally draining lacustrine basin (Paleo-Lake Rukwa) much earlier than has been recognized previously in the basin or elsewhere along the western branch (Roberts et al., 2012).

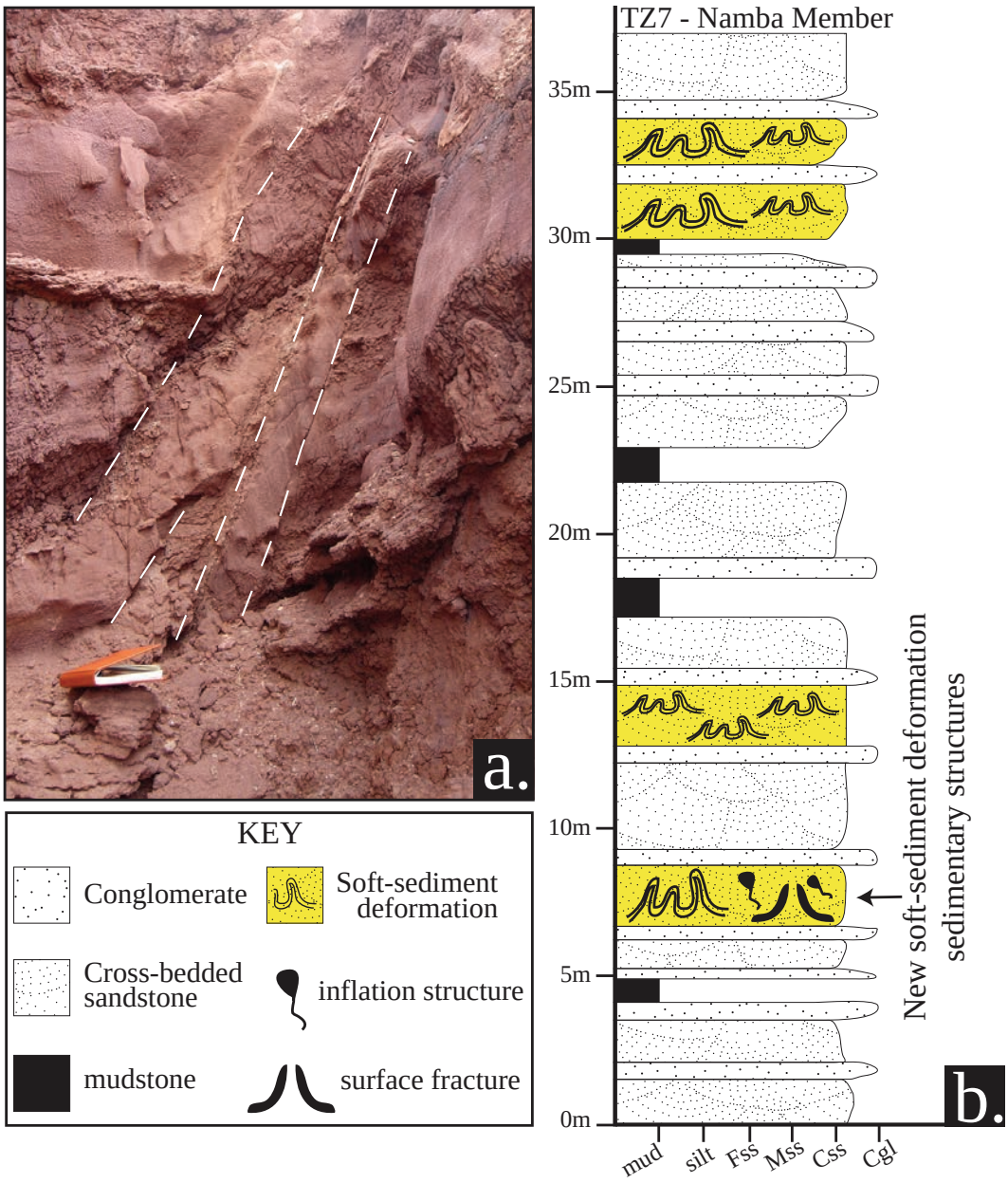

Fig. 2. Stratigraphic section and field photo of syndepositional growth faults. (a) Growth faults in the Namba Member found along a linear trend in close proximity (< 50 m away) to soft-sediment deformation structures. (b) Stratigraphic section through the TZ7 study site highlighting horizons affected by seismogenic soft-sediment deformation. See Roberts et al. (2004) for a detailed stratigraphic section through the Namba Member at the TZ7 site.

Major Late Jurassic to Early Cretaceous rifting is supported by apatite fission track dates from the Rukwa and Malawi Rift flanks (Van der Beek, 1998). Additionally, Delvaux et al. (2012) recognize a succession of rifting stages spanning the Late Cretaceous, Paleogene, and Neogene (components of stress stage 3) that correspond to preserved seismogenic sedimentary structures. Continuous and widespread tectonic activity and associated seismicity during the Cretaceous is clearly recognizable in the Rukwa Rift Basin sandstones (Figs. 2a and 3). Milga (1994) and Roberts et al. (2010) report extensive syndepositional soft-sediment deformation features from the Namba Member of the Galula Formation, including: fluid-escape structures, clastic dykes, and growth faulting. These features are linked with intense tectonic activity and the emplacement of local intrusive/extrusive igneous bodies, such as the Panda Hill and Mbalizi carbonatites (Roberts et al., 2010; Fig. 1). Hydrothermal activity and CO2 vents are current features of the basin system that may also influence the deformation of sediment.

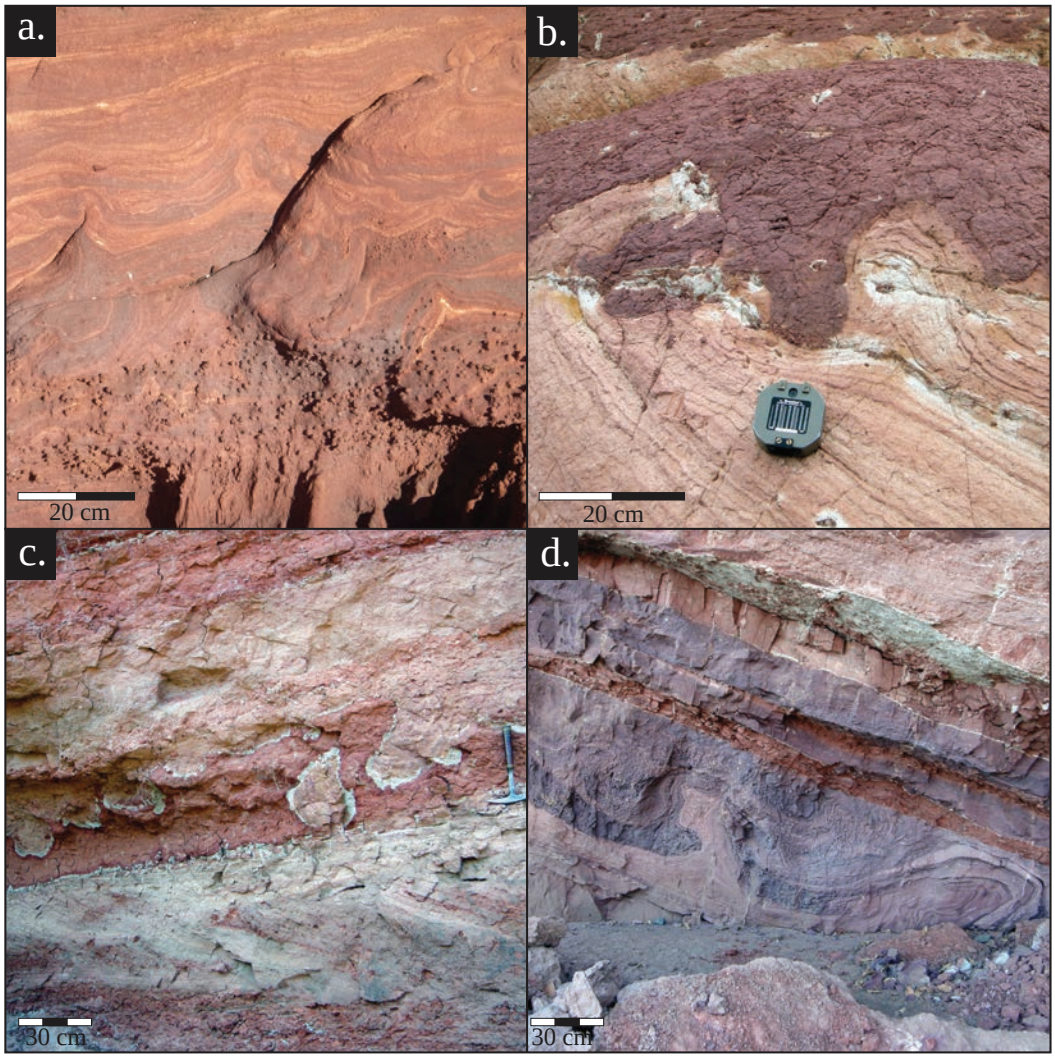

Fig. 3. Field photographs of seismogenic soft-sediment deformation features recorded throughout the Cretaceous red-beds of the Rukwa Rift Basin. (a) Folded, convoluted units showing evidence of fluidization. (b) Load structures and diapir-like features. The plastic intrusion furthest to the left shows evidence of halted injection. (c) Detached load structures. (d) Fluidized and folded beds with diapir-like structure.

3. Description of soft-sediment deformation

The soft-sediment deformation features discussed in this paper are located in the Songwe Valley, west of Mbeya, along the TanZam Highway at a locality called TZ7 (Fig. 1). At least four distinct 2-3.5 m-thick horizons with extensive soft-sediment deformation structures are recognized throughout the exposed Cretaceous Namba Member section. Each is overlain and underlain by undeformed strata and is horizontally continuous for a minimum of 200 m across the outcrop (Fig. 2b). The deformation includes cm- to m-scale convoluted bedding, folds, and flame structures preserving evidence of fluidization and water-escape (Fig. 3).

The two new types of soft-sediment deformation features we report from the Cretaceous Namba Member include: 1) balloon-shaped inflation structures and 2) associated linear surface fractures with linked sandstone splays. The site preserving these features is located in the middle part of the Namba Member of the Galula Formation, roughly 8 m above the base of the local section, in a three-dimensionally exposed outcrop (Fig. 2b). This interval is characterized by a series of upward-fining, medium- to fine-grained arkosic to sub-arkosic sandstones with erosive, basal pebble lags and well-developed, medium-scale trough and tabular cross-stratification throughout (Roberts et al., 2004; 2010). The inflation structures and surface fractures occur in the lowest recognized seismite horizon, specifically in an amalgamated tabular sandstone bed. They occur near the up-dip portion of one of many, small synsedimentary growth faults that are located in this part of the stratigraphy (Fig. 2a), dominated by a large braid plain system. Relative to the preserved Cretaceous land surface, the balloon structures and expulsion cracks with sandstone splays represent both near subsurface- and surface-linked, soft-sediment deformation features.

3.1. Inflation structures and gas-discharge pits

The inflation structures consist of an upper oblate spheroid- to teardrop-shaped chamber connected to a narrow cylindrical shaft that widens vertically from sub-cm to 1 cm or more in diameter (Figs. 4 and 5). Most shafts originate in an underlying structureless to weakly stratified sandstone bed, bend at varying angles and crosscut planar to low-angle stratification (Fig. 4). Internally, the shafts consist of massive, fine- to medium-grained sandstone with no discernable difference in grain size from the surrounding sediments. At their uppermost extent, just below the paleosurface, the shafts are connected to asymmetrical ovoid structures. The ovoid structures are wider near the tops than at the bases, resembling the shape of an inflated balloon (Figs. 4 and 5), and range from 3-10 cm in diameter. Finer-grained sandstone appears in the outer shell of the ellipsoid compared

to the core sandstone. Some ovoid structures deflect the overlying stratified sandstone beds vertically into small anticlines that commonly encase multiple asymmetrical ovoid structures (Fig. 4). Inflation structures occur in isolation (Fig. 5) as well as in small clusters (Fig. 4). Many of the inflation structures breach the paleosurface and are preserved in planar cross-section as circular pits with concentric, fine-grained sandstone laminations (Fig. 5b).

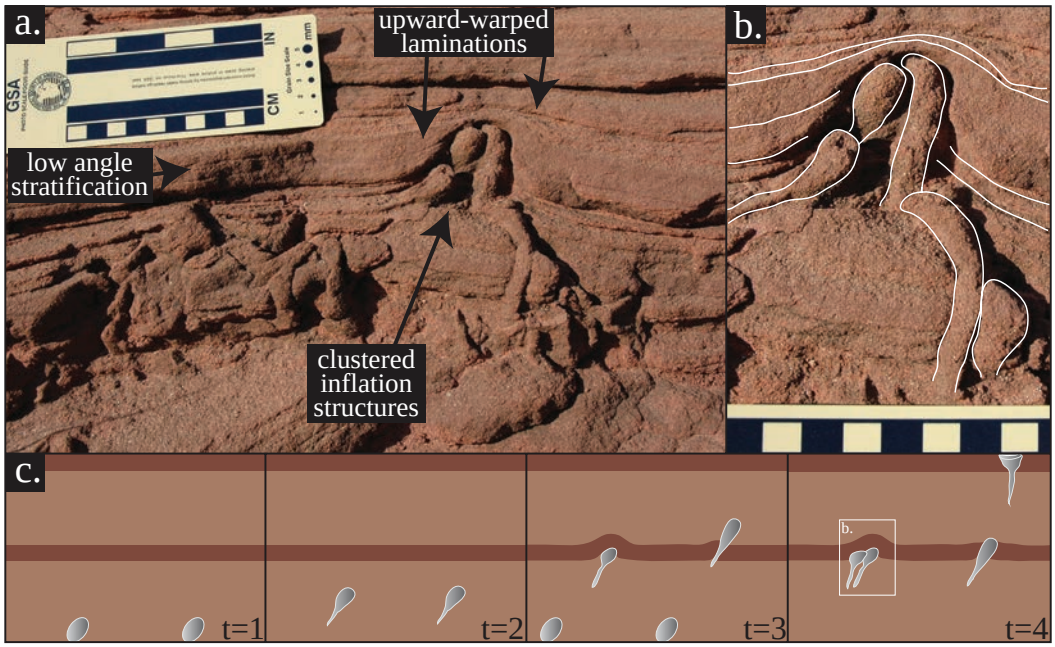

Fig. 4. Field photographs of balloon-shaped inflation structures in the Cretaceous Namba Member. (a) Note the upward-arching laminations and clustering of ovoid structures at the crest. Low-angle stratification is preserved above the structures, and massive sandstone is present below the structures. (b) Line sketch highlighting individual inflation structures within the gas-cluster of (a). (c) Time-series cartoons illustrating the likely genesis of inflation structures and surficial gas-discharge pits. At t=3, heterogeneities in the Namba Member sediments trapped some rising gas bubbles (forming balloon-shaped inflation structures), while other gas bubbles successfully rise to the paleosurface and rupture (t=4), forming gas-discharge pits.

3.2. Surface fractures with sandstone splays

Surface fractures are structures formed by fluidized conduits that have breached the paleosurface (Fig. 6). The surface fractures are restricted to the top of the unit and bend the upper 15-50 cm of fine- to medium-grained, low-angle laminated sandstone immediately surrounding the conduit upward (bent perpendicular to the undisturbed bedding; Fig.7). In the subsurface the conduits crosscut low-angle, stratified sandstone and originate from an underlying structureless to weakly stratified sandstone bed. Internally the conduits have vertically oriented, irregular–shaped, and upward bending folded laminations. The slightly sinuous cracks on the paleosurface display numerous associated smaller splay fractures (Fig. 6). The surface and subsurface strata are upturned adjacent to, and paralleling, the fractures.

A key feature of surface fractures is the common co-occurrence of narrow, linear to branching networks of finger-like sandstone that emanate from the numerous expulsion cracks (Fig. 6). These features are termed “sandstone splays” and together, both surface fractures and sandstone splays are observed in the same bed and horizon as the balloon-like inflation structures. Sandstone splays branch in a dendritic pattern and represent granular flows that moved down-slope of the paleo-topographic surfaces onto lower elevations on the undisturbed sandstone surface (Fig. 6). Splay sandstones display no apparent internal structure nor do they change in grain size along the length of the splay, but do show a decrease in flow thickness away from the rupture breach.

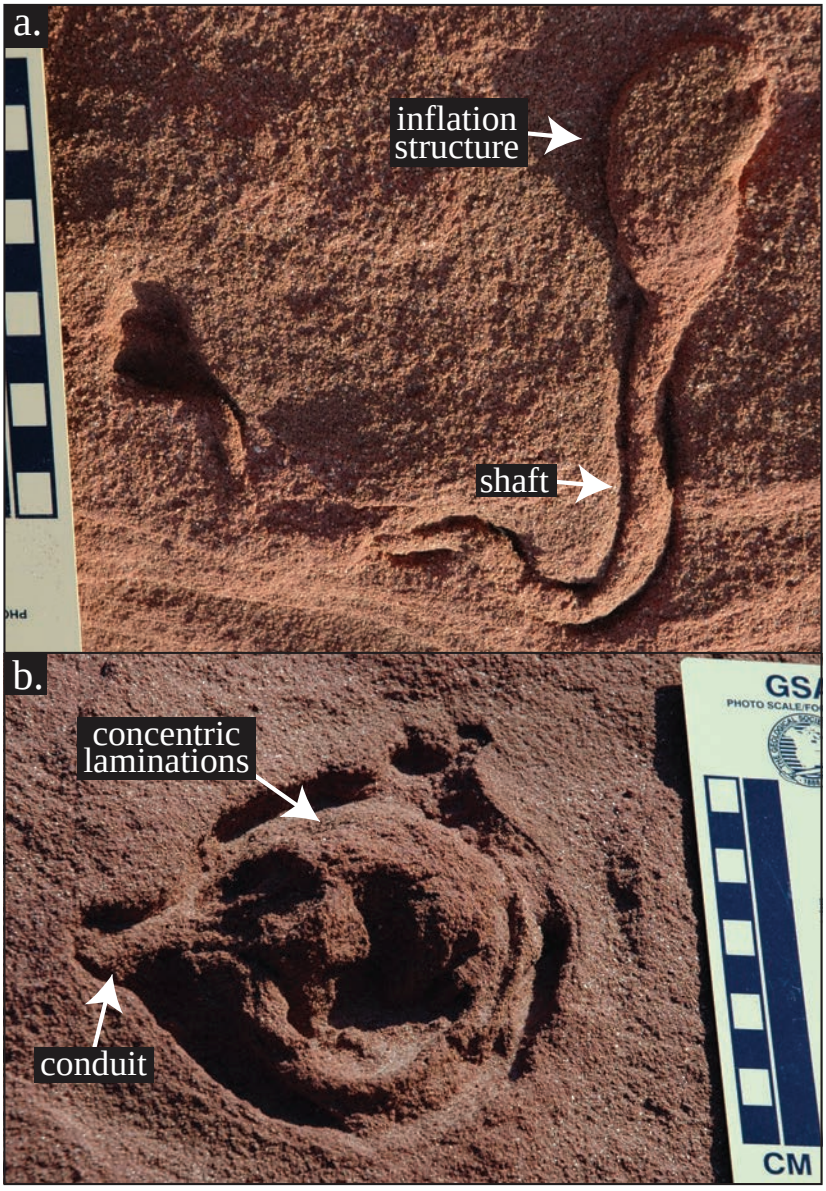

Fig. 5. Field photographs of inflation structure and gas-discharge pit. (a) Isolated, asymmetric ovoid structure and winding shaft. The ovoid inflation structure is oriented near-parallel to the bedding and the shaft crosscuts cm-scale bedding below the ovoid structure. Note the fine laminations preserved in the top half of the ovoid feature that parallel the ovoid edge. (b) A gas-discharge pit, preserving the rupture of gas onto the paleosurface. No obvious shaft is visible, although there is a suspicious conduit-like feature on the left side of the ovoid. Note the concentric laminations.

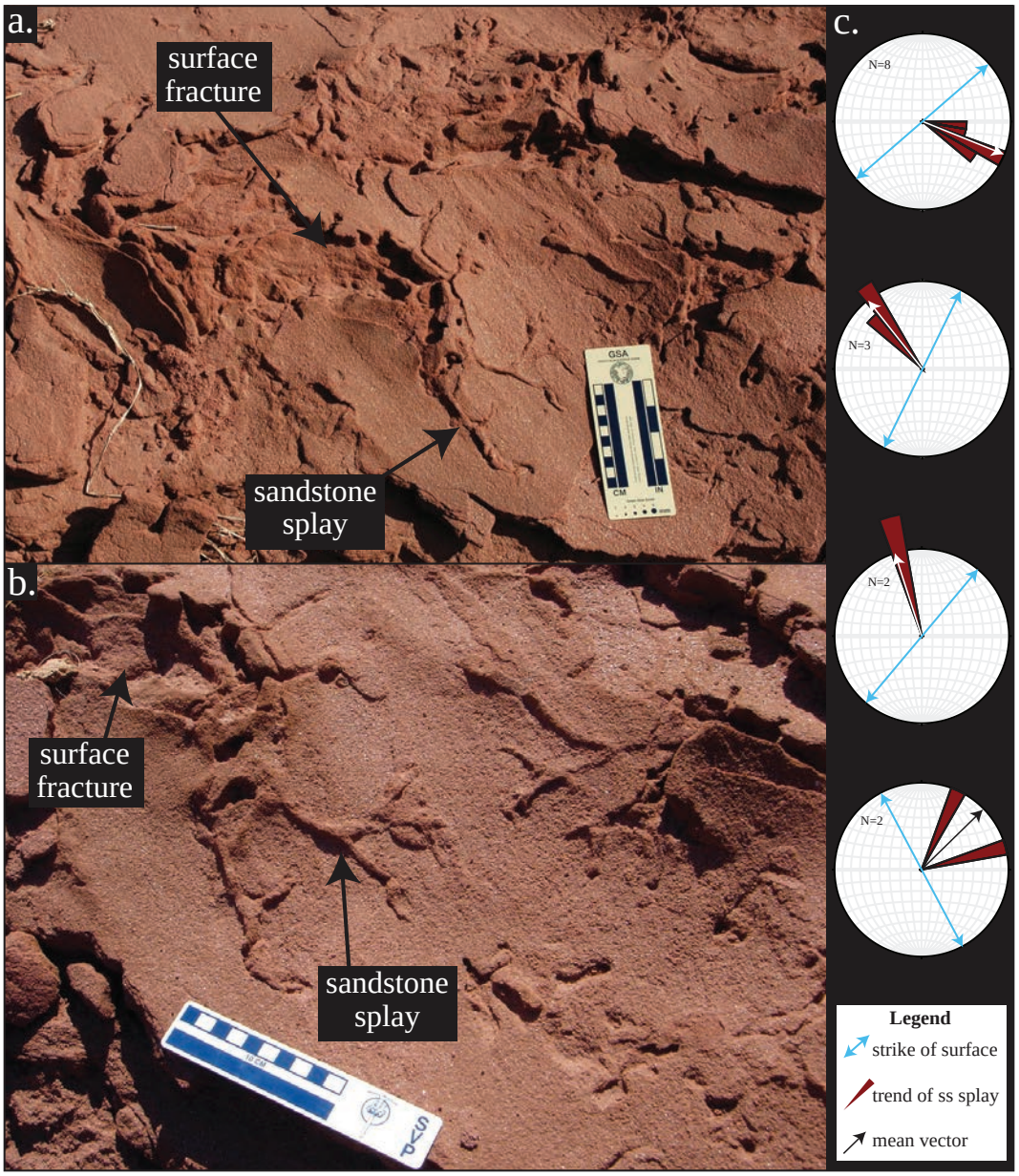

Fig. 6. Field photographs of surface fractures with linked sandstone splays in the Namba Member. (a) Irregular surface rupture with upward bending of laminations. Sandstone splays run from the highest to the lowest elevations of the flanks of the fractures and run out onto the Cretaceous land surface. Left scale bar is in cm. (b) Surface fractures with linked sandstone splays. Note the reduction in thickness of the splay away from the rupture. Top scale bar is in cm. (c) Rose diagrams illustrating the near-perpendicular orientations of the sandstone splays with the strike of the paleosurface, documenting that these hyperconcentrated flows moved down the Cretaceous topography.

4. Interpretations and Discussion

4.1. Evidence for a seismic origin

A succession of rift stages affected the Tanganyika-Rukwa-Malawi lineament during the Cretaceous (Delvaux et al., 2012), repeatedly reactivating the structural weaknesses in the Precambrian basement underlying the RRB. Thermochronology studies have identified

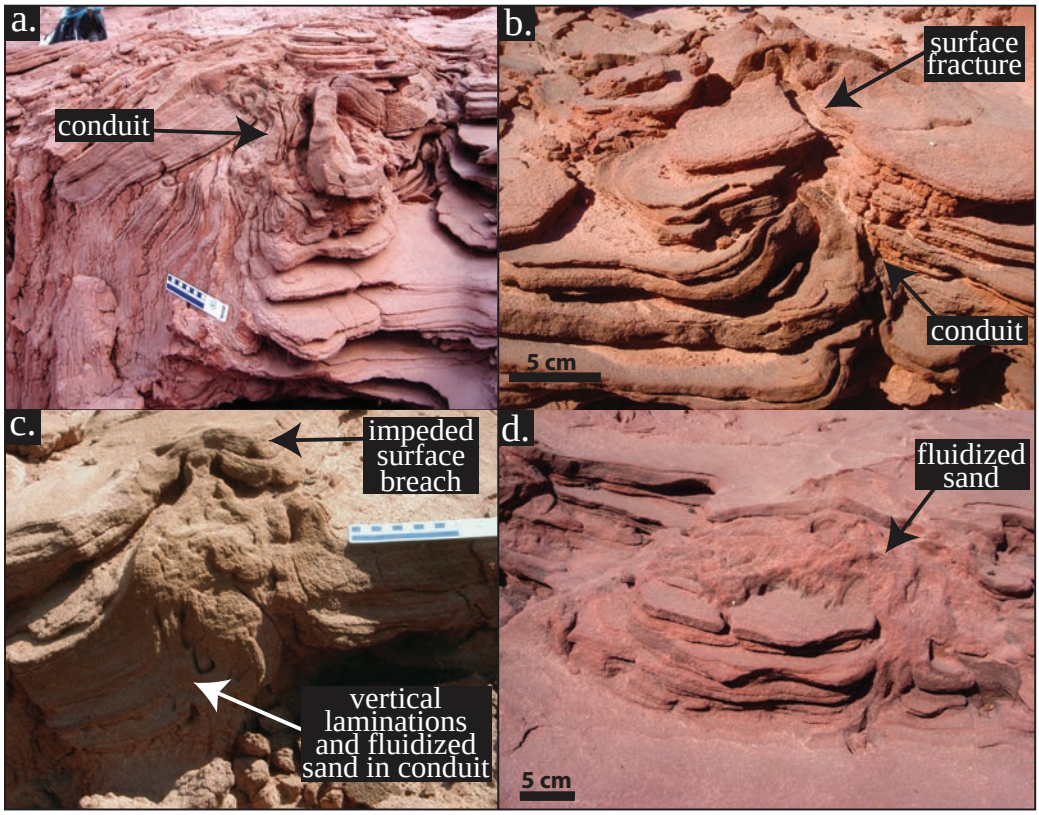

Fig. 7. Field photographs illustrating fluidized sandstone conduits and various interactions with the paleosurface in the Namba Member. Upper scale bars in photographs are in cm. (a) Cross section view of sandstone conduit. Note the truncation of near horizontal stratification, terminated vertically trending stratification, and the conduit surface rupture. Top scale bar is in cm. (b) Cross-section of fluidized sandstone conduit and associated surface fracture. No expelled material is evident on the paleo-surface. (c) Cross section of sandstone conduit. Note truncation of near horizontal stratification and complexly folded internal stratification. The conduit deforms the top laminations into a dome shape, but does not breach the paleosurface. Top scale bar is in cm. (d) Fluidized sand erupting from the surface fracture.

evidence for Late Jurassic-Early Cretaceous rifting (Van der Beek et al., 1998). Continent-scale tectonic reactivation of major rifts and structural sutures is recognized from 140-120 Ma (Foster and Gleadow, 1992) and is related to far-field stresses associated with the rifting of the African and South American plates. These tectonic events are often associated with syntectonic Cretaceous sedimentary successions (Roberts et al., 2010). Additionally, within a few kilometers of the study area are the Panda Hill and Mbalizi carbonatite volcanoes, which were putatively active during the Cretaceous (Pentelkov and Voronovskii, 1977; Van Straaten, 1989). Crosscutting field relationships and volcaniclastic sediments in the Namba Member strongly suggest that the Namba Member was deposited contemporaneously with the carbonatite volcanism (Fawley and James, 1955; Roberts et al., 2010). Throughout the Cretaceous Galula Formation sandstones, there are abundant and repeated horizons that show evidence for laterally continuous liquefaction and fluidization. In some cases, soft-sediment deformation features in the Namba Member have been directly traced back to syndepositional faults in the rift basin (Fig. 2a; Roberts et al., 2010). More specifically,

the inflation structures and surface fractures described here occur directly in a line with a series of small, syndepositional normal faults that are observed a short distance away at the top of a highly deformed, 2.5 m-thick interval with convoluted bedding, folded laminations and fluidized beds (Fig. 2a). The presence of these soft-sediment deformation features in a long-lived half-graben basin, directly linked with syndepositional growth faults, points to a seismic trigger for the soft-sediment deformation, and hence these newly reported sedimentary structures are best interpreted as seismites.

Although the presence of soft-sediment deformation features such as convoluted bedding, flame structures and other features in these deposits can easily be explained by liquefaction and fluidization of water and sediment during seismic shaking, the morphologies of the newly documented balloon-shaped inflation structures and surface fractures with sandstone splays are unique in the sedimentary record. Comparison with recent empirical investigations suggests an additional element of gas-escape was significantly involved in their genesis.

4.2. The role of gas-escape in soft-sediment deformation

4.2.1. Formation of inflation structures and gas-discharge pits

The balloon-shaped inflation structure, consisting of a subvertical, cylindrical shaft leading to a larger, ovoid form, is a unique sedimentary structure formed via gas-expulsion near, but not breaching, the paleosurface. Experiments illustrate a significant morphological difference between water- and gas-escape generated structures (Furniss et al., 1998; Frey et al., 2009). Comparable to experimental structures formed by Furniss et al. (1998) and Frey et al. (2009), gas moved upwards through the sandstone in straight to semi-winding paths, probably following minor heterogeneities in the sediments, until it reached a barrier and stalled, as an ovoid chamber, a typical gas bubble morphology (Fig. 8; Boudreau, 2012). As the ovoid-to-spherical bubble grows in soft, sandy sediment, the pressure difference between the tip and the tail of the bubble becomes larger, and the bubble shape deviates from an oblate spheroid, adopting an inverted teardrop shape, as seen in the preserved balloon-shaped inflation structures (Figs. 4 and 5; Boudreau et al., 2005; Boudreau, 2012).

The shafts are preserved fractures in soft-sediments through which gases rose (i.e., creation of a bubble tube or path, sensu Boudreau et al., 2005). The multi-directional shafts are likely an indication that the gas was under low pressure, as slight differences in the permeability of surrounding sediments deflected the gas escape path. Sediments experiencing liquefaction and fluidization (e.g., due to earthquake activity) could provide

such a low-pressure, low yield-strength environment. Experiments of bubble propagation through soft-sediment and observations in the rock record generally report on muddy sediment and/or movement through gelatin. The structures reported here are consequential in that they preserve movement paths (shafts) through fine- to medium-grained sand, a less elastic medium in comparison to mud. Most balloon structures are oriented vertically, however, a few are subvertical with shafts preserved near-parallel to the bedding (Fig. 5a). In these cases, gas bubbles moved laterally along more permeable bedding planes when the vertical resistance was encountered (e.g., Boudreau et al., 2005).

Under abnormal stress, as gas moves through water-saturated sediment, the sediment dewaters and increases the viscosity of the surrounding material over time (Furniss et al., 1998). The closer to the surface the gas moved, the more viscous, and impermeable the surrounding sand became, eventually trapping the gas, where it formed ovoids. In addition to this autogenic control, timing might have also played a role in impeding gas movement. During liquefaction, due to the loss of grain-to-grain contacts, sediment behaves as a viscous fluid with little or no yield strength (Owen and Moretti, 2011). After liquefaction, grains settle to close packing, leading to the displacement of excess pore fluid (Owen and Moretti, 2011). Assuming the sediment underwent liquefaction and fluidization, then it is possible that the gas flowed freely while the yield strength of the sediment was reduced, and was trapped following fluid expulsion and subsequent 'stiffening' of the surrounding sand via dewatering. The rising gas pulled sediment entrained in water behind it, effectively pumping the pores and also leading to compaction of the sediment. When conditions were right to prevent the gas from moving towards the surface, the gas expanded at the end of its trail (the preserved shafts), creating the ovoid structures (Fig. 8). This bubble morphology mimics the results of numerical experiments by Katsman (2015) who showed that methane bubbles achieve an inverted teardrop shape and are much bigger and more inflated when moving through stronger, coarser sediment with a high value of fracture toughness.

The ovoid structures and up-warped, anticlinal laminations above collection points of multiple balloon structures are evidence for impeded gas movement (Fig. 4). These accumulations of gas bubbles created gas domes (Fig. 8), some of which erupted, forming surface fractures (see section 4.2.2). Early cementation or a biogenic mat may have formed a less-permeable Cretaceous surface, trapping the gas as individual ovoids, or together in pockets. At higher effusive rates or where slight differences in surface permeability existed, the gas bubbles breached the paleosurface, forming gas-discharge pits (Fig. 5; sensu Jianhua et al., 2004). The concentric fabric in both subsurface and ruptured (gas-discharge pits) inflation structures is attributable to gas pulses through a single conduit that pulled along pulses of watery sediment (Cloud, 1960). An upward directed flow generated in the wake of the bubbles entrains and transports sediment. The fine-grained outer laminae of

the ovoids may represent the initial sediments that were more easily transported by the gas. The ovoid chambers of the inflation structures were eventually filled by watery sediment as the gas escaped via hair-like cracks and/or dissolving into the water. Vertical conduits and concentric laminations in air-discharge pits have previously been attributed to gas-escape features on the Yellow River delta plain (Jianhua et al., 2004). According to Jianhua et al., (2004), air-discharge pits form only in the presence of water, where the environment is pressurized enough for gas to 'erupt' and form a pit.

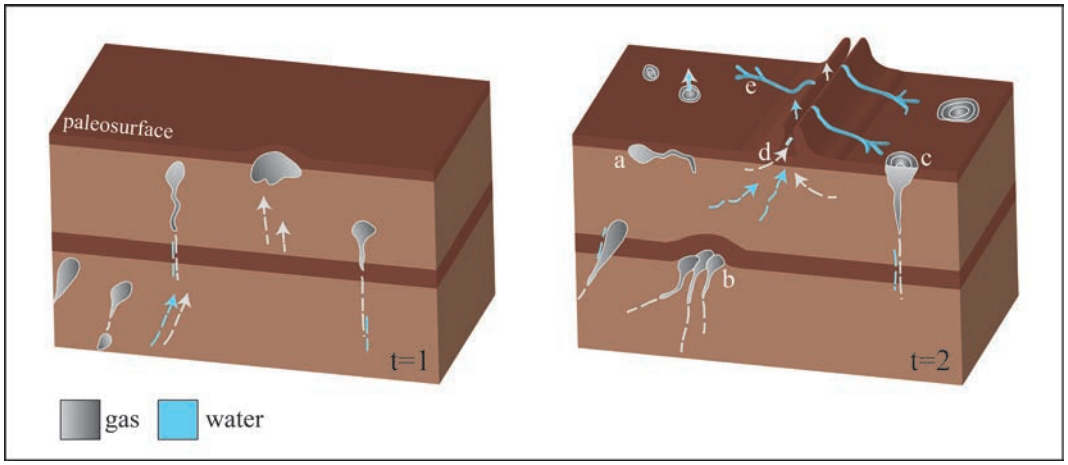

Fig. 8. Time-series cartoon illustrating the genesis of the newly described sedimentary features primarily by gas expulsion. White-grey colors indicate gas, and blue colors indicate a secondary water component. Heterogeneities in the sediment deflected, impeded, and facilitated gas-escape, as manifested by the variety of sedimentary structures preserved in different stages of gas- and water-escape onto the paleosurface. a – inflation structure, see Fig. 5a; b – collection of gas bubbles forming a gas dome, see Fig. 4; c – gas-discharge pit, see Fig 5b; d – surface fracture, see Figs. 6 & 7; e – sandstone splays, see Fig. 6.

4.2.2. Formation of surface fractures with sandstone splays

The surface fractures with associated sandstone splays are evidence of overpressured gas rupturing the early-cemented Cretaceous paleosurface forming a linear fracture (Fig. 8). This is comparable to experiments by Frey et al. (2009) where gas bubbles were observed moving upwards in long, linear fractures. In contrast to the inflation structures described above, the surface fractures represent higher gas effusion rates. The build-up of gas bubbles (now preserved as balloon-shaped inflation structures) beneath an impassable layer suggests permeability heterogeneities in the Namba Member that impeded vertical gas movement. Once formed, the path of a gas bubble is slow to anneal (Boudreau et al., 2005) and so becomes a conduit for the movement of subsequent gas bubbles. At such obstructions, gas likely accumulated and built up to a critical pressure, fracturing the overlying sediment and erupting onto the surface (e.g., Boudreau et al., 2005). The flanks of the surface fractures are marked by upward turned (nearly vertical) laminations (Fig. 7). This characteristic upward warping of laminations is considered a critical point of differentiation of gas-escape, as compared to water-escape, in experiments of Frey et

al. (2009). Continued passage of gas bubbles created chaotic and convoluted bedding in the conduits leading to the surface fractures (also noted by Frey et al., 2009). Subsurface cracks commonly coalesce into conduits or ruptures that may breach the sediment surface, forming mud volcanoes, individual sediment flows, or pools of sediment (Nichols et al., 1994; Pralle et al., 2003; Ross et al., 2011). The thin, finger-like, branching sand splays preserved on the bottom, distal edges of the crack flanks likely formed as small-scale hyperconcentrated flows that were entrained in the wake of moving gas, erupted at the paleosurface, flowed down the flanks of the surface fractures towards topographic lows, and then frictionally froze due to rapid dewatering. Similar gas-driven water expulsion is reported from gas chimneys, which are known to propel water upwards (Cathles et al., 2010).

Experimentally, gas-generated features are not uniformly distributed across the surface, but cluster due to heterogeneities (e.g., bioturbation, cross-laminations, etc.) in the subsurface (Pralle et al., 2003). Heterogeneities are best called upon to explain the horizontal variation in the Cretaceous gas features described here. Additionally, in experiments Pralle et al. (2003) observed that the main formation phase of gas-escape structures was swift (30 minutes) and the interstitial fluid flow due to excess pore pressure causing fluids to migrate vertically destroyed the structure over the following 12 hours.

4.3. A model for gas-generated seismites in the Rukwa Rift

Gas saturated pore waters necessary to produce the features documented in the study area were likely generated and overpressured due to seismic activity along localized faults, as suggested by the region's active tectonic history. We hypothesize that seismicity generated overpressured gas pulses that were released and migrated through the groundwater system, deforming the sediment as the gas passed through (Fig. 8; e.g., Pralle et al., 2003; Frey et al., 2009; Ross et al., 2011). The gas likely moved through the sediment in the form of bubbles (aggregative fluidization), as the density contrast between the fluid and sediment is high (Allen, 1982; Frey et al., 2009). Under static loading conditions, gas bubbles tend to be stable (Wheeler, 1990). Weakening the surrounding sediment can induce gas bubble movement. Cyclic stresses from seismic activity can initiate liquefaction (Owen and Moretti, 2011), creating the conditions necessary to release gas bubbles (Wheeler, 1990). There are few reported examples of shallow, gas-generated features associated with modern earthquakes with which to compare these structures from the Namba Member. Examples include coseismic gas generation by the 7.7 magnitude Bhuj earthquake, as documented by surface vents without associated sand volcanoes and then late stage fluid leakage vents with associated sand volcanoes (Rajendran et al., 2001), and the deformation of clay sediments by CO_2 gas jets associated with seismicity along a shear zone (Bankwitz et al., 2003).

However, taking into consideration the depositional and tectonic environments, morphologies and spatial relationship between these sedimentary structures, and by comparison with the literature and experimental works, the inflation structures and surface fractures reported here most likely formed primarily by gas-escape, with a minor component of water-escape, close to and at the paleosurface of an ancient channel bank deposit (Fig. 8). An initial gas expulsion phase is favored for the generation of these structures rather than water because of: 1) an absence of extensive water-related fluidization features, such as sand volcanoes, sediment pools, and down-turned laminations (e.g., Montenat et al., 2007), and 2) the manner in which the physical structure of balloon-shaped inflation structures appears to mimic gas expansion. The inflation structures are likely shallow subsurface structures formed by lower gas effusion rates, and where they breached the paleosurface, formed gas-discharge pits, comparable to those described by Jianhua et al. (2004; "air-discharge pits" from modern fluvial deposits from the Yellow River). The surface fractures with linked sandstone splays also formed primarily through gas-discharge. The large sandstone conduits linked to the surface fractures reflect a greater effusive rate than the cylindrical shafts linked to the balloon structures, which more aggressively ruptured the paleosurface. This argument is based on conduit diameters, evidence of generation and deformation of internal laminations, as well as potential for paleosurface breaching and deformation. Missing from the Cretaceous pedogenic surface is evidence of large amounts of elutriated sediment, indicating that water was less likely involved in the deformation process than was gas.

Changes in porosity and pressure due to seismic stresses are capable of initiating gas release, and/or increasing gas release rates. Genetic relationships between seismicity and gas discharge of carbon dioxide (Irwin and Barnes, 1980; Mörner and Etiope, 2002), methane (Etiope and Klusman, 2002), and radon (Hauksson, 1981) have been documented. The nearby Panda Hill carbonatite complex represents a proximal source of seismicity in the Rukwa Rift that might best explain the abundance of small-scale syndepositional faulting and seismite features documented in the study area. Pulses of overpressured gas during Cretaceous deposition in the Rukwa Rift Basin may have also been generated by this volcanic/seismic activity. Potential gas sources include: collapsed pores, fractured interbedded anoxic lacustrine deposits (CH_4), volcanogenic degassing (CO_2), CO_2 released from hydrothermal springs, and/or thermogenic gas from the underlying Karoo shales. Non-marine limestone is reported from the Galula Formation near Usevia and may also indicate a hydrothermal gas source, similar to the present-day CO_2–rich geothermal system in the Mbeya area.

5. Summary

Cretaceous rift strata in Tanzania exhibit unique sedimentary structures developed in a low groundwater setting, including: 1) balloon-shaped inflation structures and 2) surface fractures with linked sandstone splays. The expressions of soft-sediment deformation are attributable to localized seismic events in the Cretaceous East African Rift that generated gas release coupled with a subsequent water-escape phase. These new sedimentary structures are easily recognizable and allow more detailed interpretation of the impact of seismic activity, and generally of gas-release by any triggering mechanism. Observations further support the possibility of preserving gas-escape related deformation structures in the rock record, and emphasize the significant role gas can play as an agent of sediment transport and mechanism of sedimentary structure formation and alteration. For shallow deformation within 10 meters of the surface, over pressuring of water rather than gas is more often called upon to generate soft-sediment deformation associated with seismic activity (Obermeier, 1996). However, gas-generated soft-sediment deformation features are observed (Jianhua et al., 2004) and experimentally generated (Wheeler, 1990; Furniss et al., 1998) in near-surface environments. Although gas-escape generated sedimentary structures are rarely identified from ancient environments, they are likely more common than documentation reveals due to the difficulties in differentiating between gas- and water-escape mechanisms. It is important to continue to refine the classification schemes for soft-sediment deformation structures to accommodate for the genesis of sedimentary structures by gas-escape, which is traditionally not appreciated, and it is fruitful to investigate both empirically and experimentally.

Chapter Three

Application of U-Pb detrital zircon geochronology to drill cuttings for age control in hydrocarbon exploration wells: a case study from the Rukwa Rift Basin, Tanzania

In press: *The AAPG Bulletin*

Abstract

Precise dating and correlation of drilled wells through continental successions is challenging for hydrocarbon exploration, especially where preservation and recovery of age-diagnostic fossils is poor. As a complement or alternative to biostratigraphic dating we demonstrate the effectiveness of U-Pb geochronology via LA-ICP-MS on detrital zircon from well cuttings. In basins with syndepositional volcanic input, the youngest zircons in a stratigraphic interval can refine and serve as a proxy for the age of deposition. We demonstrate the reliability of this technique when applied to hydrocarbon exploration wells by analyzing drill cuttings through a continental interval of the Galula-1 well in the Rukwa Rift Basin, East African Rift System, Tanzania, which previously yielded conflicting biostratigraphy results. The lower 1/3 of the well section reveals a late Miocene to Pliocene up-hole younging trend in the youngest detrital zircon populations, which matches new radioisotopic ages on volcanic tuffs from a correlative outcrop section. This is followed by an interval with recycled young zircons, followed by a zircon-free interval, interpreted to correspond with changes in magma composition of the nearby Rungwe Volcanic Province. This study provides the first radioisotopic age constraints for the Lake Beds in the Rukwa Rift, and demonstrates that sedimentation in the basin began by 8.7 Ma, critical for burial and thermal history modeling and establishing the probability of a working hydrocarbon system. Correspondence in age and zircon preservation between well and outcrop samples from the same intervals provides strong support for applying U-Pb detrital zircon geochronology to well cuttings, as a rapid, inexpensive approach for hydrocarbon exploration.

1. Introduction

Critical decisions made during exploration and field development of prospective hydrocarbon bearing plays are underpinned by accurate stratigraphic control and correlation within and between wells. Biostratigraphy, the conventional method for such dating and correlation of sedimentary rocks, is not always possible or reliable. For example, oxidized red-bed successions and other, typically continental, intervals commonly yield depauperate microfossil and/or pollen assemblages, and in some cases lack preservation altogether. Accurate dating and correlation of sequences where microflora and fauna are limited or absent is now more critical than ever, as global hydrocarbon exploration moves to consider biostratigraphically-lean frontier basins.

As one of the next hydrocarbon frontiers, East Africa hosts a suite of prospective rift basins with characteristics amenable to hydrocarbon generation, including deep depocenters with rapid sediment accumulation and high heat flow, promoting early thermal maturation ('petroleum kitchens'; Tiercelin et al., 2012). However, an absence of reliable index fossils in these non-marine, intracratonic rift basins often limits the use of traditional biostratigraphic dating methods. Assessing essential elements of the petroleum system such as basin structure; composition and architecture of sedimentary successions; and thermal history (Cohen, 1989; Nelson et al., 1992; Morley, 1995), hinges on the accurate dating of sedimentary successions; and where biostratigraphy is poor, alternative means of dating are important. Rift settings, in particular, require temporal resolution for understanding their complex tectonic histories and the timing between such key events as rift lake development, volcanism, and uplift, all of which have a major impact on hydrocarbon prospectivity. Recent onshore successes, such as hydrocarbon discoveries in the Turkana (Lokichar) and Albertine rift basins, have renewed interest in exploring other rift segments along the East African Rift System (EARS). In particular, the western branch of the EARS has seen considerable hydrocarbon exploration since 2007, when the Kingfisher-1 discovery in the Albertine Graben demonstrated the commercial hydrocarbon potential of these rift basins (Logan et al., 2009).

Other innovative approaches to correlation and depositional age approximation have been used successfully, such as chemostratigraphic techniques (Ratcliffe et al., 2015), Sm-Nd isotope analysis (Dalland et al., 1995), and fission track dating (Carter et al., 1995), though not all of these approaches provide age constraint. Radioisotopic dating of ash beds in core samples, or correlation of wells to dated ash beds in outcrop, is the most common alternative for dating sedimentary units where biostratigraphy is problematic or greater precision is required. In recent years the increasing throughput and decreasing costs of laser ablation-inductively coupled plasma-mass spectrometry (LA-ICP-MS) U-Pb

detrital zircon geochronology have opened this technique to a much greater number of applications. In particular, recent papers have highlighted the potential of dating large numbers of detrital zircons from sedimentary units with the express intent of identifying the youngest population of grains as a means of constraining the maximum depositional age (Dickinson and Gehrels, 2009; Lawton et al., 2010; Tucker et al., 2013). Although studies have focused on the application of detrital zircons and other minerals for maximum depositional age constraint, it is noteworthy that in petroleum geology, a field for which this approach has great potential, there has been limited application of this technique to date. This is perhaps due to the uncertainty of applying the technique to well cuttings (for which sample sizes are typically limited), concerns about possible contamination issues, as well as issues associated with proprietary data.

A primary concept in the use of detrital zircons for dating the deposition of sediments is that the radiometric age of zircons derived from volcanic sources record the date of the eruptive event(s). The technique is most useful where eruptive volcanic events occur in proximity to active sedimentary basins and there is an expectation that the erupted zircons are essentially coeval in age to the sediments into which they are deposited. This assumption is likely to widely pertain to much of the East African Rift System. Thus, when the ages of zircon populations within the sediments are determined, the older populations, while useful in provenance studies, can be excluded, and the youngest population can be used to define the maximum age of sediment deposition. In such cases, the maximum depositional age (i.e., the age of the youngest zircon population, for which the sediments cannot be older than) is a proxy for the depositional age of the sedimentary unit from which the zircons derive (Dickinson and Gehrels, 2009; Lawton et al., 2010; Tucker et al., 2013).

Here we apply detrital zircon geochronology to systematically investigate maximum depositional ages from well cuttings through the Miocene-Recent Lake Beds succession in the Galula-1 well in the Rukwa Rift of Tanzania (Fig. 1). This work has been undertaken in combination with stratigraphic investigations and radioisotopic dating of volcanic tuffs from a control section logged through the Lake Beds succession in outcrop. This approach is designed to provide an independent test of this method via correlation between the subsurface and outcrop. This paper evaluates the application of U-Pb detrital zircon geochronology for age control of stratigraphic units and correlation in petroleum exploration wells, which has great potential for refining depositional ages of continental sedimentary basins around the world that are often notorious for ambiguous biostratigraphy and poor age constraint. Using these ages in combination with absolute ages dated herein from newly discovered volcanic tuffs in outcrop, we are able to delineate the timing of sedimentation (and therefore, late Cenozoic rifting) in this part of the western branch of the East African Rift System for the first time. These results are highly encouraging and

strongly support the potential for applying U-Pb detrital zircon geochronology via LA-ICP-MS to well cuttings in certain basin types as an effective exploration tool in petroleum geology for improving temporal resolution in wells through poorly constrained intervals.

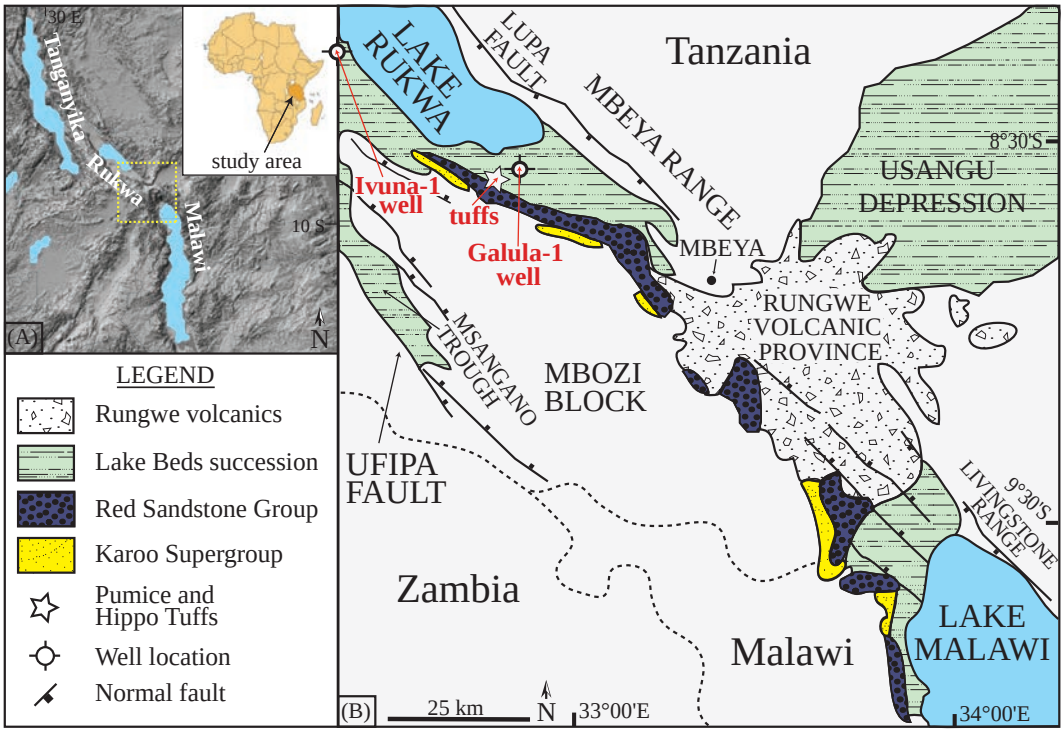

Fig. 1. A) Map of the Tanganyika-Rukwa-Malawi rift segment (western branch, East African Rift System) modified from the NASA Shuttle Radar Topography Mission collection. Inset map shows the location of the study area within Africa and the yellow dotted box shows the location of map B. B) Geologic map of Phanerozoic sedimentary deposits in the southern Rukwa Rift and northern Malawi Rift basins. The sample sites are labeled.

2. Rukwa Rift Basin Geology

The western branch of the East African Rift System is characterized by a series of linked, elongate sedimentary basins that typically follow preexisting Paleoproterozoic basement structures. The Rukwa Rift Basin in southwestern Tanzania is a ~300 km-long by ~50 km-wide, half graben basin occupying the middle of the Tanganyika-Rukwa-Malawi (TRM) rift segment, which forms the NW-trending southern portion of the western branch (Fig. 1). The TRM rift segment has been affected by repeated rifting cycles and fault reactivation from Paleozoic to Recent times (Delvaux et al., 2012). Initiation of Cenozoic rifting in the western branch of the EARS began by 25 Ma with the opening of the Rukwa Rift (Roberts et al., 2012), followed by development of the Tanganyika Rift between 12-9 Ma (Cohen et al., 1993), and the Malawi Rift by at least 8.6 Ma (Ebinger, 1989; Ebinger et al., 1993).

The Rukwa Rift Basin preserves a major sedimentary succession (at least 8 km thick), representing a rich archive of tectonic and environmental change (Roberts et al., 2012 and therein). Paleozoic to Holocene rifting and sedimentation is recorded in the basin by

a suite of sedimentary deposits, which are subdivided into the: 1) Permo-Triassic Karoo Supergroup, 2) Cretaceous Galula Formation, 3) Oligocene Nsungwe Formation, and 4) Miocene-Recent Lake Beds succession. The last of these depositional sequences, the Miocene-Recent Lake Beds succession, is the focus of the case study presented herein, and is the primary target for ongoing hydrocarbon exploration in the rift. The Lake Beds succession is best exposed on the basin margins, where it is composed of variably consolidated conglomerates, sandstones, siltstones, and mudstones, along with intercalated volcanic tuffs. Volcanic-rich fluvial, alluvial, and deltaic deposits are common at the peripheral basin exposures, and the depocenter is modeled as being composed of finer grained, deeper water lacustrine sequences (Kilembe and Rosendahl, 1992). The Miocene-Recent Rungwe Volcanic Province on the southern margin of the basin covers over 1500 km2 (Fig. 1), where it developed along a complex tectonic junction between multiple rift branches, including the Rukwa Rift, Usangu Basin and northern Malawi Rift. The sedimentary strata of the Lake Beds are largely derived from the uplifted metamorphic basement rock and from the Rungwe volcanics.

This study presents the first absolute age constraints on the deposition of the Lake Beds succession. There is a long history of conflicting age interpretations for strata in the rift, though it has generally been accepted that the Lake Beds are Neogene to Pleistocene in age (Stockley, 1938; Spence, 1954). Quenell et al. (1956) suggested the Lake Beds were dominantly Pleistocene strata, whereas Pentelkov (1979) assigned the lower part of the Lake Beds to the Cretaceous. Published geological survey maps over the area (e.g., van Loenen and Kennerly, 1962) ascribe a Neogene age to the Lake Beds. More recently, outcrop investigations of the uppermost portion of the Lake Beds have proposed a latest Quaternary to Holocene age for the upper 50-100 meters of the formation (Cohen et al., 2013; Hilbert-Wolf and Roberts, 2015; Mtelela et al., in press) and further biostratigraphic analyses are underway by our research group. In 1987 the Amoco Tanzania Oil Company drilled two exploration wells in the Rukwa Rift Basin, Ivuna-1 and Galula-1. In the published biostratigraphic analysis of these wells Wescott et al. (1991) were only able to assign broad ages, suggesting that the Lake Beds are for the most part Pliocene to Holocene, based on a limited range of palynomorphs and diatoms. These workers also assigned Miocene to Holocene ages to the underlying Red Sandstone Group, which has now been dated as Cretaceous to Oligocene based on extensive vertebrate biostratigraphy and high-precision radioisotopic dating (Roberts et al., 2010, 2012; Stevens et al., 2013). Stimulated by the significant Neogene discoveries in Turkana (Lokichar) and Albertine Basins, the Rukwa Rift Basin is once again a focus for investigation of its hydrocarbon potential. A critical element in the determination of the Lake Beds prospectivity, particularly source rock maturation, is clear resolution of the formations age(s). Thus, an unconventional approach for dating the well sections was sought and the possibility of using detrital zircon LA-ICP-

MS U-Pb geochronology to refine the temporal resolution of this unit was investigated.

3. Methods

3.1. LA-ICP-MS U-Pb Geochronology

The supply of cuttings from the Galula-1 and Ivuna-1 wells was very limited, so sample sizes were increased by aggregating a number of individual cuttings samples over depth ranges from 150-360 ft (46-110 m; average 226 ft / 69 m) to enhance zircon yield. Twelve composited samples were selected from the Lake Beds succession over the interval 3150-90 ft (960–27.4 m) in the Galula-1 well (0489729 E 9053938.8 N; UTM zone 36, ARC 1960 datum), with each sample initially weighing between 150 and 500g. Two samples from the Ivuna-1 well (0423732.4 E 9087313.4 N; UTM zone 36, ARC 1960 datum) were also investigated for a pilot study, but zircon yield was low, likely reflecting the dominance of fine-grained lacustrine shale facies closer to the paleo-depocenter. In outcrop, tuffs of the Lake Beds succession are distinctive and were identified by their clay-dominated composition, including relict pumice shapes and textures (now devitrified). The tuffs range in color from white, to grey, to brown, to purple. The basal, phenocryst-rich horizons were targeted for sampling.

Samples were crushed and milled (when necessary) in a tungsten carbide disc mill and sieved at various size fractions, with all grains < 500 μm recovered to enhance the possibility of sampling the widest range of zircon sizes, including distal volcanic ash derived zircons. Heavy minerals were separated using lithium polytungstate adjusted to a specific gravity of 2.85. Mineral separates were then washed, dried, and a hand magnet was used to remove strongly magnetic minerals, followed by a Frantz magnetic separator at progressively higher magnetic currents of 0.5A, 0.8A, 1.2A, and 1.4A, set at a constant 10° side slope. The non-magnetic heavy mineral separates were treated according to hybrid selection protocols that involved handpicking zircons as randomly as possible from the greater population within a defined field of view. Following this, the remainder of each sample was handpicked a second time with the intention of selecting the clearest, most euhedral grains remaining in each sample, to increase the likelihood of analyzing age constraining young zircons. Depending on sample size and zircon yield, ~60-100 grains (or as many as were recovered, if less than this) were mounted in a 25mm epoxy resin puck, polished to expose their mid-sections and imaged using a Jeol JSM5410LV scanning electron microscope with attached cathodoluminescence detector in order to document microstructures, cracks, inclusions, inherited cores, and other zircon grain complexities.

All LA-ICP-MS U-Pb analyses were conducted at the Advanced Analytical Centre of James Cook University, using a Coherent GeolasPro 193nm ArF Excimer laser ablation system connected to a Bruker 820-MS (formerly Varian 820-MS). Zircons were analyzed using the same, optimized LA-ICP-MS method outlined in Tucker et al. (2013). Laser spot sizes varied between 32 μm and 44 μm according to the size and morphology of sample and standard zircons. However, for a given set of standard and unknown analyses, spot size remained constant. The total measurement time was set at 70 seconds per analysis. The first 30 seconds were for gas blank measurement, and during the final 40 seconds the shutter was opened to allow for sample ablation and measurement. At the beginning and end of each sample, as well as after every 10 or so unknown grains, at least two analyses each of the primary zircon standard GJ1 (608.5 ± 0.4 Ma, 2σ; Jackson et al., 2004) and the secondary zircon standards Temora-2 JCU (416.8 Ma ± 1.1 Ma, 2σ; Black et al., 2003) and Fish Canyon Tuff (28.5 ± 0.03 Ma, 2σ; Schmitz and Bowring, 2001) were completed to monitor down-hole fractionation and for age and instrument-drift corrections. All secondary standard analyses were within 1-2% of the expected ages. Due to instrumental drift during the course of a day, different calibrations were used to correct for this, including either linear or average fitting of the standards. NIST 610 or 612 was analyzed at the beginning, middle, and end of each session for the purpose of calibrating Th and U concentrations. Data reduction and age calculations based on measured isotope ratios were carried out using the Glitter software (Van Achterbergh et al., 2001). All time-resolved isotope signals were filtered for signal spikes or perturbations related to inclusions and fractures, and then background and sample intervals were selected based on evaluation of the most stable and representative isotope ratios. Isoplot/Ex version 4.15 (Ludwig, 2012) was used for extracting ages from multi-grain populations (i.e., calculating weighted means). $^{206}Pb/^{238}U$ ages have been reported for zircon grains younger than 1.0 Ga and $^{207}Pb/^{206}Pb$ ages are preferred for zircon grains older than 1.0 Ga. Where applicable, $^{206}Pb/^{238}U$ ages were corrected for common Pb based on the Pb isotope evolution model of Stacey and Kramers (1975). Zircon grains with an age discordance ≥ 30% were omitted from the samples and from this study as a whole. However, in young zircon grains (e.g., < 10 Ma) the production of radiogenic Pb is typically low, and hence the $^{207}Pb/^{206}Pb$ age can be discordant, so the above criterion was not applied.

3.2. Recommendations for sampling

Sampling a well or borehole for LA-ICP-MS U-Pb zircon geochronology is dictated by the availability of well cuttings or cores, and by the project-specific aims of a dating campaign. A few general strategies may maximize the likelihood of obtaining reliable maximum depositional ages. Sandy intervals are sometimes more likely to contain zircon than muddy intervals, and similarly, volcaniclastic sandstones and tuffs are preferred because

if the volcanic source was zircon-fertile, these units are likely to contain depositional-age defining volcanic zircons. A potential limitation to applying this approach to cuttings from existing wells is the small sample sizes generally available (commonly <200 g per sample per depth interval), in comparison to outcrop detrital zircon samples where ~2-5 kg (or more) of sample is typically collected. The retention and collection of larger well cutting samples can be prearranged when detrital zircon dating is planned prior to drilling. A large sample from each targeted depth would be preferable to combining smaller volume well cuttings over longer intervals, to minimize mixing and to increase dating resolution. However, in studies involving legacy wells and well cuttings, large sample sizes may not be possible and the approach utilized in this study to increase sample size by combining cuttings over a few hundred feet may still be the best option. We also recommend that care is taken in the selection and recording of the drilling fluids that are used, in order to avoid or recognize potential contamination issues. If possible, it is best not to pre-wash well cuttings before the mineral separation process, as this may lead to the unnecessary loss of very fine-grained zircon crystals. All mineral separates should be retained for alternative dating approaches (e.g., U-Pb on titanite; Ar/Ar on detrital sanidine). In some cases, through careful mineral separation, this approach may be a gateway to discovering other datable radiogenic minerals capable of recording depositional age, such as detrital apatite, titanite, monazite, or sanidine.

3.3. Calculating maximum depositional ages

Due to the uncertainties associated with U-Pb isotopic systematics, multiple approaches are often used to define the youngest detrital zircon age population (Dickinson and Gehrels, 2009). When working with detrital minerals it is important to compare and evaluate results from each approach and to assess maximum depositional ages by correlation with existing biostratigraphy, well-dated tuffs, or other means if available. We applied four robust approaches to each sample for determining maximum depositional ages, including: 1) youngest single grain (YSG); 2) weighted mean of the 3 youngest grains (WM); 3) weighted mean age of the youngest cluster of two or more grains overlapping in age at 1σ (YC1σ; Dickinson and Gehrels, 2009); and 4) weighted mean age of the youngest cluster of three or more grains overlapping in age at 2σ (YC2σ; Dickinson and Gehrels, 2009). Other calculations may also be applied to determine maximum depositional ages (e.g., "TuffZirc" algorithm of Ludwig and Mundil, 2002), however here we have chosen robust approaches that are most suitable to the size and nature of our dataset. Approaches 2, 3, and 4 produced similar maximum depositional ages where there were enough grains to calculate a mean age, and all revealed a younging trend in the bottom three to four Galula-1 well samples (Fig. 2). Similarly, the youngest single grain ages through the ~950-625 m intervals in the Galula-1 well show a zircon younging trend (i.e., a depositional age younging trend),

although these ages are ≤1 Ma younger than calculated maximum depositional ages using methods 2-4. While it may be best practice to consider the youngest population (n ≥ 2) of zircons when estimating depositional age, as shown in Figure 2, the youngest single grains throughout the Galula-1 well are also reliable indicators of depositional age, as it is unlikely these crystals experienced Pb-loss due to their young crystallization ages and the lack of late Cenozoic metamorphic activity affecting this region. However, maximum depositional ages based on the youngest populations of zircons, rather than on single grain ages, are more consistently compatible with depositional ages (Dickinson and Gehrels, 2009). In all cases, biostratigraphy, dating tuffs where available, and knowledge of the age of contemporaneous, nearby volcanic deposits is ideal for evaluating such maximum depositional ages (Fig. 3).

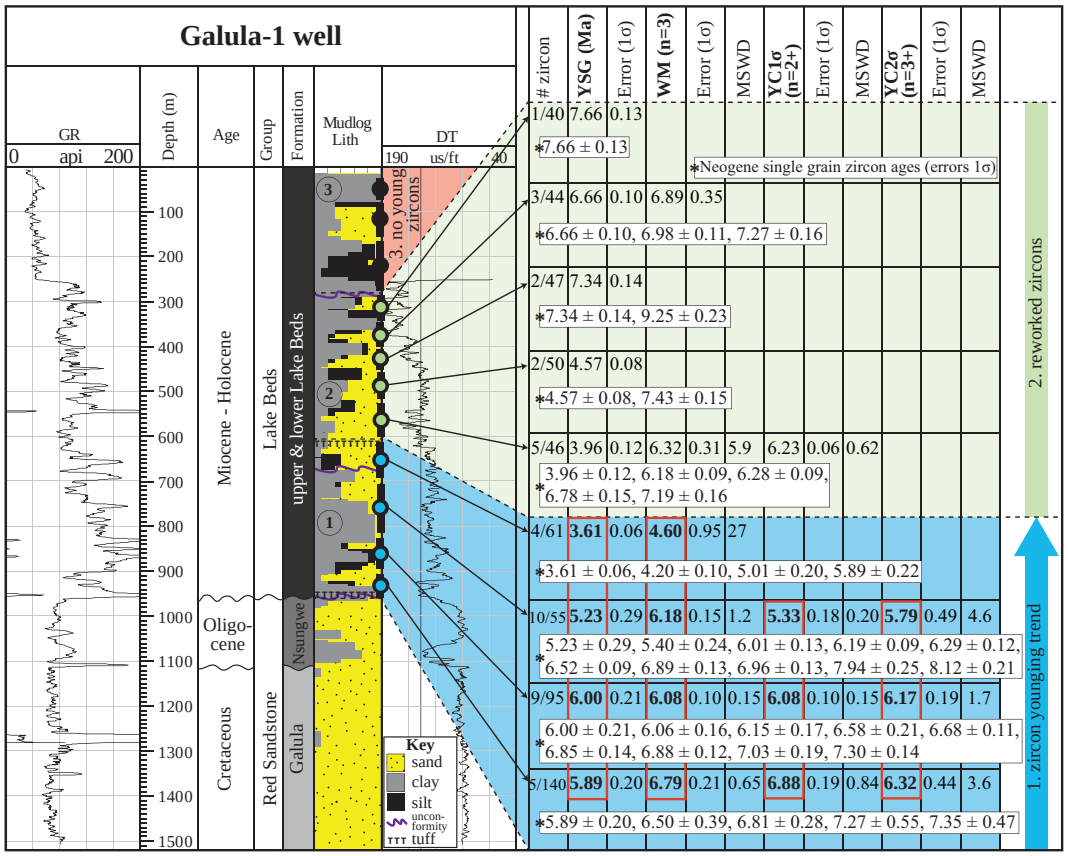

Fig. 2. Stratigraphically ordered display of all Neogene zircons recovered from the Galula-1 well cuttings (single grain ages are listed in white boxes). The results of four different methods for calculating maximum depositional age for each sample interval are shown, and up-hole younging trends are highlighted by rectangles (red, in color version of figure). See text for details about the calculations. # zircon = number of Neogene zircon ages / total number of concordant zircon ages acquired; YSG = youngest single grain; WM = weighted mean; YC1σ (2+) = weighted mean of youngest zircon cluster of ≥ 2 grains overlapping in age at 1σ; YC2σ (3+) = weighted mean of youngest zircon cluster of ≥ 3 grains overlapping in age at 2σ; MSWD = mean square weighted deviation. Galula-1 well log data was provided by Heritage Rukwa Tanzania Limited. Stratigraphic interpretations are based on Roberts et al. (2004; 2010) and all available well data sets (not all presented here). Dashed lines through the 'mudlog lithology' are suggested unconformities, based on three distinct detrital zircon zones: (1) up-hole zircon younging trend (zircons of Neogene age); (2) reworked Neogene zircons; (3) no Neogene zircons. Wavy lines (purple in colored figure) represent correlated unconformities recognized in outcrop and rows of "T" symbols show the correlated stratigraphic positions of tuffs from outcrop (see Fig. 3).

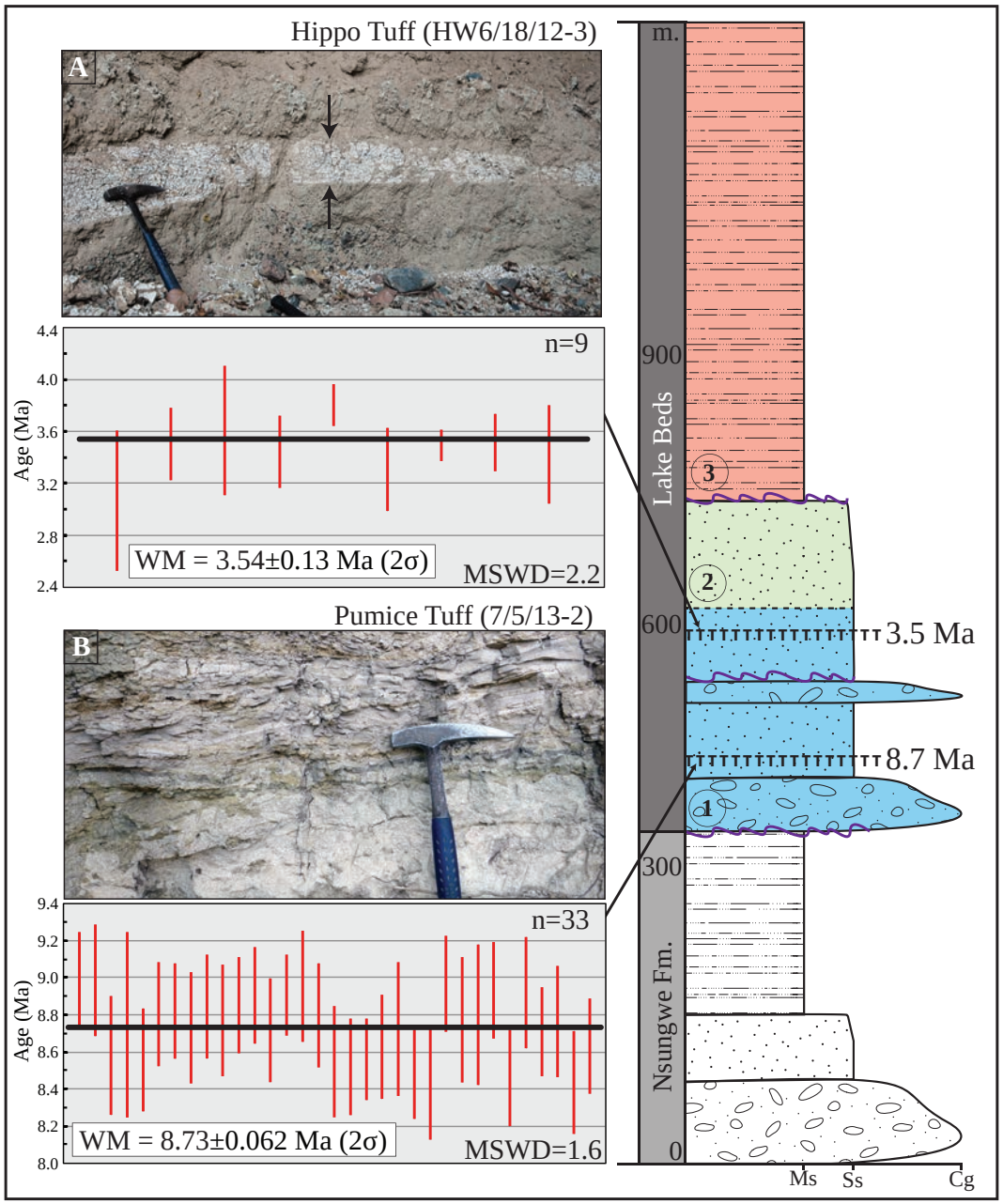

Fig. 3. LA-ICP-MS U-Pb ages of two newly dated volcanic tuffs from the Lake Beds in outcrop, located within a composite stratigraphic section (position of tuffs denoted by rows of "T" symbols). The three indicated zones correlate with the zones distinguished in Fig. 2. Wavy lines (purple in color figure) represent unconformities recognized in outcrop. Ms = mudstone; Ss = sandstone; Cg = conglomerate.

4. Reliable depositional age constraints acquired from well cuttings

4.1. Geochronology results

Twelve samples from the Galula-1 exploration well yielded 638 concordant U-Pb detrital zircon ages. The dominant detrital zircon age populations for the Lake Beds include: 1) 3100-2500 Ma, 2) 2200-1800 Ma, 3) 1050-950 Ma, 4) 900-500 Ma, and 5) 8.7-3.5 Ma. Young, Neogene zircons (< 10 Ma) are present in the nine deepest Lake Beds samples and

constitute 2.5 - 18.2% of the dated zircons from each interval. All Neogene zircon ages are reported in Table 1 and in Figure 2 in the white boxes corresponding to each sampled well interval. For the purposes of this study, only the youngest detrital zircon populations are reported in Figure 2 and Table 1. However, the full detrital zircon datasets for each of the 12 samples from the Galula-1 well are available via the AAPG's Datashare. All tuff zircon ages acquired from this study are reported in Figure 3 and Table 2. Zircon recovery decreased significantly from the deepest (960 m / 3,150 ft) to shallowest (27.5 m / 90 ft) intervals sampled from the Lake Beds in the Galula-1 well.

Maximum depositional ages for Neogene zircon-bearing samples were calculated via the four methods described above (YSG, WM, YC1σ, and YC2σ). The deepest four Lake Beds samples reveal maximum depositional ages that young from ~6.9 to 4.6 Ma towards the top of the Galula-1 well (Fig. 2), which correlate well with the ages of two tuffs recognized in outcrop, also from the lower part of the Lake Beds strata. These two tuffs from the Lake Beds were identified in the field along the Hamposia River Section (Figs. 1 and 3). Volcanic zircons from each tuff were sampled and dated using the same LA-ICP-MS U-Pb methodology as applied to the Galula-1 well cuttings (Fig. 3). The lower tuff (Pumice Tuff: 7/5/13-2; 0480150 E 9045105 N; UTM zone 36, ARC 1960 datum), 29 m from the base of the Lake Beds, yields a U-Pb zircon age of 8.7 ± 0.03 Ma (1σ; Fig. 3 and Table 2). The Hippo Tuff (HW6/18/12-3; 0480513 E 9047045 N; UTM zone 36, ARC 1960 datum), approximately 75 m above the Pumice Tuff, yields a U-Pb zircon age of 3.5 ± 0.07 Ma (1σ; Fig. 3 and Table 2).

4.2. Interpretation of zircon depositional ages for the lower Lake Beds

The U-Pb zircon ages we report here are the first radioisotopic ages for the lower Lake Beds succession. The Pumice Tuff, which sits 29 m above the base of the Lake Beds, yields a depositional age of 8.73 ± 0.06 Ma (2σ), which we interpret to record the age of the initiation of the last major phase (Miocene-Recent) of basin development and sedimentation in the Rukwa Rift. The age of this tuff corresponds to the initiation of the Rungwe Volcanic Province, and is possibly correlative with the early Rungwe volcanic activity, such as the 8.60 ± 0.01 and 8.15 ± 0.02 Ma (1σ) Songwe phonolitic tuffs in the Karonga Basin of the northern Lake Malawi Rift (Ebinger et al., 1993) or to the 9.2 ± 0.4 Ma trachyte dome in the Usangu Basin (Ivanov et al., 1999).

Subdivision of the Lake Beds in the Galula-1 well is possible based on the presence or absence of Neogene, depositional-age-constraining zircons. The Lake Beds in the Galula-1 well can be divided into three zones based on patterns of Neogene-aged detrital zircons (Fig. 2): 1) zone of maximum depositional age-constraining zircons that progressively

Galula-1 well	**930'-1120'** (n=1)		**1140'-1310'** (n=3)		**1330'-1480'** (n=2)		**1500'-1690'** (n=2)		**1730'-1970'** (n=5)	
	$^{206}Pb/^{238}U$ age (Ma)	Error (1σ) (Ma)	$^{206}Pb/^{238}U$ age (Ma)	Error (1σ) (Ma)	$^{206}Pb/^{238}U$ age (Ma)	Error (1σ) (Ma)	$^{206}Pb/^{238}U$ age (Ma)	Error (1σ) (Ma)	$^{206}Pb/^{238}U$ age (Ma)	Error (1σ) (Ma)
Youngest (Ma)	**7.66**	**0.13**	**6.66**	**0.10**	**7.34**	**0.14**	**4.57**	**0.08**	**3.96**	**0.12**
			6.98	0.11	9.25	0.23	7.43	0.15	6.18	0.09
			7.27	0.16					6.28	0.09
									6.78	0.15
									7.19	0.16
WM (Ma) n=3	*n/a*		*6.89*	*0.35*	*n/a*		*n/a*		*6.32*	*0.31*
YC1σ (2+; Ma)	*n/a*		*n/a*		*n/a*		*n/a*		*6.23*	*0.06*
YC2σ (3+; Ma)	*n/a*		*n/a*		*n/a*		*n/a*		*n/a*	

Galula-1 well	**2010'-2270'** (n=4)		**2310'-2670'** (n=10)		**2710'-2930'** (n=9)		**2970'-3150'** (n=5)	
	$^{206}Pb/^{238}U$ age (Ma)	Error (1σ) (Ma)	$^{206}Pb/^{238}U$ age (Ma)	Error (1σ) (Ma)	$^{206}Pb/^{238}U$ age (Ma)	Error (1σ) (Ma)	$^{206}Pb/^{238}U$ age (Ma)	Error (1σ) (Ma)
Youngest (Ma)	**3.61**	**0.06**	**5.23**	**0.29**	**6.00**	**0.21**	**5.89**	**0.20**
	4.20	0.10	5.40	0.24	6.06	0.16	6.50	0.39
	5.01	0.20	6.01	0.13	6.15	0.17	6.81	0.28
	5.89	0.22	6.19	0.09	6.58	0.21	7.27	0.55
			6.29	0.12	6.68	0.11	7.35	0.47
			6.52	0.09	6.85	0.14		
			6.89	0.13	6.88	0.12		
			6.96	0.13	7.03	0.19		
			7.94	0.25	7.30	0.14		
			8.12	0.21				
WM (Ma) n=3	*4.6*	*0.95*	*6.18*	*0.15*	*6.08*	*0.10*	*6.79*	*0.21*
YC1σ (2+; Ma)	*n/a*		*5.33*	*0.18*	*6.08*	*0.10*	*6.88*	*0.19*
YC2σ (3+; Ma)	*n/a*		*5.79*	*0.49*	*6.17*	*0.19*	*6.32*	*0.44*

WM = weighted mean; YC1σ = weighted mean of youngest cluster of two or more grains overlapping in age at 1σ;
YC2σ = weighted mean of youngest cluster of three or more grains overlapping in age at 2σ

Table 1. $^{206}Pb/^{238}U$ ages of youngest detrital zircon populations from the Galula-1 well cuttings. Maximum depositional ages are calculated (italics).

Pumice Tuff (7/5/13-2)			Hippo Tuff (HW6/18/12-3)		
Spot ID	$^{206}Pb/^{238}U$ age (Ma)	Error (1σ) (Ma)	Spot ID	$^{206}Pb/^{238}U$ age (Ma)	Error (1σ) (Ma)
7-5-13-2-1	8.99	0.13	HW6/18/12-3-5	3.06	0.27
7-5-13-2-2	8.98	0.15	HW6/18/12-3-8	3.50	0.14
7-5-13-2-4	8.58	0.16	HW6/18/12-3-19	3.61	0.25
7-5-13-2-5	8.75	0.25	HW6/18/12-3-31	3.44	0.14
7-5-13-2-6	8.56	0.14	HW6/18/12-3-32	3.80	0.08
7-5-13-2-7	8.80	0.14	HW6/18/12-3-33	3.30	0.16
7-5-13-2-8	8.82	0.13	HW6/18/12-3-36	3.49	0.06
7-5-13-2-9	8.73	0.15	HW6/18/12-3-45	3.51	0.11
7-5-13-2-10	8.84	0.14	HW6/18/12-3-50	3.42	0.19
7-5-13-2-11	8.77	0.15	*weighted mean*	*3.54*	*0.07*
7-5-13-2-14	8.85	0.13			
7-5-13-2-15	8.90	0.13			
7-5-13-2-16	8.72	0.14			
7-5-13-2-17	8.91	0.11			
7-5-13-2-18	8.95	0.15			
7-5-13-2-19	8.79	0.14			
7-5-13-2-20	8.55	0.15			
7-5-13-2-21	8.52	0.13			
7-5-13-2-22	8.56	0.11			
7-5-13-2-23	8.62	0.14			
7-5-13-2-24	8.72	0.18			
7-5-13-2-25	8.48	0.12			
7-5-13-2-26	8.43	0.15			
7-5-13-2-28	8.97	0.13			
7-5-13-2-29	8.77	0.17			
7-5-13-2-30	8.80	0.19			
7-5-13-2-31	8.93	0.13			
7-5-13-2-32	8.46	0.13			
7-5-13-2-34	8.92	0.15			
7-5-13-2-35	8.71	0.12			
7-5-13-2-36	8.76	0.15			
7-5-13-2-39	8.44	0.14			
7-5-13-2-40	8.63	0.13			
weighted mean	*8.73*	*0.03*			

Table 2. $^{206}Pb/^{238}U$ ages of tuff zircons from outcrop samples 7/5/13-2 (Pumice Tuff) and HW6/18/12-3 (Hippo Tuff).

young upwards (blue zone 1); 2) zone of reworked Neogene zircons (i.e., no younging trend; green zone 2); and 3) zone containing no Neogene zircons (red zone 3). A zircon younging trend recorded in the four deepest sampled Lake Beds intervals (Fig. 2: zone 1) establishes maximum depositional ages from 6.88 ± 0.19 to 4.60 ± 0.95 Ma (1σ) in the well. A combination of zircon zonal partitioning, lithostratigraphy, and zircon-based maximum depositional ages allows for a strong correlation between the Galula-1 well and the two dated tuffs and stratigraphic unconformities identified in outcrop (Figs. 2 and 3). The two dated tuffs bracket zone 1 stratigraphically (Figs. 2 and 3). Zone 1 is underlain by the 8.73 ± 0.06 Ma (2σ) Pumice Tuff and capped by the 3.54 ± 0.13 Ma (2σ) Hippo Tuff (Fig. 3), which nicely fits the upward younging trend of depositional age-defining detrital zircons

from ~6.9 to 4.6 Ma that is recorded in the well samples that correlate stratigraphically to between these two tuffs. This provides corroborating evidence to support the accuracy of maximum depositional ages recorded by detrital zircon in the Galula-1 well, strongly supporting the application of this approach.

After ~3.5 Ma, zircon-generating volcanism capable of reaching the southern end of the Rukwa Rift Basin apparently ceased in the Rungwe Volcanic Province, as the middle of the Lake Beds Succession recorded in the Galula-1 well contains only reworked ~9-4 Ma Neogene zircons and no tuffs were identified in outcrop from this level (Fig. 2: zone 2). An increase in the proportion of sandy facies in Galula-1 also occurs at the point where the younging zircon trend shuts off (between zones 1 and 2; Fig. 2), suggesting a period of volcanic inactivity characterized instead by fluvial reworking within the basin. At the top of the well, in units characterized by clay- and silt-rich lacustrine facies, no Neogene-age zircons were recovered; a trend that was also observed in detrital zircon samples collected from outcrops through this interval (Fig. 2: zone 3). Radiocarbon analyses from the uppermost Lake Beds succession suggest an age of 27,750 ±110 Cal BP to 7,270 ±60 Cal BP (Cohen et al., 2013; Hilbert-Wolf and Roberts, 2015; Mtelela et al., in press) for the uppermost Lake Beds Succession. The presence or absence of syndepositional zircon age populations in the sedimentary record is coincident with changing magma compositions within the Rungwe Volcanic Province between trachytes, phonolites, and basalts (Ebinger et al., 1989, 1993). The Rungwe Volcanic Province evolved from dominantly phonolitic magmas between 9.2-5.4 Ma to dominantly zircon-free olivine basalts and trachytes from 3-1.5 Ma and 0.6 Ma to the present (Ebinger et al., 1989; Fontijn et al., 2012), although each of these compositions is recognized to some extent in each of the three major Rungwe Volcanic Province phases. First-cycle, ~8.7-3.4 Ma zircons occur in zone 1, the most zircon-fertile interval that coincides with the earliest, phonolitic dominated magmas (9.2-5.4 Ma; Fontijn et al., 2012). Above this stratigraphic interval, reworked 9-4 Ma zircon grains (zone 2) and an absence of zircons in zone 3 suggest deposition during a period of predominantly olivine basalt-producing volcanism with very low zircon fertility.

5. Discussion

In a pioneering study on the relationship between detrital zircon age populations in sedimentary strata and basin types, Cawood et al. (2012) found that the crystallization age of the youngest detrital zircon population tends to very closely approximate the timing of sediment deposition in certain basin types. For example, convergent margin basins are typically associated with felsic-to-intermediate, arc-related volcanism and tend to produce sedimentary sequences with a high proportion of young, near syndepositional detrital zircon populations. An implication of this and other recent detrital zircon studies (e.g.,

DeCelles et al., 2007; Barbeau et al., 2009; Park et al., 2010; Tucker et al., 2013; Gehrels, 2014) is that certain basins are suited for the application of detrital zircon geochronology, such as foreland, forearc, backarc, as well as volcanic retroarc foreland basins and rift basins, where this technique has the potential to be used as a stratigraphic tool for refining the age of successive stratigraphic units.

However, collisional and extensional basins, which include peripheral (pro) foreland basins, passive margins and intracratonic basins, as well as rifts, tend to record a proportionally smaller volume of young, age constraining syndepositional zircons (Cawood et al., 2012). Nonetheless, with a statistically significant number of detrital zircons grains (Vermeesch, 2004), one should expect to recover a population of depositional age-constraining detrital zircons, even if the population is a very minor constituent of the total zircon volume. Although recovering >100 detrital zircons may not be possible with small-volume samples from well cuttings, this study makes it evident that other basin types (in addition to convergent margins) associated with active volcanism (such as the intracratonic Rukwa Rift Basin) can be rich sources of syndepositional volcanic zircons for depositional age constraint, and do not require 100+ detrital zircons for the detection of young syndepositional zircon grains. Since zircon populations are not equally abundant (sensu Anderson, 2005), in the right tectonic setting, dating fewer total detrital zircon grains (here, for example, as few as 46) can still successfully reveal depositional age-constraining populations. This being said, if possible, it would still be advantageous to plan for detrital zircon work prior to drilling and collect larger cutting samples for this work.

For provenance studies, to be certain that all zircon populations are sampled, recommendations vary from dating 35-117 zircon grains (Vermeesch, 2004; Anderson, 2005) to 300-1,000 zircon grains (Pullen et al., 2014). With the 150-500g well cutting samples from Galula-1, we were able to recover 40-140 concordant zircon grains from each sample (full detrital zircon datasets available via the AAPG Datashare). Since we are concerned only with the presence of one particular zircon population (i.e., that which constrains the sediment depositional age), the number of zircons dated per sample is not an imperative statistic. The presence of a zircon population in a very small data set suggests that the origin of such zircons is a significant sediment source. When seeking a maximum depositional age via detrital zircon in any volcanically influenced basin, the presence of just $\geq$ 2-3 young zircons is typically admissible for constraining or greatly refining the depositional age of sediments (e.g., Dickinson and Gehrels, 2009), providing it is a geologically and tectonically sensible age.

No matter the size of the data set, of greatest importance when deciding to use this method

for maximum depositional age control and temporal refinement of stratigraphic intervals is the likelihood that a syndepositional magmatic source (zircon fertile) contributed significantly to the zircon content of the sediment (Sláma and Košler, 2012). Although extensional basins tend to have a high proportion of reworked zircons derived from the basement (Cawood et al., 2012), volcanism is commonly present along rift zones such as in the EARS, and these basin types are potential targets for applying detrital zircon geochronology for maximum depositional age constraint of their stratigraphic successions. If the youngest sediment source is greatly overshadowed by zircon input from older sources due to drainage patterns, the depositional age population is likely to be overlooked even with a large number of detrital zircon analyses (Anderson, 2005). Similarly, many volcanic centers, particularly those that are rift-related, tend to evolve through time, meaning that zircon fertility changes. As a result of this, a modified approach to dating well cuttings may yield even better results. Particularly one in which radioisotopic dating of other mineral phases, such as titanite, monazite, apatite, or rutile, is applied alongside detrital zircon geochronology.

One caveat of the approach applied here is an explicit understanding that the maximum depositional age of detrital zircons (or other detrital minerals) is not necessarily the same as depositional age. In many volcanically active settings, it has been clearly demonstrated that the maximum depositional age from zircons does closely correspond to the depositional age of the sediments from which the zircons were recovered (e.g., Dickinson and Gehrels, 2009; Cawood et al., 2012; Tucker et al., 2013). However, a good understanding of tectonics and other supporting geologic data is critical to the accurate interpretation of the results. Correspondence with known stratigraphic superposition in the well and other associated geologic data, such as dated tuffs or volcanic strata and well-constrained biostratigraphic intervals, is an excellent indication that the youngest population of detrital zircon grains were generated concurrently with strata deposition. Similarly, younging maximum depositional ages upwards through a well supports such interpretations. Knowledge of the ages of nearby zircon sources (particularly volcanic sources), as well as assessing mineral shape for signs of weathering and reworking, can also contribute significantly to assigning a depositional age based on the youngest zircon population. In addition to the likelihood that a basin collects and preserves syndepositional volcanic sediment, consideration must be made for analytical uncertainties and for the possibility of disturbance of the U-Pb system in zircons (e.g., Pb loss), which may result in age underestimations.

6. Implications for the development of the East African Rift

The Rukwa Rift Basin is an important segment of the East African Rift System, in the sense that it preserves sedimentary rocks from the Permo-Triassic to Recent times, and

due to its superposition on top of a structurally weak shear zone, the Rukwa Rift Basin has been subject to rifting, subsidence, and uplift repeatedly throughout its history. The Oligocene onset of rifting in the western branch of the East African Rift System has been determined through the dating of tuffs from the Nsungwe Formation, which underlies the Lake Beds in the Rukwa Rift Basin (Roberts et al., 2012). Until this study, accurate age constraints on the initiation of the most recent phase of sedimentation (i.e., the Lake Beds) were absent due to conflicting biostratigraphic age information. U-Pb zircon ages from the basal part of the Lake Beds succession reported here are significant for placing age constraints on this most recent phase of Late Cenozoic rifting, demonstrating that renewed sedimentation commenced at ~8.7 ± 0.06 Ma (2σ). Significantly, these dates show that initiation of Late Cenozoic sedimentation was coeval with the first phase of Late Cenozoic volcanism in the Rungwe Volcanic Province. This demonstrates that reactivation of the Rukwa Rift Basin was heralded by both volcanism and sedimentation (i.e., rifting and basin filling).

The characteristics of sedimentary fill in a rift basin depend on climate, provenance, and subsidence rates. Since extensional events in the East African Rift System are marked by sedimentation and magmatism, the age and provenance of both detrital and tuffaceous zircons from the Rukwa Rift strata provide reliable insight into the timing of rift development and likely regional uplift in the western branch. Our new constraints on the timing of this most recent phase of rifting are consistent with demonstrated rifting and uplift in Uganda (Bauer et al., 2010) and Malawi (Ebinger et al., 1993), as well as with the initiation of the Rungwe Volcanic Province at the southern end of the Rukwa Rift (Ebinger et al., 1993; Ivanov et al., 1999), and the estimated development of Lake Tanganyika to the north (Cohen et al., 1993).

Constraining the timing of rifting and deposition of the Lake Beds also allows us to investigate links between critical climate events, landscape changes, and evolutionary patterns. Specifically, understanding the timing of the Lake Beds deposits has the potential to help understand the tempo and extent of Late Cenozoic uplift. Along the East African Rift, as uplift of the rift shoulders commenced, the climate of eastern Africa changed, putatively driving patterns of vertebrate evolution (e.g., Sepulchre et al., 2006). Recently, a large number of previously unknown species have been discovered in the Rukwa Rift Basin. These discoveries reveal that this part of the East African Rift was an important setting for the evolution of unique flora and fauna (e.g., Feldmann et al., 2007; Stevens et al., 2013; Gorscak et al., 2014; McCartney et al., 2014). The radioisotopic ages presented here allow us to confirm a late Miocene – Pliocene age for the lower Lake Beds and place critical constraints on newly discovered vertebrate-bearing deposits in the Rukwa Rift. This discovery is significant because it represents the only known fossil-

bearing deposit of this age exposed in the western branch of the East African Rift System between lakes Edward and Malawi. Therefore, the detrital and tuff-derived zircons dated here provide important temporal context for the rich vertebrate record described from the East African Rift, and help to illuminate the tectonic backdrop and timing of important large-scale faunal shifts in East Africa.

7. Summary

The ages of sedimentary basins along the Cenozoic East African Rift System, the World's archetypal continental rift system, figure prominently into our understanding of the timing of rift formation, evolution of topography and climate, hydrocarbon generation, and other fundamental geologic questions. Detrital zircon geochronology of the Galula-1 well cuttings, combined with U-Pb tuff dating from correlative outcrops has provided the first radioisotopic age constraints on deposition of the lower Lake Beds Succession of the Rukwa Rift Basin, from ~8.7 ± 0.06 to 3.5 ± 0.13 Ma (2σ), suggesting that Neogene rift reactivation, volcanism, and sedimentation began coevally. These results strongly support the application of detrital zircon geochronology in hydrocarbon exploration, specifically where small-volume well cuttings may limit samples. U-Pb LA-ICP-MS detrital zircon geochronology is economic and now widely available, and should be considered as a standard complementary tool to biostratigraphy for refining the depositional age of the strata in wells, particular through intervals with limited or conflicting biostratigraphy. This approach has the potential to: 1) closely approximate the depositional age of stratigraphic units; 2) estimate and provide constraints on sedimentation rates; and 3) provide intrabasinal correlation of units using detrital zircon fingerprinting; thereby resolving a variety of stratigraphic, burial, time, and thermal history questions critical to hydrocarbon exploration and the potential development of these resources.

Chapter Four

Insights into the accordion-like behavior of the Rukwa Rift Basin from detrital geochronology and thermochronology

Abstract

We have applied a multifaceted approach to sedimentary basin analysis, which includes geo- and thermochronology of sedimentary outcrop and well cutting samples, to assess the timing and magnitude of Paleogene-Recent tectonic events, sedimentation, and landscape development in the Rukwa Rift, a segment of the western branch of the East African Rift System in Tanzania. To detect varying magnitudes of tectonic events and provide greater resolution for tracing sediment provenance, U-Pb geochronology has been combined with fission track and (U-Th)/He low-temperature thermochronology of zircon and apatite from both sandstones (i.e., detrital grains) and volcanic tuffs in order to take advantage of a range of closure temperatures across each isotopic system. Integration of these data sets has allowed us to relate the initiation of rifting events to sedimentation patterns within the basin, to localized volcanic centers, and to dynamic uplift of the Rukwa Rift and surrounding regions.

Investigation of well cuttings and outcrop samples from the largely unstudied, uppermost succession in the Rukwa Rift Basin, the Lake Beds, reveals a suite of previously unrecognized tuffaceous deposits at the base of the succession. U-Pb geochronology on both the volcanic tuffs exposed at the surface and on the detrital zircons from well cuttings establishes a Miocene to Pliocene age for the basal Lake Beds deposits, implying that Neogene rifting and volcanism began by at least 8.7 Ma. Moreover, detrital zircon maximum depositional ages from unconformity-bound stratigraphic units in the lower Lake Beds suggests episodic sedimentation in the rift, punctuated by long hiatuses or uplift, rather than steady subsidence and sedimentation. A distinct, upward-younging trend in maximum depositional ages of detrital zircon through the lower portion of the well stratigraphy is documented and linked to initiation of the Rungwe Volcanic Province, coincident with Late Miocene initiation of rifting and subsidence in the basin. Detrital zircon populations from the Lake Beds are dominated by Paleoproterozoic grains of the same age as the metamorphic Ubendian Belt that underlies the rift basin and forms the flanks. The volcaniclastic nature of the Lake Beds in combination with this provenance signature suggests an internally draining basin associated with the most recent rifting episode. Neoproterozoic and Mesoproterozoic zircon populations, likely reworked from the underlying Cretaceous sandstones and derived from younger metamorphic terranes of the Ubendian Belt, are also present in the samples. Thermochronology data suggests that the Rukwa Rift Basin experienced localized uplift and reheating due to volcanic eruptions

during the earliest episodes of rifting and volcanism in the western branch of the East African Rift System (~25 Ma). A key implication of this work is that there appears to be minimal uplift associated with either of the initial two pulses of rifting, volcanism and sedimentation at ~25 Ma and ~9 Ma. This suggests that the high-topography observed in this part of eastern Africa is a very recent phenomenon, which therefore must have developed sometime during the late Pliocene to Quaternary.

1. Introduction

The East African Rift System (EARS) extends over 4,000 km from the Afar triangle in the north to Lake Malawi in the south. Multiple rift basins connect to form two rift branches, the eastern and western, which are surrounded by the uplifted East African Plateau. The Ethiopian and Kenyan domes are linked to the EARS and are thought to be related to a single or multiple mantle plumes, which are suspected to have initiated in the Eocene (Ebinger and Sleep, 1998; Pik et al., 2008). The tectonic evolution of the rift valleys is of immense interest, especially for understanding fundamental mechanisms and controls on rifting and volcanism, but also for investigating the relationships between landscape development associated with rifting and surface uplift and putative climatic and environmental change in Africa.

The causal relationships between mantle plumes, rifting, and volcanism during continental breakup are the subject of debate, particularly because these have significant effects on topographic evolution. Together these consequences of rift activity are thought to have had a profound influence on the development of the modern African flora and fauna, and on human evolution in eastern Africa (Sepulchre et al., 2006; Jung et al., 2015). Recently, the long-held paradigm that rifting of the western branch of the East African Rift System initiated between 10-7 Ma, post-dating the already established eastern branch, was challenged by Roberts et al. (2012), who found evidence for rifting and volcanism in portions of the western branch between 26-24 Ma. However, the timing of associated regional and local uplift of the East African Plateau remains poorly resolved (Roberts et al., 2012). A number of fundamental questions still remain unanswered about the initiation of the western branch, including: 1) did significant surface uplift of the East Africa Plateau accompany the Oligocene rifting event?; 2) how many discrete phases of rifting have occurred since 25 Ma, how long did these phases last, and were they accompanied by rock or surface uplift?; and 3) if uplift was not in sync with rifting episodes, then when did uplift and the establishment of the high-elevation topography of the East African Plateau develop?

In order to understand these processes and their effects, accurate chronologies of rifting, volcanism, and uplift must be resolved for key portions of the East African Rift System. Here we attempt to address these questions from the perspective of the sedimentary record preserved in the Rukwa Rift Basin of the western branch of the EARS, by applying a combination of U-Pb geochronology and low-temperature thermochronology on detrital zircon and apatite grains in combination with U-Pb dating of newly discovered volcanic tuffs from the base of the Neogene rift-fill package (Lake Beds succession). Over the last 25 years a number of studies have sought to address similar questions by focusing on low-temperature thermochronology investigations of the flanks of the Malawi and Rukwa rifts (e.g., Van der Beek et al., 1998). However, because these studies were based on apatite fission track analyses of a limited number of transects along the rift flanks, the spatial and temporal resolution of rifting and uplift in the western branch, particularly the more subtle uplift events, remains poorly resolved (i.e., existing constraints on uplift are of a low resolution). Hence, additional work and new approaches are needed for investigating the chronology and magnitude of rifting and uplift in the western branch.

The eastern branch of the East African Rift System is well known for its effusive volcanism (e.g. Afar region), whereas the less volcanically active western branch is defined by its deep lakes and thick sedimentary successions. Until recently, relatively little work had been conducted on the stratigraphy of the sedimentary successions in the western branch rift segments, in large part due to the deep water nature of the overlying lakes, lack of exploration wells, and limited exposure of these strata. The Rukwa Rift Basin, which lies between the Albertine and Malawi rift segments of the western branch in southwestern Tanzania (Fig. 1A), represents one of the best opportunities to resolve some of these outstanding questions. This is in large part because the basin contains the thickest continental sedimentary sequence in Africa (~9-11 kms; Kilembe and Rosendahl, 1992) and is only partially covered by a shallow rift lake in the north. Major Holocene lake regression, coupled with faulting and inversion along the rift flanks, particularly within the Songwe Valley (southern end of the basin), has exposed significant portions of the stratigraphy, which provide an unparalleled opportunity to better understand the tectonic and sedimentary evolution of this portion of the western branch of East African Rift System.

Over the last 15 years, sedimentological, paleontological, and geochronological approaches have documented a complex, long-lived history for the western branch of the EARS (O'Connor et al., 2006; Roberts et al., 2012; Stevens et al., 2013), and progress has been made towards unraveling the kinematic history of rifting and the timing of corresponding sedimentation in the Rukwa Rift Basin (Delvaux et al., 2012). Superimposed on a structurally weakened, Paleoproterozoic shear belt, the Rukwa Rift has been tectonically

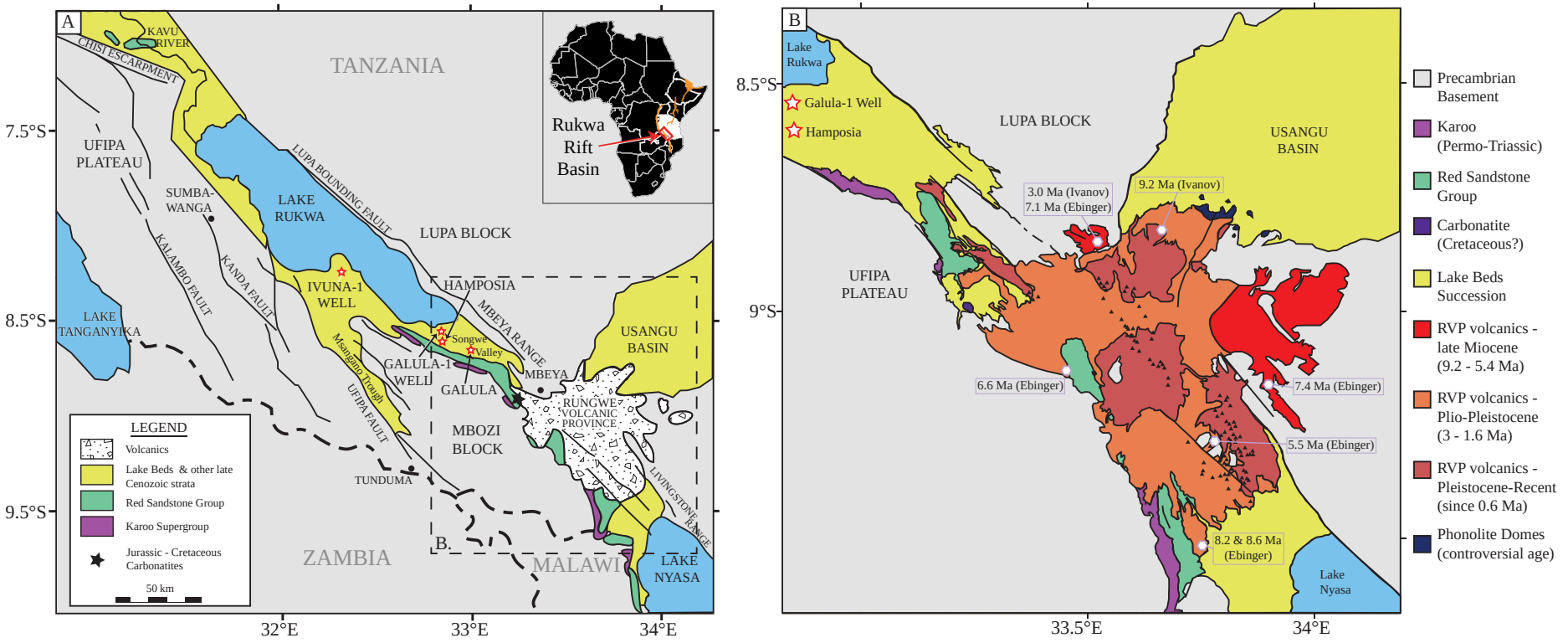

Fig. 1. A. Geologic map of the Rukwa Rift Basin showing major tectonic elements and the distribution of Phanerozoic sedimentary deposits. The two exploration wells and other key localities are labeled. B. Geologic map of the Rungwe Volcanic Province modified after Ebinger et al. (1989) and Fontijn et al. (2012). Holocene explosive eruptions are not shown, as they cover most of the region. The ages of representative Miocene-Pliocene volcanics are displayed. The ages from Ivanov et al. (1999) and Ebinger et al. (1989; 1993) are derived from K-Ar and 40Ar/39Ar analysis of whole rock samples.

reactivated numerous times since the Late Paleozoic. Four depositional successions comprise the thick sedimentary package (Roberts et al., 2010) preserved in the Rukwa Rift Basin, which includes: the Permo-Triassic Karoo Supergroup; the Cretaceous and Oligocene Red Sandstone Group; and the Miocene-Recent Lake Beds succession. Importantly, the Rukwa Rift Basin preserves the only continental Oligocene sedimentary sequence in Africa south of the equator, and likely has the best and most extensive exposures of Neogene to Recent sedimentary strata in the western branch. This rare window into end of the Paleogene in East Africa records the onset of rifting of the western branch of the East African Rift System, and is therefore critical to reconstructing climate and landscape change at this time, and also during the collision of the Afro-Arabian and Eurasian landmasses that initiated faunal exchange (Winkler, 1994). Moreover, we have recently identified and dated basal strata of the uppermost stratigraphic unit in the Rukwa Rift, the Lake Beds succession, and documented a late Miocene to Pliocene age for the lower portion of these deposits (see Chapter Three), temporally coincident the proposed initiation of the Rungwe Volcanic Province and Neogene rifting in the southern portion of the western branch. These newly identified units are rich in fossils, including the discovery of a new species of Hippopotamidae (N. Stevens, pers. comm.) among other previously unknown Mio-Pliocene fossil fauna from the western branch of the EARS. Given these discoveries, geochronologic and thermochronologic investigations of the Lake Beds succession are now critical for not only understanding the latest phase of rifting in the western branch but also for giving important context to an ancient ecosystem that set the stage for human and other vertebrate evolution.

Differentiating, correlating, and dating the sedimentary units in the East African Rift System is central to understanding the timing and relationships between volcanism, rifting, rock and surface uplift, and sedimentation over the rift's long-lived tectonic history. Understanding the sources and timing of ancient terrestrial sedimentary deposits can be challenging, particularly when biostratigraphic control is lacking. Post-depositional tectonic movements, erosion events, and scarce outcrop exposure can further complicate correlations. Therefore, assigning ages and differentiating the depositional sequences in the Rukwa Rift Basin has historically proven problematic (e.g., Wescott et al., 1991; Kilembe and Rosendahl, 1992; Morley et al., 1999; Roberts et al., 2004, 2010). Much still remains unresolved concerning the age and the spatial and temporal continuity of rifting during the earliest depositional phases in the western branch rifts. Combining multiple geochronological and thermochronological methods for analyzing detrital grains from the Rukwa Rift Basin has allowed us to begin to unravel the sediment source and basin tectonic histories. Hence, the aims of this study are to: 1) constrain post-Oligocene rifting activity in the Rukwa Rift Basin by using detrital- and tuff-geochronology to determine the depositional age for the youngest portion of the stratigraphy in the rift (the Lake Beds

deposits); 2) unravel the temporal development of volcanism in this portion of the western branch from the Miocene - Recent; and 3) investigate uplift and drainage development via detrital zircon and apatite geochronology and thermochronology throughout the rift stratigraphy, from the Cretaceous to Pliocene deposits.

2. Geology of the Rukwa Rift Basin

2.1. Structure and tectonics

The Rukwa Rift Basin is bounded by the Ufipa Fault and Plateau to the southwest, the Lupa Fault to the northeast, the Ubende Plateau to the north, and the Mbozi Block and Rungwe Volcanic Province to the southwest and south, respectively (Ebinger et al., 1989; Kilembe and Rosendahl, 1992; Fig. 1). The regional cross-sectional morphology of the Rukwa Rift Basin is a northeastern-tilted half graben. The Rukwa Rift is unusual within the EARS because the eastern escarpment adjacent to the bounding fault only rises ~ 400 m above the East African Plateau (total of ~1200 m high), whereas the western side of the rift is nearly 1,000 m higher (Ebinger et al., 1989). The majority of the intrabasinal faults trend parallel to the NW-SE structural direction of the Ubendian basement rocks on top of which the Rukwa Rift has developed, although a few trend NE-SW. The uplift of the Mbeya Range caused the narrowing of the Rukwa depression at its southeastern extremity (Camelbeeck and Iranga, 1996), where it splits into two troughs: the Songwe (study area) and the Msangano valleys, separated by the Precambrian Mbozi Block (Fig. 1).

The major Precambrian tectono-metamorphic cycles and resulting high-grade metamorphic belts in eastern Africa include the Pan-African (~700-500 Ma), Kibaran (~1200-900 Ma), Ubendian (~2-1.8 Ga), and Archean (>2.5 Ga) cycles (Fritz et al., 2005). In East Africa, the Archean Congo, Bangweulu, and Tanzania cratons have acted as rigid blocks while the flanking mobile belts experienced metamorphism and deformation during these successive orogenies. The resulting lithologic and tectonic complexes (mobile belts) together with the Archean cratons characterize the basement geology of this part of East Africa (Fig. 2). Regionally, the location of the two rift braches (eastern and western) follows Proterozoic orogenic belts and goes around the central Tanzanian craton, reflecting the heterogeneity in the lithosphere across eastern Africa. Metamorphic basement beneath the western rift is characterized by northwest, northeast, and north-south trending mylonites and shear zones (Daly et al., 1989). The Rukwa Rift Basin has formed on top of the Ubendian Belt; a shear zone that is part of a larger Paleoproterozoic orogen that developed around the west and southwest margins of the Archean Tanzanian Craton. The metamorphic and metasedimentary rocks of the Ubendian belt cover an area over 90,000 km2, separating the western margin of the Tanzanian Craton from the Archean Congo Craton and

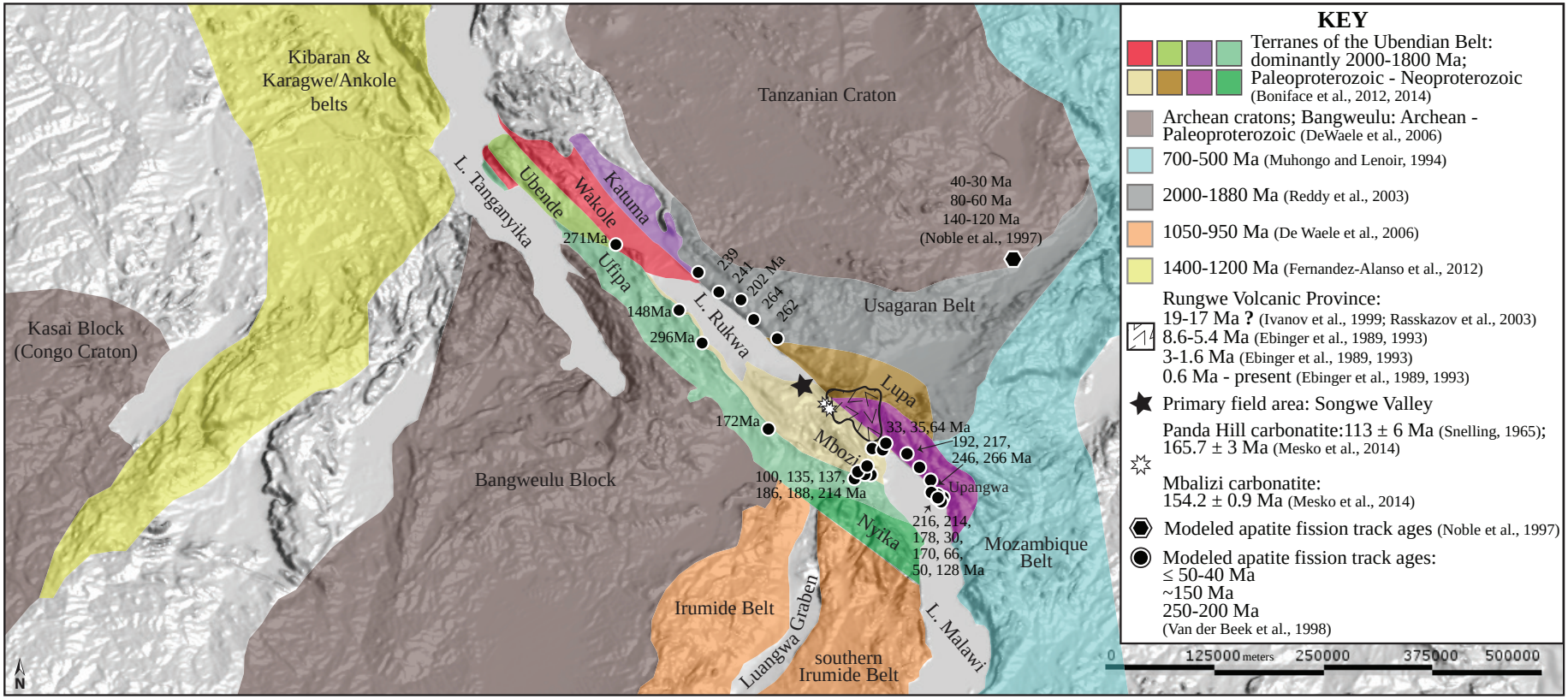

Fig. 2. DEM map of the southern part of the western branch of the East African Rift System modified from the Arc-Minute Global Relief Model (Amante and Eakins, 2009). Boundaries of terranes, cratons, metamorphic belts, and shear zones surrounding the Rukwa Rift Basin are overlain on the map, highlighting the source areas of the majority of sediments deposited in the Rukwa Rift Basin. Age ranges for each source area are presented in the key, and a key reference is provided. The grey-scale of the map indicates sediment cover. Important volcanic regions are highlighted between the Rukwa and Malawi rifts. Individual apatite fission track ages labeled on the map are from Van der Beek et al. (1998) unless otherwise labeled, and the resulting modeled periods of uplift are presented in the key.

Bangweulu Block (Lenoir et al., 1994; Fig. 2). The Ubendian Belt is composed of eight terranes that have differentially been affected by at least three distinct orogenic events: the Ubendian, Kibaran, and Pan African (Lawley et al., 2013; Fig. 2). The protracted accretionary and tectonic history of the Ubendian Belt has influenced the repeated subsidence and filling of the Rukwa Rift Basin.

2.2. Sedimentology and stratigraphy

Four distinct phases of deposition are recorded in the Rukwa Rift Basin, including the: 1) Permian Karoo Supergroup, 2) Cretaceous Galula Formation, 3) Oligocene Nsungwe Formation, and 4) Miocene-Recent Lake Beds succession. The continental strata of the oldest unit, the Karoo, is characterized by glacial, lacustrine, and fluvial deposits, and has been assigned a late Carboniferous to Late Permian age based on palynology (Semkiwa et al., 1998). An angular unconformity separates the Karoo Supergroup from the overlying Red Sandstone Group, the age of which has historically been contentious. Biostratigraphy results from two hydrocarbon exploration wells through the Rukwa Rift Basin in the 1980s (Galula-1 and Ivuna-1, Fig. 1) yielded a Miocene - Pliocene age for the Red Sandstone Group (Wescott et al., 1991), yet others found evidence for a Middle Jurassic – Middle Cretaceous depositional age (Kilembe and Rosendahl, 1992). Extensive paleontologic (O'Connor et al., 2006) and sedimentologic (Roberts et al., 2010; 2012) investigations have since resolved this issue, demonstrating that the Red Sandstone Group consists of at least two different stratigraphic units. The lower unit, termed the Galula Formation, has been grossly dated as mid-Cretaceous, and the upper unit, the Nsungwe Formation, is late Oligocene. Whereas a paucity of volcanic tuffs has precluded exact radioisotopic dating of the fluvial-dominated Galula Formation, the lacustrine and fluvial claystones, siltstones and sandstones of the upper member of the Nsungwe Formation (Songwe Member) are intercalated with devitrified volcanic tuffs that constrain deposition very well to 26-24 Ma (Roberts et al., 2012; Stevens et al., 2013). Exposures of the Nsungwe Formation are very limited, but they preserve an extremely important window into the tectonics, climate, fauna, and landscape of this region at the onset of rifting of the western branch. The Lake Beds succession, best exposed at the basin margins, is the youngest of the sedimentary successions, and is composed of conglomerates, sandstones, siltstones, and mudstones, along with intercalated volcanic tuffs. Where exposed, the Lake Beds is dominated by volcanic-rich fluvial, alluvial, and deltaic deposits, and the depocenter contains finer grained, deeper water lacustrine sequences (Kilembe and Rosendahl, 1992; Mtelela et al., in press). The age of the Lake Beds succession has also been plagued by confounding biostratigraphy from the Galula-1 and Ivuna-1 hydrocarbon exploration wells, though it has generally been accepted that the Lake Beds are Neogene to Pleistocene in age (Stockley, 1938; Spence, 1954). However, the Lake Beds have been assigned an age as old

as Cretaceous (Pentelkov, 1979).

2.3. Volcanism

A major tectonic feature adjacent to the southern end of the Rukwa Rift is the 1500 km2 Rungwe Volcanic Province (Fig. 1), which developed at a triple junction between the Malawi, Rukwa, and Usangu rift segments (Delvaux, 2001). Volcanism in the Rungwe Volcanic Province is thought to have initiated ~9 Ma (Ebinger et al., 1989), although volcanic rocks as old as ~19-17 Ma have been dated (Ivanov et al., 1999; Rasskazov et al., 2003). Rungwe volcanic activity has been subdivided into three stages, based on radiometric ages from volcanic rocks exposed in the area: 1) ~8.6 – 5.4 Ma; 2) ~3-1.6 Ma; and 3) ~0.6 Ma to present (Ebinger et al., 1989, 1993; Delvaux et al., 1992; Ivanov et al., 1999). The volcanism is dominated by effusive and explosive eruptions of basalt, trachyte, and phonolite magmas (Fontijn et al., 2012).

The oldest and only other existing volcanic center from prior to the development of the Rungwe Volcanic Province, is a suite of carbonatites, comprised of at least four known complexes, including: Panda Hill, Mbalizi, Sengeri Hill, and Musensi (Fig. 1; Van Straaten, 1989). This carbonatite suite has been assigned a Jurassic to Cretaceous age (Fawley and James, 1955) from the interpretation of sediments truncating a carbonatite dyke. Snelling (1965) dated a part of the complex as Early Cretaceous (113 ± 6 Ma) on the basis of K-Ar dating of phlogopite. Carbonatitic breccia exhumed along the Songwe scarp is presumed to have been emplaced during the same period as these Early Cretaceous carbonatites exposed in the Songwe Valley (Brown, 1962; Pentelkov and Voronovskii, 1977). The exact ages of the carbonatite centers that form this volcanic suite remain contentious, and recently, samples from two of the carbonatite complexes in the southern Rukwa Rift Basin were dated via $^{40}Ar/^{39}Ar$ and yielded Jurassic ages of 165.7 ± 3 Ma (for Panda Hill, which forms the highest topographic feature in the Songwe Valley) and 154.2 ± 0.9 Ma (for Mbalizi), which are older than prior Cretaceous age estimates (Mesko et al., 2014).

Oligocene-aged volcanic tuffs are abundant in the Songwe Member of the Nsungwe Formation, although no Paleogene volcanic sources have yet been identified in the region. The alkaline composition of these Oligocene tuffs suggests an association with the Jurassic-Cretaceous carbonatite suite at the southern end of the basin. One hypothesis is that carbonatite volcanism from the region around Panda Hill was renewed with the initiation of the western branch around 25 Ma. Alternatively, the Oligocene alkaline tuffs could represent an early stage of the Rungwe Volcanic Province, the evidence of which has since been eroded or buried (Roberts et al., 2010). A newly discovered tuff in the Nsungwe Formation around the Ikumbi area was recently dated via LA-ICP-MS U-Pb

geochronology on titanite and is slightly older (~29 Ma) than those tuffs in the Songwe Valley (Spandler et al., 2016). However, Sm-Nd isotope analysis (Spandler et al., 2016) strongly supports a similar alkaline source for all of the Oligocene tuffs.

3. Approaches

To overcome the difficulties inherent in studying the tectonic history of a complex rift basin we have combined a suite of geochronometers and thermochronometers and applied them to both detrital and tuff zircons and to detrital apatites from the sedimentary successions in the Rukwa Rift Basin. This approach entails: 1) tephrochronology via U-Pb geochronology on zircon; 2) U-Pb geochronology of detrital zircon and apatite; 3) detrital zircon and apatite fission track analysis; and 4) low temperature thermochronology via the (U-Th)/He method on detrital apatites. Performing these analyses on detrital minerals is challenging, but particularly insightful, because we are able to reconstruct the responses of source terrains as well as the rift basin and rift flanks to various tectonic events through geologic history. Since the sediments in the Rukwa Rift Basin have not been thermally reset after deposition, they preserve the thermal histories of their source regions. The provenance, geochronology, and thermal history of syntectonic sedimentary rocks deposited in the Rukwa Rift Basin provide valuable information about the location, age, and exhumation history of source terranes (including the rift flanks) and therefore about the dynamics of rifting and landscape evolution in the western branch of the East African Rift System.

Geochronology of detrital minerals in the sedimentary record allows us to reconstruct past sediment routing systems, and therefore gain insights into changing topography through time. Zircon has proven particularly well suited for U-Pb geochronology because of its relative abundance in a variety of rock types, resistance to physical and chemical weathering, and tendency to include uranium and thorium in the crystal structure, but not common lead. U-Pb detrital zircon ages are particularly important for reconstructing the sedimentary provenance of a sedimentary rock, but in some cases, they can also provide maximum depositional ages, which is particularly valuable in stratigraphic investigations. While U-Pb geochronology of zircon is now a widely applied approach to sediment provenance studies (e.g., Fedo et al., 2003; Dickinson and Gehrels, 2010; Gehrels, 2014), the dating of other heavy minerals such as apatite, titanite, monazite, etc. for provenance studies is still uncommon. Targeting non-traditional minerals in addition to zircon is advantageous in rift settings, where magma compositions change through time and non-zircon bearing volcanic rocks such as carbonatites and kimberlites are common and may provide a powerful means of determining the maximum depositional ages of sedimentary units. Volcanism in the Rukwa Rift Basin (e.g., the Rungwe Volcanic Province) is dominantly carbonatitic and mafic in nature, meaning that syndepositional volcanic zircon grains may

not be especially abundant in all sedimentary units derived from these sources. Therefore, we have also targeted apatite, a common uranium and thorium bearing detrital component of many clastic sedimentary rocks, for detrital geochronology and thermochronology. A number of important provenance sources are known from the region that do not produce significant zircon, but are known to produce abundant apatite (e.g., carbonatite suite in the Songwe Valley), hence both minerals were applied to this study. An advantage of detrital apatite is that it is much softer than zircon, and because of this, it is unlikely to have survived multiple stages of transport and erosion from one sedimentary unit to the next. This is in contrast to zircon, which is extremely resistant to weathering, and so it can be difficult to differentiate first-cycle and polycyclic grains (Carrapa, 2010). The disadvantage of using apatite, is that it commonly contains low uranium, thorium, and radiogenic lead concentrations, and is elevated common lead.

In this study, fission track and (U-Th)/He data were used to interpret uplift and denudation of local and regional sediment sources, and by proxy the rift flanks themselves. These techniques have been little applied in eastern Africa. The advantage to using many techniques in combination across mineral types is that this widens the temperature spectrum over which we can detect thermal perturbations in the Rukwa Rift area, signaling tectonic events of different magnitudes. For example, U-Pb closure temperatures range from 450-550°C for apatite (Dodson, 1973) and >900°C for zircon (Lee et al., 1997). The partial annealing zone for fission tracks in zircon ranges from 170-260°C (typically ~240°C; Yamada et al., 1995), and for apatites ranges from 100-120°C (Gleadow and Duddy, 1981). The closure temperature for the (U-Th)/He system in apatites is estimated to be 70-50°C (Flowers et al., 2009). Double-dating of detrital apatite and zircon grains (via U-Pb and fission track) was performed to better understand and trace sediments back to their main sediment sources and to determine the uplift and denudation history of the different sources.

Great care was taken during field sampling, mineral separation, through to data acquisition, interpretation, and display to reduce all possible sources of bias. Detrital zircon, detrital apatite, and tuff samples were collected from outcrops spanning four field seasons in the Rukwa Rift Basin. The Tanzania Petroleum Development Corporation and Heritage Rukwa Tanzania Limited provided well cuttings samples from the Ivuna-1 and Galula-1 exploration wells. Zircon and apatite grains were separated from bulk rock samples using standard rock pulverization techniques, followed by sieving, density separation using a Wilfley Table, magnetic separation, and heavy liquid separation techniques. Note that all double-dated grains (i.e., U-Pb and fission track on the same grain) were analyzed at Apatite to Zircon Inc. All other U-Pb analyses were performed at James Cook University's Advanced Analytical Centre (i.e., well cutting samples and Lake Beds outcrop samples). All (U-Th)/He analyses were done at the Scottish Universities Environmental Research

Centre in collaboration with the University of Glasgow. Histograms, probability density curves, and kernel density estimation curves were plotted using the DensityPlotter program (http://densityplotter.london-geochron.com; Vermeesch, 2012).

3.1 LA-ICP-MS U-Pb geochronology

U-Pb dating of tuff and detrital zircons was conducted at James Cook University's Mineral Separation Lab and Advanced Analytical Centre. Separated zircon grains were mounted with internal and external zircon standards in epoxy discs. For each detrital sample, roughly 100 unknown zircon grains (or as many as were recovered) and the standard grains were mounted close to each other in the inner 0.5 inches of the mount to minimize U-Pb fractionation related to spatial variation of the carrier gas over the sample surface (Gehrels et al., 2008). Small sample volumes from the Ivuna-1 and Galula-1 well cuttings limited some samples to < 100 grains (see Chapter Three and Hilbert-Wolf et al., in press, for further details). The epoxy surface was ground down to expose the interior portions of most grains. Scanning electron microscope (SEM)–Cathodoluminescence (CL) and SEM-secondary electron images (Jeol JSM5410LV) were taken for each sample, enabling the placement of laser pits in specific portions of the zircon crystals. These images were used with caution, so as to avoid a biased age spectra based on the selection/rejection of grains according to CL or SE characteristics.

All LA-ICP-MS U-Pb analyses conducted at the Advanced Analytical Centre of James Cook University used a Coherent GeolasPro 193nm ArF Excimer laser ablation system connected to a Bruker 820-MS (formerly Varian 820-MS). Zircons were analyzed using the same, optimized LA-ICP-MS method outlined in Tucker et al. (2013). Laser spot sizes varied between 32 μm and 44 μm according to the size and morphology of the sample and standard zircons. However, for a given set of standard and unknown analyses, spot size remained constant. The total measurement time was set at 70 seconds per analysis. The first 30 seconds were for gas blank measurement, and during the final 40 seconds the shutter was opened to allow for sample ablation and measurement. At the beginning and end of each sample, as well as after every 10 or so unknown grains, at least two analyses each of the primary zircon standard GJ1 (608.5 ± 0.4 Ma, 2σ; Jackson et al., 2004) and the secondary zircon standards Temora-2 JCU (416.8 Ma ± 1.1 Ma, 2σ; Black et al., 2003) and Fish Canyon Tuff (28.5 ± 0.03 Ma, 2σ; Schmitz and Bowring, 2001) were completed to monitor down-hole fractionation and for age and instrument-drift corrections. All secondary standard analyses were within 1-2% of the expected ages. Due to instrumental drift during the course of a day, different calibrations were used to correct for this, including either linear or average fitting of the standards. NIST 610 or 612 was analyzed at the beginning, middle, and end of each session for the purpose of calibrating Th and U concentrations.

Data reduction and age calculations based on measured isotope ratios were carried out using the Glitter software (Van Achterbergh et al., 2001). All time-resolved isotope signals were filtered for signal spikes or perturbations related to inclusions and fractures, and then background and sample intervals were selected based on evaluation of the most stable and representative isotope ratios. Isoplot/Ex version 4.15 (Ludwig, 2012) was used for extracting ages from multi-grain populations (i.e., calculating weighted means). $^{206}Pb/^{238}U$ ages and errors have been reported for grains < 1 Ga and $^{206}Pb/^{207}Pb$ ages and errors are reported for grains > 1 Ga, as $^{206}Pb/^{207}Pb$ ages are less sensitive to the Pb loss that is more common in older systems. Where applicable, $^{206}Pb/^{238}U$ ages were corrected for common Pb based on the Pb isotope evolution model of Stacey and Kramers (1975). Zircon grains with an age discordance ≥ 30% were omitted from the samples and from this study as a whole. However, in young zircon grains (e.g., < 10 Ma) the production of radiogenic Pb is typically low, and hence the $^{207}Pb/^{206}Pb$ age can be discordant, so the above criterion was not applied.

3.2. Fission track and U-Pb double dating

Low-temperature thermochronology is more time intensive and costly than U-Pb geochronology. Due to this barrier, only one sample from each of the Cretaceous, Oligocene, and Pliocene sequences was analyzed via low-temperature thermochronology techniques. Therefore, the data reported here does not necessarily account for all detrital zircon and apatite populations, although it is still of great use for exploring uplift and denudation in and around the Rukwa Rift Basin. One challenge to using detrital minerals for thermochronology work is the ability to link a crystallization age with a cooling age. This was accomplished by "double dating" detrital zircon and apatite grains via both U-Pb and fission track analysis. Fission track and U-Pb dating are two of the most useful (and most rapid) techniques in sedimentary provenance studies. They yield complementary information, with the fission track system yielding low-temperature cooling ages and the U-Pb system yielding high temperature crystallization ages. Three key samples ("TZ7", "Big Wall", and "Hippo Quarry") representative of the Red Sandstone Group and the Lake Beds succession were chosen for detrital zircon and apatite double dating via fission track and LA-ICP-MS U-Pb geochronology on the same grain. Zircon and apatite separates were double dated at Apatite to Zircon Inc.

At Apatite to Zircon Inc., zircon and apatite fission tracks were revealed via standard procedures, by embedding grains in Teflon, polishing the grains to expose internal grains surfaces, and lastly, etching the fission tracks. The fission track sample preparation methods and analytical procedures are presented in detail in Donelick et al. (2005). Durango apatite (31 Ma; McDowell et al., 2005) was used as the apatite fission track zeta age calibration

standard and the Fish Canyon Tuff (28 Ma; Gleadow et al., 2015) was used as the zircon fission track zeta age calibration standard. Fission tracks were viewed, counted, and measured at 1562.5x (Nikon Optiphot2 microscope; analyst Raymond A. Donelick) or 2000x (Zeiss Axioplan microscope; analyst Paul B. O'Sullivan) dry magnification using plain, transmitted light with or without reflected light. Analyzed zircons and apatites were selected so as to sample the greatest range of observable grain characteristics (e.g., size, roundness, color). Fission track ages were calculated using the scheme presented by Donelick et al. (2005) using a modified zeta calibration approach after Hurford and Green (1983).

For U-Pb dating, the standards used by Apatite to Zircon Inc. include the Duluth Complex zircon (1099±0.6 Ma; FC primary standard; Paces and Miller, 1993) and the Fish Canyon Tuff zircon (28.2±0.012 Ma; IF secondary standard; Kuiper et al., 2008). A minimum of two primary and two secondary standard spots were analyzed prior to and following each group of ~25-40 unknown sample spots. For apatite, fractionation factors and their absolute errors were determined using the scheme described by Chew et al. (2012). Since apatite generally exhibits low Pb signals and relatively high common Pb values, isotopic sums were used instead of values for individual scans. Additionally, apatite and zircon chemistry on the three double dated samples was measured by Apatite to Zircon Inc. Major, minor, and trace element chemistries of each successful spot analysis via LA-ICP-MS on zircon and apatite grains were calculated using isotopic 'counts per second' data summed over seven scans exhibiting the highest scan background-corrected signal intensities for the primary cation for each mineral (primary cation is 43Ca for apatite and 91Zr for zircon). The apatite and zircon geochemistry was analyzed in an attempt to differentiate sources by REE signatures (Hoskin and Ireland, 2000). Geochemistry can be a potential provenance indicator, but only when the zircon or apatite chemistry is sufficiently variable in different source rocks. Geochemistry data proved to be of limited use for this study.

3.3 Apatite (U-Th)/He thermochronology

Detrital apatite (U-Th)/He thermochronology was performed at the Scottish Universities Environmental Research Centre in collaboration with the University of Glasgow. Heavy mineral separates were first produced at James Cook University via standard procedures as outlined above. At the University of Glasgow 3.3 g/ml diiodomethane was used to separate apatite from zircon, and then apatites suitable for (U-Th)/He analysis were hand picked using a petrographic microscope. Grains were chosen that lacked visible fractures or mineral or fluid inclusions. Care was taken not to bias the sample based on number of terminations, grain shape, physical surficial weathering, or size. The ages reported here are of single crystals. Twenty apatite grains from each sample ("Hippo Quarry" and "Big Wall") were

individually packed in Pt-foil tubes and loaded into a 6 cm diameter Cu planchet for He extraction. He extraction from the apatite grains was performed using a diode laser beam focused using a binocular microscope, attaining temperatures of 500-600°C, heating to 0.5 W for 30 seconds to achieve He release. See Foeken et al. (2006) for a more detailed analytical procedure. After each initial heating, the apatites were re-heated to check for optically undetectable inclusions. Outgassed apatite grains were retrieved, dissolved in nitric acid, and analyzed via ICP-MS to measure U, Th, and Sm quantities, using a spike of 230Th, 235U, and 149Sm. The Durango apatite (31 Ma; McDowell et al., 2005) was used as a standard throughout the procedure, and blank Pt-foil tubes were included in the sample set to check the instrument background levels.

LA-ICP-MS U-Pb ages could not be obtained for the apatite grains that underwent (U-Th)/He analysis, as it is important to retain the entire grain for He-extraction. Therefore, the (U-Th)/He ages presented in this work cannot definitively be assigned to a U-Pb age (i.e., to a discrete source). In an effort to group detrital grains by something other than their crystallization ages, the geochemistry of some apatite and zircon samples was investigated. For example, trace element partition coefficients in igneous apatite are commonly very sensitive to changes in magmatic conditions and can exhibit large variations in concentrations. Hence, the trace element composition of igneous apatite can yield useful provenance information (e.g., Sell and Samson, 2011). For this study, such work proved to be of limited use. The major challenge for interpreting low-temperature thermochronology data for detrital grains is the inability to model the calculated ages, track lengths, etc., without knowing the crystallization age (i.e., the source) of the dated grain, to put some initial constraints on the grain's history. Despite this limitation, useful information can still be derived from the cooling ages at face value, as demonstrated below.

4. Results: detrital geochronology and thermochronology

4.1 Galula Formation

For comparison to the Late Cenozoic strata in the Rukwa Rift Basin, a representative detrital sandstone sample ("TZ7") from the Namba Member of the Galula Formation was dated. U-Pb ages were acquired for 54 detrital apatite grains, which reveal one dominant population at ~540 Ma, but with a spread between ~690-350 Ma (Fig. 3). The youngest single apatite grain is 125 Ma. Thirty-nine of these detrital apatite grains were double dated, via fission track analysis, and show a spread of cooling ages from ~375-50 Ma (Fig. 4).

Detrital zircon from sample "TZ7" was also double dated (Fig. 4). Twenty-one detrital

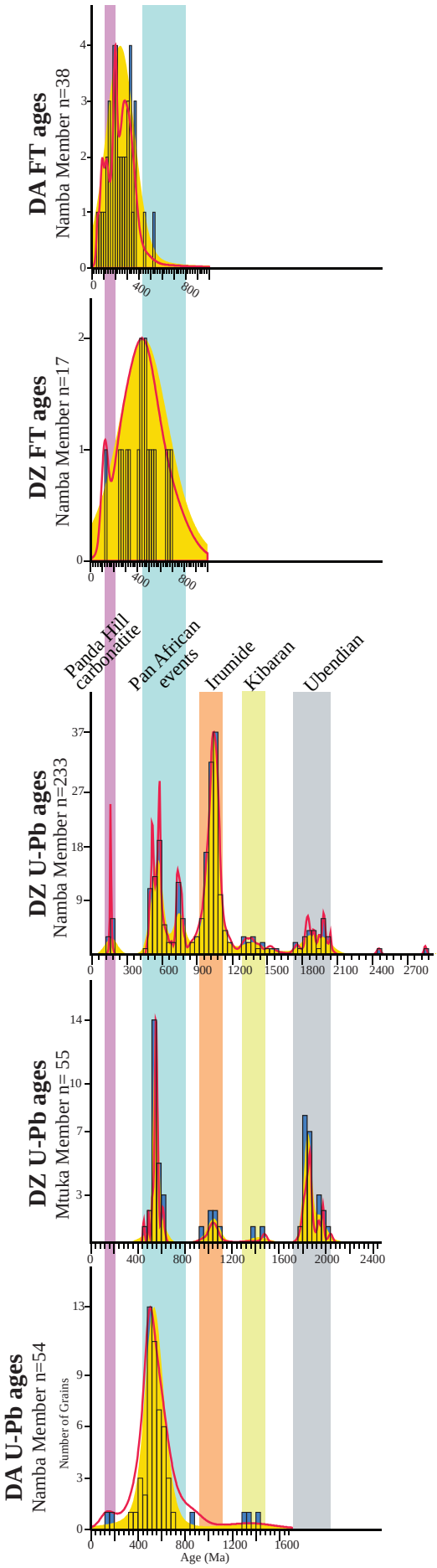

Fig. 3. Histograms (blue) with probability density curves (red) and kernel density estimates (KDE; yellow) comparing U-Pb and fission track (FT) ages of detrital apatites (DA) and zircons (DZ) from the Mtuka and Namba members of the Galula Formation. KDE plots are adaptive and use a Gaussian kernel. The detrital zircon U-Pb ages from the Mtuka Member are sourced from Roberts et al. (2012), and all other data was generated in this study. Vertical colored bars are interpretations of sediment provenance, and correspond to the maps in figures 2 and 14.

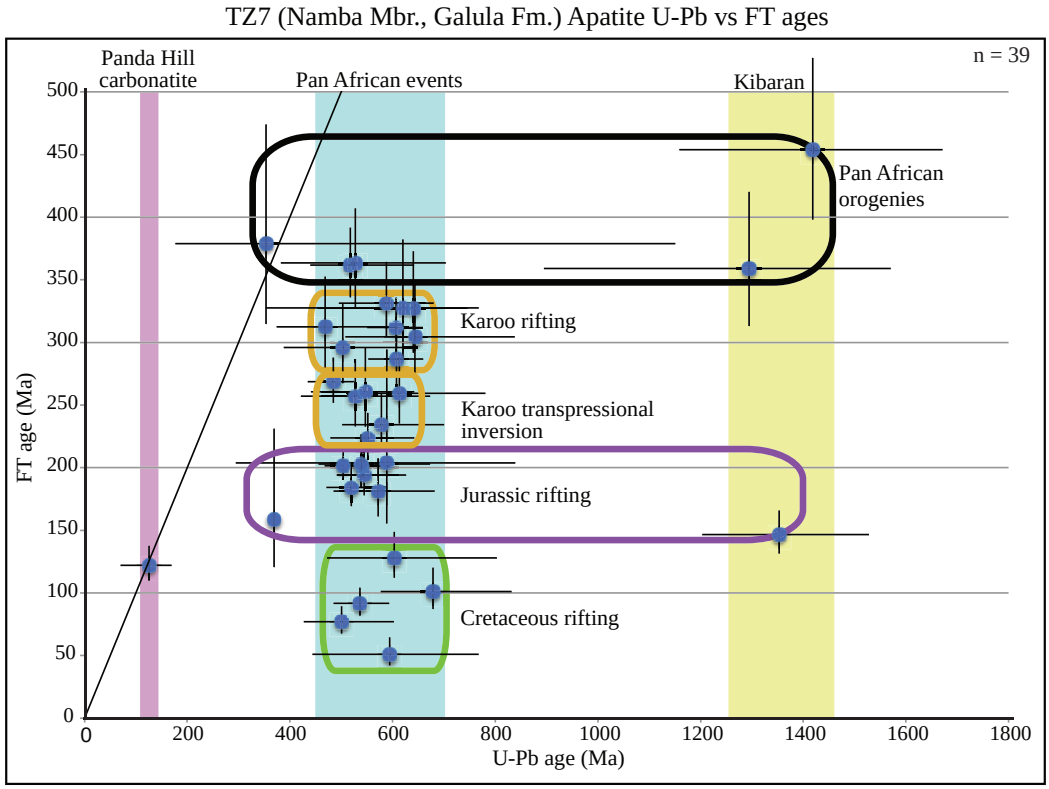

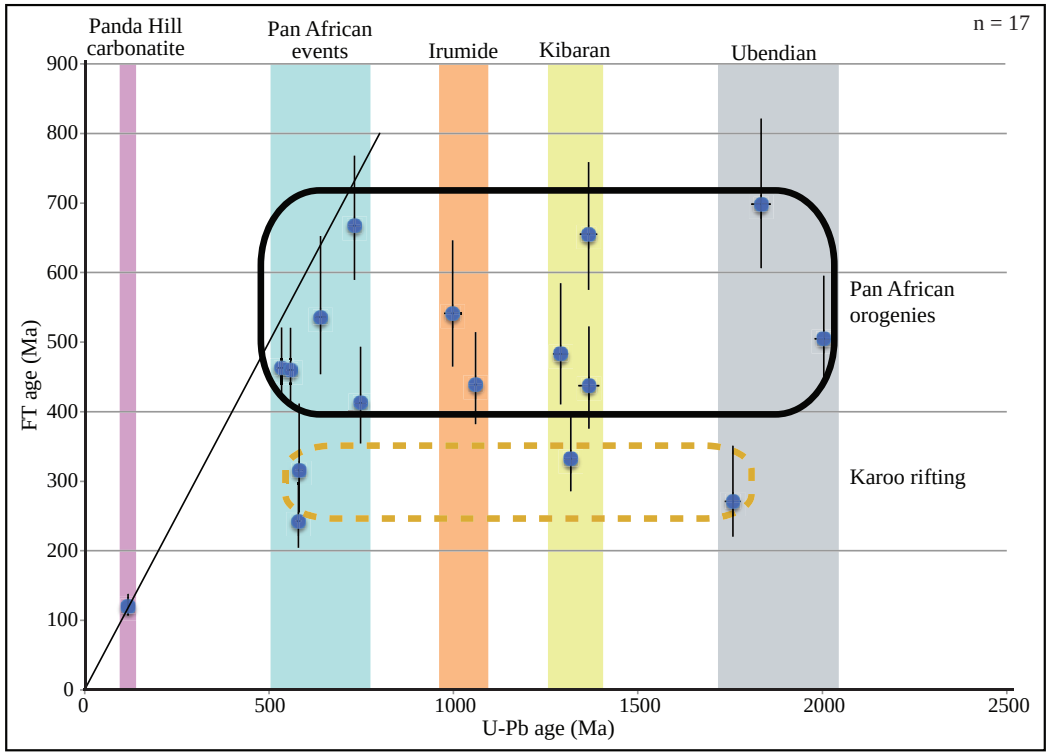

Fig. 4. Low-temperature thermochronology data for sample "TZ7" from the Cretaceous Namba Member of the Galula Formation. Each blue data point represents a single detrital apatite or zircon grain that was double dated via U-Pb geochronology and fission track analysis. Vertical colored bars are sediment provenance interpretations (see figures 2 and 14). Colored ovals represent interpretations of populations of detrital zircon or apatite grains with cooling ages that correspond to tectonic events known to have affected eastern Africa and the Rukwa Rift region. The diagonal black line represents where x=y (i.e., where U-Pb date = fission track date). All error bars represent 1-sigma errors.

zircon U-Pb ages were obtained, and the age population signature matches detrital zircon ages reported in Roberts et al. (2012) for this unit, with a minor 2000-1750 Ma population, a minor 1600-1200 Ma population, a slightly more significant 800-450 Ma population, and dominated by a 1100-900 Ma population (Fig. 3). The youngest single detrital zircon grain detected is 118 Ma. Seventeen of these detrital zircon grains were double dated via the fission track method. The results suggest a period of cooling from ~700-400 Ma. There is also a less clearly defined cooling episode distinguishable from ~350-225 Ma, although two grains from this younger zircon fission track age population overlap in error with the older population.

4.2 Nsungwe Formation

A critical sample ("BigWall") from the Songwe Member of the Nsungwe Formation was chosen for geochronologic and thermochronologic studies. This sandstone sample comes from a major vertebrate fossil locality termed "BigWall", which is a heavy mineral-rich sandstone characterized by a distinct assemblage of volcanic minerals (zircon, apatite, titanite, sanidine, andradite garnet, pyrochlore, and phlogopite) and is stratigraphically situated between two well-dated (via U-Pb CA-TIMS) tuffs. The lower tuff ("TZ61911-1") has been dated at 25.237 ± 0.098 Ma, whereas the overlying tuff ("TZ62512-3") yielded an age of 25.214 ± 0.021 Ma (Stevens et al., 2013). The detrital geochronology and thermochronology results obtained here can therefore be precisely constrained in time by these two tuffs. One hundred thirty-nine detrital apatite grains were dated via LA-ICP-MS U-Pb analysis, revealing a dominant apatite population around 200-170 Ma, a less abundant apatite population around 150-25 Ma, and a small population of apatites ~950 Ma (Fig. 5). From this unit, 102 apatite grains were double dated via fission track analysis, yielding Jurassic through Cretaceous cooling ages, as well as a population of apatites with cooling ages that are equal to their crystallization age of ~25 Ma, equivalent to both the depositional age of the strata ("BigWall" locality) and to the magmatic age associated with the volcanic ash beds bracketing the site (Fig. 6; Roberts et al., 2012; Stevens et al., 2013).

U-Pb LA-ICP-MS was also used to date 140 detrital zircon grains, which show two dominate age populations, one at ~2800-2600 Ma, and a second at ~2000-1800 Ma (Fig. 5). Two ~25 Ma zircons were also recovered. Twenty of the detrital zircons were double dated via fission track analysis (Fig. 6). The main period of cooling that is recorded spans ~600-400 Ma. Finally, thirteen detrital apatites from "BigWall" yielded acceptable (U-Th)/He ages, comprising one population at ~25 Ma, with a range of other single grain ages up to ~160 Ma (Fig. 7).

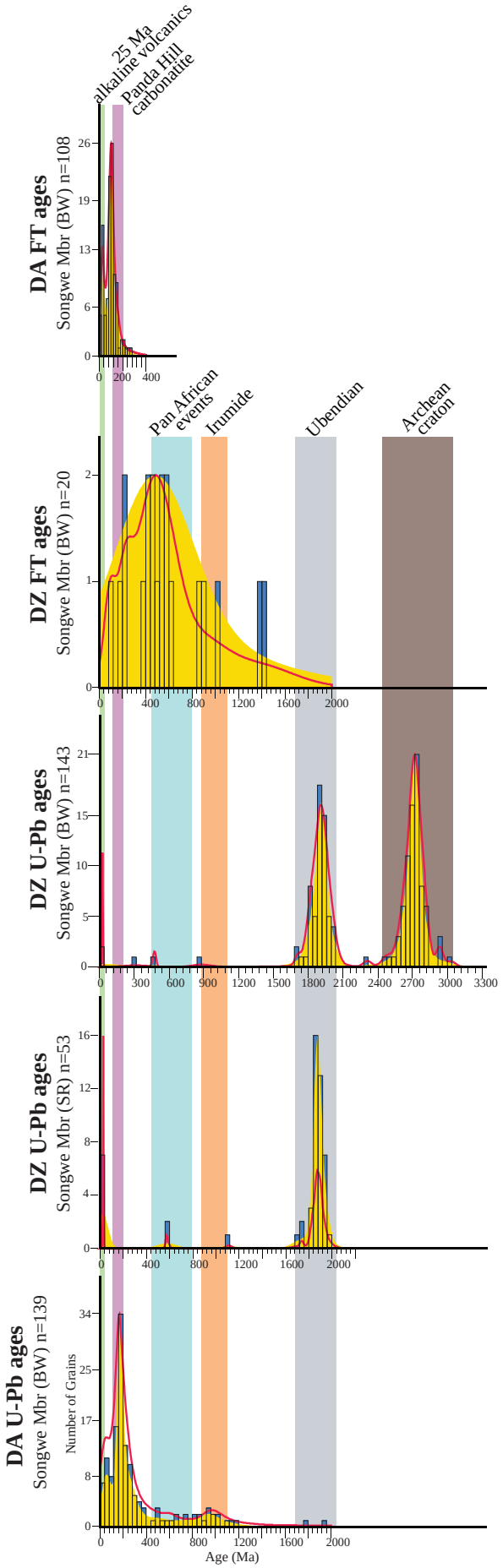

Fig. 5. Histograms (blue) with probability density curves (red) and kernel density estimates (KDE; yellow) comparing U-Pb and fission track (FT) ages of detrital apatites (DA) and zircons (DZ) from the Songwe Member of the Nsungwe Formation. KDE plots are adaptive and use a Gaussian kernel. The detrital zircon U-Pb ages from the Songwe Member marked "SR" are sourced from Roberts et al. (2012), and all other data was generated in this study (BW = "BigWall"). Vertical colored bars are interpretations of sediment provenance, and correspond to the maps in figures 2 and 15.

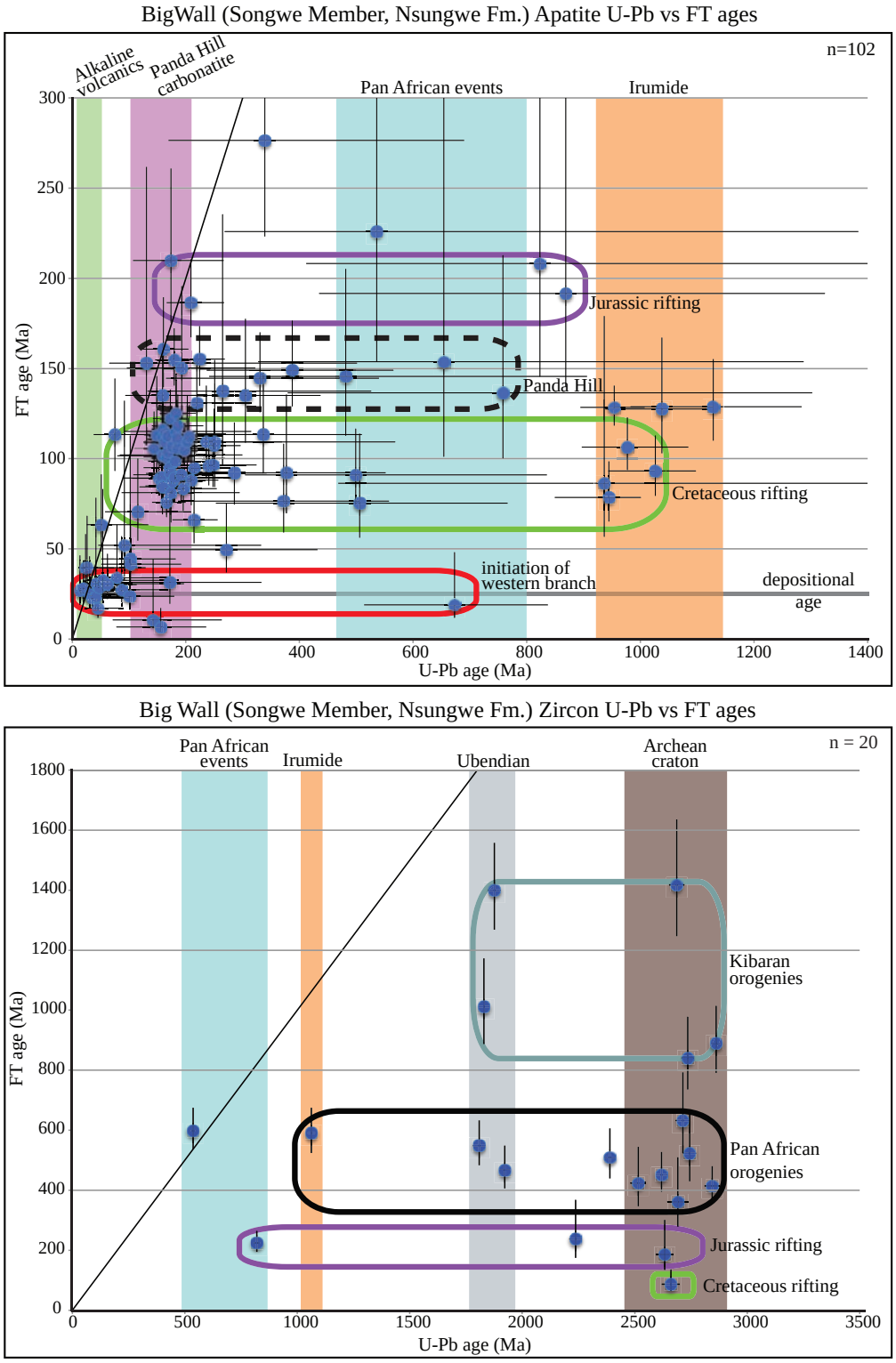

Fig. 6. Low-temperature thermochronology data for sample "BigWall" from the Oligocene Songwe Member of the Nsungwe Formation. Each blue data point represents a single detrital apatite or zircon grain that was double dated via U-Pb geochronology and fission track analysis. Vertical colored bars are sediment provenance interpretations (Figs. 2 and 15). Colored ovals represent interpretations of populations of detrital zircon or apatite grains with cooling ages that correspond to tectonic events known to have affected eastern Africa and the Rukwa Rift region. The diagonal black line represents where x=y (i.e., where U-Pb date = fission track date). All error bars represent 1-sigma errors.

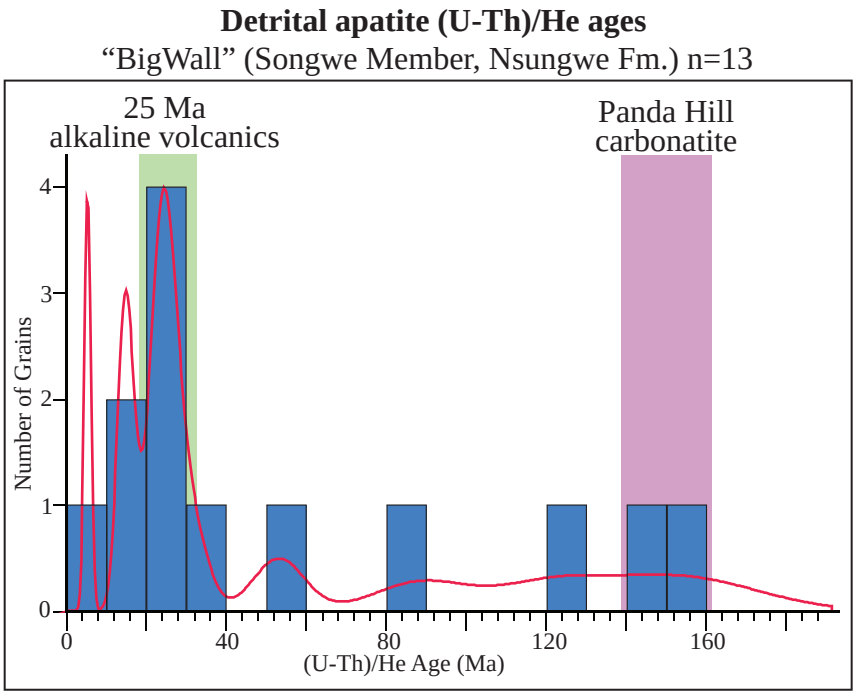

Fig. 7. Histogram (blue) with probability density curve (red) displaying detrital apatite (U-Th)/He ages for 13 apatite grains from the "BigWall" sample of the Oligocene Songwe Member of the Nsungwe Formation. The vertical colored bars mark time periods of volcanic activity in the immediate vicinity of the study area, in the southern Rukwa Rift Basin.

4.3. Lake Beds succession

The continental Lake Beds succession was the primary focus of this project and hence is represented by the most extensive U-Pb detrital zircon campaign. Both outcrop samples and samples from two hydrocarbon exploration wells were investigated, with the combined purpose of trying to refine the depositional ages of the Lake Beds units for the first time, understand its sedimentary provenance, and date the timing and frequency of EARS-related Neogene-Quaternary rifting in the basin, following its initiation in the late Oligocene. Cutting samples from the Galula-1 and Ivuna-1 hydrocarbon exploration wells (see Fig. 1 for locations) were analyzed via LA-ICP-MS U-Pb detrital zircon geochronology (Figs. 8 and 9). Previously, samples from these wells have yielded conflicting biostratigraphic age results (see Chapter Three). The supply of cuttings from the Galula-1 and Ivuna-1 wells was very limited, so to enhance the detrital zircon yield sample sizes were increased by aggregating a number of individual cuttings samples over depth ranges from 150-360 ft (46-110 m; average 226 ft / 69 m) in the Galula-1 well (see Chapter Three and Hilbert-Wolf et al., in press). A larger sample from each targeted depth in the Galula-1 well would be preferable to combining smaller volume well cuttings over longer intervals, but this was not possible in this study utilizing legacy well cuttings. While this may somewhat compromise the resolution of the U-Pb datasets through the Galula-1 well, this approach to increase sample size by combining cuttings over a few hundred feet was adequate, as evidenced

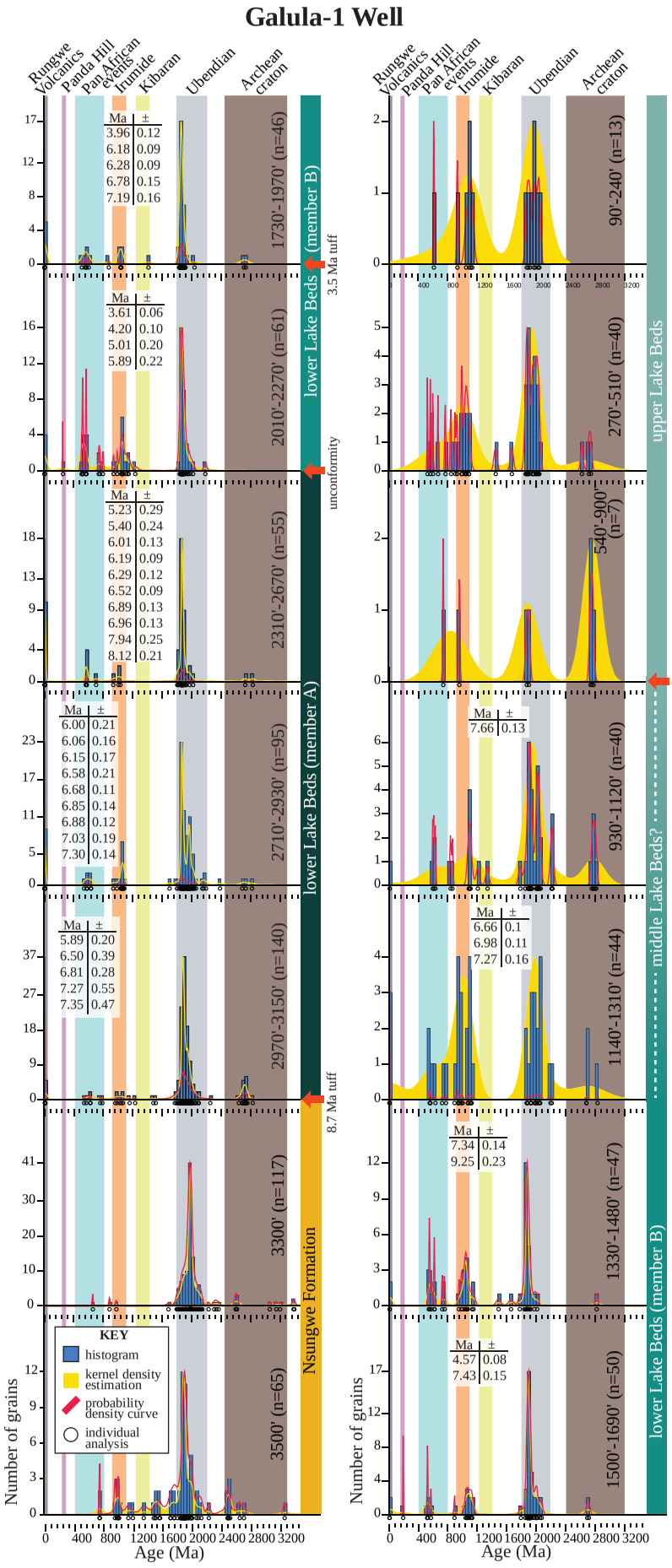

Fig. 8. Detrital zircon U-Pb age data for 14 well cutting samples through the Galula-1 exploration well. Samples are labeled with the depth(s) that each was retrieved from. Histograms (blue) with probability density curves (red) and kernel density estimates (KDE; yellow) are plotted for each sample. KDE plots are adaptive and use a Gaussian kernel. Colored bars represent interpreted source regions, and correlate to the provenance map in Fig. 2. Note that the scaling of the y-axis changes depending on the number of analyses represented for each sample. Young (<10 Ma) detrital zircon ages capable of refining maximum depositional age assignments for the Lake Beds strata are highlighted in the white boxes (see Chapter Three for further details). Red arrows indicate stratigraphic tie points between the Galula-1 well and dated tuffs and unconformities documented in outcrop (see Chapter Three).

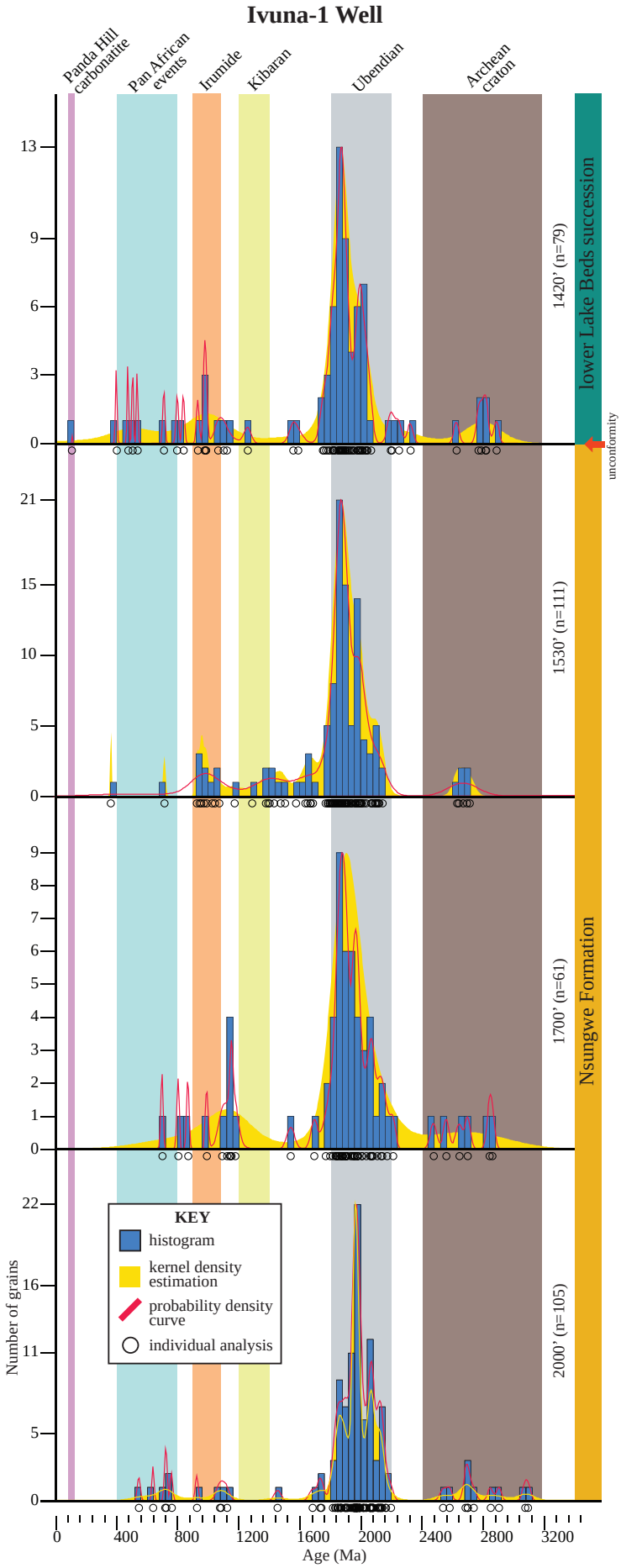

Fig. 9. Detrital zircon U-Pb age data from four well cutting samples through the Ivuna-1 exploration well. Samples are labeled with the depth that each was retrieved from. Colored bars represent interpreted source regions, and correlate to the provenance map in Fig. 2. Note that the scaling of the y-axis changes depending on the number of analyses represented for each sample.

by correlation of detrital zircon population patterns between Galula-1 well samples and outcrop samples from the Lake Beds, and by the identification of a detrital zircon maximum depositional age younging trend upward through the Galula-1 well (see discussion below and Hilbert-Wolf et al., in press). Fourteen composited samples were selected from the Galula-1 well (0489729 E 9053938.8 N; UTM zone 36, ARC 1960 datum), two of which are from the Nsungwe Formation (from 3500 ft / 1067 m and 3300 ft / 1006 m depth) and the remaining 12 are from the Lake Beds succession over the interval 3150-90 ft (960–27.4 m), with each sample initially weighing between 150-500g. Well cutting samples from the Galula-1 well yielded a total of 820 concordant detrital zircon U-Pb ages (Fig. 8).

Four samples were investigated from the Ivuna-1 well (0423732.4 E 9087313.4 N; UTM zone 36, ARC 1960 datum); two from the Nsungwe Formation and two from the Lake Beds succession, yielding a total of 356 concordant detrital zircon U-Pb ages (Fig. 9). All four samples from the Nsungwe Formation, across both wells, record nearly identical detrital zircon signatures. The dominant detrital zircon age population ranges from ~2120-1860 Ma. Very minor age populations (1-4 grains per sample) exist at ~2700 Ma and between ~1160-1100 Ma. The Lake Beds samples from the Ivuna-1 and Galula-1 wells display a dominant detrital zircon population between ~2200-1800 Ma. The two Lake Beds samples from Ivuna-1 (1530 ft and 1420 ft) and the lower seven Lake Beds samples from Galula-1 (3150 ft to 1330 ft) contain minor detrital zircon age populations spanning ~1200-400 Ma (each group consisting of 1-5 detrital zircon grains). The top five Lake Beds samples from Galula-1 record a shift in detrital zircon age populations. These samples exhibit two dominant detrital zircon populations from ~1100-900 Ma and from ~2200-1800 Ma, the latter of which also dominates each of the Lake Beds samples lower in the well. Take note that these provenance shifts could be affected by the composite samples representing the Galula-1 well as well as by differences in the number of recovered detrital zircons from each sample (i.e., different n, see Fig. 8). The lower nine Lake Beds samples from the Galula-1 well also have a young Neogene zircon population spanning 9-3 Ma, which yield a distinct up section younging trend (see Chapter Three and Hilbert-Wolf et al., in press, for a discussion of these young zircons).

Four sandstone samples from outcrops of the Lake Beds succession in the Hamposia and Galula areas were analyzed, yielding 419 concordant detrital zircon ages (Fig. 10). Samples “7/5/13-2”, “Hippo Quarry”, and “HW6/18/12-3” are derived from the lower Lake Beds succession, and sample “HW6/16/12-1” was collected from the upper Lake Beds succession (presented in stratigraphic order in Fig. 10). “7/5/13-2” and “Hippo Quarry” are precisely constrained in time by two tuffs dated at 8.7 Ma and 3.5 Ma, via U-Pb LA-ICP-MS on zircon (Fig. 10; see Chapter Three for details). All four samples contain a few (1-4) Archean-aged grains. The three lower Lake Beds samples are dominated by Paleoproterozoic zircons

that form a distinct population between ~2150-1800 Ma. This population remains present in the stratigraphically highest sample from the upper Lake Beds (HW6/16/12-1), however this sample is dominated by Mesoproterozoic-Neoproterozoic zircons forming a single population between 1200-850 Ma. This sample also contains a minor Neoproterozoic-Cambrian zircon population (660-520 Ma). Additionally, sample 7/5/13-2 contains a minor

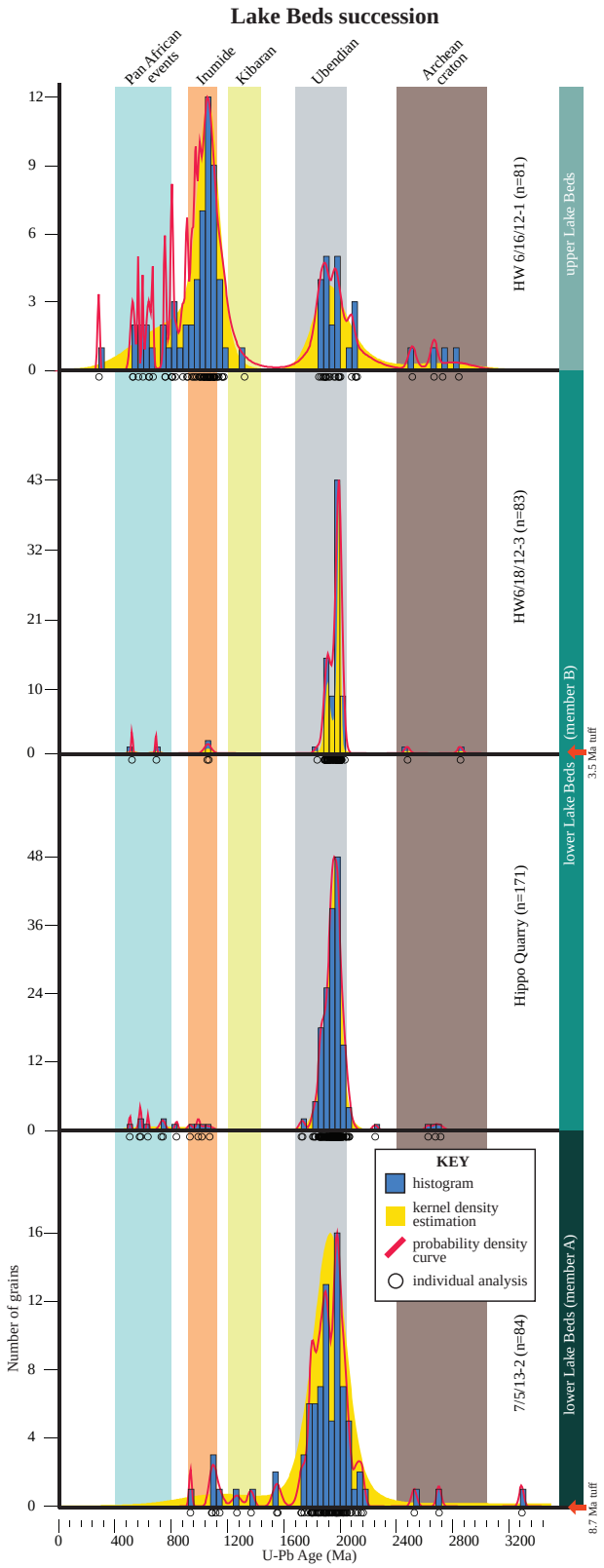

Fig. 10. Detrital zircon U-Pb age data from four outcrop samples from the Lake Beds succession from the Galula and Hamposia study areas (Fig. 1). Colored bars represent interpreted source regions, and correlate to the provenance map in Fig. 2. Note that the scaling of the y-axis changes depending on the number of analyses represented for each sample. The red arrow indicates the stratigraphic locations of the 3.5 and 8.7 Ma dated tuffs, which are intercalated with the detrital zircon samples at the Hamposia study site (Chapter Three).

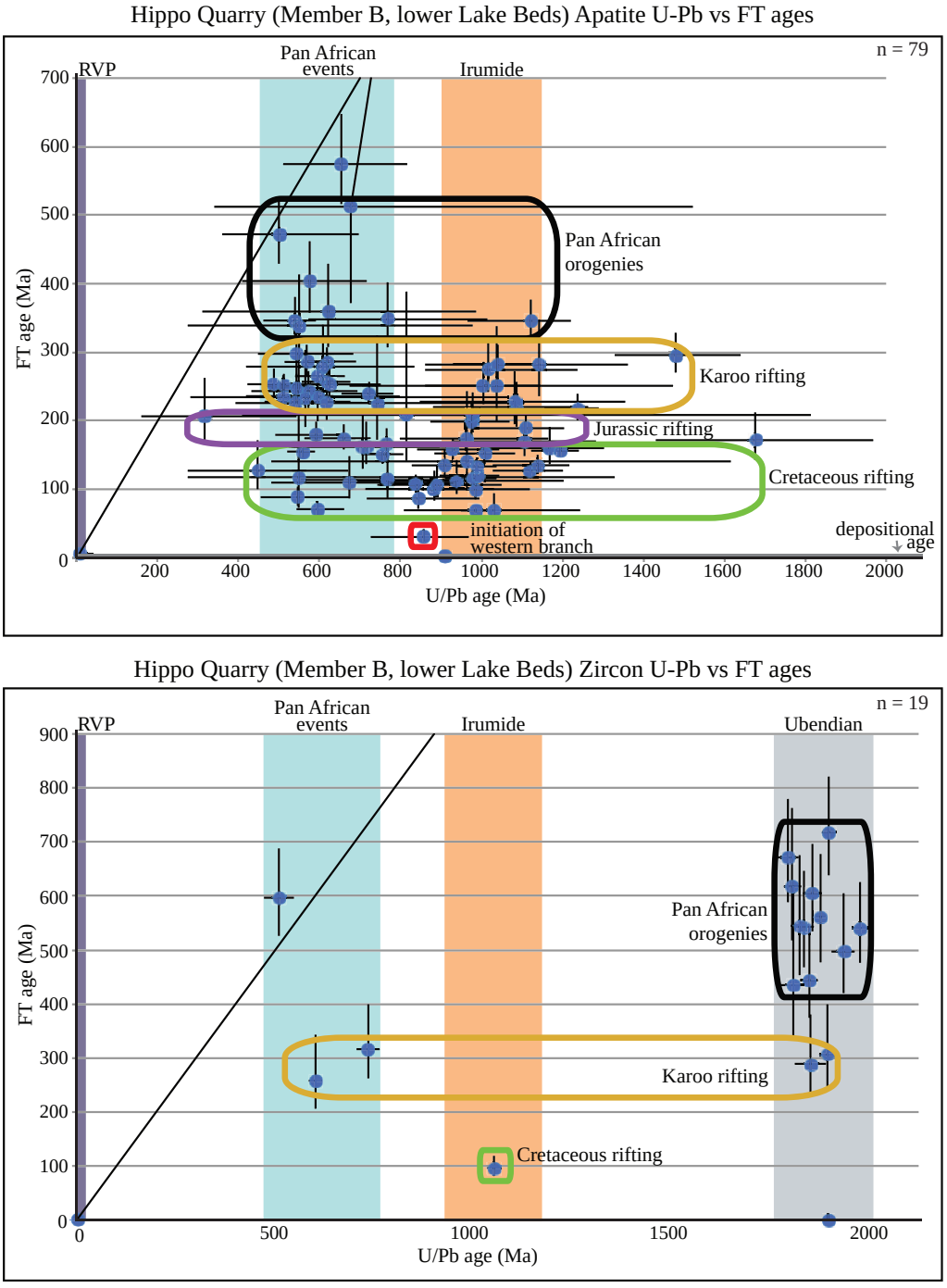

Fig. 11. Low-temperature thermochronology data for sample “Hippo Quarry” from member B of the lower Lake Beds. Each blue data point represents a single detrital apatite or zircon grain that was double dated via U-Pb geochronology and fission track analysis. Vertical colored bars are sediment provenance interpretations (see Figs. 2 and 15). Colored ovals represent interpretations of populations of detrital zircon or apatite grains with cooling ages that correspond to tectonic events known to have affected eastern Africa and the Rukwa Rift region. The diagonal black line represents where x=y (i.e., where U-Pb date = fission track date). All error bars represent 1-sigma errors.

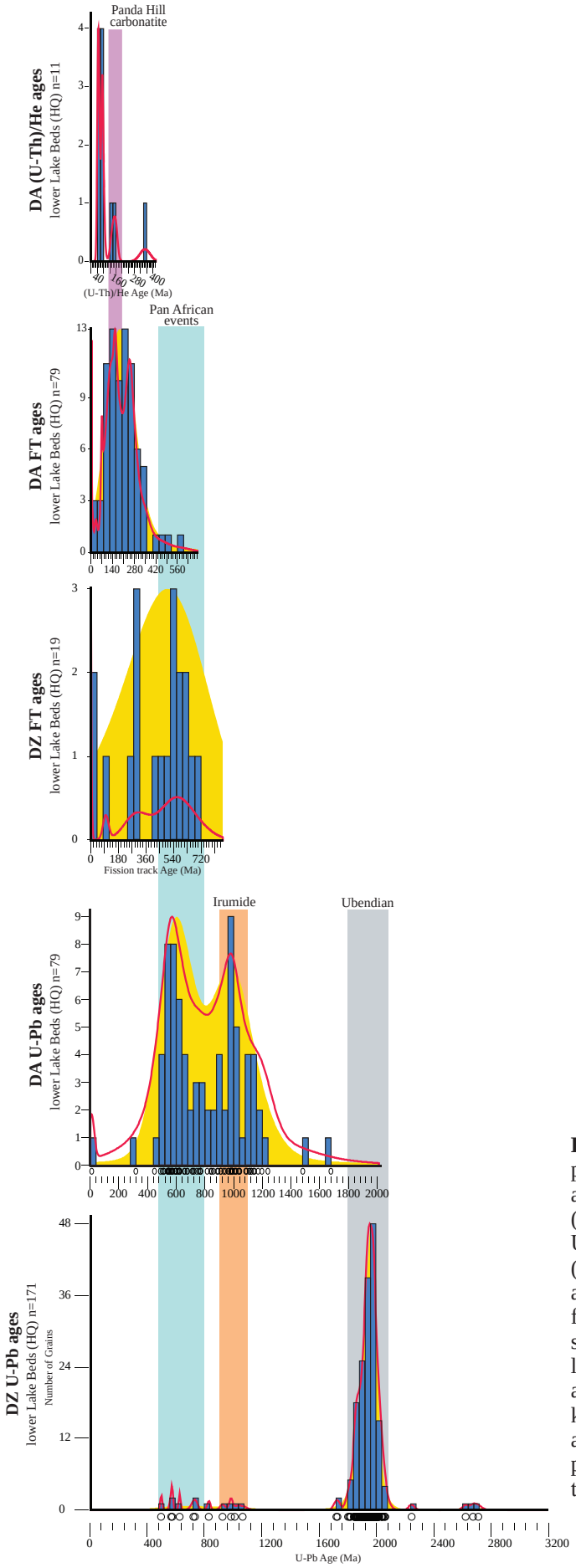

Fig. 12. Histograms (blue) with probability density curves (red) and kernel density estimates (KDE; yellow) comparing U-Pb, fission track (FT), and (U-Th)/He ages of detrital apatites (DA) and zircons (DZ) from the "Hippo Quarry" sandstone of member B of the lower Lake Beds. KDE plots are adaptive and use a Gaussian kernel. Vertical colored bars are interpretations of sediment provenance, and correspond to the maps in figures 2 and 15.

population of zircons (<10 grains) ranging in age from ~1600-900 Ma. The two middle samples (Hippo Quarry and HW6/18/12-3) each contain <10 zircon grains ranging in age from ~1100-500 Ma.

The lower Lake Beds "Hippo Quarry" sample from the informal upper "member B" was selected for detrital apatite and zircon fission track and LA-ICP-MS U-Pb double dating (Fig. 11). The "Hippo Quarry" sandstone sample entombs the skull of a recently discovered, potentially new species of Hippopotamidae (N. Stevens, pers. comm.), and therefore represents a critical interval of the Lake Beds succession that is yielding an entirely new and previously unknown Mio-Pliocene fossil fauna from this portion of the East African Rift System. Seventy-nine detrital apatite grains were dated via LA-ICP-MS and yielded two distinct populations of U-Pb ages ranging from ~1200-900 Ma and from ~800-600 Ma (Figs. 11 and 12). These same apatite grains yielded fission track cooling ages spanning ~500-75 Ma, with the majority less than 300 Ma. Four detrital apatite fission track age populations can be discerned, including a population spanning 500-350 Ma, a population from 300-200 Ma, a population from 200-175 Ma, and the youngest population ranges in age from 175-75 Ma. Nineteen detrital zircons were double dated, 15 of which ranged in U-Pb age from ~2000-1800 Ma, and the others from ~1100-500 Ma. Fourteen zircons yielded fission track ages between ~700 and ~425 Ma. Four zircons recorded Carboniferous-Permian fission track ages (~325-250 Ma), and one zircon recorded cooling at ~100 Ma. We also report eleven detrital apatite (U-Th)/He ages from the "Hippo Quarry" sample (Fig. 12). The two minor populations span ~160-140 Ma (2 grains) and ~80-40 Ma (8 grains). There is one older zircon (U-Th)/He age of 350 Ma.

5. Interpretation and Discussion of the uplift history of the Rukwa Rift Basin

5.1. Accordion-like rift tectonics

Certain rift segments that now comprise the East African Rift System are clearly much older than the Cenozoic EARS. The Rukwa Rift is a classic example of one of these long-lived basins, as it has developed within a Precambrian shear zone, which has a prolonged infill history recording repeated accordion-like rifting behavior in response to repeated, far-field tectonic stresses affecting the African continent through the Phanerozoic (Fig. 13). What is remarkable is that rift basins like the Rukwa appear to continuously record these tectonic perturbations via their infill history, and these events can be identified via a combination of careful investigations of the sedimentary depositional record, dating of intercalated volcanics, and deciphering of denudation/uplift events recorded by detrital grains shed into the basin over time via low-temperature thermochronology. Unlocking

this history of the continent is not easy though, as the sedimentary infill is these basins is complex and in the case of the Rukwa Rift Basin, difficult to unravel via traditional lithostratigraphy and biostratigraphy alone, particularly because of the common issue of reworking and deposition of lithologically similar stratigraphic units through time (e.g., see Roberts et al., 2010 for a review of the debate over the age and stratigraphy of the Red Sandstone group).

Low-temperature thermochronology analyses (fission track and (U-Th)/He) of detrital zircon and apatite grains from Cretaceous – Pliocene sedimentary strata in the Rukwa Rift Basin document the long-lived cooling, rock uplift, and denudation histories of the source terranes immediately surrounding this part of the EARS. From the new data sets presented here it is clear that the southern part of the western branch and surrounding regions were repeatedly affected by tectonic events since the Proterozoic. This is made evident in the spread of detrital apatite fission track ages (and to a lesser extent detrital zircon fission track ages) from the Namba Member, Songwe Member, and lower Lake Beds samples, which show more-or-less continuous cooling of the source areas from 700 to 76 Ma (Figs. 4, 6, and 11). Due to the nature of apatite U-Pb geochronology and detrital fission track thermochronology, these particular datasets have large errors, and also sometimes low numbers of grains per sample (particularly for zircon fission track ages), which together limits the resolution of these datasets, and therefore caution is exercised in their interpretation. However, while fission track age uncertainties cause many of the interpreted periods of cooling to overlap, the delineation of these zones is still possible based upon the correlation of our data with already known periods of tectonic activity that have affected eastern Africa. For example, the three double dated samples have four common fission track age populations: 1) 700-350 Ma (Pan African), 2) 350-225 Ma (Karoo rifting), 3) 200-150 Ma (Jurassic rifting), and 4) 150-76 Ma (Cretaceous rifting) (Figs. 4, 6, and 11). All of these cooling ages can be linked to orogenic and rifting events that affected eastern and southern Africa. These cooling ages reflect the thermal and tectonic histories of the various sediment source areas (typically mobile belts that have been reactivated by tectonic events) that have provided sediment to the Rukwa Rift Basin, which includes the Ubendian, Mozambique, Usugaran, Kibaran, and Irumide belts, as well as the southern Songwe Valley carbonatite suite. Most cooling ages are recorded by apatites with Pan African crystallization ages, which can be derived from a number of these previously mentioned sources. The Pan African orogenies in particular left the most extensive regional thermal signature according to the data we have collected from the Rukwa Rift Basin, as 800-500 Ma fission track ages are common across all detrital zircon and apatite data sets (except for apatites from the Songwe Member), and affect grains derived from over four different source areas (Figs. 2, 4, and 11). After the conclusion of the Pan African orogenies, rifting dominated the tectonic evolution of this part of eastern

Africa (Delvaux, 1991; see section 5.1 above).

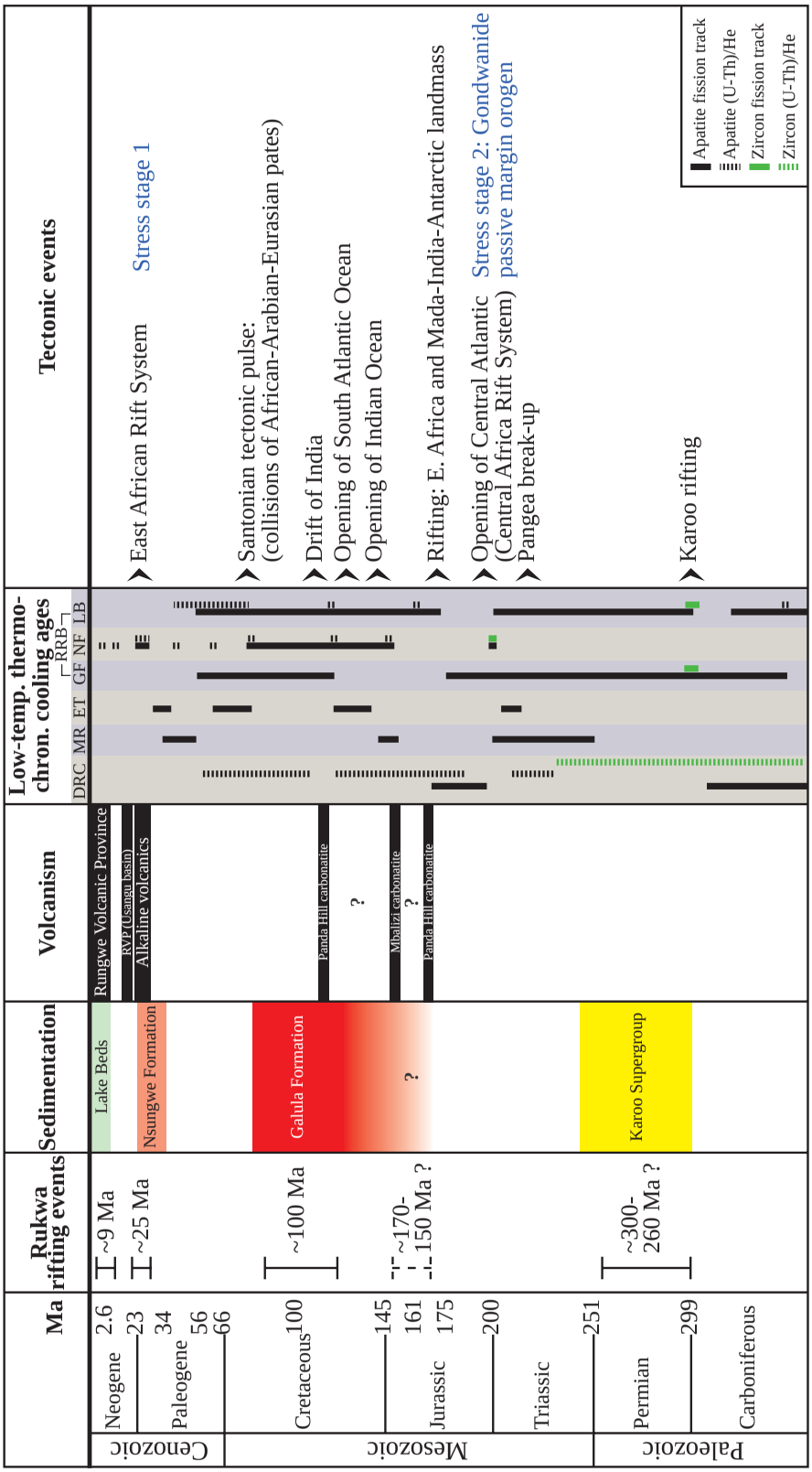

Fig. 13. Summary diagram showing the chronology of rifting, sedimentation, and volcanism in the Rukwa Rift region based on both new and existing geologic analyses, geochronology, and low-temperature thermochronology data. These data are displayed alongside the stress stages of Delvaux et al. (2012) for the Tanganyika-Rukwa-Malawi rift segments and possible regional-scale tectonic drivers. Low-temperature thermochronology data is presented as age ranges, and the colored bars serve only to differentiate each data set for visualization purposes. DRC = western flank of Albertine Rift (Bauer et al., 2015); MR = Malawi Rift (Van der Beek et al., 1989); ET = eastern Tanzania (Noble et al., 1997); RRB = Rukwa Rift Basin (this study; GF = Galula Fm., NF = Nsungwe Fm., LB = Lake Beds succession).

5.2. Timing of rifting and uplift

5.2.1. Late Paleozoic

The Rukwa Rift Basin has been active, experiencing repeated episodes of subsidence and sediment deposition since the Permo-Triassic, as recorded by deposition of the Karoo Supergroup (Wopfner, 2002; Fig. 13). During all phases of extension and basin filling, rifting is primarily controlled by preexisting basement structures (i.e., the Ubendian Belt). Little work has been conducted to date on the timing and duration of rifting during the late Paleozoic; however it appears as though the Karoo strata preserved in the Rukwa Rift Basin terminate prior to the Triassic. Sediments from the Galula Formation and the lower Lake Beds succession contain populations of detrital apatite and zircons with fission track ages spanning 350-225 Ma (Figs. 4 and 11), derived from Pan African, Irumide, and Ubendian-aged sources that record this Karoo-associated rifting and subsequent inversion. Van der Beek et al. (1998) recorded a phase of rapid cooling and denudation of the rift flanks from ~250-200 Ma, and interpreted this as an erosional event that marked the termination of Karoo activity in eastern and southern Africa.

5.2.2. Late Mesozoic

The second major episode of sedimentation in the rift is also poorly constrained and has remained controversial for many years (Dypvik et al., 1990; Damblon et al., 1998; Roberts et al., 2004; 2010; 2012). This is represented by the Red Sandstone Group, which has since been shown to actually represent two discrete late Mesozoic and late Paleogene rifting events (Roberts et al., 2010). A wealth of recent paleontological discoveries and sedimentological analyses has demonstrated that the Mesozoic Galula Formation has two members. The depositional age of the lower Mtuka Member is still unclear, but likely somewhere between Middle Jurassic and mid-Cretaceous. However, the upper Namba Member has produced an important assemblage of vertebrate fossils that indicate a mid to Late Cretaceous age (O'Connor et al., 2006; 2010).

There is little consensus on the initiation of rifting during the late Mesozoic, however, Van der Beek et al. (1998) recorded a phase of rapid cooling and uplift of the western flank of the Rukwa Rift at ~150 Ma, which can be linked to far-field stresses due to the breakup of Gondwana, as South America began to move away from Africa in the Late Jurassic – Early Cretaceous (Nürnberg and Müller, 1991). At the same time, sea floor spreading between Africa and Madagascar occurred between 165-80 Ma, which represents the beginning of Gondwanan break-up (Coffin and Rabinowitz, 1988). What is now the eastern branch of the East African Rift System was affected as well, as revealed by rapid denudation

around the central Kenya Rift recorded from 140-120 Ma (Foster and Gleadow, 1992). Detrital apatites from this study from the Namba Member of the Galula Formation show a single population of grains (n=5) with Cretaceous fission track ages (128-77 Ma; Fig. 4), perhaps partially recording the Santonian tectonic pulse (related to the opening of the Atlantic Ocean; Fig. 13) that affected much of Africa (Guiraud and Bosworth, 1997) and likely caused the folding and faulting of the Namba Member as seen in outcrop. What is significant though, is that this Cretaceous cooling recorded by detrital apatite fission track ages helps to constrain radioisotopically for the first time the depositional age of the Namba Member to ~130-80 Ma. Since this Early-Late Cretaceous cooling event did not affect all of the detrital apatites analyzed from the Namba Member (i.e., the entire Namba Member was not thermally reset; Fig. 4), the Pan African-aged source area from which these grains were derived (Figs. 2 and 14) must have been uplifted / denuded at this time, prior to sediment deposition in the Rukwa Rift Basin. One reason that this Cretaceous cooling/denudation signal is not better represented in the Namba Member detrital zircon and apatite record is due to sediment drainage patterns at the time. Sediment was sourced primarily from the south (Fig. 14), and therefore not from the rift flanks, where Cretaceous uplift and denudation was expressed (particularly the western flank) as suggested by Van der Beek et al. (1998). Additionally, throughout all the sedimentary units of the Rukwa Rift, Ubendian-aged (i.e., derived from the rift flanks) apatites were not recovered, and therefore signals recording rift flank activity were not detectable from the detrital apatite fission track or detrital apatite (U-Th)/He data. This new age constraint is in agreement with faunal data that indicate a "middle" Cretaceous age (~120-90 Ma; O'Connor et al., 2006), and refines the ~150 Ma detrital zircon maximum depositional age of Roberts et al. (2007).

The Jurassic-Cretaceous carbonatite suite at the southern end of the Songwe Valley is the most proximal volcanic center approximately corresponding in time to this rifting event. While Jurassic-Cretaceous volcanic grains are not common in the Namba Member, detrital apatites from the Oligocene Songwe Member ("BigWall" sample) are dominated by 200-150 Ma (U-Pb) apatites (Fig. 5), likely derived from this nearby carbonatite suite, and which record fission track ages of 125-75 Ma (Fig. 6). This suggests that the carbonatite suite perhaps experienced multiple eruptions over a time period of ~100 million years, exhumed slowly over time, and that younger eruptions (e.g., 113 Ma carbonatite; Snelling, 1965) may have reheated the older carbonatite deposits (e.g., 165.7 - 154.2 Ma carbonatites; Mesko et al., 2014).

5.2.3. Early Cenozoic

An unusual population of (U-Th)/He detrital apatite ages is present in both the Songwe Member and lower Lake Beds samples, ranging in age from 80-40 Ma (HQ: n=8/11;

BW: n=2/13; Figs. 7 and 12). These particular ages stand out because they cannot be linked to known volcanism or sedimentation. However, this age range is similar to other thermochronologic ages recorded from the East African Rift System. Van der Beek et al. (1998) reported cooling of the western Rukwa Rift at <50-40 Ma, and rapid denudation are the central Kenya Rift is reported from 70-60 Ma (Foster and Gleadow, 1992; 1996). Deciphering the possibility of another widespread surface or rock uplift event spanning the Late Cretaceous – Paleogene could be critical for understanding the tectonic history of East Africa just prior to the onset of the development of the East African Rift System.

5.2.4. Late Cenozoic

In concert with the eastern branch, the Rukwa Rift was the earliest of the western branch basins to have been (re)activated as a consequence of the Late Cenozoic development of the East African Rift System, as recorded by the 26-24 Ma Nsungwe Formation sediments and tuffs (Roberts et al., 2012). The Ubendian Belt again responded to rifting stresses and controlled the location of basin development. Low-temperature detrital thermochronology data from this study does not support the hypothesis of major surface or rock uplift of the Rukwa Rift flanks or basin at the onset of the development of the western branch at ~25 Ma (Fig. 15B). A population of detrital apatite grains (n=12) from the Songwe Member of the Nsungwe Formation with fission track ages < 30 Ma (average: 21.5 Ma; Fig. 6) may indicate local volcanic reheating and subsequent cooling, or local rock uplift, but all other detrital apatites have cooling ages older than the deposition age of the Songwe Member. All of the detrital apatites with < 30 Ma fission track ages have U-Pb crystallizations ages corresponding to volcanic sources; either the Jurassic-Cretaceous Panda Hill, Mbalizi, and other carbonatites or to the 26-24 Ma alkaline volcanism recognized from tuffs in the Songwe Member (Fig. 6; Roberts et al., 2012). Since this 25 Ma cooling event did not thermally affect much of the Rukwa Rift Basin (i.e., the Songwe Member apatites were not all reset at 25 Ma), we can hypothesis that this 25 Ma cooling age corresponds to a volcanic event, and the provenance of the affected grains may suggest a potential source area for the 25 Ma alkaline volcanics: on top of or near to the existing Mesozoic carbonatite bodies (Fig. 15 B).

Since no other basins along the western branch predate the Miocene, the Rukwa Rift Basin is the best archive of tectonics, sedimentation, and climate in the western branch of the East African Rift System, and possibly of the entire EARS. In the Rukwa Rift Basin there is a strong link between subsidence, sediment accumulation, and volcanic episodes. The tuff-rich Oligocene Songwe Member and Lake Beds succession exemplify this and allow us to place radioisotopic constraints on the age of rift reactivation. The existence of the thick sedimentary package overlying the Galula and Nsungwe formations, known as the

Lake Beds, has been known about for decades (Quenell et al., 1956; Wescott et al., 1991; Roberts et al., 2010), but its exact age and relationship to the East African Rift System has remained largely unexplored until this study. A basal tuff from the Lake Beds at the Hamposia locality (Fig. 1) was identified and dated to 8.73 ± 0.06 Ma (Chapter Three; Hilbert-Wolf et al., in press), constraining for the first time the age of the next depositional sequence following the Oligocene Nsungwe Formation. This new age for the base of the Lake Beds (~8.7 Ma) is a regionally significant date, as it corresponds to the first stage of Late Cenozoic volcanism in the Rungwe Volcanic Province (Figs. 1 and 16) that spans ~9.2 - 5.4 Ma (Ebinger et al., 1989, 1993). In particular, Ebinger et al. (1993) dated the Songwe Tuff to 8.60 ± 0.04 Ma (40Ar/39Ar on anorthoclase separates), which also occurs in the region of northern Lake Malawi (Fig. 1B) and serves as the earliest evidence of Cenozoic rifting, or the initiation of rifting in the Malawi Rift. A second tuff higher in the sequence at Hamposia yielded an age of 3.54 ± 0.13 Ma (Chapter Three), and maximum depositional ages calculated from detrital zircon geochronology through the Galula-1 well cuttings demonstrate episodic deposition and periodic volcanic eruptions from ~9 – 3.5 Ma (Fig. 16). What is particularly striking about these new 'young' zircon ages is that they reveal a chronology of volcanism (and by proxy rift activity) that has been concealed before. In addition to the three active volcanoes of the Rungwe Volcanic Province, there are more than 100 geomorphically new cones and domes that are interpreted as being part of the most recent phase of volcanism (i.e., 0.6 Ma – Recent; Harkin, 1960; Fontijn et al., 2010). Therefore, whole rock radioisotopic dating of exposed volcanic rocks cannot reach volcanic sequences that are buried under the presently exposed cones. The detrital zircon and apatite record, particularly from subsurface samples, therefore reveal a more detailed chronology of volcanism in the Rungwe Volcanic Province (Fig. 16). This study does clearly link volcanism and sedimentation together, and provide new insights into the onset and duration of rifting. This coincidence was also noted by Ebinger et al. (1989), who observed that the location of volcanic provinces in the western branch (such as Toro-Ankole, Virunga, South Kivu, and Rungwe) show correlations with rift basin development and coincide with interbasinal accommodation zones.

Low-temperature thermochronology studies on the detrital zircon and apatite grains from a key unit of the Songwe Member ("BigWall") and a key unit of the lower Lake Beds ("Hippo Quarry") were aimed at detecting uplift events associated with rifting. The results consist of multiple populations of cooling ages in both members, recording several tectonic events (i.e., uplift/denudation) that affected the sediment source terranes since the Paleoproterozoic (see section 5.3 below). Detrital low-temperature thermochronology data does not suggest that at any time between 25 and 3.5 Ma the Rukwa Rift Basin was significantly inverted (Figs. 6, 11, and 12). Nor is there any evidence of significant surface uplift of the rift flanks during this time. For much of the history of rifting in the western

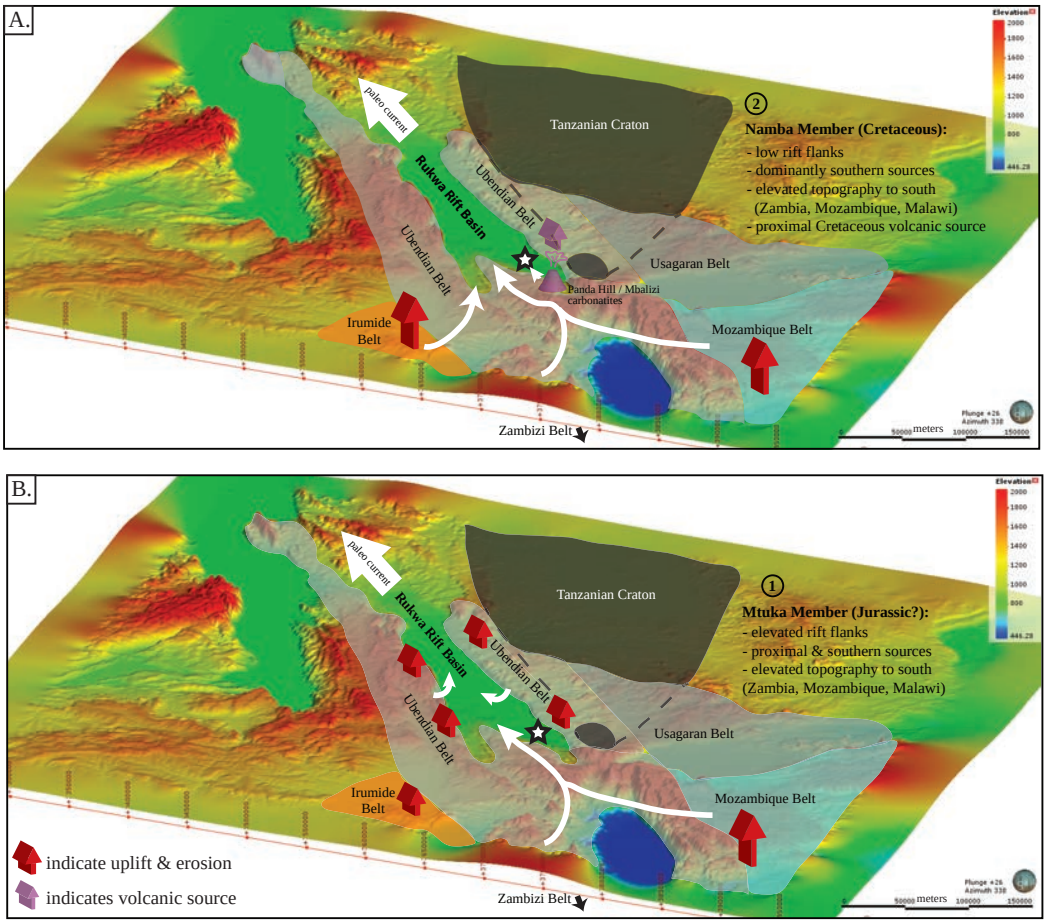

Fig. 14. Provenance and drainage evolution models for the Cretaceous Galula Formation (A: Namba Member and B: Mtuka Member) showing the proposed evolution of sediment routing patterns and source areas that were actively uplifting/eroding (i.e., topographic highs) during the Jurassic – Cretaceous deposition of the two members based on detrital zircon and apatite age data (Figs. 3 and 4). DEM maps were modified from the Arc-Minute Global Relief Model (Amante and Eakins, 2009). Paleocurrent direction is shown by white arrows and is modified from Roberts et al. (2012).

branch associated with the East African Rift System, it appears that significant uplift of the basin or rift flanks does not accompany subsidence, deposition, or volcanic events (i.e., rifting). Alternatively, it is possible that the Rukwa Rift Basin and/or rift flanks did undergo rock uplift and exhumation, which is not recorded in the detrital record. This data could suggest that the detrital minerals in the basin sediments were not sufficiently reheated prior to more recent exhumation to reset the thermochronometers. Perhaps rock uplift of the rift flanks is too recent (and/or small in magnitude) to have been exposed and subject to erosion by the time of deposition of the Lake Beds sediments.

Given the absence of uplift from the Oligocene – Pliocene, we hypothesize that the elevated rift flanks and deep incisions into the sedimentary strata in the Rukwa Rift (Karoo through Lake Beds) is a very recent (e.g., Pleistocene or younger) occurrence, not able to be detected by the geochronology and thermochronology techniques used in this study. This conclusion is supported by changes in the drainage patterns across the rift flank plateaus, which

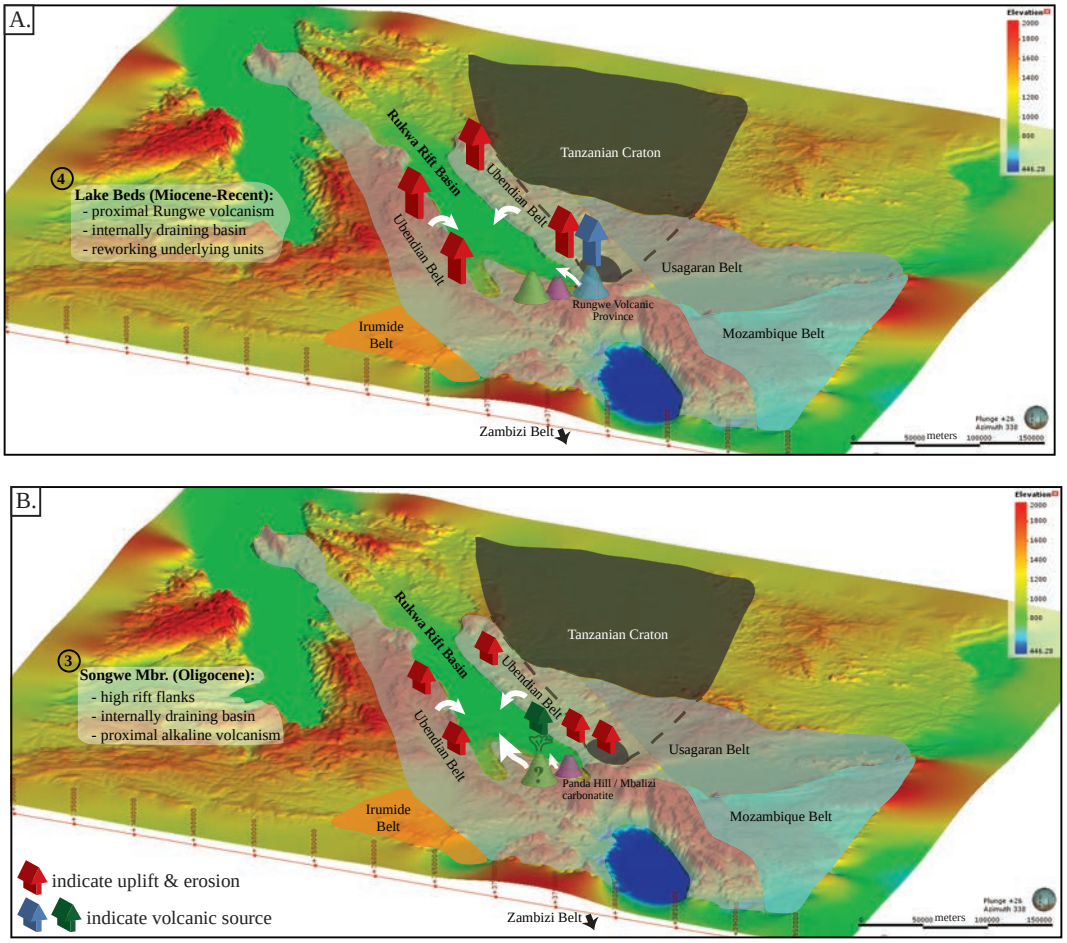

Fig. 15. Provenance and drainage evolution models for the Oligocene Songwe Member of the Nsungwe Formation (B) and for the Miocene – Pliocene lower Lake Beds (A), showing the proposed evolution of sediment routing patterns and source areas that were actively uplifting/eroding (i.e., topographic highs) during the deposition of the two units based on detrital zircon and apatite age data (Figs. 5-12). DEM maps were modified from the Arc-Minute Global Relief Model (Amante and Eakins, 2009). Paleocurrent direction is shown by white arrows and is modified from Roberts et al. (2012).

suggest that flank uplift was most rapid during the late Pliocene – Pleistocene (Grove, 1983; Baker, 1986), as rates of uplift along the northeastern flanks of the western rift system exceeded rates of downcutting along several rivers that previously flowed north into the Nile drainage basin. Additionally, rivers that originally flowed west into the Congo basin were diverted by uplift along the eastern flanks of the rift (Holmes, 1978; Grove, 1983; Baker, 1986). These rivers are now ponded in shallow lakes in the central uplifted plateau between the western and eastern rift systems (Ebinger, 1989). Uplift of the regions flanking the Songwe, Usangu, and Karonga basins has tilted Miocene and Pliocene Rungwe volcanic units away from the present axis of the rift valley; additional evidence for uplift postdating volcanism (and therefore basin subsidence as well; Ebinger et al., 1989).

5.3. Drainage evolution and sediment provenance of the Lake Beds

Roberts et al. (2010; 2012) provided the first geochronological constraints on sediment

provenance for strata in the Rukwa Rift Basin, which uncovered the sediment source areas and drainage patterns for the Cretaceous and Oligocene successions. These authors discovered fluvial drainage reversals that recorded the onset of topographic surface uplift caused by the African Superswell and the initiation of the western branch of the EARS contemporaneously with the eastern branch ~25 million years ago. At first, large-scale braided fluvial systems flowed northwest from highlands in Mozambique, Malawi, and Zambia during the middle Cretaceous, passing through the Rukwa Rift and ultimately draining into the Congo Basin. At this time subsidence of the Rukwa Rift Basin is thought to have been limited, with decreasing accommodation space throughout the deposition of the Galula Formation. Detrital zircon age spectra and paleocurrent measurements reveal that the Early-middle Cretaceous sediments are dominated by zircon from the proximal Ubendian Belt basement terranes of the Rukwa Rift margins, and from the southern Zambezi-Mozambique belts (Fig. 14). In the upper Namba Member, flank uplift and subsidence slowed, so proximal sediment from the Ubendian Belt ceased and was replaced by southern sources, including the Zambezi-Mozambique and Irumide belts (Fig. 14). Later, the Eocene-Oligocene initiation of the modern East African Rift System reactivated the Rukwa Rift ~24.9 Ma, renewing deposition via a predominantly interior-draining basin within a wetland environment dominated by active alkaline volcanics. A major drainage reversal between the deposition of the Galula Formation and that of the Nsungwe Formation is recorded by a zircon provenance shift in the Utengule Member, indicated by northern-derived zircons from the Karagwe-Ankole Belt and an increase in Ubendian-aged, or possibly Rusizian-derived zircon grains (Roberts et al., 2012). Deposition of the Songwe Member (coeval with the initiation of the western branch of the EARS) shows another provenance shift to almost exclusively Ubendian belt sediments, heralding the onset of an internally draining rift basin enclosed by elevated rift flanks. Significant scatter in paleocurrent directions and a shift from fluvial and alluvial fan to shallow-lacustrine depositional environments also corroborates a tectonically forced change in sedimentation in the Rukwa Rift Basin. By 26 to 25 Ma the Rukwa Rift Basin had developed into an internally draining basin with border faults, uplifted rift shoulders, and an active volcanic system (Fig. 15 B). Sediments from the modern Songwe River mirror the sediment provenance pattern of the Songwe Member, except they lack the Oligocene volcanic grains. The new detrital zircon data from this study provides data to fill this Neogene – Quaternary gap in understanding of sediment provenance and drainage patterns, allowing us to expand what we know about basin evolution over the Late Cenozoic, as the EARS was continuing to develop.

Deciphering the sediment provenance of the late Miocene Lake Beds succession and reconstructing sediment pathways demonstrates that the Rukwa Rift Basin remained an internally draining basin throughout the most recent episodes of rifting, beginning around

8.7 Ma and continuing through to the late Quaternary (Fig. 15 A). A significant population of detrital zircon grains with U-Pb ages ranging from ~2200-1800 Ma dominates all Lake Beds intervals, including samples from both outcrop and the Galula-1 and Ivuna-1 exploration wells (Figs. 8-12). The source of these Paleoproterozic zircons is the Ubendian Belt, which forms the basement and flanks of the rift and exerts a major control on basin development (Figs. 2 and 15A). While detrital zircon and apatite low-temperature thermochronology did not reveal major surface or rock uplift events associated with rifting, the significant Ubendian signal that dominates the detrital zircon record from the Oligocene - Quaternary suggests that at the very least, the Ubendian rift flanks were elevated and actively eroding sediment into the basin. Perhaps if Ubendian-aged detrital zircons and apatites were specifically targeted for low-temperature thermochronology work, this rift flank signal may be captured. Pebbles from the large perennial rivers and braided channels of the lower Lake Beds and from coarse conglomerates that characterize the base of the upper Lake Beds are compositionally dominated by vein-quartz, meta-granitoids, and meta-volcanics, supporting the interpretation of a major proximal rift flank (Ubendian Belt) source for the Lake Beds succession.

All of the Lake Beds samples also contain Pan African (~800-400 Ma) and Irumide age (~1100-900 Ma) detrital zircon grains (Figs. 8-10 and 12). Rarely do these grains form a statistically significant population, but rather in each sample, three to ten grains are spread out over this long age range (~1100-400 Ma). These grains are interpreted to also originate from the Ubendian Belt metamorphic complex, which is known to contain zircons spanning this significant period of time (Boniface et al., 2012; 2014), as a result of tectonic reactivation of this belt from the Mesoproterozoic through to the early-mid Paleozoic (Fig. 2). There are both igneous and metamorphic events that have affected the Ubendian terrane, and many Paleoproterozoic zircons (main peak Ubendian metamorphism: 1831 ± 11 to 1886 ± 16 Ma) have Meso- and Neoproterozoic overprinting (Boniface et al., 2012; 2014). Four main igneous phases (Usagaran: 2.05-1.93 Ga; Ubendian: 1.88-1.85 Ga; Lukamfwa: 1.65-1.55 Ga; and Irumide: 1.05 – 0.95 Ga) and Paleoproterozoic to Neoproterozoic orogenies (Eburnian: 2200-1800 Ma; Kibaran 1350-950 Ma; and Pan African: 800-500 Ma) have affected primarily the margins of the older (usually Archean) cratons (DeWaele et al., 2006). The Rukwa Rift Basin and hinterland, lying between the Tanzanian craton and the cratonic Bangweulu block, has therefore been affected by each of these events, and their signatures can be found in the U-Pb ages of detrital zircon and apatite from the basin. For example, the Wakole Terrane of the Ubendian Belt records zircons with ages of 1166 ± 14 and 1007 ± 6 Ma in addition to Paleoproterozoic ages, the former associated with granitoid emplacement in the Karagwe-Ankolean/Kabaran Belt and the later resulting from orogenesis associated with the assembly of Rodinia (Fig. 2). Zircons of Pan African age have also been recorded from the Ufipa (600-520 Ma), Mbozi

(740-685 Ma), and the Upagwa (920-720 Ma) terranes (Boniface et al., 2012; Fig. 2). During deformation, Meso- and Neoproterozoic sedimentary basins developed along ductile shear zones in the Ubendian Belt, and these metasedimentary sources contributed to the mixed signal of Ubendian ages observed in these samples. Additionally, there is a long history of crustal recycling of a somewhat ambiguous Archean basement complex. Reworked Archean cratonic zircon grains have been discovered in many of the immediate tectonic belts surrounding the Rukwa Rift Basin. For example, the Usagaran Belt contains zircons with 2.64-2.4 Ga and 3.0-2.5 Ga ages, identical to those of the Tanzanian craton, despite its dominantly ~2.0 Ga age. With this in mind, and without additional isotopic fingerprinting such as Hf-isotopic analysis, Almost 100% of the detrital zircon grains recovered from the lower Lake Beds can be attributed to the many ages of igneous and metamorphic activity of the Ubendian Belt.

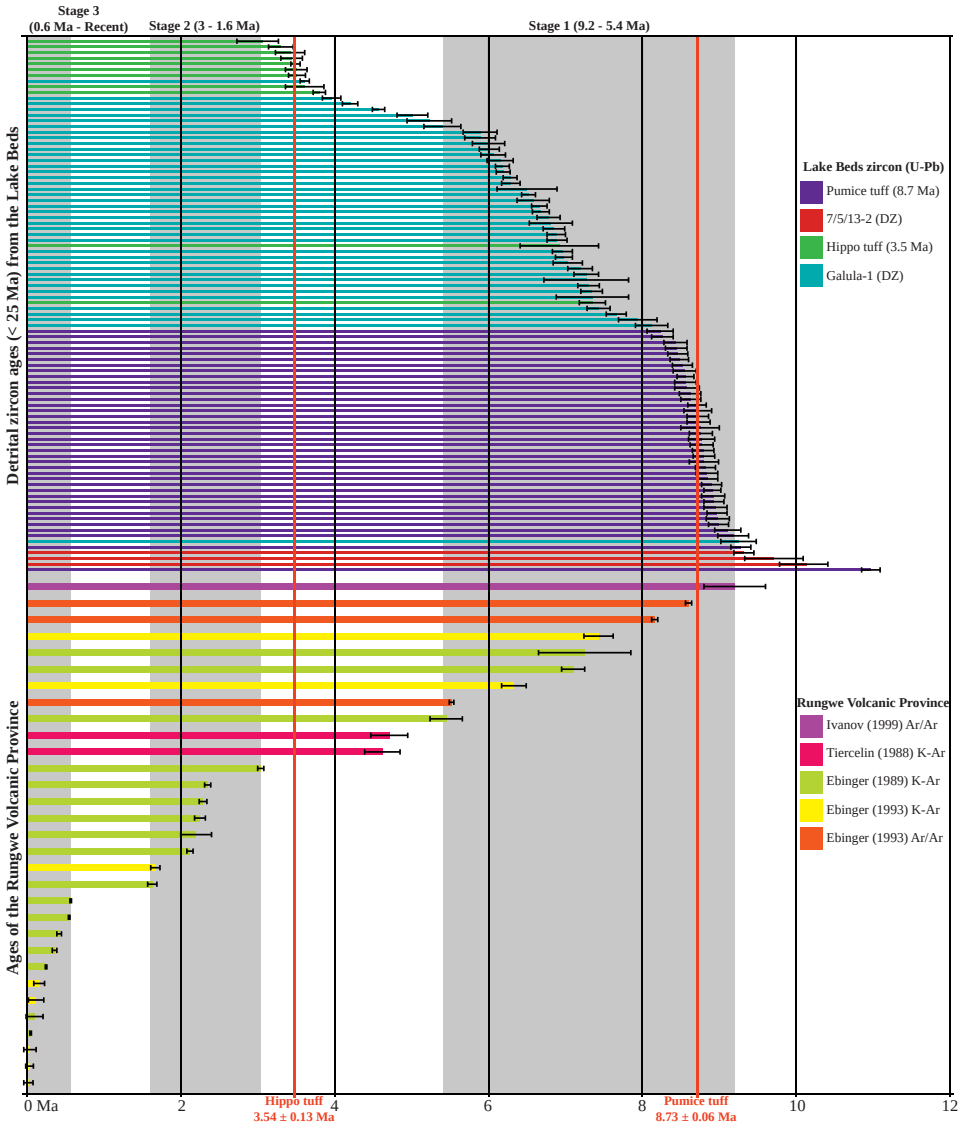

Fig. 16. Comparison of radioisotopic dates reported from the Rungwe Volcanic Province (mostly K-Ar ages) with comparable U-Pb detrital zircon ages recovered from the Lake Beds succession during this study. The three active stages of the Rungwe Volcanic Province are highlighted by the thick vertical grey bars (Ebinger et al., 1989) and U-Pb ages for two volcanic tuffs from the lower Lake Beds (this study) are shown by thin vertical red bars (errors are 2σ).

The Lake Beds succession and the underlying Songwe Member of the Nsungwe Formation share a similar detrital zircon signature (Figs. 8 and 9), yet major reworking seems unlikely since the exposure of the Songwe Member is extremely limited. What quantitatively sets these two units apart, however, are their differing detrital apatite U-Pb signatures. The Songwe Member is dominated by ~200 Ma apatites (Fig. 5), whereas the Lake Beds sample is dominated by apatites with Pan African (~600-500 Ma) and Irumide (~1000-900 Ma) crystallization ages (Fig. 12). Additionally, there is a notable absence of ~25 Ma zircon and apatite grains in the Lake Beds samples, suggesting that the Oligocene volcanic center that influenced so much of the deposition of the Songwe Member of the Nsungwe Formation (Roberts et al., 2012) had since been eroded or buried by the time of Lake Beds deposition. Alternatively, the developing Rungwe Volcanic Province to the south may have blocked the sediment route.

A commonly encountered bias in detrital provenance reconstructions is the zircon fertility of source rocks (Moecher and Samson, 2006). One of the challenges of working in a rift setting is the consequence of bimodal volcanism. For the Rukwa Rift Basin, the range of igneous compositions has a significant effect that can be detected by comparing the detrital zircon and apatite signatures within the same sample. A series of Jurassic-Cretaceous carbonatite complexes, including the Panda Hill, Mbalizi, Sengeri Hill, Musensi, and possibly other carbonatites, is located at the southern end of the Songwe Valley, in close proximity to the study area. While these sources are undetected in the detrital zircon signature, Jurassic-Cretaceous age detrital apatites dominate the Nsungwe Formation "BigWall" sample (Fig. 5), suggesting the carbonatites as major sources of sediment during the Oligocene. Conversely, the detrital apatite data do not record any Ubendian grain ages, which is worth noting because this source terrane dominates the detrital zircon record, for both the Galula Formation and Lake Beds succession.

Although the Ubendian belt signature remains dominant throughout all Lake Beds samples, there is a noticeable sediment provenance shift between the lower Lake Beds (both members A and B) and the upper Lake Beds (Figs. 8 and 10). In the upper Lake Beds the proportion of Irumide (~1000-900 Ma) to Ubendian grains increases, as the two populations become nearly equal in magnitude towards the top of the stratigraphy. This change is detected in both the samples from outcrop and those from the Galula-1 well cuttings and can be used a diagnostic signature for distinguishing lower from upper Lake Beds units. The zircon age population distribution pattern of the upper Lake Beds samples mirrors that of the Namba Member sandstone of the Cretaceous Galula Formation (Red Sandstone Group; Roberts et al., 2012). The Mesoproterozoic through Cambrian zircons found in the Namba Member of the Galula Formation are southerly derived, from the Irumide, Zimbabwe, and Mozambique belts. At many outcrops in the Songwe Valley the upper Lake Beds sits unconformably on

top of the Cretaceous Namba Member, and multistory conglomerate units at the base of the lower Lake Beds erosionally scour into the underlying Galula Formation. This clearly demonstrates localized recycling of underlying Cretaceous sediments as the likely cause of the provenance shift in the upper Lake Beds, rather than a change in the drainage system. Likewise, the volcaniclastic nature of the upper Lake Beds, which is dominated by ash deposition into shallow lakes and streams, shows no indication for major river systems that may have routed sediments from the far south Irumide belt. While the Rukwa Rift Basin remained an internally draining basin fed by transverse-flowing small streams throughout the deposition of the entire Lake Beds Succession, the recycled detrital zircon signature in the upper Lake Beds succession also suggests that there was at least local basin inversion along the basin margins during the deposition of the upper Lake Beds (i.e., after 3.4 Ma: Hippo Tuff age at the top of the lower Lake Beds succession).

A second significant 'young' population of detrital zircons with crystallization ages of < 10 Ma is recorded in nine out of twelve samples from the Galula-1 well (n = 1-10; Fig. 8). We interpret these to be derived from the Rungwe Volcanic Province (origins discussed in detail in Chapter Three and above in section 5.1; Figs. 1 and 16). While the number of analyzed samples significantly differs between the Ivuna-1 and Galula-1 wells, it is interesting to note that no young zircons were recovered from the lower Lake Beds of Ivuna-1 (Fig. 9). The proximity of the Galula-1 well to the Rungwe Volcanic Center perhaps is accountable for this. Small transverse streams brought sediment from the rift flanks into the basin, and these likely did not extend into 'deeper' waters that developed closer to the basin bounding Lupa fault on the east side of the basin nearer to the Ivuna-1 well site (Fig. 1). Many of the tuffs and tuffaceous units in the lower Lake Beds are preserved as shallow filling of ponds or volcaniclastic choking of small streams. This also indicates that much of the material erupted from the Rungwe Volcanic Province was deposited as air-fall tuffs that were locally reworked. In contrast, the upper Lake Beds is distinguished by a distinct lack of syn-depositional aged detrital zircons (i.e., no 'young' zircons). The Rungwe volcanic center almost certainly formed a formidable physiographic barrier between the Rukwa, the Malawi, and the Usangu drainage basins, and therefore controlled the thickness and composition of late Cenozoic sedimentary and volcanic sequences, which do vary locally and regionally. Much of the now 2,100 m-high Rungwe shield complex formed in the Pleistocene (Ebinger et al., 1989), so it is conceivable that material from late Cenozoic volcanic eruptions was blocked from entering the Songwe Valley. Additionally, the latest phase of Rungwe volcanism from 0.6 Ma to the present is dominated by zircon-free olivine basalts and trachytes (Ebinger et al., 1989; Fontijn et al., 2012).

6. Conclusions

A combination of detrital zircon and apatite U-Pb geochronology, tephrochronology, and detrital zircon and apatite low-temperature thermochronology techniques applied to Cretaceous through Pliocene strata of the Rukwa Rift Basin reveal a long-lived, pre-EARS tectonic history, and provide important insights about the Lake Cenozoic development of the western branch of the East African Rift System. Among the most significant results of this work is a clear understanding of the timing of rifting and sedimentation events in the Rukwa Rift Basin from the Neogene to Recent. In particular, recovery and dating of young (9-3 Ma) detrital zircons from well cuttings and in situ volcanic tuffs in outcrop reveal several phases of rifting, volcanism, and sedimentation in the Neogene, which appear to have initiated by ~9 Ma. Significant uplift accompanying initial rifting of the Rukwa Rift at ~25 Ma was not detected via detrital apatite and zircon double dating, nor was major uplift associated with later Neogene rifting episodes in the late Miocene-early Pliocene, suggesting perhaps that the incised and uplifted landscapes present today in this part of the EARS are Pleistocene or later developments. Detrital zircon provenance of the Lake Beds sediments indicates that the Rukwa Rift Basin has remained an internally draining basin throughout its history, and therefore drainage entrances and exits to the basin have been limited both by rift flank topography and also by volcanic topography in the south of the basin (Fig. 15A). Both the Rungwe Volcanic Province and the earlier Mesozoic carbonatite complexes to the south of the Songwe Valley were major sources of sediment and had a significant influence on sedimentation (i.e., both as a source and as a barrier blocking sediment input from southerly sources) during the Oligocene and Miocene-Pliocene. Detrital low-temperature thermochronology has also shed light on the Late Cretaceous depositional age of the Namba Member of the Galula Formation. This data suggests a Late Cretaceous to Paleogene thermal event that is recorded by both the sediments in the Rukwa Rift Basin and by the rift flanks (Van der Beek et al., 1998). Double dating of detrital apatites derived from the Jurassic carbonatite complex at the southern end of the basin show evidence for prolonged volcanism and reheating, and suggests that the as-yet-undiscovered Oligocene alkaline volcanic source was likely near the Jurassic-Cretaceous carbonatite suite in the Songwe Valley (Fig. 6). The detrital zircon and apatite grains across all sedimentary units are derived from a mixture of regional and rift flank sources, and show an extended range of cooling ages, from the Paleoproterozoic to Late Cretaceous; evidence that the Rukwa Rift and immediate region has been tectonically active repeatedly and frequently throughout the Phanerozoic. The cooling ages acquired collectively overlap independently known tectonic events that have affected eastern Africa, which we now know must have affected the cooling history of the basin sediment sources. Taken together, these new findings tell of a long-lived tectonic history for the Rukwa Rift Basin and surrounding terranes, which have had an accordion-like response to both far-field tectonic

events that are known to be widespread over much of eastern and southern Africa as well as the development of the East Africa Rift System (Fig. 13). The rift complexities that have been elucidated here attest to the capability of the sedimentary record to preserve tectonic histories, particularly in volcanic settings.

Chapter Five

Thesis summary and future work

Detailed sedimentary-based investigations of the Rukwa Rift Basin have greatly enhanced and expanded our knowledge and understanding of rifting, volcanism and sedimentation in the western branch of the East African Rift System. The multifaceted approaches used in this study have demonstrated the effectiveness of using detrital minerals and sedimentation patterns as proxies for constraining the timing of rifting, volcanism, and uplift, as well as the magnitude of denudation of regional and local source areas surrounding the rift. Sedimentary basins are the most important archives of past environments, landscapes, and seismicity, particularly in places such as continental rifts, where the Earth's surface continually undergoes rapid and drastic geomorphic changes. The results of these studies include the following advancements: discovering evidence for the magnitude and timing of Late Pleistocene earthquakes in the Rukwa Rift Basin region and understanding their impact on shallow, subsurface deformation; recognizing new morphologies of soft-sediment deformation formed by seismogenic gas-escape during the Cretaceous and the implications of this for studying ancient earthquakes; dating a new phase of Late Miocene rifting, sedimentation, and volcanism in the Rukwa Rift Basin starting by 8.7 Ma; proof of concept for applying U-Pb detrital zircon geochronology to well cuttings for stratigraphic control; and the creation of a suite of detrital apatite and zircon geochronologic and thermochronologic data that has revealed that the Rukwa Rift Basin and surrounding tectonic terranes have experienced cooling more-or-less continuously throughout the rift's long-lived history.

This thesis, which is divided into two main themes and presented as four independent studies, provides new information about a variety of different aspects of this continental rift system, particularly with regard to geologic hazards and the long-lived tectonic history of the region. Probing the record of ancient seismicity, as revealed in the first two chapters of this thesis, has led to better understanding of how earthquakes have deformed the near-surface in the Rukwa Rift region. These investigations described new soft-sediment deformation sedimentary features (e.g., balloon structure) and new expressions of large-scale seismites, such as the megablock complex. Adding to the catalogue of known seismically generated sedimentary structures, and critically evaluating the origins of these structures (e.g., water-escape vs. gas-escape in Chapter Two) is essential for planning for and predicting how earthquakes may deform the Earth's surface, especially in places like the tectonically active southern Rukwa Rift Basin, an important region with a rapidly expanding population. Furthermore, the decameter-scale seismites from the upper Lake Beds extend the record of large-magnitude earthquakes back into the Late Pleistocene, and perhaps the identification and study of additional seismite horizons throughout the Lake Beds units in the future will allow us to reconstruct recurrence intervals for such large-magnitude, hazardous earthquakes.

Results from Chapters Three and Four indicate that after initial rifting of the western branch in the Oligocene, a new phase of Late Miocene rifting, sedimentation, and volcanism in the Rukwa Rift Basin began again by at least 8.7 Ma, as suggested by newly dated volcanic tuffs and detrital zircons from hydrocarbon exploration well cuttings through the lower Lake Beds. An up-well younging trend in maximum depositional ages acquired from detrital zircon from throughout the Galula-1 well, paired with ages on tuffs from outcrop, also demonstrate that deposition and volcanic eruptions were episodic after the late Miocene rift initiation, from ~9–3.5 Ma. A combination of detrital zircon and apatite geochronology and thermochronology data sets indicate that the Rukwa Rift and surrounding regions behaved in an accordion-like fashion in response to repeated episodes of far-field stresses from tectonic episodes that are known to have disturbed much of eastern and southern Africa since the Precambrian. Additionally, this data shows that neither the late Oligocene nor the Late Miocene western branch rifting events were accompanied by significant inversion of the Rukwa Rift Basin or uplift of its flanks, suggesting instead that the high topography and incised landscape present today must have developed since the Pleistocene. Resolving a more detailed uplift history might entail higher-resolution (i.e., more samples throughout the stratigraphy) low-temperature thermochronology and geochemistry data on detrital minerals and an increased number of grains analyzed per sample, particularly for low-temperature thermochronology analyses that are both time intensive and costly. Moreover, different techniques such as clumped isotope analyses on carbonates (i.e., paleoaltimetry) could help to resolve and constrain the suggested late Quaternary uplift of the Rukwa Rift Basin margins. Detailed low-temperature thermochronologic analysis of transects up the rift flanks, particularly those that surround the Songwe Valley, will also be a critical data set in the future for refining the timing of uplift, and for comparison with the detrital signatures obtained here.

Detrital zircon analyses from this study (Chapter Three) were specifically applied to test the possibility of using small-volume well cuttings, in lieu of diagnostic biostratigraphy, for refining stratigraphic age assessments in hydrocarbon exploration wells. This method has proven to be effective, and the re-examination of well cuttings from the Lake Beds in the Rukwa Rift Basin has renewed interest in hydrocarbon exploration in this portion of the rift. It is envisioned that such an approach has the potential to provide significant benefits to the hydrocarbon industry, particularly by helping to resolve similar hydrocarbon exploration uncertainties elsewhere in the East African Rift System frontier.

Another significant result of this work was the discovery and U-Pb dating of new volcanic tuffs from both the late Oligocene Nsungwe Formation (see authors contribution in Spandler et al., 2016) and the lower portion of the Lake Beds succession. The volcanic tuffs from the Oligocene Songwe Member contain other volcanic minerals in addition to zircon

and apatite such as abundant titanite, phlogopite, and andradite garnet, and tuffs from the late Miocene Lake Beds also contain sanidine. A natural progression from this work will be to isotopically fingerprint and date other mineral phases. Pilot work of this nature is presented in Spandler et al. (2016) in Appendix 2.

Active landscapes such as continental rifts can provide landscape complexity (i.e., barriers), fertility (e.g., from volcanic input), and complex ecologic environments that can significantly influence the development of flora and fauna. This project as a whole has focused on using non-traditional approaches to understanding how the landscape has changed over time, specifically by focusing on the sedimentary record, rather than on the structural geology of the rift or thermochronology of the rift flanks. The sediments preserved in the Rukwa Rift Basin contain high-resolution records that can be used to decipher the interplay between rifting, volcanism, uplift, and sedimentation. Radioisotopic dating provides important constraints for interpreting the influences of diverse tectonic, environmental, and volcanic processes on depositional patterns, in an effort to better understand the evolution of the dynamic topography of rift basins, and better understand how to interpret this history from the sedimentary record. For example, the new radioisotopic age constraints for the lower Lake Beds presented in Chapter Three suggests late Miocene reactivation of the Rukwa Rift Basin, and coeval volcanism and sedimentation. These dates place critical temporal and environmental constraints on newly discovered vertebrate-bearing deposits in the Lake Beds succession in the Rukwa Rift, which are the first discovered of their age in the western branch of the East African Rift System between lakes Edward and Malawi.

These studies were conducted as a part of the Rukwa Rift Basin Project, which is comprised of an international team of geologists and paleontologists exploring the Rukwa Rift Basin in southern Tanzania, which preserves one of the most complete, and indeed only successions of well-exposed, fossiliferous Cretaceous through Neogene continental sedimentary sequences in sub-equatorial Africa. The tectonic framework resulting from these studies is important for contributing to hypotheses about the Cretaceous evolution of southern hemisphere faunas after the breakup of Gondwana and isolation of landmasses, as it is also critical for constraining Neogene faunal changes brought about by the collision of the Afro-Arabian and Eurasian landmasses, not to mention evolutionary changes ensuing from pressures associated with continental rifting and consequent dynamic landscapes. Therefore, the much-improved temporal constraints on sediment deposition, rifting, volcanism, seismicity, and uplift that have resulted from this study are critical for placing important new fossil discoveries into proper geologic context. For instance, recent fossil discoveries in the Rukwa Rift Basin have begun to shed new light on large-scale evolutionary and ecological hypotheses, including establishing the timing of divergence between Old World monkeys and apes (Stevens, et al., 2013), the evolution of mammal-like

crocodyliforms in Gondwana (O'Connor et al., 2010), the evolution of booid and colubroid snakes (McCartney et al., 2014), and the antiquity of symbiotic mutualism between fungus farming termites (the Macrotermitinae) and their fungal symbionts (Microfavichnus alveolatus; Roberts et al., in review). However, one of the most exciting discoveries that resulted directly from this thesis project was the identification and radioisotopic dating of a previously unknown Mio-Pliocene stratigraphic succession with abundant vertebrate fossils exposed in the southern end of the Rukwa Rift Basin (i.e., the lower Lake Beds succession). Although paleontologic exploration of these strata has only just begun, a sensational fauna is already starting to emerge, which includes mammal, crocodilian, fish, turtle, mollusk, and continental trace fossils. Considering that the East African Rift has long been considered the Cradle of Human Kind, and has undoubtedly shaped the evolution of hominins and other flora and fauna, the discovery of a new Mio-Pliocene fossil-bearing sequence in the Rukwa Rift is particularly exciting. It is hoped that the work presented in this thesis, which has aimed to understand the interplay of rifting and its consequences and has helped to reconstruct ancient landscapes via the sedimentary record, has the potential to provide significant insights into the framework for the evolution of humans, and other vertebrates.

References

Allen, J.R.L., 1982, Sedimentary Structures: Their character and physical basis: Developments in Sedimentology, 30B, Elsevier, Amsterdam.

Allen, J.R.L., 1986, Earthquake magnitude-frequency, epicentral distance, and soft-sediment deformation in sedimentary basins: Sedimentary Geology, v. 46, p. 67-75.

Alsop, G.I., and Marco, S., 2013, Seismogenic slump folds formed by gravity-driven tectonics down a negligible subaqueous slope: Tectonophysics, v. 605, p. 48-69.

Amante, C., and Eakins, B.W., 2009, ETOPO1 1 Arc-Minute Global Relief Model: Procedures, Data Sources and Analysis: NOAA Technical Memorandum NESDIS NGDC-24, National Geophysical Data Center, NOAA.

Ambraseys, N.N., 1988, Engineering seismology: Earthquake Engineering and Structural Dynamics, v. 17, p. 1-105.

Ambraseys, N.N., and Adams, R.D., 1991, Reappraisal of major African earthquakes, south of 20°N, 1900-1930: Natural Hazards, v. 4, p. 389-419.

Ambraseys, N.N., 1991, The Rukwa earthquake of 13 December 1910 in East Africa: Terra Nova, v. 3, p. 203-208.

Anderson, T., 2005, Detrital zircons as tracers of sedimentary provenance: limiting conditions from statistics and numerical simulation: Chemical Geology, v. 216, p. 249-270.

Anketell, J.M., Cegla, J., and Dzulynski, S.T., 1969, Unconformable surfaces in the absence of current erosion: Geologica Romana, v. 8, p. 41-46.

Atkinson, G., 1984, Simple computation of liquefaction probability for seismic hazard applications: Earthquake Spectra, v. 1, p. 107-123.

Audemard, F.A., and de Santis, F., 1991, Survey of liquefaction structures induced by recent moderate earthquakes: Bulletin of the International Association of Engineering Geologists, v. 44, p. 5-16.

Backeberg, N.R., and Rowe, C.D., 2009, Mega-scale (~50M) Ordovician load casts at De Balie, South Africa: Possible sediment fluidization by thermal destabilization: South African Journal of Geology, v. 112, p. 187-196.

Baker, B.H., 1986, Tectonics and volcanism of the southern Kenya Rift Valley and its influence on rift sedimentation: Geological Society, London, Special Publications 25, p. 45–57.

Barbeau Jr., D.L., Olivero, E.B., Swanson-Hysell, N.L., Zahid, K.M., Murray, K.E., and Gehrels, G.E., 2009, Detrital-zircon geochronology of the eastern Magallanes foreland basin: Implications for Eocene kinematics of the northern Scotia Arc and Drake Passage: Earth and Planetary Science Letters, v. 284, p. 489-503.

Bauer, F.U., Glasmacher, U.A., Ring, U., Schumann, A., and Nagudi, B., 2010, Thermal and exhumation history of the central Rwenzori Mountains, Western Rift of the East

African Rift System, Uganda: International Journal of Earth Sciences, v. 99, p. 1575-1597, Doi: 10.1007/s00531-010-0549-7.

Bauer, F.U., Glasmacher, U.A., Ring, U., Grobe, R.W., Mambo, V.S., Starz, M., 2015, Long-term cooling history of the Albertine Rift: new evidence from the western rift shoulder, D.R. Congo: International Journal of Earth Science. Doi: 10.1007/s00531-015-1146-6.

Bezerra, F.H.R., da Fonseca, V.P., Vita-Finzi, C., Lima-Filho, F.P., Saadi, A., 2005, Liquefaction-induced structures in Quaternary alluvial gravels and gravelly sediments: Engineering Geology, v. 76, p. 191-208.

Black, L.P., Kamo, S.L., Allen, C.M., Aleinikoff, J.N., Davis, D.W., Korsch, R.J., and Foudoulis, C., 2003, TEMORA 1: a new zircon standard for Phanerozoic U–Pb geochronology: Chemical Geology, v. 200, p. 155–170.

Boniface, N., Schenk, V., and Appel, P., 2012, Paleoproterozoic eclogites of MORB-type chemistry and three Proterozoic orogenic cycles in the Ubendian Belt (Tanzania): Evidence from monazite and zircon geochronology, and geochemistry: Precambrian Research, v. 192-195, p. 16-33.

Boniface, N., Schenk, V., and Appel, P., 2014, Mesoproterozoic high-grade metamorphism in politic rocks of the northwestern Ubendian Belt: Implication for the extension of the Kibaran intra-continental basins to Tanzania: Precambrian Research, v. 249, p. 215-228.

Boudreau, B.P., Algar, C., Johnson, B.D., Croudace, I., Reed, A., Furukawa, Y., Dorgan, K.M., Jumars, P.A., and Grader, A.S., 2005, Bubble growth and rise in soft sediments: Geology, v. 33, p. 517-520.

Boudreau, B.P., 2012, The physics of bubbles in surficial, soft, cohesive sediments: Marine and Petroleum Geology, v. 38, p. 1-18.

Brown, P.E., 1962, The tectonic and metamorphic history of the Pre-Cambrian rocks of the Mbeya region, South-West Tanzania: Quarterly Journal of the Geological Society of London, v. 118, p. 295-317.

Camelbeeck, T., and Iranga, M.D., 1996, Deep crustal earthquakes and active faults along the Rukwa trough, eastern Africa: Geophysical Journal International, v. 124, p. 612-630.

Carrapa, B., 2010, Resolving tectonic problems by dating detrital minerals: Geology, v. 38, no. 2, p. 191-192. Doi: 10.1130/focus022010.1.

Carter, A., Bristow, C.S., and Hurford, A.J., 1995, The application of fission track analysis to the dating of barren sequences: examples from red beds in Scotland and Thailand, in R.E. Dunay, and E.A. Hailwood, eds., Non-biostratigraphical methods of dating and correlation: Geological Society Special Publication No. 89, p. 57-68.

Cartwright, J., 2010, Regionally extensive emplacement of sandstone intrusions: a brief review: Basin Research, v. 22, p. 502-516.

Cathles, L.M., Su, Z., and Chen, D., 2010, The physics of gas chimney and pockmark formation, with implications for assessment of seafloor hazards and gas sequestration: Marine and Petroleum Geology, v. 27, p. 82-91.

Cawood, P.A., Hawkesworth, C.J., and Dhuime, B., 2012, Detrital zircon record and tectonic setting: Geology, v. 40, p. 875-878. Doi: 10.1130/G32945.1.

Chew, D.M., and Donelick, R.A., 2012, Combined apatite fission track and U-Pb dating by LA-ICP-MS and its application in apatite provenance analysis, in P. Sylvester, Quantitative mineralogy and microanalysis of sediments and sedimentary rocks: Mineralogical Association of Canada Short Course 42, St. John's, Newfoundland and Labrador, p. 219-247.

Chew, D.M., Sylvester, P.J., and Tubrett, M.N., 2011, U-Pb and Th-Pb dating of apatite by LA-ICPMS: Chemical Geology, v. 280, n. 1-2, p. 200-216.

Chorowicz, J., 2005, The East African Rift System: Journal of African Earth Sciences, v. 43, p. 379-410.

Cloud, P.E., Jr., 1960, Gas as a sediment and diagenetic agent: American Journal of Science, Bradley Volume 258-A, p. 35-45.

Coffin, M.F., and Rabinowitz, P.D., 1988, Evolution of the conjugate East African-Madagascan margins and the western Somali Basin: Geological Society of America Special Paper 226, 78 p.

Cohen, A.S., 1989, Facies relationships and sedimentation in large rift lakes and implications for hydrocarbon exploration: Examples from lakes Turkana and Tanganyika: Palaeogeography, Palaeoclimatology, Palaeoecology, v. 70, p. 65-80.

Cohen, A.S., Soreghan, M.J., and Scholz, C.A., 1993, Estimating the age of formation of lakes: An example from Lake Tanganyika, East African Rift System: Geology, v. 21, p. 511-514.

Cohen, A.S., Van Bocxlaer, B., Todd, J.A., McGlue, M., Michel, E., Nkotagu, H.H., Grove, A.T., and Delvaux, D., 2013, Quaternary ostracodes and molluscs from the Rukwa Basin (Tanzania) and their evolutionary and paleobiogeographic implications: Palaeogeography, Palaeoclimatology, Palaeoecology, v. 92, p. 79-97.

Dalland, A., Mearns, E.W., and McBride, J.J., 1995, The application of samarium-neodymium (Sm-Nd) Provenance ages to correlation of biostratigraphically barren strata: a case study of the Statfjord Formation in the Gullfaks Oilfield, Norwegian North Sea, in R.E. Dunay, and E.A. Hailwood, eds., Non-biostratigraphical methods of dating and correlation: Geological Society Special Publication No. 89, p. 201-222.

Daly, M.C., Chorowicz, J., and Fairhead, J.D., 1989, Rift basin evolution in Africa: the influence of reactivated steep basement shear zones, in M.A. Cooper and G.D. Williams, eds., Inversion tectonics: Geological Society Special Publications No. 44, p. 309-334.

Damblon, F., Gerrienne, P., D'Outrelepont, H., Delvaux, D., Beeckman, H., and Back,

S., 1998, Identification of a fossil wood specimen in the Red Sandstone Group of southwestern Tanzania: stratigraphic and tectonic implications: Journal of African Earth Sciences, v. 26, p. 387–396.

DeCelles, P.G., Carrapa, B., and Gehrels, G.E., 2007, Detrital zircon U-Pb ages provide new provenance and chronostratigraphic information from Eocene synorogenic deposits in northwestern Argentina: Geology, v. 35, p. 323-326.

Delvaux, D., 1991, The Karoo to Recent rifting in the western branch of the East-African rift system: A bibliographical synthesis: Royal Museum for Central Africa Annual Report 1989-1990, p. 63-83.

Delvaux, D., Levi, K., Kajara, R., and Sarota, J., 1992, Cenozoic palaeostress and kinematic evolution of the Rukwa – North Malawi rift valley (East African Rift System): Bulletin des Centres de Recherches Exploration – Production Elf Aquitaine 16, p. 383–406.

Delvaux, D.F., and Hanon, M., 1993, Neotectonics of the Mbeya area, SW Tanzania: Royal Museum for Central Africa Annual Report 1991-1992, p. 87-97.

Delvaux, D., Kervyn, F., Vittorl, R.S., Kajara, E., Kilembe, S.A., 1998, Late quaternary tectonic activity and lake level change in the Rukwa Rift Basin: Journal of African Earth Sciences, v. 26, p. 397-421.

Delvaux, D., 2001, Tectonic and paleostress evolution of the Tanganyika-Rukwa-Malawi rift segment, East African Rift System, in P.A. Ziegler, W. Cavazza, A.H.F. Robertson, and S. Crasquin-Soleau, S., eds., Peri-Tethys Memoir 6: PeriTethyan Rift/Wrench Basins and Passive Margins, Mémoire Musée National Histoire naturelle, v. 186, p. 545-567.

Delvaux, D., Kervyn, F., Macheyeki, A.S., and Temu, E.B., 2011, Active faulting in W-Tanzania: Coupling between tectonics, volcanism & climate?: abstract, 23rd Colloquium of African Geology, Johannesburg, South Africa, v. 112.

Delvaux, D., Kervyn, F., Macheyeki, A.S., Temu, E.B., 2012, Geodynamic significance of the TRM segment in the East African Rift (W-Tanzania): Active tectonics and paleostress in the Ufipa plateau and Rukwa basin: Journal of Structural Geology, v. 37, p. 161-180.

DeWaele, B., Kampunzu, A.B., Mapani, B.S.E., and Tembo, F., 2006, The Mesoproterozoic Irumide belt of Zambia: Journal of African Earth Sciences, v. 46, p. 36-70.

Dickinson, W.R., and Gehrels, G.E., 2009, Use of U-Pb ages of detrital zircons to infer maximum depositional ages of strata: A test against a Colorado Plateau Mesozoic database: Earth and Planetary Science Letters, v. 288, p. 115-125.

Dickinson, W.R., and Gehrels, G.E., 2010, Insights into North American paleogeography and paleotectonics from U-Pb ages of detrital zircons in Mesozoic strata of the Colorado Plateau, USA: International Journal of Earth Science, v. 99, p. 1247-1265.

Dodson, M.H., 1973, Closure temperatures in cooling geochronological and petrological systems: Contributions to Mineralogy and Petrology, v. 40, p. 259–274.

Donelick, R.A, O'Sullivan, P.B., Ketcham, R.A., 2005, Apatite fission-track analysis: Reviews in Mineralogy and Geochemistry, Mineralogical Society of America, v. 58, p. 49-94.

Dypvik, H., Nesteby, H., Ruden, F., Aagaard, P., Johansson, T., Msindai, J., Massay, C., 1990, Upper Paleozoic and Mesozoic sedimentation in the Rukwa-Tukuyu region, Tanzania: Journal of African Earth Sciences, v. 11, p. 437–456.

Ebinger, C.J., 1989, Tectonic development of the western branch of the East African rift system: Geological Society of America Bulletin, v. 101, p. 885-903.

Ebinger, C.J., Deino, A.L., Drake, R.E., and Tesha, A.L., 1989, Chronology of volcanism and rift basin propagation: Rungwe Volcanic Province, East Africa: Journal of Geophysical Research, v. 94, no. B11, p. 15785-15803.

Ebinger, C.J., Deino, A.L., Tesha, A.L., Becker, T. and Ring, U., 1993, Tectonic controls on rift basin morphology: Evolution of the northern Malawi (Nyasa) Rift: Journal of Geophysical Research, v. 98, no. B10, p. 17821-17836.

Ebinger, C.J., and Sleep, N.H., 1998, Cenozoic magmatism throughout east Africa resulting from impact of a single plume: Nature, v. 395, p. 788-791.

Etiope, G., and Klusman, R. W., 2002, Geologic emissions of methane to the atmosphere: Chemosphere, v. 49, no. 8, p. 777-789.

Ettensohn, F.R., Rast, N., and Brett, C.E., eds., 2002, Ancient Seismites: Geological Society of America Special Publication 359, 200 pp.

Fawley, A.P., James, T.C., 1955, A pyrochlore carbonatite from Southern Tanganyika: Economic Geology, v. 50, p. 571-585.

Fedo, C.M., Sircombe, K.N., Rainbird, R.H., 2003, Detrital-zircon analysis of the sedimentary record, in J.M. Hanchar, and P. Hoskin, P., eds., Zircon: Experiments, Isotopes, and Trace Element Investigations: Mineralogical Society of America, Reviews in Mineralogy, v. 53, p. 277–303.

Feldmann, R.M., O'Connor, P.M., Stevens, N.J., Gottfried, M.D., Roberts, E.M., Ngasala, S., Rasmusson, E.L., and Kapilima, S., 2007, A new freshwater crab (Decapoda: Brachyura: Potamonautidae) from the Paleogene of Tanzania, Africa: Neues Jahrbuch fur Geologie und Palaontologie-abhandlungen, v. 244/1, p. 71-78.

Fernandez-Alonso, M., Cutten, H., De Waele, B., Tack, L., Tahon, A., Baudet, D., and Barritt, S.D., 2012, The Mesoproterozoic Karagwe-Ankole Belt (formerly the NE Kibara Belt): The result of prolonged extensional intracratonic basin development punctuated by two short-lived far-field compressional events: Precambrian Research, v. 216-219, p. 63-86.

Field, M.E., Gardner, J.V., Jennings, A.E., Edwards, B.D., 1982, Earthquake-induced sediment failures on a 0.25° slope, Klamath River delta, California: Geology, v. 10, p. 542–546.

Fleischer, P., Orsi, T.H., Richardson, M.D., and Anderson, A.L., 2001, Distribution of free

gas in marine sediments: a global overview: Geo-Marine Letters, v. 21, p. 103-122.

Flowers, R.M., Ketcham, R.A., Shuster, D.L, and Farley, K.A., 2009, Apatite (U-Th)/He thermochronometry using a radiation damage accumulation and annealing model: Geochemica et Cosmochimica Acta, v. 73, p. 2347-2365.

Foeken, J.P.T., Stuart, F.M., Dobson, K.J., Persano, C., and Vilbert, D., 2006, A diode laser system for heating minerals for (U-Th)/He chronometry: Geochemistry Geophysics Geosystems, v. 7, no. 4. Doi: 10.1029/2005GC001190.

Fontijn, K., Delvaux, D., Ernst, G.G.J., Kervyn, M., Mbede, E., and Jacobs, P., 2010, Tectonic control over active volcanism at a range of scales: Case of the Rungwe Volcanic Province, SW Tanzania; and hazard implications: Journal of African Earth Sciences, v. 58, p. 764-777.

Fontijn, K., Williamson, D., Mbede, E., and Ernst, G.G.J., 2012, The Rungwe Volcanic Province, Tanzania – A volcanological review: Journal of African Earth Sciences, v. 63, p. 12-31.

Foster, D.A., and Gleadow, A.J.W., 1992, The morphotectonic evolution of rift margin mountains in central Kenya—constraints from apatite fission track thermochronology: Earth and Planetary Science Letters, v. 113, p. 157–171.

Foster, D.A., and Gleadow, A.J.W., 1996, Structural framework and denudation history of the flanks of the Kenya and Anza Rifts, East Africa: Tectonics, v. 15, p. 258-271.

Frey, S.E., Gingras, M.K., and Dashtgard, S.H., 2009, Experimental studies of gas-escape and water escape structures: mechanisms and morphologies: Journal of Sedimentary Research, v. 79, p. 808-816.

Fritz, H., Tenczer, V., Hauzenberger, C.A., Wallbrecher, E., Hoinkes, G., 2005, Central Tanzanian tectonic map: a step forward to decipher Proterozoic structural events in the East African Orogen: Tectonics, v. 24, TC6013.

Furniss, G., Rittel, J. F., and Winston, D., 1998, Gas bubble and expansion crack origin of “molar-tooth” calcite structures in the middle Proterozoic belt Supergroup, western Montana: Journal of Sedimentary Research, v. 68, p. 104-114.

Galli, P., 2000, New empirical relationships between magnitude and distance for liquefaction: Tectonophysics, v. 324, p. 169-187.

Gehrels, G.E., Valencia, V.A., and Ruiz, J., 2008, Enhanced precision, accuracy, efficiency, and spatial resolution of U–Pb ages by laser ablation–multicollector–inductively coupled plasma–mass spectrometry: Geochemistry, Geophysics, Geosystems, v. 9, no. 3. Doi: 1029/2007GC001805.

Gehrels, G., 2014, Detrital zircon U-Pb geochronology applied to tectonics: Annual Review of Earth and Planetary Sciences, v. 42, p. 127-149.

Gleadow, A.J.W., and Duddy, I.R., 1981, A natural longterm track annealing experiment for apatite: Nuclear Tracks, v. 5, p. 169–174.

Gleadow, A., Harrison, M., Kohn, B., Lugo-Zazueta, R., and Phillips, D., 2015, The Fish

Canyon Tuff: A new look at an old low-temperature thermochronology standard: Earth and Planetary Science Letters, v. 242, p. 95-108. Doi: 10.1016/j.epsl.2015.05.003.

Gorscak, E., O'Connor, P.M., Stevens, N.J., and Roberts, E.M., 2014, The basal titanosaurian Rukwatitan bisepultus (Dinosauria, Sauropoda) from the middle Cretaceous Galula Formation, Rukwa Rift Basin, southwestern Tanzania: Journal of Vertebrate Paleontology, v. 34, no. 5, p. 1133-1154, Doi: 10.1080/02724634.2014.845568.

Gottfried, M.D., O'Connor, P.M., Jackson, F.D., Roberts, E.M., and Chami, R., 2004, Dinosaur eggshell from the Red Sandstone Group of Tanzania: Journal of Vertebrate Paleontology, v. 24, p. 494-497.

Grantham, D.R., Teale, E.O., Spurr, A.M., Harkin, D.A., and Brown, P.E., 1958, Quarter Degree Sheet 244 (Mbeya): Geological Survey of Tanganyika, Dodoma.

Grove, A.T., 1983, Evolution of the physical geography of the East African rift valley region, in R.W. Sims, J.H. Price, and P.E.S. Whalley, eds., Evolution, time, and space: The emergence of the biosphere: Academic Press, London, United Kingdom, p. 115-155.

Guiraud, R., and Bosworth, W., 1997, Senonian basin inversion and rejuvenation of rifting in African and Arabia: synthesis and implications to plate-scale tectonics: Tectonophysics, v. 282, p. 39-82.

Harkin, D.A., 1960, The Rungwe volcanics at the northern end of Lake Nyasa: Geological Survey Tanganyika Memoir II, 172 p.

Haub, C., and Kaneda, T., 2012, World Population Data Sheet 2012: Population Reference Bureau.

Hauksson, E., 1981, Radon content of groundwater as an earthquake precursor: Evaluation of worldwide data and physical basis: Journal of Geophysical Research. Doi: 10.1029/JB086iB10p09397.

Hempton, M.R., and Dewey, J.F., 1983, Earthquake-induced deformational structures in young lacustrine sediments, East Anatolian fault, southeast Turkey: Tectonophysics, v. 98, p. T7-T14.

Hilbert-Wolf, H.L., Simpson, E.L., Simpson, W.S., Tindall, S.E., and Wizevich, M.C., 2009, Insights into syndepositional fault movement in a foreland basin; trends in seismites of the Upper Cretaceous, Wahweap Formation, Kaiparowits Basin, Utah, USA: Basin Research, v. 21, p. 856-871.

Hilbert-Wolf, H.L., and E.M. Roberts, 2015, Giant seismites and megablock uplift in the East African Rift: Evidence for Late Pleistocene large magnitude earthquakes: PLOS One. Doi: 10.1371/journal.pone.0129051.

Hilbert-Wolf, H.L., Roberts, E.M., and Simpson, E.L., 2016, New sedimentary structures in seismites from SW Tanzania: Evaluating gas- vs. water-escape mechanisms of soft-sediment deformation: Sedimentary Geology. Doi: 10.1016/j.sedgeo.2016.03.011.

Hilbert-Wolf, H., Roberts, E., Downie, B., Mtelela, C., Stevens, N.J., and O'Connor, P.,

in press, Application of U-Pb detrital zircon geochronology to drill cuttings for age control in hydrocarbon exploration wells: a case study from the Rukwa Rift Basin, Tanzania: The AAPG Bulletin.

Holmes, A., 1978, Holmes principles of physical geology: New York, John Wiley & Sons, p. 647-657.

Hoskin, P.W.O., and Ireland, T.R., 2000, Rare earth element chemistry of zircon and its use as a provenance indicator: Geology, v. 28, p. 627–30.

Hurford, A.J., and Green, P.F., 1983, The zeta age calibration of fission-track dating: Isotope Geoscience, v. 1, p. 285-317.

Hurst, A., and Cartwright, J.A., 2007, Relevance of sand injectites to hydrocarbon exploration and production, in A. Hurst and J.A. Cartwright, eds., Sand injectites: implications for hydrocarbon exploration and production: American Association of Petroleum Geologists Memoir 87, p. 1-19.

Hurst, A., Scott, A., and Vigorito, M., 2011, Physical characteristics of sand injectites: Earth-Science Reviews, v. 106, p. 215-246.

Huuse, M., Cartwright, J., Hurst, A., and Steinsland, N., 2007, Seismic characterization of large-scale sandstone intrusions, in A. Hurst and J. Cartwright, eds., Sand injectites: Implications for hydrocarbon exploration and production: AAPG Memoir 87, p. 21-35.

International Seismological Centre, 2012, On-line Bulletin: Available: http://www.isc.ac.uk.

Irwin, W.P., Barnes, I., 1980, Tectonic relations of carbon dioxide discharges and earthquakes: Journal of Geophysical Research, v. 85, p. 3115-3121.

Ivanov, A.V., Rasskazov, S.V., Boven, A., Punzalan, L, Brandt, I.S., Brandt, S.B., and Fernandez-Alonso, M., 1999, Timing of Late Cenozoic volcanic activity and rift basin formations in the Rungwe province of Tanzania substantiated by K-Ar and 40Ar/39Ar dating, in Third Annual Meeting and Field Excursion: Rifting in intracontinental setting: Baikal Rift System and other Continental Rifts, Abstract Book: Russia 22-30 August 1999.

Jackson, S.E., Pearson, N.J., Griffin, W.L., and Belousova, E.A., 2004, The application of laser ablation-inductively coupled plasma-mass spectrometry to in situ U-Pb zircon: Geochronology, v. 211, p. 47-69.

Jianhua, Z., Zhifeng, W., Guanmin, W., Xibin, W., Hongbo, L., and Xiaohua, S., 2004, Air-charge pits on the Yellow River delta plain: Sedimentary Geology, v. 170, p. 1-20.

Jones, A.P., and Omoto, K., 2000, Towards establishing criteria for the identifying trigger mechanisms for soft-sediment deformation: A case study of Late Pleistocene lacustrine sands and clays, Onikobe and Nakayamadaira Basins, northeastern Japan: Sedimentology, v. 47, p. 1211-1226.

Jung, G., Prange, M., and Schulz, M., 2015, Influence of topography on tropical African vegetation coverage: Climate Dynamics. Doi: 10.1007/s00382-015-2716-9.

Katsman, R., 2015, Correlation of shape and size of methane bubbles in fine-grained muddy aquatic sediments with sediment fracture toughness: Journal of Structural Geology, v. 70, p. 56-64.

Kervyn, F., Ayub, S., Kajara, R., Kanza, E., and Temu, B., 2006, Evidence of recent faulting in the Rukwa rift (West Tanzania) based on radar interferometric DEMs: Journal of African Earth Sciences, v. 44, p. 151-168.

Kilembe, E.A., and Rosendahl, B.R., 1992, Structure and stratigraphy of the Rukwa rift: Tectonophysics, v. 209, p. 143–158.

Kuiper, K.F., Deino, A., Hilgen, P.J., Krijgsman, W., Renne, P.R., and Wijbrans, J.R., 2008, Synchronizing rock clocks of Earth history: Science, v. 320, p. 500-504.

Lawley, C.J.M., Selby, D., Condon, D.J., Horstwood, M., Millar, I., Crowley, Q., and Imber, J., 2013, Lithogeochemistry, geochronology and geodynamic setting of the Lupa Terrane, Tanzania: Implications for the extent of the Archean Tanzanian Craton: Precambrian Research, v. 231, p. 174-193.

Lawton, T.F., Hunt, G.J., and Gehrels, G.E., 2010, Detrital zircon record of thrust best unroofing in Lower Cretaceous synorogenic conglomerates, central Utah: Geology, v. 38, no. 5, p. 463-466.

Lee, J.K.W., Williams, I.S., and Ellis, D.J., 1997, Pb, U, and Th diffusion in natural zircon: Nature, v. 390, p. 159-162.

Lenoir, J.L., Liégeois, K., Theunissen, K., and Klerkx, J., 1994, The Paleoproterozoic Ubendian shear belt in Tanzania: geochronology and structure: Journal of African Earth Science, v. 19, no. 3, p. 169-184.

Logan, P., Curd, S., Downie, B., Weston, J., and Shaw, D., 2009, Exploration on the frontier: towards an understanding of the Albert Basin: American Association of Petroleum Geologists Search and Discovery Article #10192, http://www.searchanddiscovery.com/documents/2009/10192logan/index.htm.

Loope, D.B., Elder, J.F., Zlotnik, V.A., Kettler, R.M., Pederson, D.T., 2013, Jurassic earthquake sequence recorded by multiple generations of sand blows, Zion National Park, Utah: Geology, v. 41, no. 10, p. 1131-1134.

Løseth, H., Rodrigues, N., Cobbold, P.R., 2012, World's largest extrusive body of sand: Geology, v. 40, p. 467-470.

Lowe, D.R., 1975, Water escape structures in coarse-grained sediments: Sedimentology, v. 22, p. 157-204.

Ludwig, K.R., 2012, User's Manual for Isoplot 3.75. A Geochronological Toolkit for Microsoft Excel: Berkley Geochronology Centre Special Publication No.5.

Ludwig, K., and Mundil, R., 2002, Extracting reliable U-Pb ages and errors from complex populations of zircons from Phanerozoic tuffs: Geochimica et Cosmochimica Acta, v. 66, no. 15A, p. A463.

Maxson, J. H., 1940, Gas pits in non-marine sediments: Journal of Sedimentary Petrology,

v. 10, p. 142-145.

McCalpin, J., ed., 1996, Paleoseismology: Academic Press, New York, 588 pp.

McCartney, J.A., Stevens, N.J., and O'Connor, P.M., 2014, The earliest colubroid-dominated snake fauna from Africa: Perspectives from the Late Oligocene Nsungwe Formation of Southwestern Tanzania: PLoS One. Doi: 10.1371/journal.pone.0090415.

McDowell, F.W., McIntosh, W.C., and Farley, K.A., 2005, A precise 40Ar-39Ar reference age for the Durango apatite (U-Th)/He and fission-track dating standard: Chemical Geology, v. 214, p. 249-263.

Mesko, G.T., Class, C., Maqway, M.D., Boniface, N., Manya, S., and Hemming, S.R., 2014, The timing of early magmatism and extension in the southern East African Rift: Tracking geochemical source variability with 40Ar/39Ar geochronology at the Rungwe Volcanic Province, SW Tanzania: American Geophysical Union, Fall Meeting 2014, abstract #V51A-4730.

Milga, N.R., 1994, Depositional environments, stratigraphy and hydrocarbon potential of the Rukwa Rift Basin–SW Tanzania: Ph.D. Dissertation, Duke University, 156 pp.

Moecher, D.P., and Samson, S.D., 2006, Differential zircon fertility of source terranes and natural bias in the detrital zircon record: Implications for sedimentary provenance analysis: Earth and Planetary Science Letters, v. 247, p. 252-266.

Molina, J.M., Alfaro, P., Moretti, M., and Soria, J.M., 1998, Soft-sediment deformation structures induced by cyclic stress of storm waves in tempestites (Miocene, Guadalquivir Basin, Spain): Terra Nova, v. 10, p. 145-150.

Montenat, C., Barrier, P., Ott d'Estevou, P., and Hibsch, C., 2007, Seismites: An attempt at critical analysis and classification: Sedimentary Geology, v. 196, no. 1-4, p. 5-30.

Moretti, M., and Sabato, L., 2007, Recognition of trigger mechanisms for soft-sediment deformation in the Pleistocene lacustrine deposits of the Sant'Arcangelo Basin (Southern Italy): seismic shock vs. overloading: Sedimentary Geology, v. 196, p. 31-45.

Morley, C.K., 1995, Developments in the structural geology of rifts over the last decade and their impact on hydrocarbon exploration, in J.J. Lambiase, ed., Hydrocarbon Habitat in Rift Basins: Geological Society Special Publication No. 80, p. 1-32.

Morley, C.K., Wescott, W.A., Harper, R.M., and Cunningham, S.M., 1999, Geology and Geophysics of the Rukwa Rift, in C.K. Morley, ed., Geoscience of Rift Systems – Evolution of East Africa: AAPG Studies in Geology, no. 44, p. 91-100.

Morley, C.K., Vanhauwaert, P., and De Batist, M., 2000, Evidence for high-frequency cyclic fault activity from high-resolution seismic reflection survey, Rukwa Rift, Tanzania: Journal of the Geological Society, London, v. 157, p. 983-994.

Mörner, N.-A., and Etiope, G., 2002, Carbon degassing from the lithosphere: Global Planetary Change, v. 33, p. 185-203.

Mörz, T., Karlik, E.A., Kreiter, A., and Kopf, A., 2007, An experimental setup for fluid

venting in unconsolidated sediments: new insights to fluid mechanics and structures: Sedimentary Geology, v. 196, p. 251-267.

Mtelela, C., Roberts, E.M., Downie, B., and Hendrix, M.S., in press, Interplay of structural, climatic and volcanic controls on Quaternary lacustrine-deltaic sedimentation patterns in the Western Branch of the East African Rift System, Rukwa rift, Tanzania: Journal of Sedimentary Research, manuscript #2015-088.

Muhongo, S., and Lenoir, J.-L., 1994, Pan-African granulite-facies metamorphism in the Mozambique Belt of Tanzania: U-Pb zircon geochronology: Journal of the Geological Society, v. 151, p. 343-347.

Nelson, R.A., Patton, T.L., and Morley, C.K., 1992, Rift-segment interaction and its relation to hydrocarbon exploration in continental rift systems: The American Association of Petroleum Geologists Bulletin, v. 76, no. 8, p. 1153-1169.

Nichols, R.J., Sparks, R.S.J., and Wilson, C.J. N., 1994, Experimental studies of the fluidization of layered sediments and the formation of fluid escape structures: Sedimentology, v. 41, p. 235-253.

Noble, W.P., Foster, D.A., and Gleadow, A.J.W., 1997, The post-Pan-African thermal and extensional history of crystalline basement rocks in eastern Tanzania: Tectonophysics, v. 275, p. 331-350.

Nürnberg, D., and Müller, R.D., 1991, The tectonic evolution of the South Atlantic from Late Jurassic to Present: Tectonophysics, v. 191, p. 27–53.

Obermeier, S.F., Martin, J.R., Frankel, A.D., Youd, T.L., Munson, P.J., Munson, C.A., et al., 1993, Liquefaction evidence for one or more strong Holocene earthquakes in the Wabash Valley of Southern Indiana and Illinois: U.S. Geological Survey Professional Paper 1536, 27 pp.

Obermeier, S.F., 1996, Use of liquefaction-induced features for paleoseismic analysis – An overview of how seismic liquefaction features can be distinguished from other features and how their regional distribution and properties of source sediment can be used to infer the location and strength of Holocene paleo-earthquakes: Engineering Geology, v. 44, p. 1-76.

Obermeier, S.F., 2009, Using liquefaction-induced and other soft-sediment features for paleoseismic analysis, in J.P. McCalpin, ed., Paleoseismology (2nd edition): Academic Press, Burlington, Massachusetts, p. 497-564.

O'Connor, P.M., Gottfried, M.D., Stevens, N.J., Roberts, E.M., Ngasala, S., Kapilima, S., and Chami, R., 2006, Dinosaurs and other vertebrates from the Cretaceous Red Sandstone Group, Rukwa Rift Basin, Southwestern Tanzania: Journal of African Earth Sciences, v. 44, p. 277-288.

O'Connor, P.M., Sertich, J.J.W., Stevens, N.J., Roberts, E.M., Gottfried, M.D., Hieronymus, T.L., Jinnah, Z.A., Ridgely, R., Ngasala, S.E., and Temba, J., 2010, The evolution of mammal like crocodyliforms in the Cretaceous of Gondwana: Nature, v. 466, p. 748-

751, doi 10.1038/nature09061.

Owen, G., 1996, Experimental soft-sediment deformation: structures formed by liquefaction of unconsolidated sands and some ancient examples: Sedimentology, v. 43, p. 270-293.

Owen, G., 1997, Deformational processes in unconsolidated sands, in M.E. Jones and R.M.F. Preston, eds., Deformation of sediments and sedimentary rocks: Geological Society of London Special Publication 29, p. 137-146.

Owen, G., and Moretti, M., 2011, Identifying triggers for liquefaction-induced soft-sediment deformation in sands: Sedimentary Geology, v. 235, p. 141-147.

Paces, J.B., and Miller, J.D., 1993, Precise U-Pb ages of Duluth Complex and related mafic intrusions, northeastern Minnesota: Geochronological insights to physical, petrogenic, paleomagnetic, and tectonomagmatic processes associated with the 1.1 Ga Midcontinent Rift System: Journal of Geophysical Research, v. 98, no. B8, p. 13997-14013.

Papathanassiou G, Pavlides S, Christaras B, Pitilakis K. Liquefaction case histories and empirical relations of earthquake magnitude versus distance from the broader Aegean region. Journal of Geodynamics. 2005; 40: 257-278.

Parize, O., and Friès, G., 2003, The Vocontian clastic dykes and sills: a geometric model, in M.E. Jones, and R.M.F. Preston, eds., Deformation of sediments and sedimentary rocks: Geological Society of London Special Publication 216, p. 51-71.

Park, H., Barbeau Jr., D.L., Rickenbaker, A., Bachmann-Krug, D., and Gehrels, G., 2010, Application of foreland basin detrital-zircon geochronology to the reconstruction of the southern and central Appalachian orogen: The Journal of Geology, v. 118, no. 1, p. 23-44.

Pentelkov, V.G., and Voronovskii, S.N., 1977, Absolute age of Mbalizi carbonatites, Tanzania, and its correlation with age of other carbonatites from Rukava-Malavi Rift Zone: Doklady Akademii Nauk SSSR, v. 235, p. 1136-1139.

Pentelkov, V.G., 1979, New data on age and correlation of Mesozoic rocks of the Rukwa trough, southwestern Tanzania: Doklady Akademiya Nauk USSR, v. 245, p. 113-116.

Pik, R., Marty, B., Carignan, J., Yirgu, G., and Ayalew, T., 2008, Timing of East African Rift development in southern Ethiopia: Implication for mantle plume activity and evolution of topography: Geology, v. 36, p. 167-170.

Pralle, N., Külzer, M., and Gudehus, G., 2003, Experimental evidence on the role of gas in sediment liquefaction and mud volcanism, in M.E. Jones, and R.M.F. Preston, eds., Deformation of sediments and sedimentary rocks: Geological Society of London Special Publication 216, p. 159-171.

Pullen, A., Ibáñez-Mejía, M., Gehrels, G.E., Ibáñez-Mejía, J.C., and Pecha, M., 2014, What happens when n=1000? Creating large-n geochronological datasets with LA-ICP-MS for geologic investigations: Journal of Analytical Atomic Spectrometry, Doi:

10.1039/c4ja00024b.

Quenell, A.M., Mcinley, A.C.M., and Aitken, W.G., 1956, Summary of the geology of Tanganyika: Geological Survey of Tanganyika Memoir, 1264 p.

Quigley, M.C., Bastin, S., and Bradley, B.A., 2013, Recurrent liquefaction in Christchurch, New Zealand, during the Canterbury earthquake sequence: Geology, v. 41, no. 4, p. 419-422.

Rajendran, K., Rajendran, C.P., Thakkar, M., and Tuttle, M.P., 2001, The 2001 Kutch (Bhuj) earthquake: Coseismic surface features and their significance: Current Science, v. 80, p. 1397-1405.

Rasskazov, S.V., Logachev, N.A., Ivanov, A.V., Boven, A.A., Maslovskaya, M.N., Saranina, E.V., Brandt, I.S., and Brandt, S.B., 2003, A magmatic episode in the western rift of East Africa (19–17 Ma): Geologiya i Geofizika, v. 44, p. 317–324.

Ratcliffe, K.T., Wilson, A., Payenberg, T., Rittersbacher, A., Hildred, G.V., and Flint, S.S., 2015, Ground truthing chemostratigraphic correlations in fluvial systems: AAPG Bulletin, v. 99, p. 155-180.

Reddy, S.M., Collins, A.S., and Mruma, A., 2003, Complex high-strain deformation in the Usagaran Orogen, Tanzania: structural setting of Paleoproterozoic eclogites: Tectonophysics, v. 375, p. 101-123.

Reicherter, K., Michetti, S.M., Silva, P.G., 2009, Palaeoseismology: historical and prehistorical records of earthquake ground effects for seismic hazard assessment, in K. Reicherter, S.M. Michetti, and P.G. Silva, eds., Palaeoseismology: historical and prehistoric records of earthquake ground effects for seismic hazard assessment: Geological Society, London, Special Publication 316, p. 1-10.

Reimer, P.J., Bard, E., Bayliss, A., Beck, J.W., Blackwell, P.G., Ramsey, C.B., et al., 2013, IntCal13 and Marine13 radiocarbon age calibration curves, 0-50,000 years cal BP: Radiocarbon, v. 55, no. 4, p. 1869-1887.

Rindsberg, A., 2005, Gas-escape structures and their paleoenvironmental significance at the Steven C. Minkin Paleozoic footprint site (Early Pennsylvanian, Alabama), in R.J. Buta, A.K. Rindsberg, and D.C. Kopaska-Merkel, eds., Pennsylvanian footprints in the Black Warrior Basin of Alabama: Alabama Paleontological Society Monograph no. 1, p. 177-183.

Roberts, E.M., O'Connor, P.M., Gottfried, M.D., Stevens, N.J., Kapilima, S., and Ngasala, S., 2004, Revised stratigraphy and age of the Red Sandstone Group in the Rukwa Rift Basin, Tanzania: Cretaceous Research, v. 25, p. 749-759.

Roberts, E.M., O'Connor, P.M., Armstrong, R.A., Stevens, N.J., and Gottfried, M.D., 2007, U–Pb geochronology of detrital zircons from the Rukwa Rift Basin, Tanzania: New data on the pre-Neogene tectonic and sedimentary evolution of the Western Branch of the East African Rift System: Geological Society of America, Abstracts with Programs 39, p. 505.

Roberts, E.M., O'Connor, P.M., Stevens, N.J., Gottfried, M.D., Jinnah, Z.A., Ngasala, S., Choh, A.M., and Armstrong, A., 2010, Sedimentology and depositional environments of the Red Sandstone Group, Rukwa Rift Basin, southwestern Tanzania: New insight into Cretaceous and Paleogene terrestrial ecosystems and tectonics in sub-equatorial Africa: Journal of African Earth Science, v. 57, p. 179-212.

Roberts, E.M., Stevens, N.J., O'Connor, P.M., Dirks, P.H.G.M., Gottfried, M.D., Clyde, W.C., Armstrong, R.A., Kemp, A.I.S., and Hemming, S., 2012, Initiation of the western branch of the East African Rift coeval with the eastern branch: Nature Geoscience, v. 5. Doi: 10.1038/NGEO1432.

Roberts, E.M., Todd, C.N., Aanen, D.K., Nobre, T., Hilbert-Wolf, H.L., O'Connor, P.M., Tapanila, L., Mtelela, C., and Stevens, N.J., 2016, Oligocene termite nests with *in situ* fungus gardens from the Rukwa Rift Basin, Tanzania, support a Paleogene African origin for insect agriculture: PLoS ONE, doi 10.1371/journal.pone.0156847.

Rodrigues, N., Cobbold, P.R., and Løseth, H., 2009, Physical modeling of sand injectites: Tectonophysics, v. 474, p. 610-632.

Rodríguez-Pascua, M.A., Calvo, J.P., De Vicente, G., and Gómez-Gras, D., 2000, Soft-sediment deformation structures interpreted as seismites in lacustrine sediments of the Prebetic Zone, SE Spain, and their potential use as indicators of earthquake magnitudes during the Late Miocene: Sedimentary Geology, v. 135, p. 117-135.

Ross, J.A., Peakall, J., and Keevil, G.M., 2011, An integrated model of extrusive sand injectites in cohesionless sediments: Sedimentology, v. 58, p. 1963-1715.

Schmitz, M.D., and S.A. Bowring, 2001, U-Pb zircon and titanite systematics of the Fish Canyon Tuff: an assessment of high-precision U-Pb geochronology and its application to young volcanic rocks: Geochimica et Cosmochimica Acta, v. 65, p. 2571-2587.

Scott, A.S.J., Vigorito, M., Hurst, A., 2009, The process of sand injection: internal structures and relationships with host strata (Yellowbank Creek Injectite Complex, California, USA): Journal of Sedimentary Research, v. 79, p. 1-18.

Sell, B.K., and Samson, S.D., 2011, A Tephrochronologic method based on apatite trace element chemistry: Quaternary Research, v. 76, p. 157-166.

Semkiwa, P., Kalkreuth, W., Utting, J., Mayagilo, F., Mpanju, F., and Hagemann, H., 1998, The geology, petrology, palynology and geochemistry of Permian coal basins in Tanzania. 1. Namwele-Mkomolo, Muze, and Galula coalfields: International Journal of Coal Geology, v. 36, p. 63-110.

Sepulchre, P., Ramstein, G., Fluteau, F., Schuster, M., Tiercelin, J.-J., and Brunet, M., 2006, Tectonic uplift and eastern Africa aridification: Science, v. 313, p. 1419-1423.

Sherry, T.J., Rowe, C.D., Kirkpatrick, J.D., and Brodsky, E.E., 2012, Emplacement and dewatering of the world's largest exposed sand injectite complex: Geochemistry Geophysics Geosystems, v.13. Doi: 10.1029/2012GC004157.

Simpson, E.L., Hilbert Wolf, H.L, Wizevich, M.C., Tindall, S.E., 2013, Implications of

the internal plumbing of a Late Cretaceous sand Blow: Grand Staircase-Escalante National Monument, Utah, in A. Titus, and M.A. Loewen, eds., At the top of the Grand Staircase: The Late Cretaceous of southern Utah: Indiana University Press, Bloomington, p. 74-84.

Sims, J.D., 1975, Determining earthquake recurrence intervals from deformational structures in young lacustrine sediments: Tectonophysics, v. 29, p. 144-152.

Skobelev, S.F., Hanon, M., Klerkx, J., Govorova, N.N., Lukina, N.V., and Kazmin, V.G., 2004, Active faults in Africa: a review: Tectonophysics, v. 380, p. 131-137.

Sláma, J., and Košler, J., 2012, Effects of sampling and mineral separation on accuracy of detrital zircon studies: Geochemistry, Geophysics, Geosystems, v. 13, no. 5.

Snelling, N.J., 1965, Age determinations on three African carbonatites: Nature, v. 205, p. 491.

Spandler, C., Hammerli, J., Sha, P., Hilbert-Wolf, H., Hu, Y., Roberts, E., and Schmitz, M., 2016, MKED1: A new titanite standard for in situ analysis of Sm–Nd isotopes and U–Pb geochronology: Chemical Geology. Doi: 10.1016/j.chemgeo.2016.01.002.

Spence, J., 1954, The geology of the Galula coalfield, Mbeya district: Geological Survey of Tanganyika Bulletin, v. 25, 34 p.

Spiegel, C., Kohn, B.P., Belton, D.X., and Gleadow, A.J.W., 2007, Morphotectonic evolution of the central Kenya rift flanks: Implications for late Cenozoic environmental change in East Africa: Geology, v. 35, no. 5, p. 427-430. Doi: 10.1130/G23108A.1.

Stacey, J.S., and J.D. Kramers, 1975, Approximation of terrestrial lead isotope evolution by a two-stage model: Earth and Planetary Science Letters, v. 26, 207-221.

Stevens, N.J., Seiffert, E.R., O'Connor, P.M., Roberts, E.M., Schmitz, M.D., Krause, C., Gorscak, E., Ngasala, S., Hieronymus, T.L., and Temu, J., 2013, Palaeontological evidence for an Oligocene divergence between Old World monkeys and apes: Nature, v. 497, p. 611-614.

Stirling, M., Rhoades, D., and Berryman, K., 2002, Comparison of earthquake scaling relations derived from data of the instrumental and preinstrumental era: Bulletin of the Seismological Society of America, v. 92, no. 2, p. 812-830.

Stockley, G.M., 1938, The geology of parts of the Tabora, Kigoma and Ufipa districts, northwest Lake Rukwa: Geological Survey of Tanganyika Short Paper 20, 33 p.

Thompson, B.J., Garrison, R.E., Moore, C.J., 2007, A reservoir-scale Miocene injectite near Santa Cruz, California, in A. Hurst, and J. Cartwright, eds., Sand Injectites: Implications for Hydrocarbon Exploration and Production: American Association of Petroleum Geologists Memoir 87, p. 151-162.

Tiercelin, J.J., Chorowicz, J., Bellon, H., Richert, J.P., Mwanbene, J.T., and Walgenwitz, F., 1988, East African Rift System: offset, age and tectonic significance of the Tanganyika-Rukwa-Malawi intracontinental transcurrent fault zone: Tectonophysics, v. 148, p. 241-252.

Tiercelin, J-J., P. Thuo, J-L. Potdevin, and T. Nalpas, 2012, Hydrocarbon prospectivity in Mesozoic and Early-Middle Cenozoic rift basins of central and northern Kenya, East Africa, in: D. Gao, ed., Tectonics and sedimentation: Implications for petroleum systems: AAPG Memoir 100, p. 179-207.

Tsuchida, H., and Hayashi, S., 1971, Estimation of liquefaction potential of sandy soils: Proceedings of the 3rd Joint Meeting US-Japan Panel on Wind and Seismic Effects, UJNR, Tokyo, p. 91-109.

Tucker, R.T., Roberts, E.M., Hu, Y., Kemp, A.I.S., and Salisbury, S.W., 2013, Detrital zircon age constraints for the Winton Formation, Queensland: contextualizing Australia's Late Cretaceous dinosaur faunas: Gondwana Research, v. 24, p. 767-779. Doi: 10.1016/j.gr.2012.12.009.

U.S. Geological Survey. ANSS Global Earthquake Catalogue. Available: http://earthquake.usgs.gov/earthquakes/search.

Van Achterbergh, E., Ryan, C.G., Jackson, S.E., and Griffin, W.L., 2001, Data reduction software for LA-ICP-MS, in P. Sylvester, ed., Laser-ablation-ICPMS in the Earth sciences: principles and applications: Mineralogical Association of Canada, Short Course Series, v. 29, p. 239-243.

Van der Beek, P., Mbede, E., Andriessen, P., Delvaux, D., 1998, Denudation history of the Malawi and Rukwa Rift flanks (East African Rift System) from fission track thermochronology, in D. Delvaux, and M.A. Khan, eds., Tectonics, sedimentation and volcanism in the East African Rift System: Journal of African Earth Sciences, v. 26, p. 363–385.

Van der Meer, J.J.M., Kjaer, K. H., Krüger, J., Rabassa, J., and Kilfeather, A.A., 2009, Under pressure: clastic dykes in glacial settings: Quaternary Science Reviews, v. 28, p. 708-720.

Van Loenen, R.E., and Kennerley, J.B., 1962, Mpui map: Geologic Survey of Tanganyika, scale 1:125,000, quarter degree sheet 225.

Van Straaten, P., 1989, Nature and structural relationships of carbonatites from Southwestern and West Tanzania, in K. Bell, K, ed., Carbonatites: Unwin-Hyman, London, p. 177-199.

Vermeesch, P., 2004, How many grains are needed for a provenance study?: Earth and Planetary Science Letters, v. 224, p. 351-441.

Vermeesch, P., 2012, On the visualisation of detrital age distributions: Chemical Geology, v.312-313, p. 190-194. Doi: 10.1016/j.chemgeo.2012.04.021.

Vigorito, M., Hurst, A., Cartwright, J., and Scott, A., 2008, Regional-scale subsurface sand remobilization: geometry and architecture: Journal of the Geological Society, v. 165, p. 609-612.

Vigorito, M., and Hurst, A., 2010, Regional sand injectite architecture as a record of pore-pressure evolution and sand redistribution in the shallow crust: insights from

the Panoche Giant Injection Complex, California: Journal of the Geological Society, London, v. 167, p. 889-904.

Vittori, E., Delvaux, D., and Kervyn, F., 1997, Kanda Fault: A major seismogenic element west of the Rukwa Rift (Tanzania, East Africa): Journal of Geodynamics, v. 24, no. 1-4, p. 139-153.

Wells, D.L., and Coppersmith, K.J., 1994, New empirical relationships among magnitude, rupture length, rupture width, rupture area, and surface displacement: Bulletin of the Seismological Society of America, v. 84, no. 4, p. 974-1002.

Wescott, W.A., Krebs, W.N., Engelhardt, D.W., and Cunningham, S.M., 1991, New biostratigraphic age dates from the Lake Rukwa Rift Basin in Western Tanzania: The American Association of Petroleum Geologists Bulletin, v. 75, no. 7, p. 1255-1263.

Wheeler, W.H., and Karson, J.A., 1994, Extension and subsidence adjacent to a "weak" continental transform: An example from the Rukwa rift, East Africa: Geology, v. 22, p. 625-628.

Winkler, A.J., 1994, The middle/upper Miocene dispersal of major rodent groups between southern Asia and Africa, in Y. Tomida, C.K. Li, and T. Setoguchi, eds., Rodent and Lagomorph Families of Asian Origins and Diversification, No. 8: National Science Museum Monographs, Tokyo, p. 173–184.

Wopfner, H., 2002, Tectonic and climatic events controlling deposition in Tanzanian Karoo Basins: Journal of African Earth Sciences, v. 34, p. 167–177.

Yamada, R., Tagami, T., Nishimura, S., and Ito, H., 1995, Annealing kinetics of fission tracks in zircon: an experimental study: Chemical Geology, v. 122, p. 249-258.

Appendix 1

Giant seismites and megablock uplift in the East African Rift: Evidence for Late Pleistocene large magnitude earthquakes

PLoS ONE

H. L. Hilbert-Wolf and E. M. Roberts, 2015

PLOS | ONE

RESEARCH ARTICLE

Giant Seismites and Megablock Uplift in the East African Rift: Evidence for Late Pleistocene Large Magnitude Earthquakes

Hannah Louise Hilbert-Wolf*, Eric M. Roberts

Department of Earth and Oceans, James Cook University, Townsville, Queensland, Australia

* hannah.hilbertwolf@my.jcu.edu.au

Citation: Hilbert-Wolf HL, Roberts EM (2015) Giant Seismites and Megablock Uplift in the East African Rift: Evidence for Late Pleistocene Large Magnitude Earthquakes. PLoS ONE 10(6): e0129051. doi:10.1371/journal.pone.0129051

Academic Editor: Fenton Cotterill, University of Stellenbosch, SOUTH AFRICA

Received: January 23, 2015

Accepted: May 3, 2015

Published: June 4, 2015

Data Availability Statement: All relevant data are within the paper.

Funding: Financial support for this study was provided by James Cook University (http://www.jcu.edu.au) and the US National Science Foundation (NSF-BCS- 127164, NSF-EAR-1349825). The funders had no role in study design, data collection and analysis, decision to publish, or preparation of the manuscript.

Competing Interests: Heritage Oil Rukwa Tanzania Ltd. provided logistical support (e.g., access to a vehicle) and advice while we were conducting

Abstract

In lieu of comprehensive instrumental seismic monitoring, short historical records, and limited fault trench investigations for many seismically active areas, the sedimentary record provides important archives of seismicity in the form of preserved horizons of soft-sediment deformation features, termed seismites. Here we report on extensive seismites in the Late Quaternary-Recent (≤ ~ 28,000 years BP) alluvial and lacustrine strata of the Rukwa Rift Basin, a segment of the Western Branch of the East African Rift System. We document examples of the most highly deformed sediments in shallow, subsurface strata close to the regional capital of Mbeya, Tanzania. This includes a remarkable, clastic 'megablock complex' that preserves remobilized sediment below vertically displaced blocks of intact strata (megablocks), some in excess of 20 m-wide. Documentation of these seismites expands the database of seismogenic sedimentary structures, and attests to large magnitude, Late Pleistocene-Recent earthquakes along the Western Branch of the East African Rift System. Understanding how seismicity deforms near-surface sediments is critical for predicting and preparing for modern seismic hazards, especially along the East African Rift and other tectonically active, developing regions.

Introduction

Earthquakes not only trigger geohazards such as surface ruptures, tsunamis, and landslides, but are also linked to significant, catastrophic soft-sediment deformation. Despite recent events associated with devastating liquefaction and fluidization of near-surface sediments, such as the 2011 New Zealand and Japan earthquakes and the ongoing Lusi mud eruptions in Indonesia, the dangers to life and infrastructure from soft-sediment deformation are often overlooked. In 1910 7.5 million people lived in Tanzania when the most powerful earthquake in Africa of the twentieth century (M_s 7.4) struck the Lake Rukwa region, collapsing houses, initiating standing waves in nearby water bodies, causing ground deformation, and triggering liquefaction and fluidization of saturated subaerial and submarine deposits [1, 2]. By 2050 roughly 138 million people will live in Tanzania [3], largely in constructed urban environments. This growth

research in the area, where they are also concurrently conducting hydrocarbon exploration reconnaissance work. The authors' interaction with Heritage Oil Rukwa Tanzania Ltd. geologists does not alter the authors' adherence to PLOS ONE policies on sharing data and materials.

particularly affects the seismically active rift valleys of East Africa, where people concentrate near productive rift lakes and volcanic soils, on substrate that is susceptible to liquefaction and seismite generation and preservation [4].

A combination of approaches to investigate prehistoric seismicity, such as archaeoseismic research, seismic-stratigraphic correlation of event horizons, and characterization of soft-sediment deformation features, are vital for constraining earthquake recurrence intervals and magnitude [4, 5]. In Africa, historical records alone can limit the recognition of long-term earthquake trends due to deficiencies in station numbers, global station distribution, epicentral accuracy, and short instrumental coverage period of only the last ~100 years. Given the potential societal impacts, understanding sediment responses to earthquake activity is an underappreciated aspect of seismic hazard evaluation. Additionally, the ability to recognize and document large-scale soft-sediment deformation and injectite features in outcrop is increasingly advantageous in light of heightened interest in the association of large-scale sandstone intrusions and hydrocarbons.

Seismicity in the Rukwa Rift

The Rukwa Rift Basin is a nexus of tectonic activity (Fig 1), and with one of the thickest continental sedimentary successions in Africa, it records repeated rifting, volcanism, and sedimentation from the Permian to Recent [6, 7]. At its southern extremity the Rukwa Rift Basin splits into the Msangano and Songwe (study area) valleys (Fig 1). Over the last century, the Songwe Valley has been characterized by particularly high micro-seismicity, moderate and strong earthquakes ($5 \leq M \leq 7.4$), and significant Holocene fault movements [6, 8–10]. Related to Miocene-Recent rifting, the Lake Beds Succession (LBS) is the youngest deposit in the Rukwa Rift Basin, comprised of semi-consolidated volcaniclastic siltstones, mudstones, sandstones and conglomerates deposited by fluvial deltaic, alluvial, and lacustrine processes.

Numerous soft-sediment deformation features of possible seismic origin have been identified at a variety of different localities spanning the Paleozoic-Recent sedimentary succession in the Rukwa Rift Basin. Indeed, a number of other workers have noted the presence of such secondary sedimentary features, particularly in the Cretaceous-Paleogene Red Sandstone Group strata, and they have also interpreted a seismic origin for many of these features [14–16]. This paper is the first to report soft-sediment deformation features from the Pleistocene-Recent Lake Beds Succession in the rift. We have documented numerous such features, of centimeter- to dekameter-scale and varying character, in the Lake Beds Succession at many stratigraphic levels and at numerous localities in the southern portion of the Rukwa Rift where we have concentrated our research. Here we focus on two particularly spectacular occurrences of soft-sediment deformation exposed at two, stratigraphically correlative outcrop localities ~35 km apart (Ilasilo 6: 502917 E 9044472 N; and the Songwe Megablock Site: 522904 E 9015130 N; zone 36, ARC 1960 datum; Fig 1).

Methods

Permits

The Tanzanian Commission for Science and Technology and the Tanzanian Antiquities Unit granted us permission to carry out our field studies and to take samples. Our field studies did not involve endangered or protected species.

Fieldwork and Analyses

Fieldwork was conducted in the southern Rukwa Rift Basin, Tanzania (Fig 1), during the Austral winter, from 2012–2014. Outcrops were evaluated using standard sedimentologic

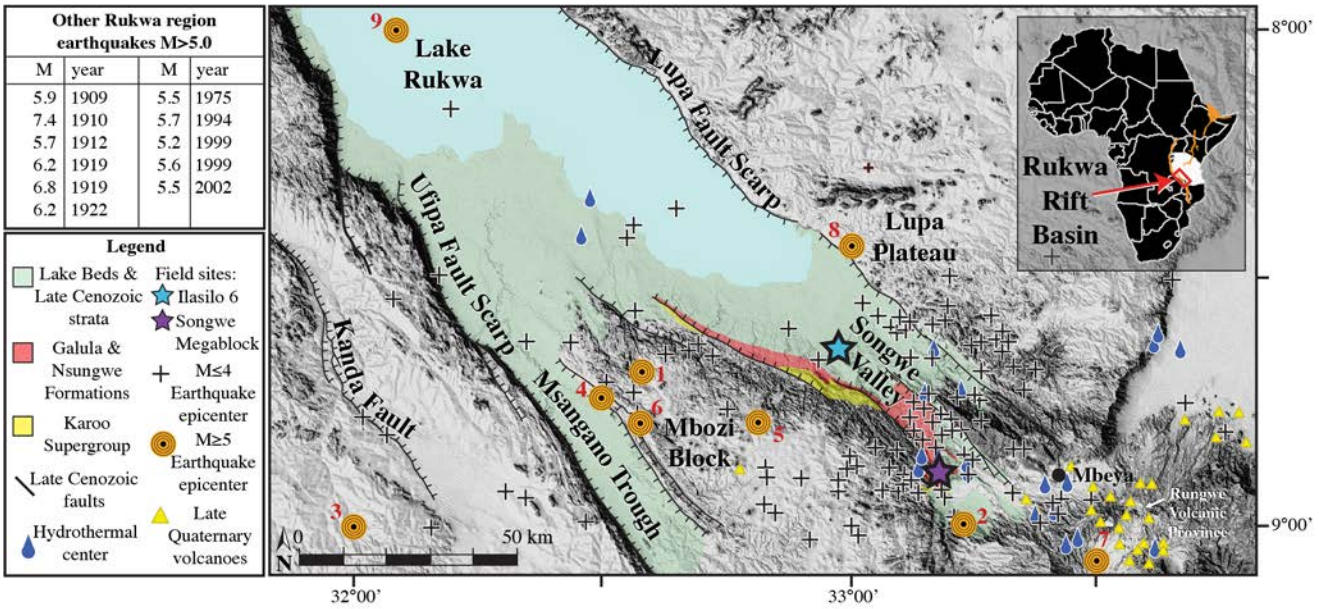

Fig 1. DEM map displaying neotectonic elements of the Songwe Valley, Rukwa Rift Basin [11]. Camelbeeck and Iranga's seismic network recorded 199 microearthquake ($M \leq 4$) events in the Rukwa Rift Basin from 1992–1994 [8]. A sample of these epicenters is plotted on the map (+ symbols) to show the general distribution of activity, highlighting the Songwe Valley as the most seismically active area [8]. Historical earthquake epicenters in the mapped region with $M \geq 5$ include: 1–1968, M 5.0; 2–1972, M 5.0; 3–1979, M 5.3; 4–1984, M 5.4; 5–1985, M 5.1; 6–1988, M 5.0; 7–1994, M 5.0; 8–2012, M 5.0; 9–2013, M 5.0. Other comparable earthquakes that plot just off the map are listed in the table [1, 12, 13].

doi:10.1371/journal.pone.0129051.g001

techniques. For example, stratigraphic sections were measured with the aid of a Jacob's staff and Brunton compass.

Data analysis was carried out at James Cook University, Australia. Sediment size and dispersion was measured on a Mastersizer 2000 via laser diffraction, capable of measuring particles of 0.02–2000 μm diameter. Five sediment samples were analyzed and corresponding liquefaction potential was modeled from the recorded data and used to create gradation curves. Sediment samples containing fossilized organic material from 1.5 m below the deformed horizon at Ilasilo 6 and in situ fossilized reed fragments from the megablock siltstone unit of the megablock complex at the Songwe Megablock Site were dated using the Accelerator Mass Spectrometry (AMS) method by Beta Analytic Inc. The samples were pretreated with an acid wash, and conventional radiocarbon ages were corrected for total fractionation effects and rounded to the nearest 10 years per conventions of the 1977 International Radiocarbon Conference. Calibrated ages were calculated using the IntCal13 database [17].

Large-Scale Soft-Sediment Deformation Features

Description

Megablock Complex. Here we describe for the first time a 50 m-tall cliff face exposure of a spectacular, large-scale (10 m-tall x 20 m-wide in cross-sectional surface area), soft-sediment deformation feature that we term the 'Songwe Megablock Complex' (Figs 2 and 3). The Songwe Megablock Site is characterized by an angular unconformity that separates the Upper Pleistocene, upper Lake Beds Succession from underlying, undeformed Cretaceous sandstones that gently dip consistently across the outcrop (~311°, 14° NE). The base of the Lake Beds Succession consists of an upward fining, polymictic, pebble-cobble orthoconglomerate. This unit preserves weak horizontal bedding, remnant trough cross-bedding, weak pebble imbrication, and

no obvious deformation. Above the conglomerate a buttress unconformity separates red, dominantly coarse-grained Lake Beds strata to the south (left of the megablock complex in Fig 2D) from dominantly fine-grained Lake Beds strata to the north (right of the megablock complex in Figs 2D and 3), which hosts the megablock complex. The coarse-grained strata is comprised of a basal conglomeratic unit, and overlain by repeated, interbedded sequences of fine-medium sandstone at the base with 1–3 mm pumice clasts, fining upwards into ash-rich siltstone with floating clasts, including $\leq$ 5 cm metamorphic and caliche pebbles. To the north, the fine-grained units are characterized by finely laminated, tuffaceous siltstone (the strata from which the megablock was derived), and were deposited within an erosionally incised depression that formed along the buttress unconformity surface, against which the fine-grained facies thin. Continuous horizons of thin (~10–20 cm) white cross-bedded ashes are present near the top of the outcrop, along with several massive, color banded, ash-rich siltstone horizons above this (Figs 2 and 3).

A large-scale, soft-sediment deformation feature dominates the finer-grained Lake Beds Succession facies. Deformation is contained between the buttress unconformity and the top of the modern-day cliff face. A 10 m-tall x 20 m-wide block of intact siltstone from the unit immediately above the basal conglomerate appears to have been uplifted ~10 m. The block is supported by a massive, fine-grained foreign body of tuffaceous material, not correlative with the laminated strata on either side of the soft-sediment deformation. This same 'parent material' that supports the megablock extends upwards via irregular dykes that surround the displaced blocks of bedded, cohesive sediment. A 5 cm-wide clastic injection dyke emerges from the top of the basal Lake Beds Succession conglomerate, crosscutting the intrusive sediment and uplifted megablock, where it expands gradually into a "V"-shape, up to 2.5 m in diameter at the top of the outcrop. The lower dyke contains metamorphic cobbles (4–20 cm diameter) from the basal Lake Beds Succession conglomerate and abundant pumice clasts (Fig 2C). Metamorphic cobbles and 5–25 cm clasts of the megablock unit infill the uppermost "V"-shaped dyke.

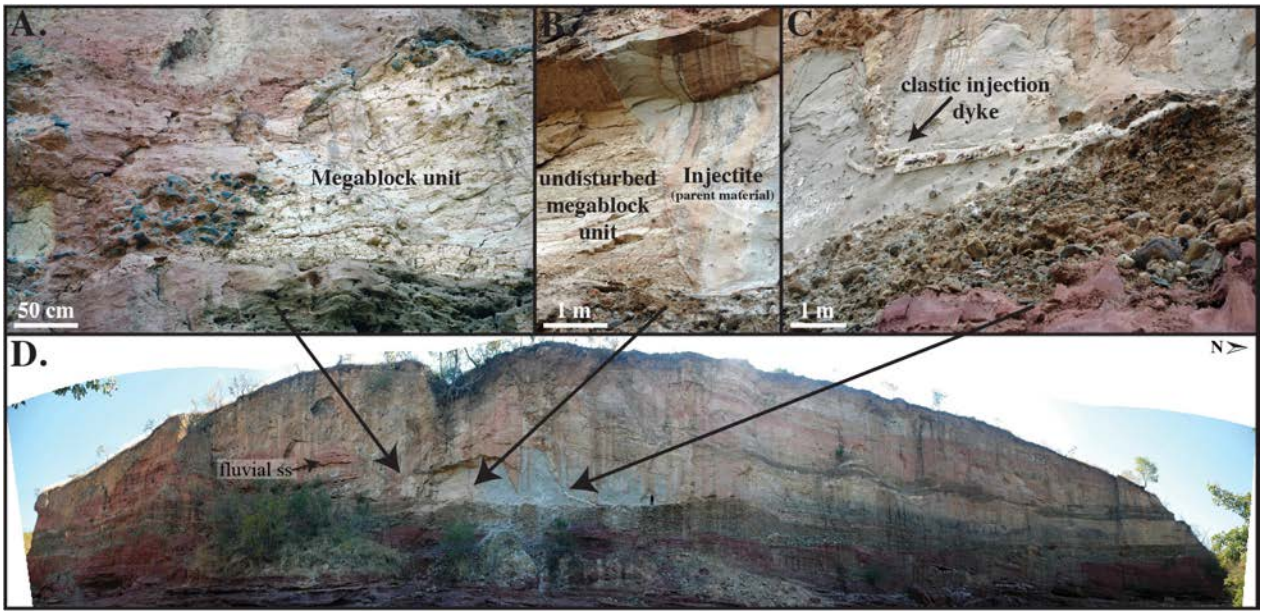

Fig 2. Field photographs of the megablock complex at the Songwe Megablock Site. (A) Megablock unit and offset conglomerate unit. (B) "Blowout" fault bounding the left side of the injectite. (C) Clastic injection dyke emerging from basal LBS conglomerate. Note the pebbles and cobbles entrained in the dyke, as well as the offset dyke segments. (D) Panoramic photograph of injectite complex outcrop, highlighting its position within undeformed, horizontal Lake Beds strata. Person is for scale on the lower right of the injectite.

doi:10.1371/journal.pone.0129051.g002

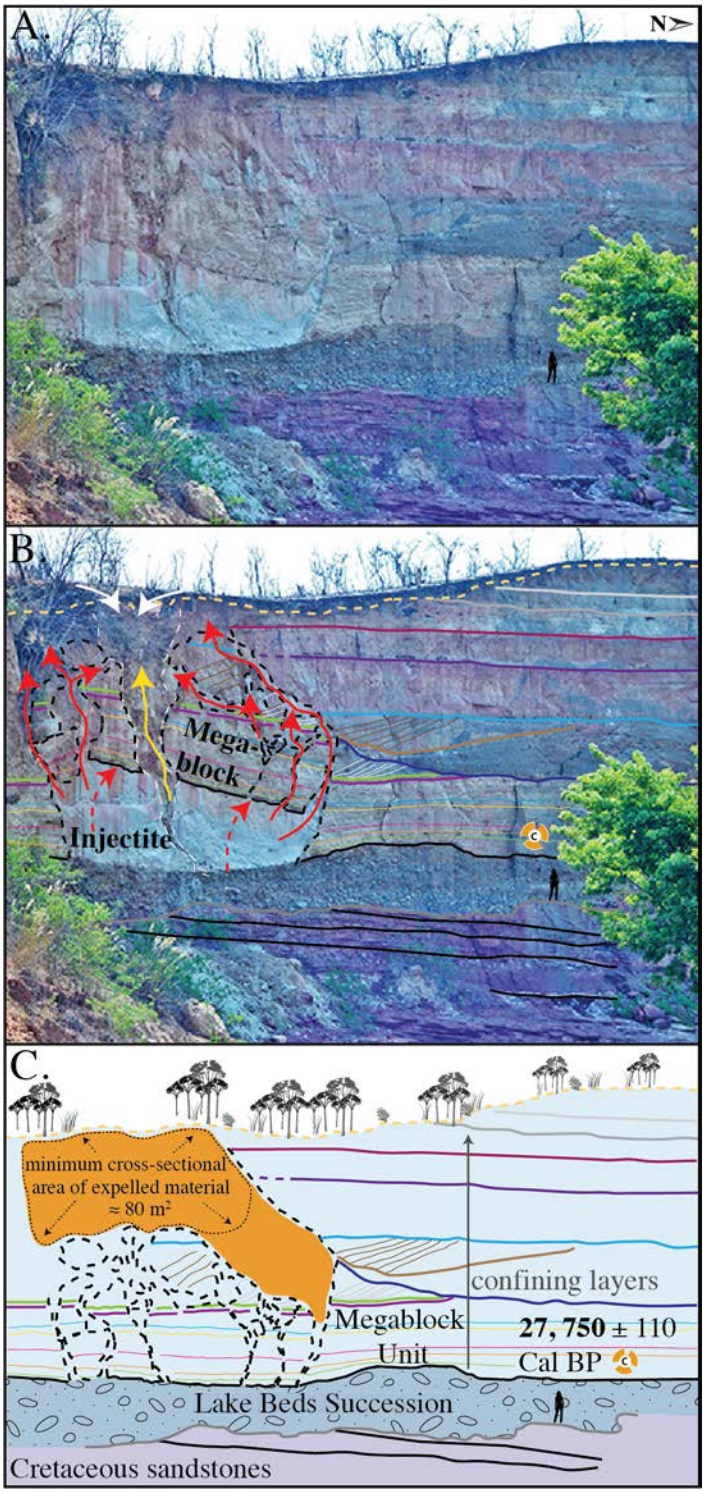

Fig 3. Outcrop exposure of injectite and megablock complex at the Songwe Megablock Site. (A) Photograph of megablock complex outcrop. (B) Trace of intact stratigraphy and displaced megablock. Red arrows indicate flow of injectite material. Yellow arrow indicates path of clastic injection dyke. White arrows represent surface alluvium and clasts of the sidewall infilling the top of the clastic injection dyke. (C) Reconstructed megablock in original stratigraphic position. An estimate is made of the cross-sectional surface area of material ejected onto the surface after formation of injectite and vertical displacement of megablock.

doi:10.1371/journal.pone.0129051.g003

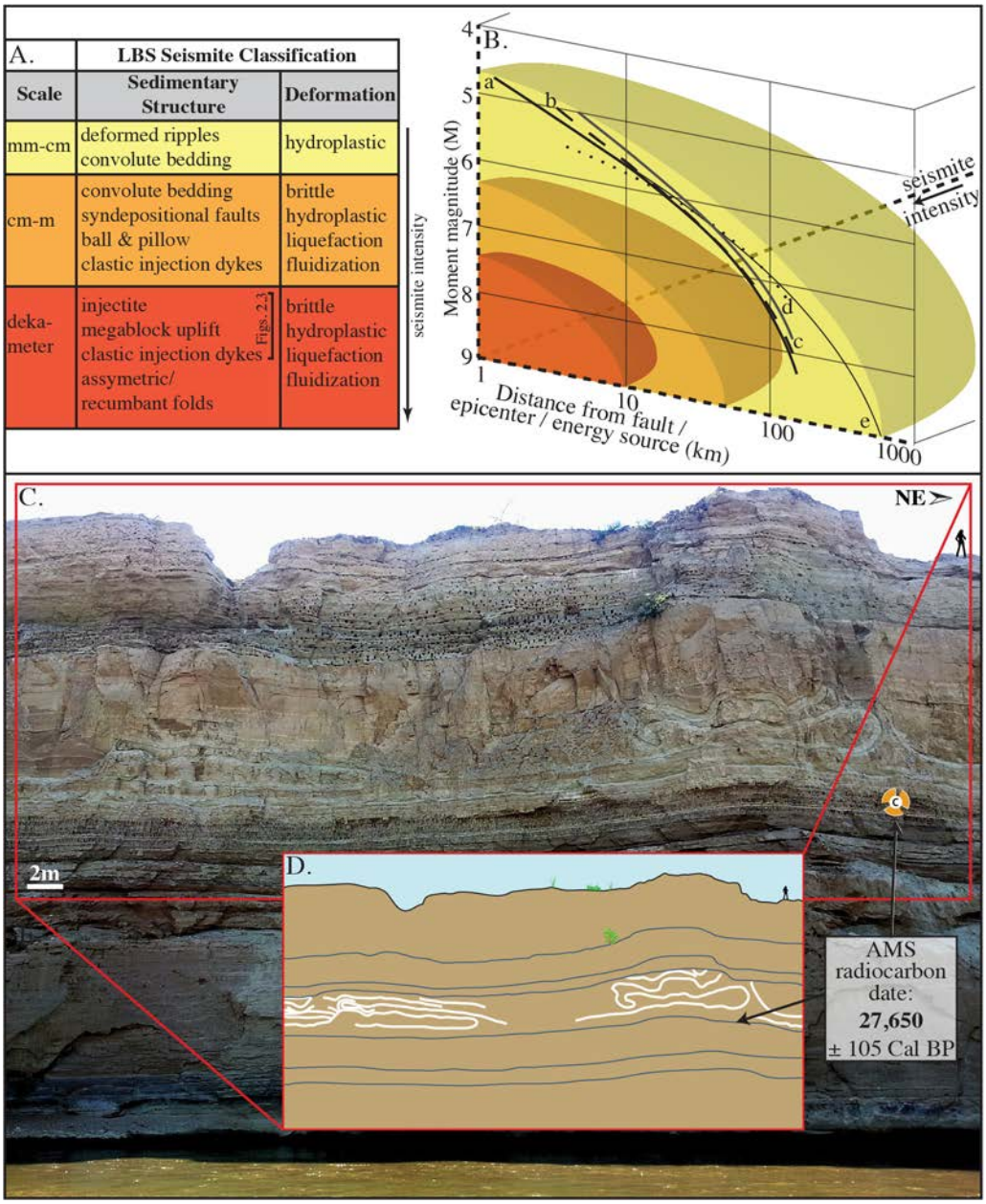

Fig 4. Classification and genetic relationship of liquefaction features in the Songwe Valley. (A) Classification scheme for seismites in the study area (after [18, 19]). (B) Model relating qualitative seismite intensity (refer to Fig 4A) to distribution (distance from fault/epicenter/energy source) and earthquake magnitude. Curve a: upper bound from energy source for worldwide, shallow focus earthquakes [20]; curves b-c: bound from fault [21]; curve d: bound from fault for earthquakes $5.5 \leq M_s \geq 7.1$ [21]; and curve e: bound from epicenter for worldwide, shallow focus earthquakes [20]. The seismite intensity scale (Fig 4A) reported here describes the soft-sediment deformation features recorded from the Lake Beds Succession only; however, the curves reported in part B are global averages. (C) Asymmetric/recumbent folds at Ilasilo 6, illustrated in (D).

doi:10.1371/journal.pone.0129051.g004

Asymmetric Recumbent Folds. Thirty-five km to the northwest of the Songwe Megablock Site, at a locality called Ilasilo 6, dekameter-scale asymmetrical, recumbent folds occur in a 3 m-thick, horizontally bedded, tuffaceous siltstone unit (Fig 4C and 4D), stratigraphically correlative to the deformed horizon (the megablock complex) at Songwe. The folds are overlain and underlain by undeformed, horizontally bedded, volcaniclastic siltstone units of the same

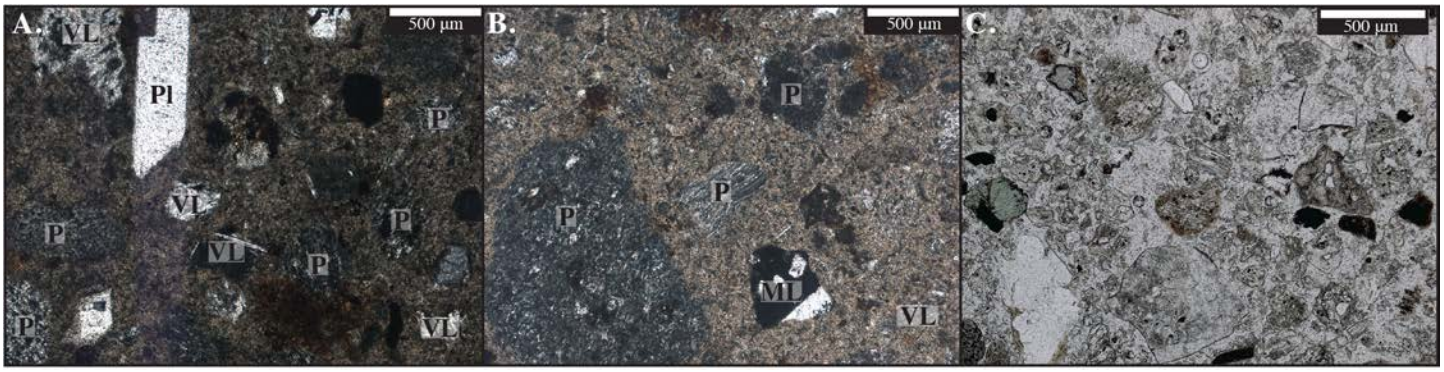

Fig 5. Thin section images from megablock complex samples. (A and B) Thin section of the clastic injection dyke in plane polarized light (PPL), containing abundant pumice and ~90% glassy fragments. (C) Thin section of grain mount of injectite material in PPL. The injectite material is composed primarily of volcanic glass, but also contains few dense mineral grains, including zircon and chlorite. "VL" = volcanic lithic; "ML" = metamorphic lithic; "P" = pumice; "Pl" = plagioclase.

doi:10.1371/journal.pone.0129051.g005

lithology. The asymmetric, recumbent fold crests are systematically directed to the southwest. The deformed horizon is truncated by the overlying siltstone, cutting off the tops of the folds.

Interpretation of Large-Scale Soft-Sediment Deformation Features

Megablock Complex. The Lake Beds Succession at the Songwe Megablock Site is characterized by older fluvial-dominated facies and younger lacustrine facies, separated by an erosional unconformity. Prior to the deposition of the lacustrine facies preserved on the north end of the outcrop, a portion of the fluvial units was deeply incised by erosional downcutting. Fluvial incision created a topographical depression, into which lacustrine sedimentation (fine-grained, siltstone dominated facies) records the presence of a network of small, isolated, shallow wetland ponds and lakes. This major decrease in grain size, coupled with a dramatic increase in volcaniclastic sediments (Fig 5) in the lacustrine facies suggests that these units (in which the megablock complex is hosted) were deposited relatively rapidly, preserving reedy plant macrofossils and are associated with a period of intense volcanism and base level rise.

The megablock complex lies on top of the undisturbed, basal Lake Beds Succession conglomerate. This soft-sediment deformation complex displays a unique combination of seismogenically-remobilized sediment coupled with brittle deformation features. It is comprised of (1) an injected body of fluidized volcanic ash that hydraulically displaced (2) an equally sized, semi-consolidated block of intact strata (megablock); both of which were subsequently intruded by (3) a clastic injection dyke (Figs 2 and 3). The buttress unconformity between the basal conglomerate and sealing siltstone above (unit from which megablock was derived) likely served as an initial conduit for lateral flow of fluidized sediment. The parent unit is not found intact or in its original stratigraphic position anywhere along the exposed cliff face. The injected material is lithologically similar to the megablock unit, so we invoke horizontal flow from a laterally correlative unit as a source for the injected parent ash/water slurry (sensu [4, 22]). The ash-dominated parent material was remobilized when pore fluid pressure rose above the hydrostatic pressure gradient [11]. When pore fluid pressure also rose above the fracture pressure gradient of the sealing siltstone unit, the confining layer was hydrofractured into an enormous megablock, along with smaller blocks, of intact strata, bound by reverse "blowout" faults [23] (Fig 2B). Once fluidized, the parent material appears to have been remobilized and driven laterally to the site of the megablock complex by overpressure, where it then hydrofractured, intruded, and hydraulically lifted the overlying volcaniclastic siltstone, similar to the

popping of a champagne cork. The megablock and smaller blocks of consolidated, undeformed siltstone were transported upward as the fluidized parent material from below was forced upwards into zones of weakness, flowing around the cohesive megablock(s) towards the paleosurface (Fig 3B).

We interpret strong ground shaking due to seismicity as the source of pore fluid overpressuring, leading to liquefaction and fluidization of the tuffaceous sediment, as discussed in detail below. Cyclic stresses (i.e. seismicity) and/or aftershocks [24] allowed for the overprinting of a brittle structure (clastic injection dyke) on ductile structures (fluidized parent unit and associated megablock), as the sediment was re-deformed after regaining strength following initial fluidization. The clastic injection dyke was formed after the uplift of the megablock complex, as evidenced by its superposition on both the injectite and megablock. Brittle fracturing of the dyke demonstrate that its emplacement was soon after the megablock uplift event, before the fluidized parent material fully dewatered, when post-seismic settling ultimately compacted the injection dyke and led to its deformation. We interpret the upper "V-shaped" portion of the clastic injection dyke as a blowout cone (sensu [25, 26]), representing the top of the dyke where it intersected with the paleosurface. Metamorphic cobbles and 5–25 cm clasts of the megablock unit infill the blowout cone, presumably after injected material was extruded onto the paleosurface [27], and material fell into the cone opening from above.

This megablock complex is significant because it is one of the few continental, outcrop examples of very large-scale soft-sediment deformation associated with injectite features [22, 27, 28], in comparison to the significant subsurface submarine record of sandstone injectite complexes. The megablock complex also stands out because it occurs in rather homogenous, tuffaceous sandstone, compared to the more common scenario of sandstone injectites in mudstone hosts [29–31]. Similarly, the hydraulic *lifting* of the megablock by fluidized injected volcanic ash, defies traditional concepts of downward displaced blocks of coherent sediment, usually due to collapse from overloading, liquefaction, and density inversions. This unique seismite formation illustrates the powerful effects of overpressured systems and active seismicity in this region on near-surface sediments. Consequently, this deformation indicates significant surface stability hazards associated with seismicity in the region, and other parts of the East African Rift System.

Asymmetric Recumbent Folds. The large-scale asymmetric, recumbent folds at Ilasilo 6 record hydroplastic soft-sediment deformation in a quiet, shallow lake or pond. The orientation of the folds suggests a very low slope (0.5°-2°) at the time of deformation. The folded horizon is truncated, indicating that the deformed unit was at the sediment/water interface at the time of deformation.

Discussion

Identification of a seismic triggering mechanism

Seismites are horizons of secondary sedimentary structures generated close to the surface by earthquakes of great enough magnitude ($M \geq 5 \pm 0.5$) [20, 32–36] to sufficiently increase intergranular pore pressure and cause liquefaction and/or fluidization of the affected sediment [18]. There are no unequivocal criteria for identifying seismogenic soft-sediment deformation structures, as morphological expression varies widely and is dependent on lithology and depositional history, no two of which are ever the same. However, many authors refer to sets of criteria proposed by Sims [37], Obermeier [38, 39], and summarized by many others, to link deformation structures with seismic events. These criteria generally include: 1) association with seismically active faults; 2) liquefiable sediments; 3) similarity to structures formed experimentally or by recent earthquakes; 4) horizons of deformation that are correlative over large areas; 5)

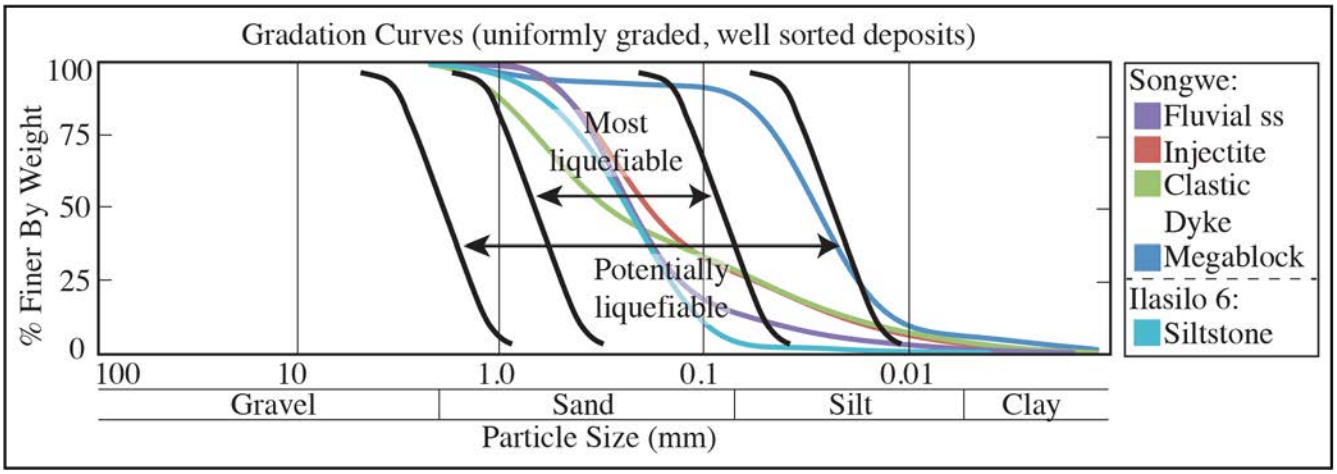

Fig 6. Gradation curves modeling the susceptibility of sediment from the Rukwa Rift Basin to liquefaction [44]. The sealing unit of the megablock complex is represented by the sample labeled "Megablock". Note that this lithology is the least liquefiable, in comparison to the fluidized parent unit ("injectite") and clastic dyke material, which plot within the "most liquefiable" zone. Sediment size and dispersion was measured on the Mastersizer 2000 via laser diffraction. The "fluvial ss" sample is located on Fig 2D. This unit represents the fluvial facies incised into by the buttress unconformity and against which the lacustrine siltstones of the megablock complex were deposited.

doi:10.1371/journal.pone.0129051.g006

deformed zones surrounded by undeformed strata; 6) deformation that increases in intensity towards the inferred epicenter; and 7) the exclusion of other triggering mechanisms [37, 39, 40].

However, the above conditions are not diagnostic, and often these criteria can also fulfill the requirements for triggers other than seismicity. In contrast, some workers advocate a context-based approach [41–43] to identify a trigger mechanism as either autogenic or allogenic, based on sedimentological and paleoenvironmental setting. In light of the problematic methodology for identifying a trigger mechanism for soft-sediment deformation, we use a combination of published criteria and depositional environment- and deformation style-based evidence to infer a seismic trigger for the large-scale megablock complex and asymmetric, recumbent folds at Ilasilo 6.

The following field-based evidence is used to meet the above criteria and to diagnose a seismic trigger for the soft-sediment deformation in the Lake Beds Succession in the southern Rukwa Rift Basin:

1. Deposition of the volcaniclastic, Late Pleistocene-Recent Lake Beds Succession occurred simultaneously with active volcanism and active faulting in the southern Rukwa Rift (Fig 1). Refer to "Implications" section below for details.
2. Grain size analysis suggests the deformed sediment is highly susceptible to liquefaction (Fig 6). The upper surface of the folded horizon at Ilasilo 6 resembles an erosional surface, an indication of liquefaction at the sediment/water interface (Fig 4C and 4D) [43]. Additionally, clastic dykes and the injectite of the megablock complex show evidence of water-escape.
3. Large-scale deformation features are correlated via radiocarbon dates over 35+ km (Figs 7 and 8).
4. Folds at Ilasilo 6 are overlain and underlain by undeformed, horizontally bedded siltstones. The megablock complex is positioned within undisturbed, horizontal bedding and preserves intact, correlative stratigraphy on either side (Figs 2, 3 and 4).

A. Sample	Conventional Radiocarbon Age	13C/12C	Calibrated Age, years BP (2σ)	
Organic sediment 710142GAL6	23,530 +/- 90 BP	-17.1 o/oo	27,650 ± 105	This study
Organic sediment 6/23/12-6	23,650 +/- 100 BP	-15.1 o/oo	27,750 ± 110	This study
Coelatura cf. *ujujiensis* Songwe section	18,360 +/- 60 BP	Indet.	22,010 ± 320	Cohen et al. (2013)
Bivalve shell S. of Galula	9,740 +/- 140 BP	-2.45 o/oo	11,070 ± 200	Cohen et al. (2013)
Bivalve shell 8 km S. of Galula	8,060 +/- 120 BP	-1.36 o/oo	8,950 ± 190	Cohen et al. (2013)
Bivalve shell S. of Galula	8,030 +/- 30 BP	Indet.	8,910 ± 90	Cohen et al. (2013)
Lavigeria sp. shell Galula Station	6,340 +/- 50 BP	-1.8 o/oo	7,270 ± 60	Cohen et al. (2013)

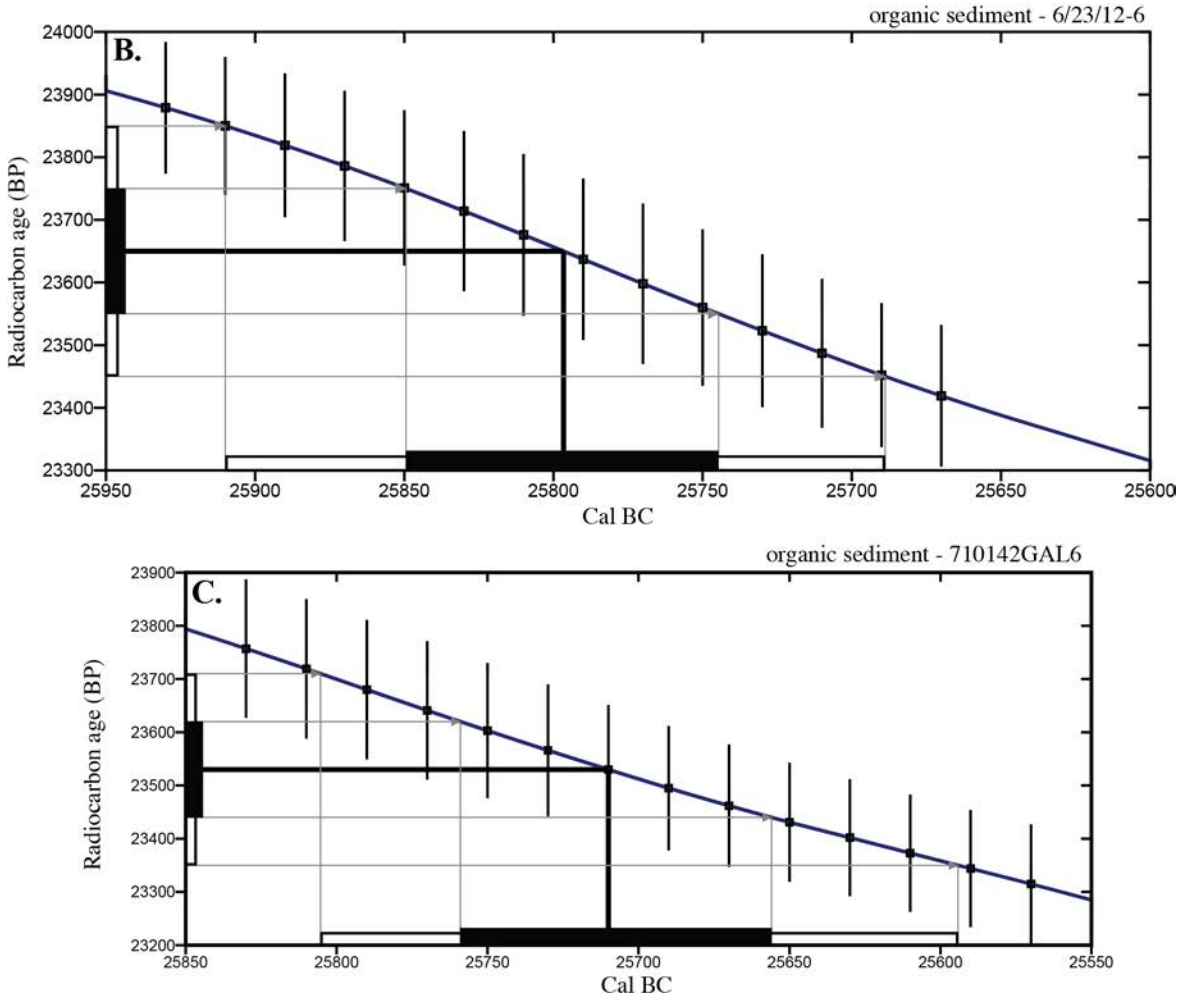

Fig 7. AMS radiocarbon dates from the Songwe Valley region. (A) Dates from the Ilasilo 6 seismite, Songwe Megablock site, and samples from Cohen et al. [45] sourced near Ilasilo 6. (B and C) The intersection of the megablock unit sample (see Fig 3) and Ilasilo 6 seismite sample radiocarbon dates (see Fig 4), respectively, with the calibration curve [17].

doi:10.1371/journal.pone.0129051.g007

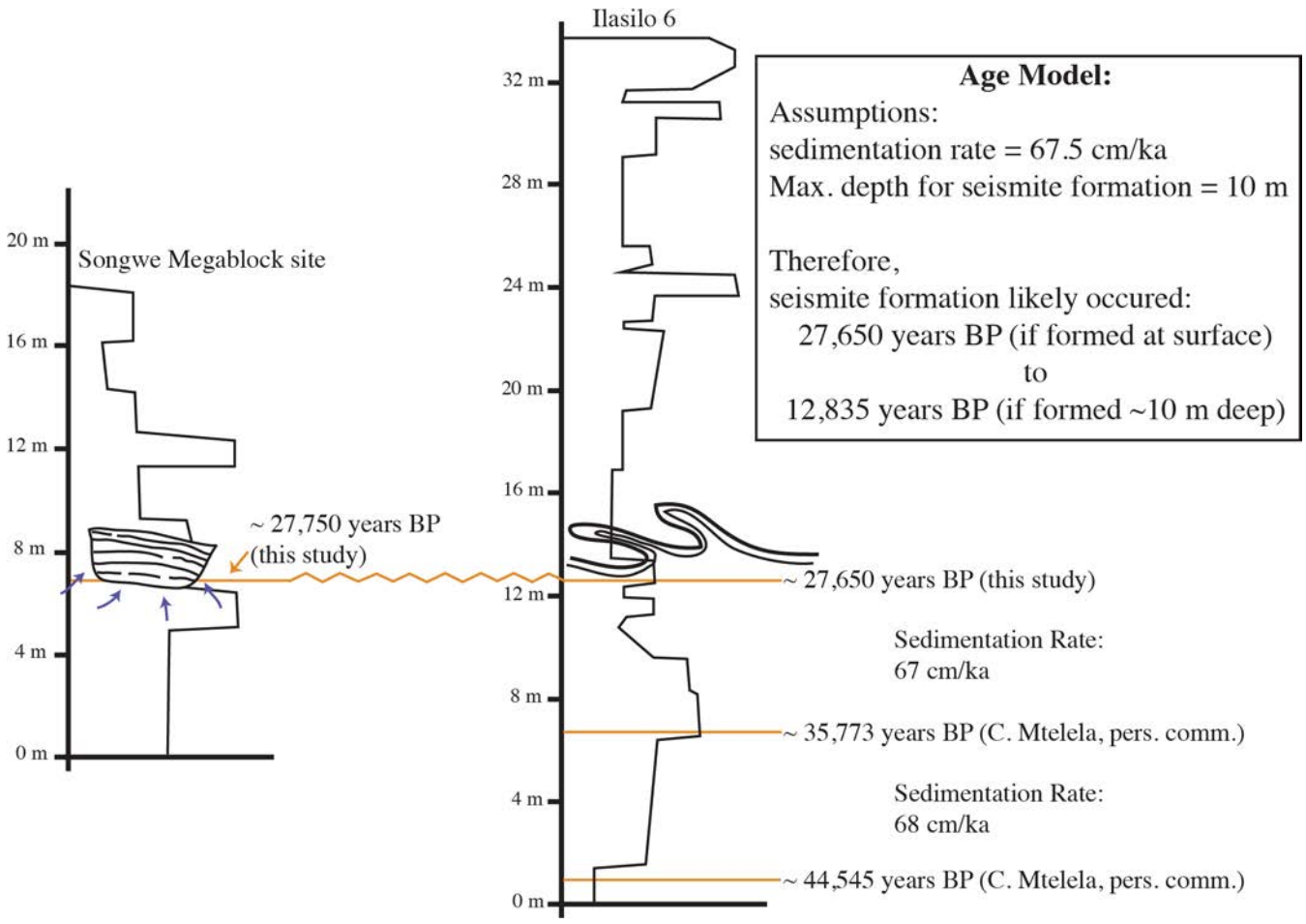

Fig 8. Correlation of Ilasilo 6 and the Songwe Megablock sites, with model approximating age of deformation. The Songwe Megablock Site radiocarbon sample is from an organic-rich layer containing macrofossil reeds of the unit that was fractured and uplifted, forming the megablock (UTM: 522904 E 9015130 N, zone 36, ARC 1960 datum). The Ilasilo 6 radiocarbon sample is from a black, fossiliferous, organic-rich unit ~1.5 meters below the large-scale seismite (UTM: 502917 E 9044472 N, zone 36, ARC 1960 datum). These two indistinguishable radiocarbon dates provide a tie point for the correlation of the two deformed outcrops over 35 km, and support the hypothesis for synchronous deformation of the megablock complex and asymmetric, recumbent folds.

doi:10.1371/journal.pone.0129051.g008

5. Soft-sediment deformation horizons are not only a common and repeated occurrence in the Lake Beds strata, but have also been abundantly recognized in Permian–Paleogene strata of the Rukwa Rift Basin. For example, stratigraphic sections at Ilasilo 6 and elsewhere in the Rukwa Rift Basin record diverse forms of soft-sediment deformation, including: flame structures; cm- to m-scale folded beds; ball-and-pillow structures; syn-sedimentary faults; sand injection features; and m-dkm-scale clastic injection dykes (Fig 9). Clastic injection dykes are most common (n >15), occurring at many localities, where they vary in length from <30 cm to >10 m, and from a few mm to >25 cm in width. Many initiate in sand beds, cut confining horizons of distinct sandstone, mudstone, or siltstone lithologies, and contain cm-scale angular fragments of the side wall rock.

The circumstantial evidence presented above strongly suggests a seismic triggering mechanism for the large-scale soft-sediment deformation in the southern Rukwa Rift Basin. However, because seismite criteria can be ambiguous, we also consider other likely triggering

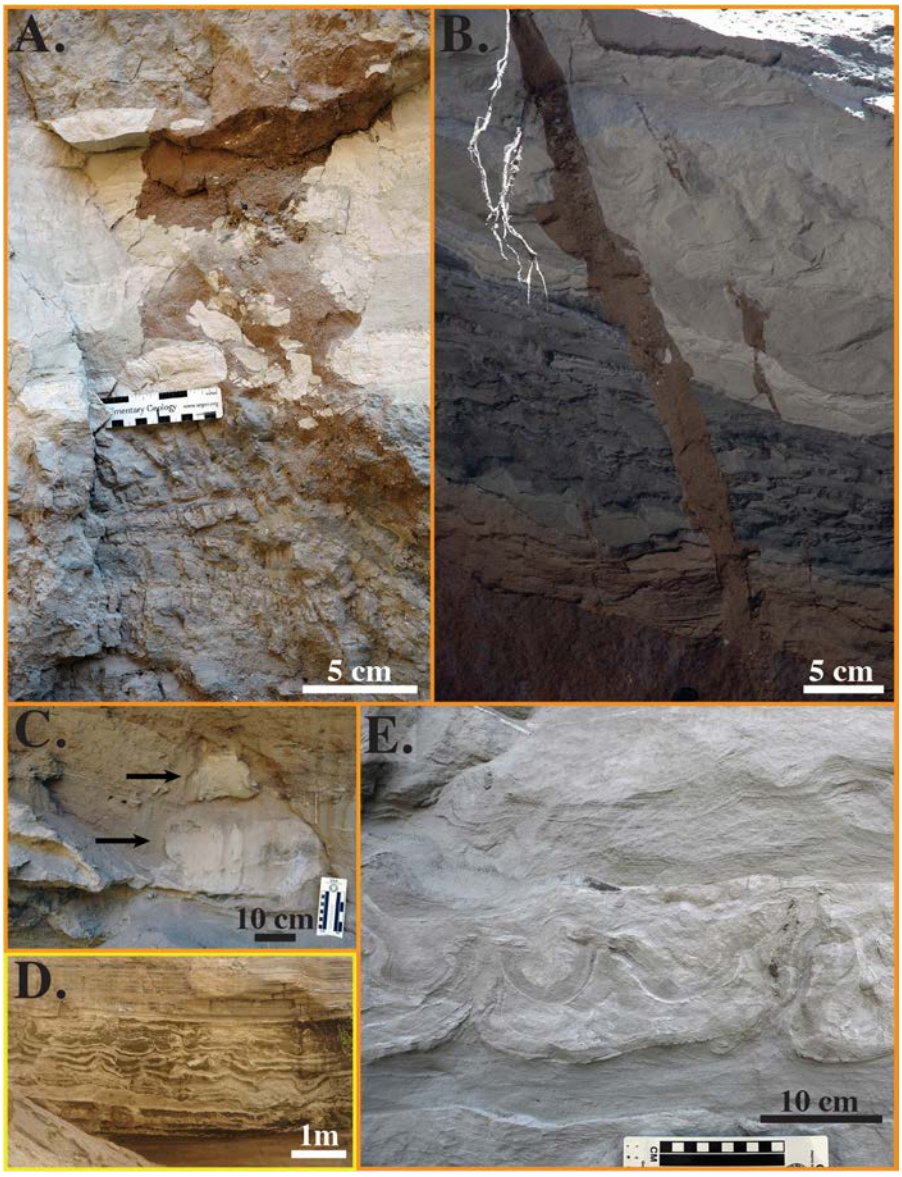

Fig 9. Seismites from the Lake Beds Succession at Ilasilo 6. (A and B) Clastic injection dykes. Vertical movement of clasts of the sidewall rock and sandstone parent bodies present below the field of view of the photographs indicate upward-directed injection. Bottom scale in (A) is in cm. (C) Ball-and-pillow structure. (D) Cm-scale convolute bedding. (E) Convolute bedding, folds, flame structures, and evidence of vertical fluid escape. Refer to Fig 4 for color-coding. Soft sediment deformation features were photographed on vertical, southwest- (A and B), northeast- (C and D), and southeast-facing (E) canyon walls of LBS strata, exposed by down cutting of modern-day rivers.

doi:10.1371/journal.pone.0129051.g009

mechanisms. Sediment loading can be ruled out because of the homogeneity of tuffaceous, silt-sized lithology that dominates the outcrops at both localities, eliminating overloading and inverse density gradients as triggers. Additionally, truncation of the folds at the top of the deformed unit at Ilasilo 6 indicates formation near the sediment/water interface [46]. Likewise, the megablock complex is positioned to within ~10 m of the paleosurface. At the Songwe site, the intrusion of massive sediment from an underlying or stratigraphically equivalent parent body demonstrates horizontal and vertical injection as the driving mechanism. At both

localities we interpret the facies to represent a flat lying lake floor unit. Vertical displacement of the megablock and block-bounding faults displaying reverse orientation also rule out a trigger originating from the sedimentary depositional environment itself. At Ilasilo 6, the directional element within the folding suggests the aid of a downslope force. Assuming paleo-slope was similar to the present day maximum lake floor slopes (0.5°-2°), and considering fold asymmetry, these seismogenic slump folds were likely gravity-driven, related to slope failure, and seismicity is again the favored mechanism to have reduced sediment shear strength to allow for such hydroplastic deformation [47–49]. Radiocarbon age correlation with the seismogenic Songwe megablock complex supports this interpretation. Storm waves are also discarded as a trigger mechanism because the finely laminated, horizontally bedded siltstone strata reflects relatively still-water conditions, and there is no evidence of tempestites, storm currents, or gravity-driven density currents. It is possible that other processes that produce high fluid pressures were present, and enhanced by seismicity. For example, abundant hydrothermal vents exist throughout the Songwe Valley and may have intensified overpressure, increasing the risk for seismically triggered liquefaction in the Rukwa Rift Basin. In summary, the large-scale dimensions; highly liquefiable, low energy, tuffaceous, lacustrine lithologies (Figs 2, 3 and 6); stratigraphic recurrence; regional extent; deformation morphology; in combination with proximity to active faults; and fulfillment of established seismite criteria, suggests deformation triggered by strong seismic shocks for the features described in this paper.

Large-scale (hundreds of meters to hundreds of kilometers) clastic injectite networks, extrudite deposits, load casts, and slumps have been previously identified, and their generation has been attributed to thermal destabilization [50], fluid overpressure due to rapid sedimentation [51], catastrophic triggering mechanism such as seismicity, subaqueous landslides, and bolide impacts [52, 53], lateral pressure transfer [53], etc., although the triggering mechanisms are not well understood [53]. The megablock complex we describe here is similar to these previously reported deformation structures only in scale, but differs in that it is the first seismically generated injectite complex that features uplifted megablocks of intact sediment, in non-marine strata, which represents a process and variety of seismite not previously recognized. This spectacular, large-scale deformation feature suggests intense, Late Pleistocene to Recent seismic shaking in the Rukwa region.

Implications: Large magnitude earthquake risk

Age Estimate for Deformation

The Songwe megablock complex and recumbent folds at Ilasilo 6 likely occur along the same stratigraphic surface, as indicated by two radiocarbon dates (Figs 7 and 8), signifying synchronous deformation. An age model (Fig 8) suggests that deformation and related seismicity occurred in the Late Pleistocene, between ~ 27,650 ± 105 and 12,835 ± ~100 years ago (based on sedimentation rates calculated from radiocarbon ages from a stratigraphic section at Ilasilo 6; Fig 8). The upper truncation of folds at Ilasilo 6 and the surface breach of the clastic dyke at Songwe imply that the deformed horizon was at or near the paleosurface at the time of liquefaction and fluidization, suggesting a significant seismic event closer to ~27,650 years ago. There is documented crustal seismicity at this time, demonstrated by fault scarps, faceted spurs, tilted Quaternary deposits, volcanism, and recorded seismicity [9], as well as by activity of Late Quaternary normal faults in the center of the basin and at the southwestern rift flank [6, 54].

Earthquake Magnitude Estimate

We suggest that earthquakes of $M \geq 6$ were responsible for the soft-sediment deformation features we report here, based on minimum magnitude capable of liquefaction, and circumstantial

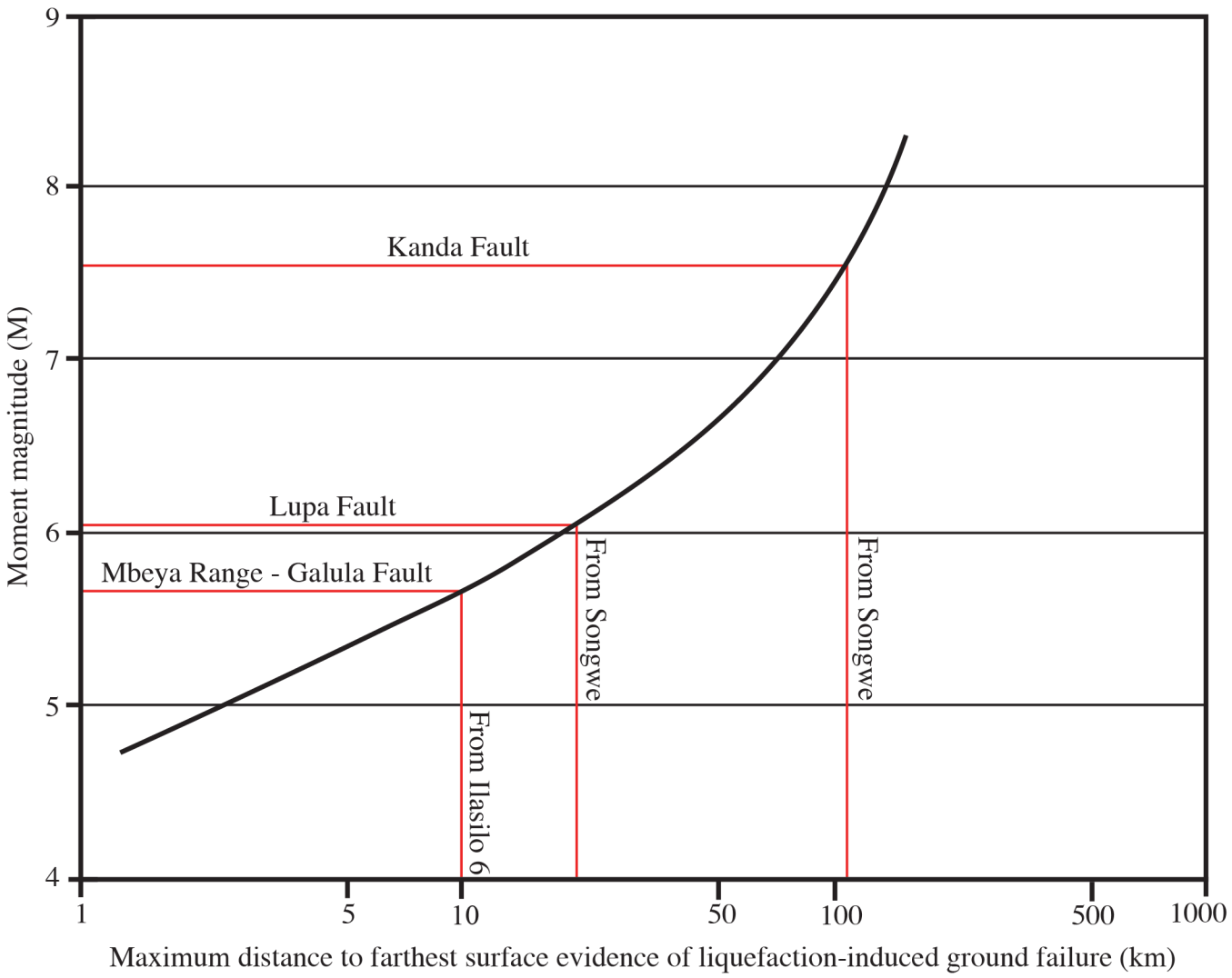

Fig 10. Paleo-earthquake magnitude estimates using the magnitude-bound method. Estimates of minimum paleo-earthquake magnitudes necessary for the formation of liquefaction features at either Ilasilo 6 or the Songwe Megablock Site using the magnitude-bound method of Ambraseys [20]. Distance to farthest evidence of liquefaction was estimated using the distance from either Ilasilo 6 or the Songwe Megablock site to each suspect fault (site furthest away was chosen). Note that this is a minimum estimate of furthest surficial liquefaction features.

doi:10.1371/journal.pone.0129051.g010

evidence, as discussed below. However, relating seismites to earthquake magnitude is equivocal, due to complexities including distance from the causal fault, attenuation of ground motion, and sediment susceptibility to liquefaction, which could not be quantitatively measured here. Many studies [20, 32–36] have reported M 5 ± 0.5 as the lower limit of earthquake energy capable of triggering liquefaction. Empirical relationships have been established between earthquake magnitude and the farthest distance of observed liquefaction [20, 21, 36], and these curves also support this estimate of minimum magnitude. Seismicity responsible for the Lake Beds Succession seismites could have originated at the Kanda Fault (also the proposed source of the 1910 Rukwa earthquake), as nearby LBS deposits record related, Pleistocene–Holocene faulting [55]. One technique for interpreting the strength of paleo-earthquakes, the magnitude-bound method [20], estimates a minimum M ~7.5 earthquake for seismites in the Songwe Valley, if sourced from the Kanda Fault (Fig 10). A second possible seismic source, the active

Mbeya Range-Galula Fault, lies just 10–15 km E/NE of the Songwe Megablock Site. This fault system continues beneath Lake Rukwa, where a series of steeply dipping faults are typically syndepositional with the youngest lake sediments. The longest segment of the Mbeya Range-Galula Fault, measuring ~23 km, could be capable of producing an earthquake of M = 6.7–7, as estimated by regression relations of moment magnitude on surface rupture length [56, 57]. A third likely candidate, the Lupa boundary fault, is continuous over 200 km, and has been significantly active, causing major basin forming events (and earthquakes) on intervals of thousands of years [58]. If we assume deformation does not extend pass the Songwe Megablock Site, the magnitude-bound method estimates a minimum earthquake M6 produced by the Lupa Fault for soft-sediment deformation ~20 km away from the source [20] (Fig 10).

Rodríguez-Pascua et al. [4] qualitatively related particular seismite morphologies to earthquake magnitudes. Clastic injection dykes in lacustrine and fluvial deposits were interpreted to form from earthquakes ranging from $5 \leq M \geq 8$ [4]. Cobbles (4–20 cm diameter) from the basal Lake Beds Succession conglomerate contained within the lower meter of the injectite and within the clastic dyke required high injection velocities [4, 22], and this displacement is additional evidence for larger magnitude earthquakes (possibly up to M8 by estimates of Rodríguez-Pascua et al.) [4]. However, we interpret these relationships with caution, as soft-sediment response to seismicity is not only dependent on magnitude, but is also related to ground acceleration, proximity to the source, and other local factors. Minimally, we estimate that the paleo-earthquake magnitude was $M > 5 \pm 0.5$, the minimum energy for triggering liquefaction. However, taking the size of the uplifted megablock and of the Ilasilo 6 folds, their morphologies, and the transport of large cobbles as proxy evidence, we suggest triggering by a higher-magnitude event at that time, especially when compared to the smaller-scale convoluted laminations, clastic dykes, and other seismites we report from underlying and overlying horizons (Fig 9). We estimate a minimum earthquake of M ~6+, taking the most conservative magnitude estimate calculated using the magnitude bound method (from the Lupa Fault). Since 1900, at least 20 earthquakes of $M \geq 5$ have been documented in the Songwe Valley region [1, 12, 13] (Fig 1). The sedimentary evidence for recurring, similarly intense palaeoseismic events presented herein emphasizes the potential for damaging surface deformation in the region, and identifies a significant seismic hazard in southwest Tanzania, and indeed throughout the East African Rift System.

Conclusions

Outcrop exposure of exceptional, large-scale soft-sediment deformation, including the uplift of a bus-sized megablock by fluidized, injected material; fluidization of large cobbles at Songwe; formation of giant, recumbent folds at Ilasilo 6; and numerous smaller scale clastic dykes and seismites, occur over at least 35 km in the RRB. These unique features suggest potential for dangerous surface deformation related to the seismically active East African Rift System. Our documentation provides evidence for M ~6+ Late Pleistocene earthquakes, similar to the M7.4 earthquake at the same location in 1910, extending the record of large-magnitude earthquakes beyond the last century, and contributing valuable data to better constrain recurrence intervals of high magnitude earthquakes in the Western Branch of the East African Rift. Our discovery is consistent with high-resolution seismic reflection data from Lake Rukwa, which provided evidence for high-frequency changes in boundary fault activity that occurs with a periodicity of thousands to tens-of-thousands of years [58]. Documenting new seismite morphologies, such as the one presented here, is essential for understanding surface dynamics and assessing seismic hazards and risks, particularly in rift settings where seismite records remain poorly studied. The nature of the Late Pleistocene to Recent deposits of the Lake Beds strata in the Rukwa

Rift Basin, typified by repeated transitions between coarse-grained alluvial/fluvial strata and fine-grained volcanic ash-rich lacustrine strata, provide perfect conditions for land surface deformation and serious hazards associated with seismic shaking, as exemplified by the unique, highly disruptive nature of the megablock complex. With population centers such as Mbeya, Tukuyu, Sumbawanga, and Mpanda all within tens of kilometers from the Songwe Megablock Site or the 1910 M7.4 earthquake epicenter, documenting and predicting the near-surface sediment behavior under seismic stress is critical information for the understanding and modeling of earthquake hazards in rift settings in East Africa.

Acknowledgments

We acknowledge C. Mtelela, N. Boniface, P. O'Connor, N. Stevens, M. Hendrix, and B. Downey for field assistance. C. DuRoss, M. Chan, A. Hurst, A. Moore, F. Cotterill, and others provided useful feedback on earlier versions of this paper. We thank the Tanzanian Commission for Science and Technology, the Tanzanian Antiquities Unit, and Heritage Oil Rukwa Tanzania Ltd. for logistical support.

Author Contributions

Conceived and designed the experiments: HLHW EMR. Performed the experiments: HLHW EMR. Analyzed the data: HLHW EMR. Contributed reagents/materials/analysis tools: HLHW EMR. Wrote the paper: HLHW EMR.

References

1. Ambraseys NN, Adams RD. Reappraisal of major African earthquakes, south of 20°N, 1900–1930. Natural Hazards. 1991; 4: 389–419.
2. Ambraseys NN. The Rukwa earthquake of 13 December 1910 in East Africa. Terra Nova. 1991; 3: 203–208.
3. Haub C, Kaneda T. World Population Data Sheet 2012. Population Reference Bureau. 2012.
4. Rodríguez-Pascua MA, Calvo JP, De Vicente G, Gómez-Gras D. Soft-sediment deformation structures interpreted as seismites in lacustrine sediments of the Prebetic Zone, SE Spain, and their potential use as indicators of earthquake magnitudes during the Late Miocene. Sedimentary Geology. 2000; 135: 117–135.
5. Obermeier SF. Use of liquefaction induced features for paleoseismic analysis. Engineering Geology. 1996; 44, 1–76.
6. Delvaux D, Kervyn F, Macheyeki AS, Temu EB. Geodynamic significance of the TRM segment in the East African Rift (W-Tanzania): Active tectonics and paleostress in the Ufipa plateau. Journal of Structural Geology. 2012; 37: 161–180.
7. Roberts EM, Stevens NJ, O'Connor PM, Dirks PHGM, Gottfried MD, Clyde WC, et al. Initiation of the western branch of the East African Rift coeval with the eastern branch. Nature Geoscience. 2012; 5: 289–294.
8. Camelbeeck T, Iranga MD. Deep crustal earthquakes and active faults along the Rukwa trough, eastern Africa. Geophysical Journal International. 1996; 124: 612–630.
9. Vittori E, Delvaux D, Kervyn F. Kanda Fault: A major seismogenic element west of the Rukwa Rift (Tanzania, East Africa). Journal of Geodynamics. 1997; 24 no. 1–4: 139–153.
10. Kervyn F, Ayub S, Kajara R, Kanza E, Temu B. Evidence of recent faulting in the Rukwa rift (West Tanzania) based on radar interferometric DEMs. Journal of African Earth Sciences. 2006; 44: 151–168.
11. Delvaux DF, Hanon M. Neotectonics of the Mbeya area, SW Tanzania. Royal Museum for Central Africa Annual Report 1991–1992. 1993: 87–97.
12. International Seismological Centre. On-line Bulletin. 2012. Available: http://www.isc.ac.uk.
13. U.S. Geological Survey. ANSS Global Earthquake Catalogue. Available: http://earthquake.usgs.gov/earthquakes/search.
14. Milga NR. Depositional environments, stratigraphy and hydrocarbon potential of the Rukwa Rift Basin–SW Tanzania. Ph.D. dissertation, Duke University. 1994; 156 p.

15. Roberts EM, O'Connor PM, Stevens NJ, Gottfried MD, Jinnah ZA, Ngasala S, et al. Sedimentology and depositional environments of the Red Sandstone Group, Rukwa Rift Basin, southwestern Tanzania: New insights into Cretaceous and Paleogene terrestrial ecosystems and tectonics in sub-equatorial Africa. Journal of African Earth Sciences. 2010; 57: 179–212.
16. Delvaux D, Kervyn F, Macheyeki AS, Temu EB. Active faulting in W-Tanzania: Coupling between tectonics, volcanism & climate? [abstract]. 23rd Colloquium of African Geology, Johannesburg, South Africa. 2011; abstract volume: 112.
17. Reimer PJ, Bard E, Bayliss A, Beck JW, Blackwell PG, Ramsey CB, et al. IntCal13 and Marine13 radiocarbon age calibration curves, 0–50,000 years cal BP. Radiocarbon. 2013; 55 no. 4: 1869–1887.
18. Lowe D. Water escape structures in coarse-grained sediments. Sedimentology. 1975; 22: 157–204.
19. Hilbert-Wolf HL, Simpson EL, Simpson WS, Tindall SE, Wizevich MC. Insights into syndepositional fault movement in a foreland basin; trends in seismites of the Upper Cretaceous, Wahweap Formation, Kaiparowits Basin, Utah, USA. Basin Research. 2009; 21: 856–871.
20. Ambraseys NN. Engineering seismology. Earthquake Engineering and Structural Dynamics. 1988; 17: 1–105.
21. Papathanassiou G, Pavlides S, Christaras B, Pitilakis K. Liquefaction case histories and empirical relations of earthquake magnitude versus distance from the broader Aegean region. Journal of Geodynamics. 2005; 40: 257–278.
22. Hurst A, Scott A, Vigorito M. Physical characteristics of sand injectites: Earth-Science Reviews. 2011; 106: 215–246. doi: 10.1093/bja/aeq296 PMID: 21037268
23. Montenat C, Barrier P, Ott d'Estevou P, Hibsch C. Seismites: An attempt at critical analysis and classification. Sedimentary Geology. 2007; 196: 5–30.
24. Quigley MC, Bastin S, Bradley BA. Recurrent liquefaction in Christchurch, New Zealand, during the Canterbury earthquake sequence. Geology. 2013; 41 no. 4: 419–422.
25. Nichols RJ, Sparks RSJ, Wilson CJN. Experimental studies of the fluidization of layered sediments and the formation of fluid escape structures. Sedimentology. 1994; 41: 233–253.
26. Loope DB, Elder JF, Zlotnik VA, Kettler RM, Pederson DT. Jurassic earthquake sequence recorded by multiple generations of sand blows, Zion National Park, Utah. Geology. 2013; 41 (10): 1131–1134.
27. Vigorito M, Hurst A, Cartwright J, Scott A. Regional-scale subsurface sand remobilization: geometry and architecture. Journal of the Geological Society. 2008; 165: 609–612.
28. Thompson BJ, Garrison RE, Moore CJ. A reservoir-scale Miocene injectite near Santa Cruz, California. In: Hurst A, Cartwright J, editors. Sand Injectites: Implications for Hydrocarbon Exploration and Production. American Association of Petroleum Geologists Memoir 87; 2007. pp. 151–162.
29. Vigorito M, Hurst A. Regional sand injectite architecture as a record of pore-pressure evolution and sand redistribution in the shallow crust: insights from the Panoche Giant Injection Complex, California. Journal of the Geological Society, London. 2010; 167: 889–904.
30. Huuse M, Cartwright J, Hurst A, Steinsland N. Seismic characterization of large-scale sandstone intrusions. In: Hurst A, Cartwright J, editors. Sand injectites: Implications for hydrocarbon exploration and production. AAPG Memoir 87; 2007. pp. 21–35.
31. Scott ASJ, Vigorito M, Hurst A. The process of sand injection: internal structures and relationships with host strata (Yellowbank Creek Injectite Complex, California, USA). Journal of Sedimentary Research. 2009; 79: 1–18.
32. Atkinson G. Simple computation of liquefaction probability for seismic hazard applications. Earthquake Spectra. 1984; 1: 107–123.
33. Allen JRL. Earthquake magnitude-frequency, epicentral distance, and soft-sediment deformation in sedimentary basins. Sedimentary Geology. 1986; 46: 67–75.
34. Audemard FA, de Santis F. Survey of liquefaction structures induced by recent moderate earthquakes. Bulletin of the International Association of Engineering Geologists. 1991; 44: 5–16.
35. Obermeier SF, Martin JR, Frankel AD, Youd TL, Munson PJ, Munson CA, et al. Liquefaction evidence for one or more strong Holocene earthquakes in the Wabash Valley of Southern Indiana and Illinois. U. S. Geological Survey Professional Paper 1536. 1993: 27 pp.
36. Galli P. New empirical relationships between magnitude and distance for liquefaction. Tectonophysics. 2000; 324: 169–187.
37. Sims JD. Determining earthquake recurrence intervals from deformational structures in young lacustrine sediments. Tectonophysics. 1975; 29: 144–152.
38. Obermeier SF. Use of liquefaction-induced features for paleoseismic analysis–An overview of how seismic liquefaction features can be distinguished from other features and how their regional

distribution and properties of source sediment can be used to infer the location and strength of Holocene paleo-earthquakes. Engineering Geology. 1996; 44 no.1-4: 1–76.

39. Obermeier SF. Using liquefaction-induced and other soft-sediment features for paleoseismic analysis. In: McCalpin JP, editor. Paleoseismology (2nd edition). Burlington, Massachusetts: Academic Press; 2009. pp. 497–564.
40. Hempton MR, Dewey JF. Earthquake-induced deformational structures in young lacustrine sediments, East Anatolian fault, southeast Turkey. Tectonophysics. 1983; 98: T7–T14.
41. Molina JM, Alfaro P, Moretti M, Soria JM. Soft-sediment deformation structures induced by cyclic stress of storm waves in tempestites (Miocene, Guadalquivir Basin, Spain). Terra Nova. 1998; 10: 145–150.
42. Jones AP, Omoto K. Towards establishing criteria for identifying trigger mechanisms for soft-sediment deformation: a case study of Late Pleistocene lacustrine sands and clays, Onikobe and Nakayamadaira Basins, northeastern Japan. Sedimentology. 2000; 47 no. 6: 1211–1226. PMID: 11130993
43. Owen G, Moretti M. Identifying triggers for liquefaction-induced soft-sediment deformation in sands. Sedimentary Geology. 2011; 235: 141–147.
44. Tsuchida H, Hayashi S. Estimation of liquefaction potential of sandy soils. In: Proceedings of the 3rd Joint Meeting US-Japan Panel on Wind and Seismic Effects, UJNR, Tokyo: 1971. pp. 91–109.
45. Cohen AS, Van Bocxlaer B, Todd JA, McGlue M, Michel E, Nkotagu HH, et al. 2013, Quaternary ostracodes and molluscs from the Rukwa Basin (Tanzania) and their evolutionary and paleobiogeographic implications. Palaeogeography, Palaeoclimatology, Palaeoecology. 2013; 392: 79–97.
46. Anketell JM, Cegla J, Dzulynski ST. Unconformable surfaces in the absence of current erosion. Geologica Romana. 1969; 8: 41–46.
47. Field ME, Gardner JV, Jennings AE, Edwards BD. Earthquake-induced sediment failures on a 0.25° slope, Klamath River delta, California. Geology. 1982; 10: 542–546.
48. Moretti M, Sabato L. Recognition of trigger mechanisms for soft-sediment deformation in the Pleistocene lacustrine deposits of the Sant'Arcangelo Basin (Southern Italy): seismic shock vs. overloading. Sedimentary Geology. 2007; 196: 31–45.
49. Alsop GI, Marco S. Seismogenic slump folds formed by gravity-driven tectonics down a negligible subaqueous slope. Tectonophysics. 2013; 605: 48–69.
50. Backeberg NR, Rowe CD. Mega-scale (~50M) Ordovician load casts at De Balie, South Africa: Possible sediment fluidization by thermal destabilization. South African Journal of Geology. 2009; 112: 187–196.
51. Løseth H, Rodrigues N, Cobbold PR. World's largest extrusive body of sand? Geology. 2012; 40 no. 5: 467–470.
52. Sherry TJ, Rowe CD, Kirkpatrick JD, Brodsky EE. Emplacement and dewatering of the world's largest exposed sand injectite complex. Geochemistry Geophysics Geosystems. 2012; 13. doi: 10.1029/2012GC004157
53. Cartwright J. Regionally extensive emplacement of sandstone intrusions: a brief review. Basin Research. 2010; 22: 502–516.
54. Skobelev SF, Hanon M, Klerkx J, Govorova NN, Lukina NV, Kazmin VG. Active faults in Africa: a review. Tectonophysics. 2004; 380: 131–137.
55. Delvaux D, Kervyn R, Vittori E, Kajara RSA, Kilembe E. Late Quaternary tectonic activity and lake level fluctuation in the Rukwa rift basin, East Africa. Journal of African Earth Sciences. 1998; 26: 397–421.
56. Wells DL, Coppersmith KJ. New empirical relationships among magnitude, rupture length, rupture width, rupture area, and surface displacement. Bulletin of the Seismological Society of America. 1994; 84 no. 4: 974–1002.
57. Stirling M, Rhoades D, Berryman K. Comparison of earthquake scaling relations derived from data of the instrumental and preinstrumental era. Bulletin of the Seismological Society of America. 2002; 92 no. 2: 812–830.
58. Morley CK, Vanhauwaert P, De Batist M. Evidence for high-frequency cyclic fault activity from high-resolution seismic reflection survey, Rukwa Rift, Tanzania. Journal of the Geological Society, London. 2000; 157: 983–994.

Appendix 2

MKED1: A new titanite standard for in situ analysis of Sm–Nd isotopes and U–Pb geochronology

Chemical Geology

C. Spandler, J. Hammerli, P. Sha, **H. Hilbert-Wolf**, Y. Hu, E. Roberts, and M. Schmitz, 2016

Chemical Geology 425 (2016) 110–126

Contents lists available at ScienceDirect

Chemical Geology

journal homepage: www.elsevier.com/locate/chemgeo

MKED1: A new titanite standard for in situ analysis of Sm–Nd isotopes and U–Pb geochronology

Carl Spandler [a,*], Johannes Hammerli [a,b], Peng Sha [a], Hannah Hilbert-Wolf [a], Yi Hu [c], Eric Roberts [a], Mark Schmitz [d]

[a] Department of Earth and Oceans, College of Science, Technology and Engineering, James Cook University, Townsville, 4811, QLD, Australia
[b] Centre for Exploration Targeting, School of Earth and Environment, University of Western Australia, 6009, WA, Australia
[c] Advanced Analytical Centre, James Cook University, Townsville, 4811, QLD, Australia
[d] Isotope Geology Laboratory, Boise State University, Boise, 83725-1535, Idaho, USA

ARTICLE INFO

Article history:
Received 22 September 2015
Received in revised form 3 January 2016
Accepted 5 January 2016
Available online 8 January 2016

Keywords:
Titanite
Sphene
Calibration standard
U–Pb dating
Sm–Nd isotopes
Trace elements

ABSTRACT

Titanite (sphene) has great potential as a petrogenetic indicator and mineral geochronometer, as it can host high concentrations of a range of trace elements and it occurs in diverse rock types. In this paper we describe a natural titanite standard material that may be used to calibrate chemical and isotopic analysis of titanite of varying age and origin. Through comprehensive bulk analysis of mm-size crystal fragments and in situ microanalysis, we show that the titanite, named MKED1, is largely free of inclusions and is homogenous at the level of analytical precision for major element, U–Pb isotope and Sm–Nd isotope composition. There is some minor zoning in trace element composition, but these zones are easily recognised using backscattered electron imaging and the trace element concentrations of each of these zones are also very homogenous. MKED1 has relatively high levels of high field strength elements (Nb, Ta, Zr, Hf, Sn), rare earth elements (REE), Th, U, and radiogenic Pb, but very low levels of common Pb. Uranium–Pb isotope data show MKED1 to be concordant with $^{206}Pb/^{207}Pb$, $^{207}Pb/^{235}U$, and $^{206}Pb/^{238}U$ ages (ID-TIMS) of 1521.02 ± 0.55 Ma, 1518.87 ± 0.31 Ma, and 1517.32 ± 0.32 Ma, respectively. Cross calibration with other titanite standards demonstrates that MKED1 can be used as a primary standard for determining U–Pb ages of titanite ranging in age from Precambrian to Neogene.

We show that MKED1 is also suitable as a Sm–Nd isotope reference material due to its relatively high REE concentrations and homogenous $^{147}Sm/^{144}Nd$ (0.127) and $^{143}Nd/^{144}Nd$ (0.5116303 ± 0.0000025) content. Isotopic homogeneity is demonstrated through extensive in situ microanalysis, which returned an average initial εNd value of −6.30 ± 0.65 that is comparable to the value obtained by TIMS of −6.13 ± 0.05.

We suggest that MKED1 can be employed as a U–Pb isotope and Sm–Nd isotope reference material for in situ or bulk analytical methods, including techniques that allow simultaneous collection of multiple elemental and/or isotopic data sets in situ. MKED1 may also be used as a standard for in situ trace element microanalysis on the provision that locations for analytical sampling are selected with consideration to grain-scale elemental zoning. To demonstrate the potential value of titanite analysis for resolving geological problems we present case studies from two very different geological settings; the first examines the timing and origin of Cu–Au-REE skarn mineralisation from the Mount Isa Inlier, Australia, and the second study investigates the timing and origin of rift related volcanism and sedimentation in the western branch of the East African Rift System.

Content has been removed
due to copyright restrictions

Content has been removed
due to copyright restrictions

Content has been removed
due to copyright restrictions

Content has been removed
due to copyright restrictions

Content has been removed
due to copyright restrictions

Content has been removed
due to copyright restrictions

Content has been removed
due to copyright restrictions

Content has been removed
due to copyright restrictions

Content has been removed
due to copyright restrictions

Content has been removed
due to copyright restrictions

Content has been removed
due to copyright restrictions

Content has been removed
due to copyright restrictions

Content has been removed
due to copyright restrictions

Content has been removed
due to copyright restrictions

Appendix 3

New sedimentary structures in seismites from SW Tanzania: Evaluating gas- vs. water-escape mechanisms of soft-sediment deformation

Sedimentary Geology

H. L. Hilbert-Wolf, E. M. Roberts, and E. L. Simpson, 2016

Sedimentary Geology xxx (2016) xxx–xxx

Contents lists available at ScienceDirect

Sedimentary Geology

journal homepage: www.elsevier.com/locate/sedgeo

New sedimentary structures in seismites from SW Tanzania: Evaluating gas- vs. water-escape mechanisms of soft-sediment deformation

Hannah L. Hilbert-Wolf [a,*], Eric M. Roberts [a], Edward L. Simpson [b]

[a] Department of Earth and Oceans, James Cook University, Townsville, QLD 4811, Australia
[b] Department of Physical Sciences, Kutztown University, Kutztown, PA, 19530, USA

ARTICLE INFO

Article history:
Received 9 September 2015
Received in revised form 21 February 2016
Accepted 15 March 2016
Available online xxxx

Keywords:
Seismites
Gas-escape
Water-escape
Soft-sediment deformation
Paleoseismology
Rukwa Rift Basin

ABSTRACT

Seismite horizons are abundant in Cretaceous sandstones of the Rukwa Rift Basin, southwestern Tanzania. Diverse morphologies of soft-sediment deformation are preserved, including two new, unusual sedimentary structures, herein referred to as 1) balloon-shaped inflation structures and 2) surface fractures with linked sandstone splays. This original description of new sedimentary structures contributes to the growing catalogue of seismically induced deformation features. Their unusual morphologies bring to the forefront an important, though seldom touched upon, question of how to differentiate between gas- and water-escape in soft-sediment deformation features. The recognition of the spectrum of soft-sediment deformation structures contained in strata and their deformational mechanisms is important because it permits the differentiation between triggering mechanisms, particularly seismic activity, and can constrain such events spatially and temporally. We interpret the surface fractures and linked sandstone splays to reflect a high gas effusion rate, formed by the release of high-pressure gas followed by a limited expulsion of water. The balloon-shaped inflation structures reflect lower gas effusion rates due to expulsion of lower pressure gas that did not breach the Cretaceous surface seal. When these gas pulses did breach the paleosurface, they formed gas-discharge pits. These seismogenic structures are consistent with deposition of Cretaceous strata in the Rukwa Rift during periods of active carbonatite volcanism, seismicity, and possibly hot spring activity. This documentation serves as an important data point for the re-examination of the classification scheme of soft-sediment deformation structures as primarily water-escape structures to accommodate for the genesis of some secondary sedimentary features by gas-escape.

Content has been removed
due to copyright restrictions

Content has been removed
due to copyright restrictions

Content has been removed
due to copyright restrictions

Content has been removed
due to copyright restrictions

Content has been removed
due to copyright restrictions

Content has been removed
due to copyright restrictions

Content has been removed
due to copyright restrictions

Appendix 4

Oligocene termite nests with *in situ* fungus gardens from the Rukwa Rift Basin, Tanzania, support a Paleogene African origin for insect agriculture

PLoS ONE

E. M. Roberts, C. N. Todd, D. K. Aanen, T. Nobre, **H. L. Hilbert-Wolf**, P. M. O'Connor, L. Tapanila, C. Mtelela, and N. J. Stevens, 2016

PLOS ONE

RESEARCH ARTICLE

Oligocene Termite Nests with *In Situ* Fungus Gardens from the Rukwa Rift Basin, Tanzania, Support a Paleogene African Origin for Insect Agriculture

Eric M. Roberts[1]*, Christopher N. Todd[1], Duur K. Aanen[2], Tânia Nobre[3], Hannah L. Hilbert-Wolf[1], Patrick M. O'Connor[4,5], Leif Tapanila[6], Cassy Mtelela[1,7], Nancy J. Stevens[4,5]

1 Department of Earth and Oceans, James Cook University, Townsville, Queensland, 4811 Australia, **2** Laboratory of Genetics, Wageningen University, Droevendaalsesteeg 1, Radix West, Building 107, 6708 PB, Wageningen, The Netherlands, **3** Institute of Mediterranean Agricultural and Environmental Sciences (ICAAM), Universidade de Évora, Núcleo da Mitra, Ap. 94, 7002–554, Évora, Portugal, **4** Department of Biomedical Sciences, Heritage College of Osteopathic Medicine, Ohio University, Athens, Ohio, 45701, United States of America, **5** Center for Ecology and Evolutionary Studies, Ohio University, Athens, Ohio, 45701, United States of America, **6** Department of Geosciences and Idaho Museum of Natural History, Idaho State University, Pocatello, Idaho, 83209, United States of America, **7** Department of Geology, University of Dar es Salaam, P.O. Box 35052, Dar es Salaam, Tanzania

* eric.roberts@jcu.edu.au

OPEN ACCESS

Citation: Roberts EM, Todd CN, Aanen DK, Nobre T, Hilbert-Wolf HL, O'Connor PM, et al. (2016) Oligocene Termite Nests with *In Situ* Fungus Gardens from the Rukwa Rift Basin, Tanzania, Support a Paleogene African Origin for Insect Agriculture. PLoS ONE 11(6): e0156847. doi:10.1371/journal.pone.0156847

Editor: Faysal Bibi, Museum für Naturkunde, GERMANY

Received: December 10, 2015

Accepted: May 20, 2016

Published: June 22, 2016

Data Availability Statement: All relevant data are within the paper and its Supporting Information files.

Funding: This research was supported by the US National Science Foundation (NSF EAR_0617561, EAR_0854218, EAR 0933619), National Geographic Society (CRE), and funding from Ohio University and James Cook University. TN was supported by a Marie Curie fellowship (FP7-PEOPLE-2012-CIG Project Reference 321725) and by the Portuguese Foundation for Science and Technology (SFRH/BCC/52187/2013).

Abstract

Based on molecular dating, the origin of insect agriculture is hypothesized to have taken place independently in three clades of fungus-farming insects: the termites, ants or ambrosia beetles during the Paleogene (66–24 Ma). Yet, definitive fossil evidence of fungus-growing behavior has been elusive, with no unequivocal records prior to the late Miocene (7–10 Ma). Here we report fossil evidence of insect agriculture in the form of fossil fungus gardens, preserved within 25 Ma termite nests from southwestern Tanzania. Using these well-dated fossil fungus gardens, we have recalibrated molecular divergence estimates for the origins of termite agriculture to around 31 Ma, lending support to hypotheses suggesting an African Paleogene origin for termite-fungus symbiosis; perhaps coinciding with rift initiation and changes in the African landscape.

Introduction

Termites are among the most diverse and ecologically important groups of insects in modern ecosystems, playing a critical role as natural decomposers of plant tissues. Termites typically rely on gut symbionts to decompose organic matter. However, members of the subfamily Macrotermitinae have turned to agriculture by developing a highly specialized, symbiotic relationship with fungi of the genus *Termitomyces* (Basidiomycotina). The fungus-growing termites cultivate fungi in gardens/chambers inside the colony and then exploit the ability of the fungi to convert recalcitrant, nitrogen-poor, plant material into a more easily digestible,

Competing Interests: The authors have declared that no competing interests exist.

protein-rich food source [1, 2]. After ingestion and brief mastication of woody material, modern Macrotermitinae excrete rounded pellets known as primary faeces or mylospheres, composed of concentrated, undigested plant fragments and *Termitomyces* spores, which germinate and colonize the plant material, thus forming fungal gardens. The critical ecological role of fungus-growing termite colonies as biodiversity and bioproductivity hotspots within African savannah ecosystems has been well documented in recent years [3, 4]. Indeed, much of the decomposition of woody plant material in Africa and Asia takes place as a result of fungus-growing termites [5], with estimates suggesting that more than 90% of dry wood in some semiarid savannahs is reprocessed by members of the Macrotermitinae [6].

A growing body of molecular evidence suggests that termite fungiculture can be traced back to a single origin around 31 Ma (19–49 Ma), when domestication of the ancestor of *Termitomyces* by the ancestor of the Macrotermitinae occurred [2, 7–10]. Once established, this symbiotic relationship is hypothesized to have remained obligate over its entire evolutionary history, with no evidence of Macrotermitinae ever forming a relationship with any other fungi or abandoning fungus farming [2, 7–9]. Until recently, little fossil evidence has been found to document the antiquity of the termite—fungus mutualism. To date only a single unequivocal report of fossilized termite fungus combs has been described, recovered from a succession of Upper Miocene-Pliocene ($\leq$7 Ma) terrestrial deposits in the northern Chad Basin, Africa [11, 12]. Intriguingly, fossilized termite nests that appear similar to those produced by fungus-farming termites have been reported from continental deposits across Afro-Arabia ranging as far back as the early Oligocene or late Eocene [13–15]. However, diagnostic evidence demonstrating the age and presence of *in situ* fungus gardens within these fossil termite nests has not yet been clearly confirmed; and hence, the timing of this important evolutionary coupling between termites and fungus (termite fungiculture) is still uncertain.

Here we report on the discovery of a new occurrence of fossilized termite nests with *in situ* fungus gardens from southwestern Tanzania. The new fossils were discovered in a paleosol horizon in a steeply dipping section of the Oligocene Songwe Member of the Nsungwe Formation in the Rukwa Rift Basin [16–18]. The aim of this study is to investigate the paleontology and geologic context of these new trace fossils, and use our findings to recalibrate the molecular phylogeny for fungus farming termites in order to test existing hypotheses regarding the timing and origin of termite-fungus symbiosis in the fossil record.

Study Area and Fossil Locality

The trace fossil locality is located near the southern end of the Rukwa Rift Basin, a segment of the Western Branch of the East African Rift System in southwestern Tanzania [17, 18] (Fig 1). Excellent exposures of fossiliferous Permian to Plio-Pleistocene strata are exposed within the basin, particularly at the southern end in the Songwe Valley [19–25]. The trace fossils described in this study come from steeply exposed type section of the Paleogene Nsungwe Formation, which represents an overall upward fining succession of alluvial fan (Utengule Member) to volcanic-rich fluvial and lacustrine (Songwe Member) facies [17, 18, 23]. The Songwe Member preserves a particularly important and rare window in the late Paleogene of continental subequatorial Africa and has produced a rich new fauna, including the earliest records of Old World monkeys and apes [16, 23], along with a diversity of other mammals, crocodiles, birds, lizards, snakes, crustaceans and mollusks [26–31].

The Songwe Member has been precisely dated as late Oligocene, between 26–24 Ma, using a combination of: (1) single-crystal laser fusion Ar/Ar dating of phlogopite; (2) U-Pb LA-ICPMS dating of titanite; and (3) U-Pb LA-ICPMS, SHRIMP and CA-TIMS dating of zircon from multiple volcanic tuffs [17, 23]. The trace fossils reported in this study come from ~265 m

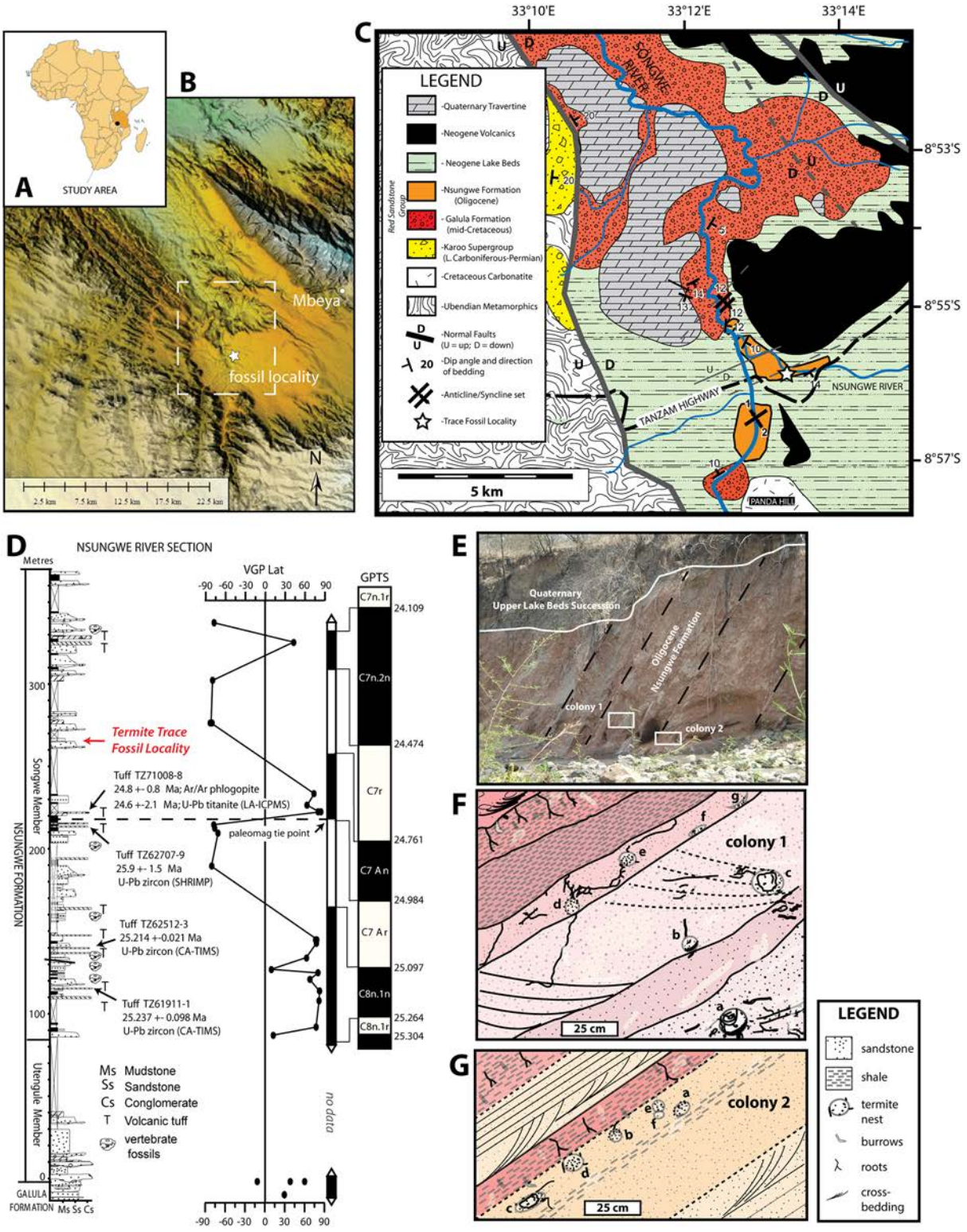

Fig 1. Location and stratigraphy of the trace fossil locality, Tanzania. (A) Location of Tanzania within Africa. (B) Digital elevation model for the study area in the southern end of the Rukwa Rift Basin (white box is shown in C). (C) Geologic map of the Songwe Valley in the southern end of the Rukwa Rift Basin, showing stratigraphy and age of fossil locality. Modified from [18]. (D) Measured section and magnetic stratigraphy through the Nsungwe Formation Type Section, with location of fossil locality shown. Modified from [18]. (E) Photograph of the nest locality in a steeply dipping cliff face along the Nsungwe River. (F, G) Sketch maps of

fossil locality showing the orientation and distribution of the termite colonies 1 (RRBP-08248) and 2 (RRBP-15106), with letters corresponding to the different nest chambers in each colony.

doi:10.1371/journal.pone.0156847.g001

above the basal contact of the Songwe Member, along the Nsungwe River Section. Based on radioisotopic dating and magnetostratigraphy, this part of the section is interpreted to fall within chron C7r of the global polarity timescale, indicating an age between ~24.8–24.5 Ma [17, 23].

The trace fossils, representing two discrete termite colonies, were all collected in the same area, but from beds several meters apart in a steeply dipping section of interbedded fluvial channel sandstones and overlying overbank mudrocks. Colony 1 was found near the top of a fine-grained, muddy sandstone complex and with seven chambers clustered in a small area spanning ~90 cm (vertically) x 150 cm (horizontally) (Fig 1). Colony 2 was found ~3 m below Colony 1 in a single 15 cm thick muddy sandstone horizon with six chambers spread out over 1.2 m (Fig 1). The sandstone beds containing Colony 1 fine upward and the densest concentration of nests were found in the finest-grained strata near the top of the bed. Colony 2 was also found in a fine-grained muddy sandstone unit. In both horizons, poorly preserved trough cross-bedding is cross-cut by the nests, associated galleries and root traces, indicating that the trace fossils formed after termination of fluvial flow and subaerial exposure at the top of the channel. Both colonies are overlain by a thin, pale orange to red color-banded sandy mudstone with abundant root mottling, horizontal and vertical burrows and minor $CaCO_3$ concretions. Considered together, these deposits are interpreted to be the top of an abandoned fluvial channel sequence, which was subjected to several flooding events followed by subaerial exposure and pedogenesis, presumably during the time of nest development and shortly after channel abandonment (see [18] for detailed interpretation of the sedimentology of section).

The site includes two termite colonies (Fig 1), each with six to seven fungus chambers, and three of which preserve fungus gardens (also called fungus combs). The trace fossils are interpreted as having formed synchronously with deposition of the Oligocene Songwe Member, rather than being modern constructions associated with recent termite activity, based on the following evidence: 1) the trace fossils are lithified; 2) some of the nests and fungus combs show compaction features, indicating that they were buried after formation; 3) galleries are infilled with similar sediment to the host rock, rather than more recent volcanic ash which is common in the present soil overlying the Oligocene strata; and 4) the nests and fungal combs are oriented parallel to the steeply dipping beds, rather than parallel to the present-day land surface.

The gross morphology of the trace fossil, its association inside *Vondrichnus*, and its peloidal construction of enclosed cells matches the diagnosis of a laminar-type fungus comb, *Microfavichnus alveolatus* [11]. Upward construction of the comb is evidenced by the concentric form and retention of alveolar form in the upper region. The fossil fungus chamber and fungus comb inside it are comparable to fungus combs produced by extant species of the genera *Macrotermes* and *Odontotermes*. However, no large hypogean chambers (calies) were observed with either colony, possibly due to the limited lateral extent of the outcrop.

Continental Ichnology

Ichnogenus *Vondrichnus* Genise & Bown, 1994

Diagnosis. Diffuse, polychambered, excavated subterranean nest systems. Obovate chambers occur in dense swarms of near 300 in cross section. Burrows simple, branched or unbranched, exiting from one or more points on periphery of chamber and comprising a dense mass of anastomosing burrows that may connect chambers [32].

Description. Thirteen specimens of *Vondrichnus planoglobus* representing two different termite colonies were discovered in the Nsungwe Formation (Fig 1). Three examples represent complete chambers and the remaining are partially eroded chambers. The chamber sizes range between 4 and 13 cm in diameter (width), but are only up to 8 cm in height because they are flattened to concave at their base (Figs 2 and 3). Flattened peloidal material, interpreted as compressed mylospheres are arranged, in part, in concentric lines from the base, as observed in polished cross-sections made from three samples (Figs 2 and 4). Some chamber peripheries consist of a 1–3 mm sediment rind that appears to differ in color and composition to the surrounding sediment, possibly due to differential composition of iron-oxides. Chamber expansion occurred in at least one example with two chambers in apposition oriented horizontally, which display meniscate shapes in cross-section. Chamber infill, subsequent to nest collapse, most often consists of fine sand or muddy sediments, however one example of coarser grained sandstone infill was observed (Figs 2–4). Although nest preservation is incomplete, the semi-spherical shape of the chambers is inferred from the cross-section shapes of the specimens. A number of galleries were observed to emanate from the top of one of the chambers, and in one case, from the bottom of the chamber, otherwise no other galleries were preserved in the next structures. A generally obovate, spaghetti-like mass composed of a meandering network of concave-up tubular shelves composed of small, white, compressed spheres was observed inside three of the nest chambers. These internal structures are interpreted as fungus combs of the ichnogenus *Microfavichnus alveolatus* [11].

Referred specimens. Twelve specimens from two separate colonies, including: (1) one housing an *in situ* fungus comb inside (*Microfavichnus alveolatus*) (RRBP 08248a); (2) one cross-sectioned specimen (RRBP 08248c) with partial fungus comb (isolated mylospheres) preserved inside; (3) one cross-sectioned specimen (RRBP08248g) showing endoecie and single chamber in apposition; (4) seven additional *in situ* specimens that were not collected; and (5) one additional collected specimen (RRBP-15106c) (Figs 2 and 3).

Locality and horizon. Nsungwe River section, late Oligocene Songwe Member (265 and 269 m levels in Fig 1D) of the Nsungwe Formation, Red Sandstone Group, Mbeya Region, southwestern Tanzania (Fig 1). The locality represents a fluvial channel succession with thin, pedogenically modified overbank deposits that host both termite colonies.

Discussion. These ichnofossils are interpreted to be polychambered subterranean termite nests. Nest density is interpreted as being low by comparison to chamber density previously reported for other fossil termite colonies [11, 14], due to the limited outcrop exposure of the Nsungwe Formation. Although the two ichnospecies of *Vondrichnus* are similar to one another, the size and shape of the Rukwa specimens are more consistent with the diagnosis of *V. planoglobus*. The concentric masses of fine-grained sediments within some of the chambers, coupled with the small size of the chambers, supports the interpretation of these nest trace fossils as *Vondrichnus*, rather than such similar ichnotaxa as *Termitichnus* and *Coatonichnus*. These specimens share many similarities with *Termitichnus*, however they can be differentiated based on their small size and morphology. Notably, nest size and the flattening of the chambers indicate that the Nsungwe nests are not *Termitichnus qatranii*, *T. namibiensis* or *T. schneideri* because they are consistently much smaller. Additionally, fungal gardens are currently only associated with the ichnospecies *Vondrichnus planoglobus*.

Ichnogenus *Microfavichnus* Duringer et al., 2007

Diagnosis. Isolated, flattened alveolar masses (~6–9 cm wide x 3–6 cm tall) that resemble a morel. Exhibits an arched-convex upper portion combined with a flattened, sub-concave

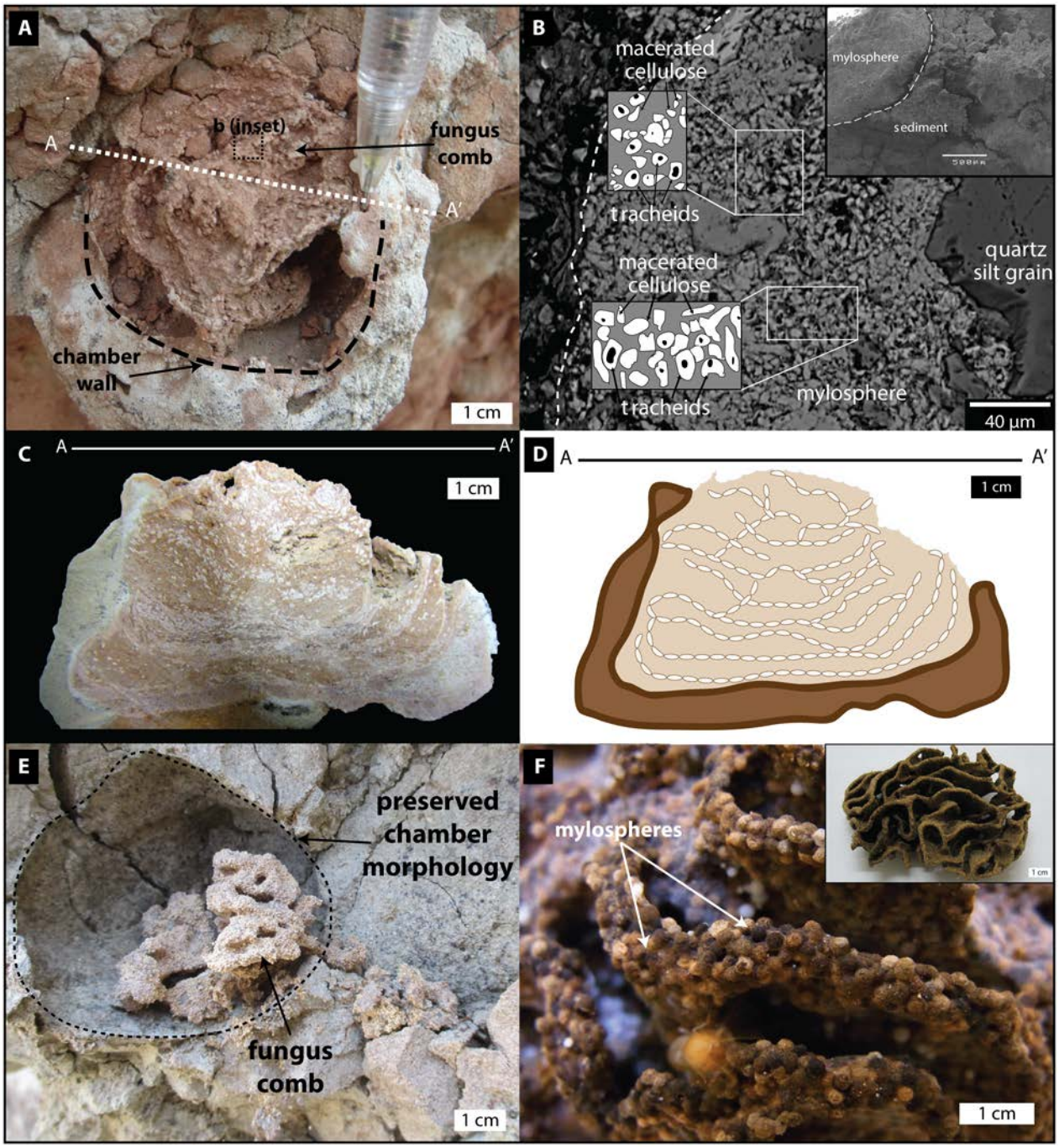

Fig 2. Fossil termite nest and fungus comb with comparative Holocene-Recent examples. (A) *In situ* fossil termite nest (*Vondrichnus planoglobus*; RRBP-08248a) with *Microfavichnus alveolatus* fungus comb trace fossil inside. (B) Backscatter electron (BSE) image of fossilized mylosphere with homogeneous composition of 5–10 µm macerated cellulose and calcified tracheids (elongated cells from the xylem of vascular plants). Inset: Scanning electron microscope (SEM) image of *Microfavichnus* in (A) showing compressed mylospheres and clay infill. (C, D) Photograph (C) and cartoon (D) of cross-section of RRBP-08248a (A). (E) Holocene fungus chamber with fungus comb, near the Galula Village along the Songwe River, Tanzania. (F) Modern *Microtermes* fungus comb, Malaysia (photo: Termite Web). Inset: Modern *Macrotermes* fungus comb.

doi:10.1371/journal.pone.0156847.g002

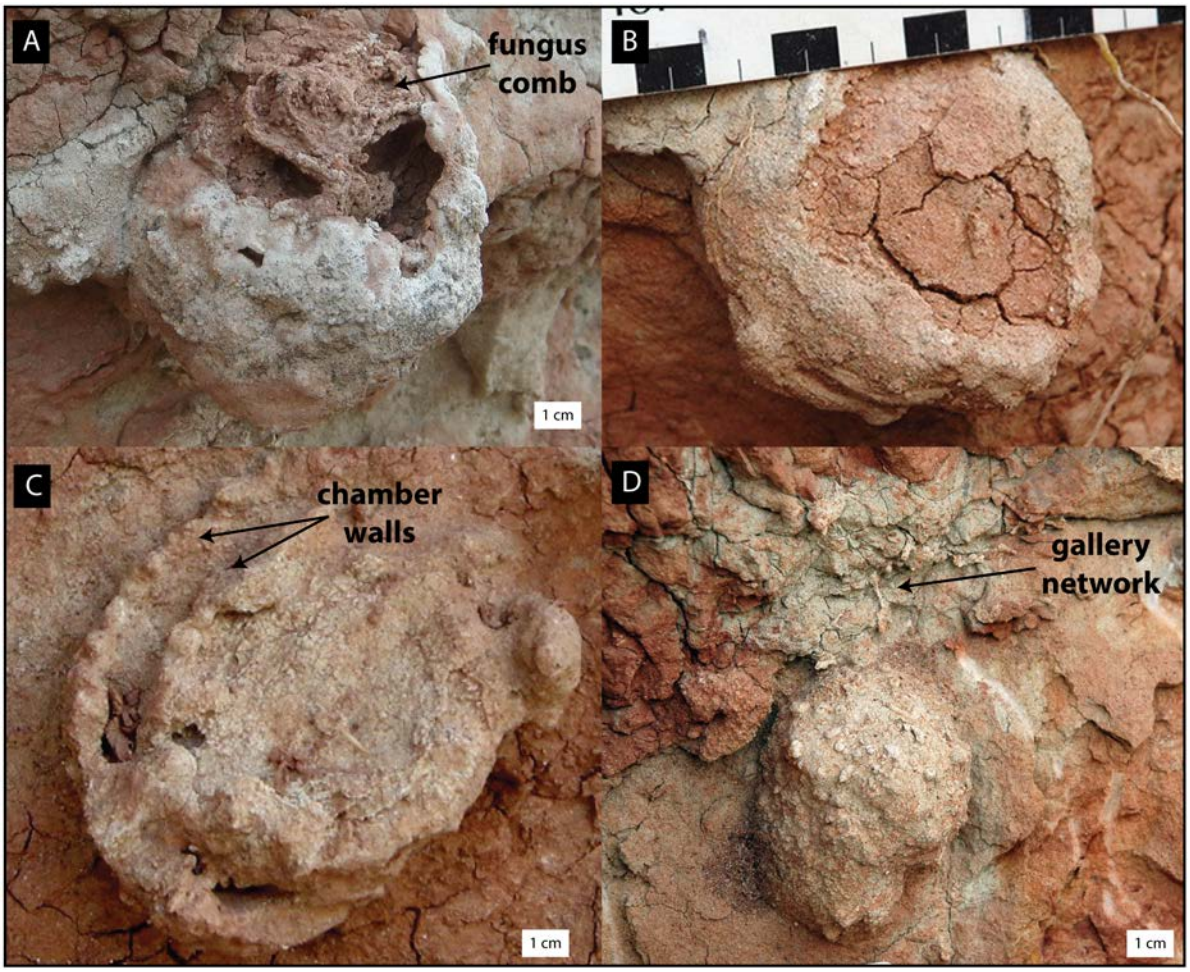

Fig 3. Photographs of specimens *in situ* displaying different morphologies and weathering stages. (A) Sample RRBP 08248a (Colony 1) with preserved fungus comb. (B) Sample RRBP 08248c (Colony 1). (C) Sample RRBP 08248g showing galleries and concentric chambers (Colony 1). (D) Uncollected nest RRBP 08248d (Colony 1) showing an external morphology and gallery network above the main nest.

doi:10.1371/journal.pone.0156847.g003

lower aspect. Specimen lacks an outer wall. The walls of the structure have peloidal texture formed by the juxtaposition and the stacking of mm-sized or smaller peloids.

Description. The outer shape of the trace fossil is hemispherical (radius 4.5 cm), with a flat to slightly concave base and no outer wall (Figs 2C, 2D and 3A). The internal fabric consists of at least eight sub-horizontal laminations or shelves of tan-colored peloids (1 mm, spherical to platelet shape) separated by red-colored, fine-grained sand and rare isolated peloids (Figs 2A–2D and 4A). The laminations (shelves) are concentrically nested from top to bottom, with the lowest levels deflecting upward at the margins of the structure. Compression of laminations and peloids is greatest near the base of the trace fossil (due to passive soil compaction), whereas the uppermost peloidal laminations show subdivision into open cells, 10 mm wide x 4 mm tall. Peloids are dominated by detrital silt grains and finely macerated cellular material, including isolated tracheids that have been replaced by calcium carbonate (Figs 2B, 2C and 4A).

Referred specimens. Three referred specimens, including one *in situ* fungus comb inside a fungus chamber (*Vondrichnus planoglobus*) (RRBP 08248a), an isolated fungus comb (RRBP

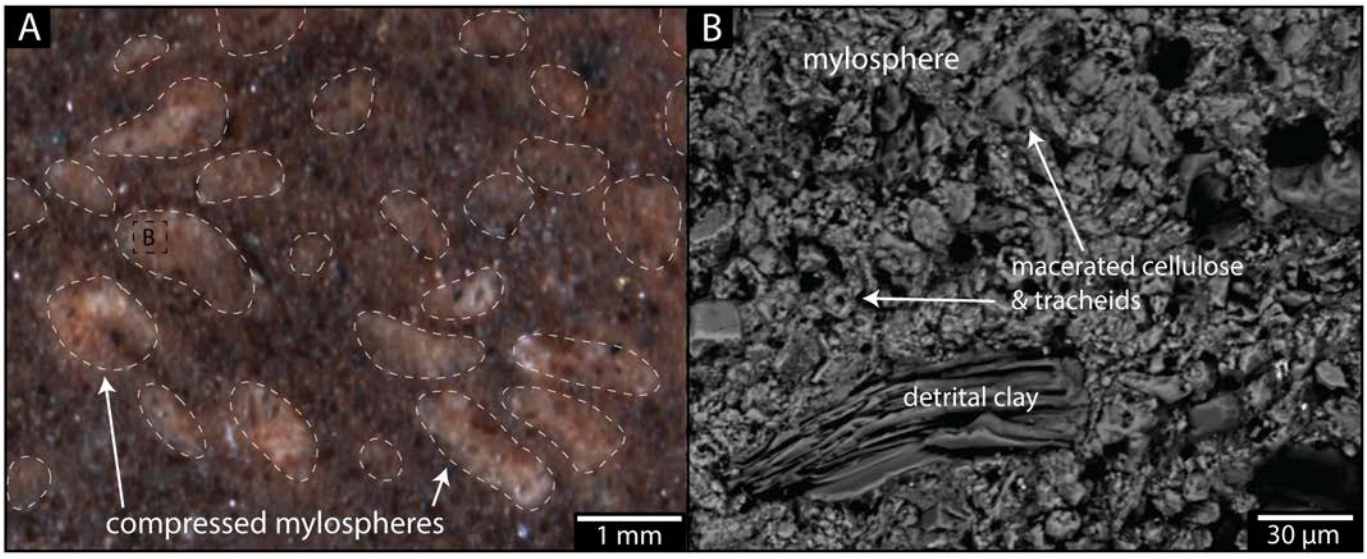

Fig 4. Structure and composition of preserved mylospheres from Macrotermitinae chamber. (A) Image of polished surface from sample RRBP 08248g (Colony 1) exposing compressed mylospheres (white) near the nest wall and detrital sediment (dark red) filling the chamber. Morphologies and chemical compositions were analyzed via energy dispersive spectroscopy (EDS) and backscattered electron imaging (BSE) by electron probe microanalysis. The sediment surrounding the mylospheres is clay-rich and contains occasional detrital quartz and feldspar grains (and accessory minerals such as monazite), deposited as the nest walls were expanded and/or through infilling of the chamber during construction of or later burial of the nest. There is a small presence of diagenetic Fe-, Mn-, and Ti-rich cement. (B) BSE image of a mylosphere from (A) revealing a homogeneous composition. Filled and hollow subcylindrical, 5–10 µm particles with a major Ca component comprise the mylospheres. We interpret the mylospheres to be composed of wood fragments now replaced by calcium carbonate, preserving the remnants of macerated cellulose and tracheids (Fig 2B).

doi:10.1371/journal.pone.0156847.g004

08248f), and one specimen (RRBP 08248c) of a cross-sectioned nest (*Vondrichnus*) with a partial fungus comb (isolated mylospheres) preserved inside (Figs 2–4).

Locality and horizon. Nsungwe River section, late Oligocene Songwe Member (265 and 269 m levels) of the Nsungwe Formation, Red Sandstone Group, Mbeya Region, southwestern Tanzania (Fig 1). Locality represents a fluvial channel succession with thin, pedogenically modified overbank deposits that host the termite colonies.

Discussion. See below.

The Fossil Record of Termites

Trace fossils provide valuable data on the role of poorly-fossilized insects in paleoecosystems through time [11, 13, 14, 33], and they are pivotal in testing the origins and timing of many different insect clades, their behaviors and niche utilization [34, 35]. Although rare, termite trace fossils have been interpreted from the Mesozoic [36–38]. The most abundant examples derive from Cenozoic deposits of Africa, and these are most closely related to nests produced by members of the fungus-growing termites (Macrotermitinae). Trace fossils interpreted as nests used for fungus growth, storage, reproduction and feeding have been assigned to several ichnogenera, including *Termitichnus* and *Vondrichnus*, and reported from the Upper Eocene—Oligocene of Libya and Egypt [13–15], the Neogene of Chad [11], and the Plio-Pleistocene of Namibia [39], Tanzania [40, 41] and South Africa [39] (Fig 5). However, the oldest example of termite nests with *in situ* fungus gardens, providing unequivocal evidence for the antiquity of termite-fungus mutualism, was reported from the late Miocene-early Pliocene in Chad [12]. These workers also reported a spectacular termite ichnofauna [12] with a number of new ichnospecies (e.g., *Termitichnus schneideri*, *Vondrichnus planoglobus*, *Coatonichnus globosus*). In

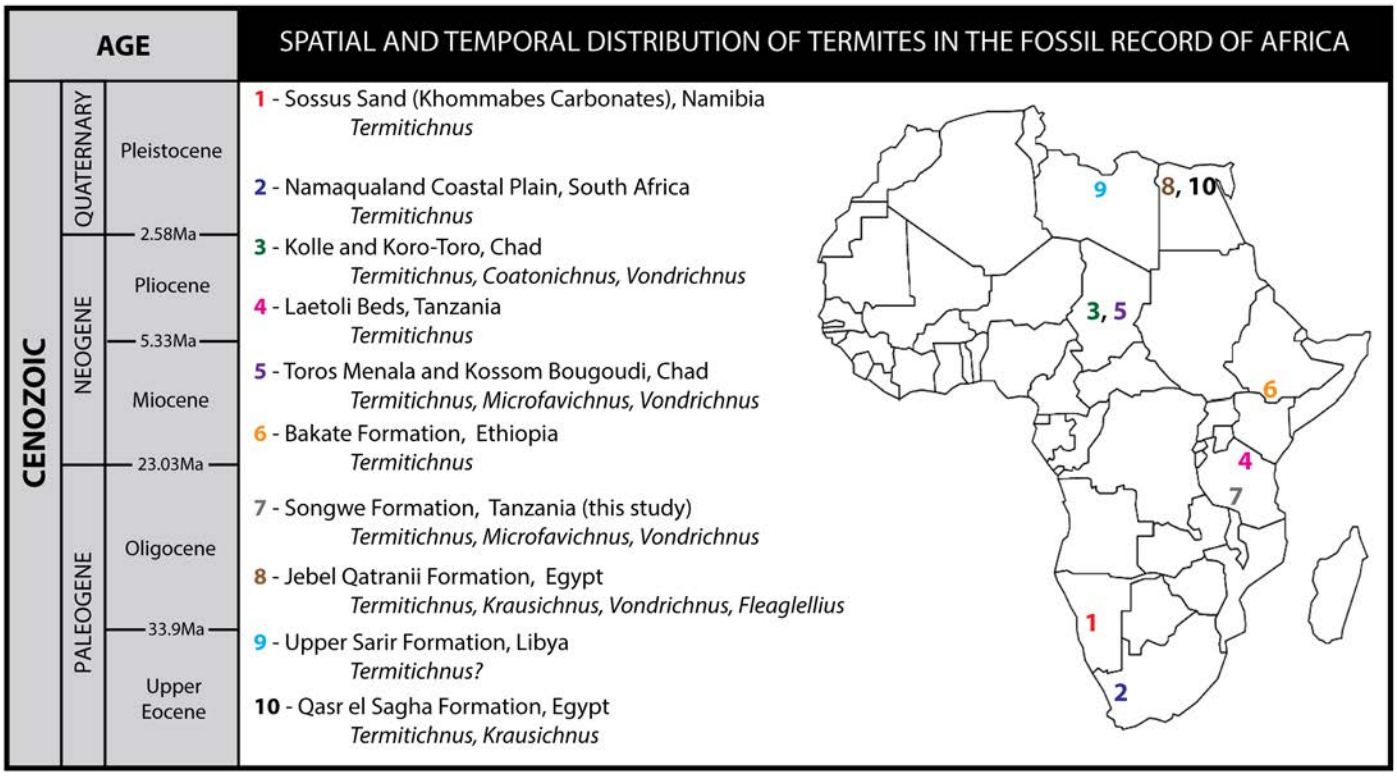

Fig 5. Temporal and spatial distribution of fossil termite nests and fungal gardens in Africa. Colored numbers represent termite trace fossil locations, along with the locality name and taxa present (*represents trace fossil localities with unequivocal fungal gardens associated with termite nests, demonstrating termite agriculture). Numbering refers to stratigraphic position as noted in reference to the Cenozoic time scale (at left). References: 1. Sossus Sand, Namibia [39]; 2. Namaqualand, South Africa [39]; 3. Kolle and Koro-Toro, Chad [11]*; 4. Laetoli, Tanzania [41, 43]; 5. Toros Menala and Kossom Bougoudi, Chad [11]*; 6. Bakate Formation, Ethiopia [44]; 7. Nsungwe Formation, Tanzania (this report)*; 8. Jebel Qatranii Formation, Egypt [14]; 9. Upper Sarir Formation, Libya [15]. 10. Qasr el Sagha Formation, Egypt [14].

doi:10.1371/journal.pone.0156847.g005

their study of this ichnological lagerstaten, these workers [11, 12, 42] documented the clear association between fungus combs, *Microfavichnus alveolatus*, and termite nests, several of which preserve *in situ* fungus combs within the ovoid chambers of the termite nest *Vondrichnus planoglobus*. These trace fossils have served as a critical calibration point in recent molecular studies and ecological modelling aimed at documenting the origins of fungus-growing termites [9]. It has been suggested that even older termite nest from the Paleogene of Egypt [13, 14] and Libya [15] may also be associated with fossil fungus combs, however due to poor preservation, confirmation of this awaits more detailed investigation of these examples.

Implications and Molecular Calibration

We used the well-dated Tanzanian fossil fungus combs reported here to recalibrate molecular divergence dates based on DNA sequences of 19 taxa and two calibration points [9] (S1 Table). First, we plotted representative examples of extant fungus gardens on a genus-level phylogeny [7, 9] (Fig 6). Based on a comparison between the fossil fungus combs and extant fungus combs, we inferred that the fossils most likely belong to the clade composed of all genera except *Pseudacanthotermes* and *Acanthotermes* (node b in Fig 6). Repeating the method used in [9], we applied the most recent common ancestor of this clade as an additional calibration point with a minimum age of 24.65 Ma (Table 1) to estimate the origin of the fungus-growing termites (node a in Fig 6) at 31.41 Ma (25.82, 39.53), which is close to previous estimates [9–10].

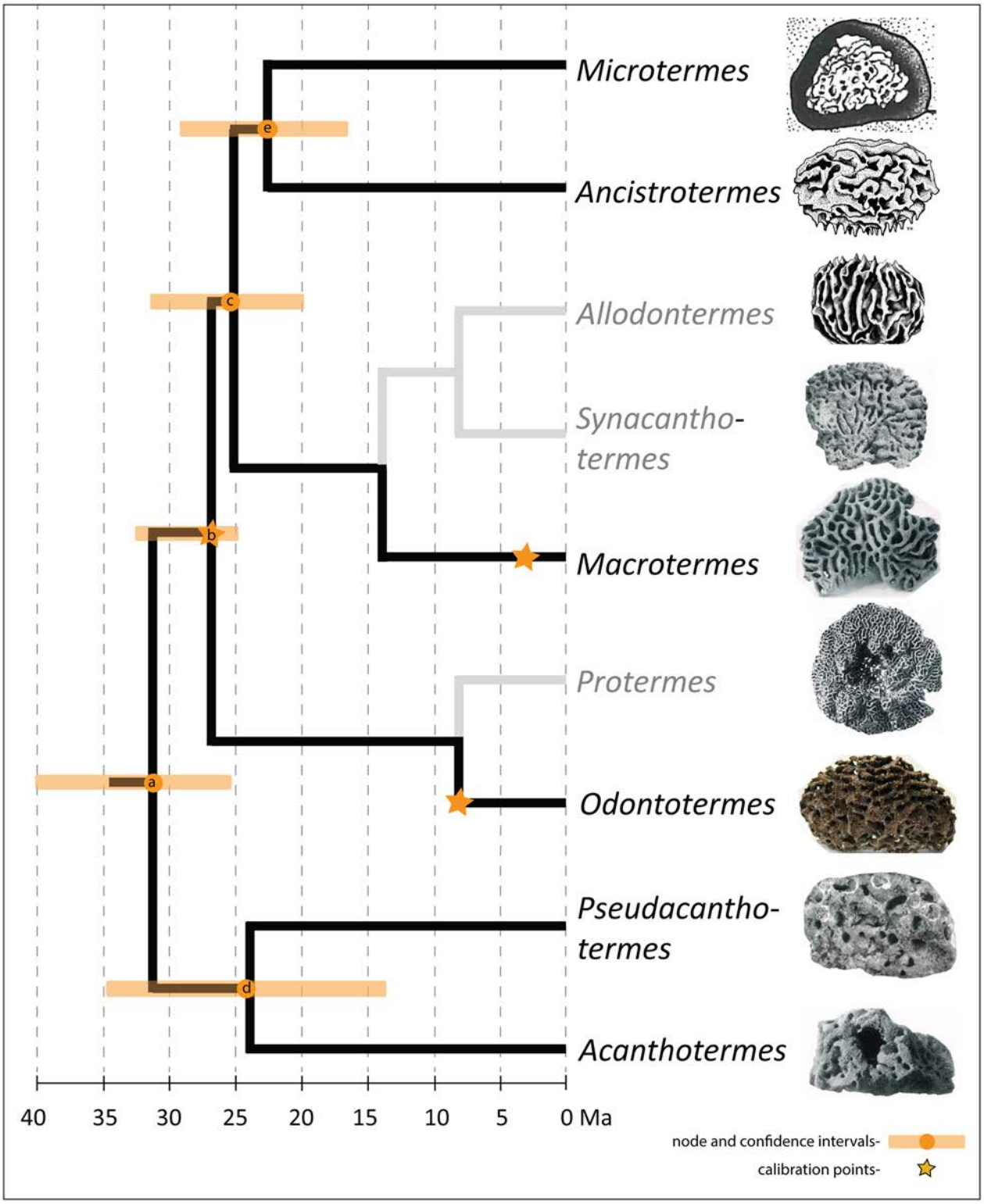

Fig 6. Schematic genus-level phylogeny [7, 9] of fungus-growing termites (Macrotermitinae) with recalibrated molecular divergence dates and confidence intervals from Table 1. This figure is based on simulation 1 and more highly resolved species trees can be found in the S1–S5 Figs. Representatives of the genera *Allodontermes*, *Synacanthotermes* and *Protermes* (faded branches) were not included in the time estimates. Images depict representative fungus combs of the different genera. Sketches of *Microtermes* and *Allodontermes* fungal combs from [45] and *Ancistrotermes* from [46]. Note: the calibration point on the Macrotermes branch corresponds to the age of the ancestor of *Macrotermes jeanneli* [41].

doi:10.1371/journal.pone.0156847.g006

Table 1. Mean estimated divergence dates and associated 95% confidence intervals for the origin of fungus-farming termites.

	(a)	(b)	(c)	(d)	(e)
Simulation 1 (node b)	31.4 Ma [25.8, 39.5]	27.1 Ma [25.0, 32.5]	25.3 Ma [20.1, 31.7]	24.5 Ma [13.7, 34.8]	22.8 Ma [16.8, 29.2]
Simulation 2 (node a)	27.1 Ma [25.0, 32.8]	22.7 Ma [16.9, 28.9]	21.2 Ma [15.4, 27.3]	20.9 Ma [11.7, 28.8]	19.2 Ma [13.3, 25.0]
Simulation 3 (node d)	32.0 Ma [25.8, 41.4]	26.6 Ma [18.7, 36.2]	24.9 Ma [17.2, 34.0]	27.1 Ma [25.0, 32.7]	22.5 Ma [14.7, 30.9]
Simulation 4 (node e)	36.1 Ma [27.8, 47.0]	31.1 Ma [25.8, 38.6]	29.3 Ma [25.2, 35.8]	28.0 Ma [13.8, 41.5]	27.0 Ma [25.0, 32.2]
Simulation 5 (genus *Microtermes*)	50.2 Ma [34.0, 70.4]	43.3 Ma [31.3, 59.1]	37.4 Ma [28.0, 49.6]	39.0 Ma [18.5, 61.0]	29.9 Ma [25.0, 31.7]

In all simulations, the *Odontotermes* node was constrained to a minimum age of 7 Ma, and the ancestor of *Macrotermes jeanneli* was constrained to a minimum age of 3.4 Ma (see Methods). We performed five analyses using alternative calibration points of the newly discovered fossils. Simulation 1 used node b as a calibration point. Alternative calibration points were: node a (Simulation 2), node d (Simulation 3), node e (Simulation 4) and the most recent common ancestor of the genus *Microtermes* (Simulation 5) (see S1 Table; S1–S5 Figs).

doi:10.1371/journal.pone.0156847.t001

Since a comparison between the fossil combs and extant combs is not unambiguous, we also tested various other possible calibration points, resulting in comparable age estimates ranging from 27 to 36 Ma (Table 1; for details see S1 Table, S1–S5 Figs). Dating phylogenies remain an uncertain process, not only depending on the fossil calibration(s) used but also on the DNA regions used and the concomitant accuracy of the recovered phylogeny and calibration methods. As such, the resulting dating should be carefully read as indicators of a time frame and not absolute ages. The proximity of this age estimate, however, is consistent with the hypothesis that the transition to fungus cultivation in the termites was followed closely by the main radiation leading to the extant genera [8, 9].

Antiquity of Insect Agriculture

Only two other insect groups are known to have derived mutualisms with fungi for agriculture: the ambrosia beetles and the leaf-cutter ants. Ants and termites are each considered to have evolved the ability to cultivate fungi for food only once, between 45–65 Ma and 24–34 Ma, respectively [47–49]. However, in ambrosia beetles, this trait may have evolved independently as many as ten different times, probably first around 50 Ma [50, 51]. It is also not clear where fungus gardening developed in ambrosia beetles, although there appears to be a strong evolutionary link to a tropical or sub-tropical forest setting [51]. Unfortunately, no fossil evidence, either in the form of fungal gardens or unequivocal ambrosia beetle borings, exists to validate molecular age estimates for ambrosia beetles or to provide direct geographic evidence on where this symbiosis originated.

The oldest evidence of fungus gardening by leaf-cutter ants dates back to the late Miocene of Argentina, between 5.7 and 10 Ma [52]. However, no fungus gardens are preserved, only fossilized ant (Attini) nests interpreted as fungus chambers based on morphology and the presence of fungal hyphae within them [52]. Together, the late Miocene Argentinian leaf-cutter nests and the macrotermitine fungus combs from Chad [11, 12] represent the oldest previously known definitive fossil evidence for insect domestication of fungi, yet both are considerably younger than the Paleogene molecular estimates for the antiquity of agriculture by insects.

Hence, the newly discovered Tanzanian trace fossils support a Paleogene record for the important evolutionary partnership between insects and fungi, and more specifically, they confirm recent molecular hypotheses for an African origin of symbiosis between the Macrotermitinae and *Termitomyces* fungi [9]. Notably, the features observed in the Tanzanian trace fossils lend support to the idea that similar Paleogene trace fossils documented across Afro-Arabia [13–15] may also represent fungus-farming termites. For instance, termite trace fossils

Vondrichnus and *Termitichnus* from Oligocene-Miocene terrestrial ecosystems in Egypt, Ethiopia, Libya and Arabia [13–15] (Fig 5) may have also been produced by fungus farming termites, however these fossils have not been described in detail and so their position on the tree is not clear (see S1 Text, S2 Table and S6 Fig for details on molecular calibrations using these taxa, which do not greatly alter the ages suggested in Simulation 1). The discoveries of fungus combs within termite nests in Chad [11] and now, in Tanzania, confirm these earlier assertions and suggest that fungus-farming termites radiated across Africa early in their evolutionary history. The diversification of the Macrotermitine termites from an African rainforest origin might have been coeval with expansion of savannahs in Africa [8]. Although the expansion of C4 grasses (and hence savannahs) are not well-documented on continental Africa until ~7–8 Ma, the presence of micromammals with crestiform teeth and active-foraging colubroid snakes from well-dated late Oligocene strata in the Rukwa Rift Basin suggest that isolated mixed forest/grassland ecosystems may have been present in ecosystems by 25 Ma, likely reflecting landscape changes associated with the initiation of the East African Rift System [17].

Methods

Permits

The Tanzanian Commission for Science and Technology (COSTECH) and the Tanzanian Antiquities Unit granted us permission to carry out our field studies and to take samples. Our field studies did not involve endangered or protected species.

Specimens

Portions of two fossilized termite colonies containing 13 individual trace fossil termite nest structures (*Vondrichnus planoglobus)*, three of which contained *in situ* fungus combs (*Microfavichnus alveolatus)*, were assigned specimen numbers: RRBP 08248a-g and RRBP 15106a-f. Due to the fragile nature of these trace fossils, only five nest structures were collected for further study. These include samples RRBP08248a, c, f, and g and RRBP 15106c. The other trace fossils were too fragile to collect and remain *in situ* or have since weathered out of the outcrop. Specimens included in the contribution are accessioned with RRBP (Rukwa Rift Basin Project) identifiers and are permanently housed through the Antiquities Division of the Republic of Tanzania (Dar es Salaam, Tanzania).

Paleontological approaches

In order to obtain a better understanding of the internal architecture of the trace fossils, three samples were cross-sectioned through a vertical mid-plane passing from the upper to lower surface using a lapidary saw with no water. One side was cross-sectioned through the equator, perpendicular to the first cut. All cut surfaces were polished for higher-resolution observation. Scanning electron microscopy (SEM) was used to image the internal structure of the trace fossils and micro-CT analysis was unsuccessfully employed to observe internal architecture of one of the trace fossils due to a lack of density differences between the different materials. One of the cross-sectioned para-types was also vacuum impregnated with epoxy and polished to observe internal structures in better detail and to construct a microprobe mount. Element concentrations were measured using EDS and BSE images of the sample were taken to examine preservation patterns of the nests and fungus combs (Figs 2 and 4). This work was conducted on an electron probe microanalyser (EPMA; Jeol JXA8200 "superprobe") at the Advanced Analytical Centre (AAC) at James Cook University.

Fungus-growing termite dating

Data and methodology used for the phylogeny calibration were the same as in Nobre et al. [9] (also see S1 and S2 Tables; S1–S7 Figs; S1 Text). Briefly, we used DNA sequences of the mitochondrial genes COI and COII and the nuclear ribosomal gene ITS2 for the 19 species of fungus-growing termites from all genera (except for the genera *Allodontermes*, *Synacanthotermes* and *Protermes*) and three outgroups [9]. Divergence dates were determined using the Bayesian relaxed-clock uncorrelated exponential approach implemented in BEAST 1.54 [53]. In the phylogeny reconstruction, the topology of the resulting tree was constrained to the genus-level phylogeny as estimated previously ([2, 7, 9] drawn schematically in Fig 6), and three Markov chain Monte Carlo searches were run for 10 000 000 generations each. Convergence was assessed using the log likelihood distributions of individual chains, and the burn-in level was assessed graphically in Tracer v1.4. In all simulations, the *Odontotermes* node was constrained to a minimum age of 7 Ma (based on the age of fossilized fungus comb associated with *Odontotermes* nest trace fossils from Chad [7]) following a lognormal distribution going as far back as the new fossil encountered (ca. 25 Ma) [8] [lognormal mean = 1.9, lognormal SD = 2.9, zero offset = 7]; and the ancestor of *Macrotermes jeanneli* was constrained to a minimum age of 3.4 Ma (based on the age of trace fossils reported from Tanzania [41]) [lognormal mean = 1.2, lognormal SD = 3.1, zero offset = 3.4]. We used the new fossils as a third node constraint of 25 Ma [lognormal mean = 3.2, lognormal SD = 2.7, zero offset = 25]. Because we inferred that the new fossils most likely belong to the clade composed of all genera except *Pseudacanthotermes* and *Acanthotermes*, the main approach applied this constraint to node b (simulation 1; the estimates from this analysis were used for the schematic Fig 6). Since the classification of the fossilized combs based on comparison with extant fungus combs is not unambiguous, we did four additional simulations (Table 1; Fig 6), using alternative calibration points of the newly discovered fossils: the most recent common ancestor of fungus-growing termites (node a; simulation 2); the most recent common ancestor of *Pseudacanthotermes* and *Acanthotermes* (node d; simulation 3); the most recent common ancestor of *Microtermes and Ancistotermes* (node e; simulation 4) and the most recent common ancestor of the genus *Microtermes* (simulation 5) (see S1–S6 Figs and S2 Table). Typically, the first 10% of the trees were discarded as burn-in, prior to results being pooled in LogCombiner v1.5.4 and tree visualization (see S1–S7 Figs; S1 Table for details concerning the details on the DNA analysis and files with raw trees produced in BEAST 1.54 [53]).

Supporting Information

S1 Fig. Simulation 1—Phylogenetic relationship of fungus-growing termites. Calibration points are indicated with ●. Each internal node is labelled with age and credibility interval of the corresponding clade; the posterior probabilities are found in italics (please note that not all posterior probability values are meaningful, since part of the topology was constrained).
(DOCX)

S2 Fig. Simulation 2—Phylogenetic relationship of fungus-growing termites. Calibration points are indicated with ●. Each internal node is labelled with age and credibility interval of the corresponding clade; the posterior probabilities are found in italics (please note that not all posterior probability values are meaningful, since part of the topology was constrained).
(DOCX)

S3 Fig. Simulation 3—Phylogenetic relationship of fungus-growing termites. Calibration points are indicated with ●. Each internal node is labelled with age and credibility interval of the corresponding clade; the posterior probabilities are found in italics (please note that not all

posterior probability values are meaningful, since part of the topology was constrained).
(DOCX)

S4 Fig. Simulation 4—Phylogenetic relationship of fungus-growing termites. Calibration points are indicated with ●. Each internal node is labelled with age and credibility interval of the corresponding clade; the posterior probabilities are found in italics (please note that not all posterior probability values are meaningful, since part of the topology was constrained).
(DOCX)

S5 Fig. Simulation 5—Phylogenetic relationship of fungus-growing termites. Calibration points are indicated with ●. Each internal node is labelled with age and credibility interval of the corresponding clade; the posterior probabilities are found in italics (please note that not all posterior probability values are meaningful, since part of the topology was constrained).
(DOCX)

S6 Fig. Simulation 6—Phylogenetic relationship of fungus-growing termites. Calibration points are indicated with ● including one for the origin of FGT based on Abouessa et al. [15]. Each internal node is labelled with age and credibility interval of the corresponding clade; the posterior probabilities are found in italics (please note that not all posterior probability values are meaningful, since part of the topology was constrained).
(DOCX)

S7 Fig. FASTA file. Original FASTA file for molecular clock calibrations from [9].
(FASTA)

S1 Table. DNA sequences from [9]. For 19 selected termite taxa, we have used 931 bp of the mitochondrial cytochrome oxidase subunit II gene (COI) using the primer pair TL1862 and TH2877 as in Aanen et al. [7], 684 bp of the mitochondrial cytochrome oxidase subunit II gene (COII) using AtLeu and B-tLys and 294 bp of part of the nuclear ribosomal internal transcribe spacer (ITS2) region using the primers ITS2 and ITS2F. Detailed methodology can be found in Nobre et al. [9].
(DOCX)

S2 Table. Alternative Calibration. Mean estimated divergence dates and associated 95% confidence intervals for the origin of fungus-farming termites (as for Table 1 in main text) considering the specimens from Libya [15] for calibration of the mrca of fungus-growing termites.
(DOCX)

S1 Text. Extra simulation for termite-fungus symbiosis excluding Rukwa specimen.
(DOCX)

Acknowledgments

We thank D. Kamamba, F. Ndunguru, and J. Temu (Tanzania Antiquities Unit), P. Msemwa (Tanzania Museum of House of Culture), and N. Boniface (University of Dar es Salaam), and the Tanzania Commission for Science and Technology (COSTECH) for logistical and administrative support; M. Gottfried, M. Hendrix, Z. Jinnah and the RRB excavation teams for field assistance. J. Hammerli, C. Pirard and K. Blake assisted with making polished slabs and microprobe mounts and imaging. We thank Termite Web for giving us permission to use photo shown in Fig 2F. We are grateful to the editor F. Bibi and two reviewers (M. Schuster and J. Scott) for their constructive feedback, which greatly improved the manuscript.

Author Contributions

Conceived and designed the experiments: EMR CNT DKA TN HLHW PMO LT CM NJS. Performed the experiments: EMR CNT DKA TN HLHW. Contributed reagents/materials/analysis tools: EMR CNT DKA TN HLHW PMO NJS. Wrote the paper: EMR CNT DKA TN HLHW PMO LT CM NJS.

References

1. Rouland-Lefèvre C. In: Takuya A, Bignell DE, Higashi M, editors. Symbiosis with Fungi. Termites: Evolution, Sociality, Symbioses, Ecology. Dordrecht: Kluwer Academic Publishers; 2000. pp. 289–306.
2. Poulsen M, Hu H, Li C, Chen Z, Xu L, Otani S, et al. Complementary symbiont contributions to plant decomposition in a fungus-farming termite. Proc. Nat. Acad. Sci. U.S.A. 2014; 111:14500–14505.
3. Pringle RM, Doak DF, Brody AK, Jocqué R, Palmer TM. Spatial pattern enhances ecosystem functioning in an African Savanna. PLoS Biol. 2010; 8:e1000377. doi: 10.1371/journal.pbio.1000377 PMID: 20520846
4. Bonachela JA, Pringle RM, Sheffer E, Coverdale TC, Guyton JA, Caylor KA, et al. Termite mounds can increase the robustness of dryland ecosystems to climate change. Science. 2015; 347:651–655.
5. Collins NM. The role of termites in the decomposition of wood and leaf litter in the southern Guinea savannah of Nigeria. Oecologia. 1981; 51:389–399.
6. Buxton RD. Termites and the turn-over of dead wood in an arid tropical environment. Oecologia. 1981; 51:379–384.
7. Aanen DK, Eggleton P, Rouland-Lefevre C, Guldberg-Froslev T, Rosendahl S, Boomsma JJ. The evolution of fungus-growing termites and their mutualistic fungal symbionts. Proc. Nat. Acad. Sci. U.S.A. 2002; 99:14887–14892.
8. Aanen DK, Eggleton P. Fungus-growing termites originated in African rain forest. Curr. Biol. 2005; 15:851–855. PMID: 15886104
9. Nobre T, Koné NA, Konaté KE, Linsenmair E, Aanen DK. Dating the fungus-growing termites' mutualism shows a mixture between ancient codiversification and recent symbiont dispersal across divergent hosts. Mol. Ecol., 2011; doi: 10.1111/j.1365-294X.2011.05090.x
10. Bourguignon T, Lo N, Cameron SL, Šobotník J, Hayahi Y, Shigenobu S, et al. The evolutionary history of termites as inferred from 66 mitochondrial genomes. Molecular Biology and Evolution. 2015; 32:406–421. doi: 10.1093/molbev/msu308 PMID: 25389205
11. Duringer P, Schuster M, Genise JF, Mackaye HT, Vignaud P, Brunet M. New termite trace fossils: Galleries, nests and fungus combs from the Chad Basin of Africa (Upper Miocene-Lower Pliocene). Palaeogeogr. Palaeoclimatol. Palaeoecol. 2007; 251:323–353.
12. Duringer P, Schuster M, Genise JF, Likius A, Mackaye HT, Vignaud P, et al. The first fossil fungus gardens of Isoptera: oldest evidence of symbiotic termite fungiculture (Miocene, Chad Basin). Naturwissenschaften. 2006; 93:610–615. PMID: 16924476
13. Bown TM. Ichnofossils and rhizoliths of the nearshore fluvial Jebel Qatrani Formation (Oligocene), Fayum Province, Egypt. Palaeogeogr. Palaeoclimatol. Palaeoecol. 1982; 40:255–309.
14. Genise JF, Bown TM. New trace fossils of termites (Insecta: Isoptera) from the late Eocene-early Miocene of Egypt, and the reconstruction of ancient isopteran social behaviour. Ichnos. 1994; 3:155–183.
15. Abouessa A, Pelletier J, Duringer P, Schuster M, Schaeffer P, Metais E, et al. New insight into the sedimentology and stratigraphy of the Dur At Talah tidal-fluvial transition sequence (Eocene—Oligocene, Sirt Basin, Libya. Journal of African Earth Sciences. 2012:72–90.
16. Stevens NJ, Gottfried MD, Roberts EM, Ngasala S, Kapilima S, O'Connor PM. Paleontological Exploration in Africa. In: Fleagle JG, Gilbert CC, editors. Elwyn Simmons: A Search for Origins. Developments in Primatology: Progress and Prospects: Springer; 2008. pp. 159–180.
17. Roberts EM, Stevens NJ, O'Connor PM, Dirks PHGM, Gottfried MD, Clyde WC et al. Initiation of the western branch of the East African rift coeval with the eastern branch. Nature Geoscience. 2012; 5:289–294.
18. Roberts EM, O'Connor PM, Stevens NJ, Gottfried MD, Jinnah ZA, Ngasala S, et al. Sedimentology and depositional environments of the Red Sandstone Group, Rukwa Rift Basin, southwestern Tanzania: New insight into Cretaceous and Paleogene terrestrial ecosystems and tectonics in sub-equatorial Africa. J. African Earth Sci. 2010; 57:179–212.
19. Grantham DR, Teale EO, Spurr AM, Harkin DA, Brown PE. Quarter Degree Sheet 244 (Mbeya). Geological Survey of Tanganyika, Dodoma; 1958.

20. Ebinger CJ. Tectonic development of the western branch of the East African rift system. Geol. Soc. Am. Bull. 1989; 101:885–903.
21. Delvaux D, Kervyn F, Vittori E, Kajara RSA, Kilembe E. Late Quaternary tectonic activity and lake level change in the Rukwa Rift Basin. J. African Earth Sci. 1998; 26:397–421.
22. Roberts EM, O'Connor PM, Gottfried MD, Stevens NJ, Kapilima S, Ngasala S. Revised stratigraphy and age of the Red Sandstone Group in the Rukwa Rift Basin, Tanzania: Cretaceous Research. 2004; 25:749–759.
23. Stevens NJ, Seiffert E, O'Connor PM, Roberts EM, Schmitz M, Krause D, et al. Palaeontological evidence for an Oligocene divergence between Old World monkeys and apes. Nature. 2013; 497:611–614. doi: 10.1038/nature12161 PMID: 23676680
24. O'Connor PM, Gottfried MD, Stevens NJ, Roberts EM, Kapilima S, Ngasala S, et al. Dinosaurs and other vertebrates from the Cretaceous Red Sandstone Group, Rukwa Rift Basin, Southwestern Tanzania. J. African Earth Sci. 2006; 44:277–288.
25. O'Connor PM, Sertich JJ, Stevens NJ, Roberts EM, Gottfried MD, Hieronymous TL, et al. The evolution of mammal-like Crocodyliforms in the Cretaceous Period of Gondwana. Nature. 2010; 466:748–751. doi: 10.1038/nature09061 PMID: 20686573
26. Stevens NJ, O'Connor PM, Gottfried MD, Roberts EM, Ngasala S. An anthropoid primate from the Paleogene of Southwestern Tanzania. J. Vertebr. Paleontol. 2005; 25:986–989.
27. Stevens NJ, Roberts EM, O'Connor PM, Gottfried MD. *Rukwalorax jinokitana* (n.gen., n.sp) (Mammalia: Hyrocoidea) in late Oligocene Rukwa Rift Basin of Tanzania. J. Vertebr. Paleontol. 2009; 29:972–975.
28. Stevens NJ, O'Connor PM, Gottfried MD, Roberts EM, Ngasala S, Dawson M. *Metaphiomys* from the Paleogene of Southwestern Tanzania: J. Paleontol. 2006; 80:407–410.
29. Stevens NJ, Holroyd PA, Roberts EM, O'Connor PM, Gottfried MD. *Kahawamys mbeyaensis* (n. gen., n. sp.) (Rodentia: *Thryonomyoidea*) from the late Oligocene Rukwa Rift Basin, Tanzania. J. Vertebr. Paleontol. 2009; 29:631–634.
30. Feldmann RM, O'Connor PM, Stevens NJ, Gottfried MD, Roberts EM, Ngasala S, et al. A new freshwater crab (Decapoda: Brachyura: Potamonautidae) from the Paleogene of Tanzania, Africa. Neues Jahrbuch fur Geologie und Palaontologie. 2007; 244:71–78.
31. McCartney J, Stevens NJ, O'Connor PM. The earliest Colubroid-dominated snake fauna from Africa: perspectives from the Late Oligocene Nsungwe Formation of southwestern Tanzania. PLOS ONE. 2014; 9(3):e90415. doi: 10.1371/journal.pone.0090415 PMID: 24646522
32. Genise JF. Ichnotaxonomy and ichnostratigraphy of chambered trace fossils in palaeosols attributed to coleopterans, ants and termites. In: McIlroy D, editor. The application of ichnology to palaeoenvironmental and stratigraphic analysis. Geological Society, London, Special Publications; 2004. pp. 419–453.
33. Genise JF, Mangano MG, Buatois LA, Laza JH, Verde M. Insect trace fossil associations in Paleosols: the Coprinisphaera Ichnofacies Palaios. 2000; 15:49–64.
34. Hasiotis ST. Complex Ichnofossils of solitary and social soil organisms: understanding their evolution and roles in terrestrial paleoecosystems. Palaeogeogr. Palaeoclimatol. Palaeoecol. 2003; 192:259–320.
35. Tapanila L, Roberts EM. The Earliest Evidence of Holometabolan Insect Pupation in Conifer Wood. PLoS ONE. 2012; 7:e31668. doi: 10.1371/journal.pone.0031668 PMID: 22355387
36. Hasiotis ST, Dubiel RF. Termite (Insecta: Isoptera) nest ichnofossils from the Triassic Chinle Formation, Petrified Forest National Park, Arizona. Ichnos. 1995; 4:119–130.
37. Bordy EM, Bumby A, Catuneanu O, Eriksson PG. Advanced Early Jurassic termite (Insecta: Isoptera) nests: evidence from the Clarens Formation in the Tuli Basin, southern Africa. Palaios. 2004; 19:68–78.
38. Bordy EM, Bumby A, Catuneanu O, Eriksson PG. Reply to a comment on advanced Early Jurassic termite (Insecta: Isoptera) nests: evidence from the Clarens Formation in the Tuli Basin, southern Africa. (Bordy et al., 2004). Palaios. 2005; 20:307–311.
39. Smith RMH, Mason TR. Sedimentary environments and trace fossils of Tertiary Oasis Deposits in the Central Namib Desert, Namibia. Palaios. 1998; 13:547–559.
40. Sands WA. Ichnocoenoses of probable termite origin from Laetoli. In: Leakey MD, Harris JM, editors. Laetoli, a Pliocene Site in Northern Tanzania. Oxford Science Publications; 1987. pp 409–433.
41. Darlington JPEC. Distinctive fossilised termite nests at Laetoli, Tanzania. Insectes Sociaux. 2005; 52:408–409.

42. Schuster M, Duringer P, Nel A, Brunet M, Vignaud P, Mackaye HT. Découverte de termitières fossiles dans les sites à vertébrés du Pliocène tchadien: description, identification et implications paléoécologiques. C. R. Acad. Sci., Paris. 2000; 331:15–20.

43. Miller WR, Mason TR. Sedimentary environments and trace fossils of Tertiary Oasis Deposits in the Central Namib Desert, Namibia. Ichnos. 2000; 7:195–215.

44. Bown TM, Genise JF. Abstracts with Programs of the Annual Meeting of the Geological Society of America. 1993; 25:58.

45. Uys VM. A Guide to the Termite genera of Southern Africa. Plant Protection Research Institute Handbook No. 15, ARC-Plant Protection Research Institute, Pretoria, South Africa. 2002. 116 pp.

46. Coaton WGH, Sheasby JL. National survey of the isoptera of Southern Africa 9. The genus *Ancistrotermes* silvestri (Termitida: Macrotermitinae). Cimbebasia (A). 1975; 3:95–104.

47. Mueller UG, Herardo NM, Aanen DK, Six DL, Schultz TR. The Evolution of Agriculture in Insects. Annu. Rev. Ecol. Evol. Syst. 2005; 36:563–595.

48. Schultz TR, Brady SG. Major evolutionary transitions in ant agriculture. Proc. Nat. Acad. Sci. U.S.A. 2008; 105:5435–40.

49. Mueller UG, Rehner SA, Schultz TR. The evolution of agriculture in ants. Science. 1998; 281:2034–2038. PMID: 9748164

50. Farrell DB, Sequeira AS, O'Meara BC, Normark BB, Chung JH, Jordal BH. The evolution of agriculture in beetles (Curculionidae: Scolytinae and Platypodinae). Evolution. 2001; 55:2011–2027. PMID: 11761062

51. Jordal BH, Cognato AI. Molecular phylogeny of bark and ambriosa beetles reveals multiple origins of fungus farming during periods of global warming. BMC Evolutionary Biology. 2012; 12:1471-2148/12/133.

52. Genise JF, Melchor RN, Sánchez MV, González MG. A Miocene record of fungus-growing ants. Palaeogeogr. Palaeoclimatol. Palaeoecol. 2013; 386:349–363.

53. Drummond A, Rambaut A. BEAST: Bayesian evolutionary analysis by sampling trees. BMC Evolutionary Biology. 2007; 7:214. PMID: 17996036